TESIS DOCTORAL
DOCTORAL THESIS
PROGRAMA DE DOCTORADO EN BIOMEDICINA
BIOMEDICINE DOCTORAL PROGRAMME

UNIVERSIDAD DE GRANADA

“Nuevos materiales biomiméticos y biotintas con aplicación en ingeniería regenerativa de cartílago y piel”

“New biomimetic materials and bioinks with application in regenerative engineering of cartilage and skin”

Memoria presentada por Carlos Chocarro Wrona

para optar a la mención de Doctor Internacional

GRANADA, Julio de 2022

Directores de tesis doctoral:

Juan Antonio Marchal Corrales,
Patricia Gálvez Martín,
y Elena López Ruiz

Editor: Universidad de Granada. Tesis Doctorales
Autor: Carlos Chocarro Wrona
ISBN: 978-84-1117-472-5
URI: http://hdl.handle.net/10481/76802

El doctorando **CARLOS CHOCARRO WRONA** y los directores de tesis **JUAN ANTONIO MARCHAL CORRALES,** CATEDRÁTICO DEL DEPARTAMENTO DE ANATOMIA Y EMBRIOLOGIA HUMANA DE LA UNIVERSIDAD DE GRANADA; **ELENA LÓPEZ RUIZ,** PROFESORA EN LA UNIVERSIDAD DE JAÉN EN EL DEPARTAMENTO DE CIENCIAS DE LA SALUD; y **PATRICIA GÁLVEZ MARTÍN,** RESPONSABLE DE PROYECTOS DE I+D EN SALUD HUMANA Y ANIMAL DE BIOBERICA S.A.U;

HACEN CONSTAR:

Que D. Carlos Chocarro Wrona ha realizado bajo su dirección el Trabajo de Tesis Doctoral:

"Nuevos materiales biomiméticos y biotintas con aplicación en ingeniería regenerativa de cartílago y piel"

durante los años 2017 – 2022, correspondiendo fielmente a los resultados obtenidos y respetándose los derechos de otros autores a ser citados cuando se han usado sus publicaciones.

Una vez redactada la siguiente memoria, ha sido revisada estando los directores conformes para que sea presentada y el doctorando pueda aspirar así al grado de Doctor Internacional por la Universidad de Granada ante el tribunal designado.

Y para que conste, en cumplimiento de las disposiciones vigentes, expedimos el presente en Granada a 25 de Mayo de 2022.

Fdo. D. Carlos Chocarro Wrona Fdo. Dr. Juan Antonio Marchal Corrales

Fdo. Dra. Elena López Ruiz Fdo. Dra. Patricia Gálvez Martín

Para optar a la mención de "Doctor Internacional", el doctorando realizó, durante un periodo de formación (Septiembre de 2021 - Diciembre de 2021), una estancia de cuatro meses en el laboratorio del Dr. Christophe Marquette en "*l'Institut de Chimie et Biochimie Moléculaires et Supramoléculaires*", donde se ubica su equipo de investigación, "*Equipe Génie Enzymatique, Membranes Biomimétiques et Assemblages Supramoléculaires (GEMBAS)*", del que forma parte la 3d.FAB platform.

Parte de los resultados de esta Tesis Doctoral han sido publicados en las siguientes publicaciones que cumplen con los criterios de calidad exigidos:

Chocarro-Wrona, C., López-Ruiz, E., Perán, M., Gálvez-Martín, P. and Marchal, J.A. (2019), *Therapeutic strategies for skin regeneration based on biomedical substitutes*. J Eur Acad Dermatol Venereol, 33: 484-496. https://doi.org/10.1111/jdv.15391

Indicios de calidad (datos del Journal Citation Reports):

Impact Factor (2019): 5.248

Categorías (posición/número de revistas): Dermatology (5/68)

Quartil: Q1 (D1)

Chocarro-Wrona, C, de Vicente, J, Antich, C, Jiménez, G, Martínez-Moreno, D, Carrillo, E, Montañez, E, Gálvez-Martín, P, Perán, M, López-Ruiz, E, Marchal, JA. *Validation of the 1,4-butanediol thermoplastic polyurethane as a novel material for 3D bioprinting applications*. Bioeng Transl Med. 2021; 6:e10192. https://doi.org/10.1002/btm2.10192.

Indicios de calidad (datos del Journal Citation Reports):

Impact Factor (2020): 10.711

Categorías (posición/número de revistas): Biomedical Engineering (4/89)

Quartil: Q1 (D1)

Criterios de calidad para optar al grado de Doctor con la mención de "Doctor Internacional" de la Universidad de Granada.

Publicaciones:

1. **Chocarro-Wrona, C**., López-Ruiz, E., Perán, M., Gálvez-Martín, P. and Marchal, J.A. (2019), *Therapeutic strategies for skin regeneration based on biomedical substitutes.* **J EUR ACAD DERMATOL VENEREOL, 33: 484-496. https://doi.org/10.1111/jdv.15391**
2. Hernández-Camarero, P., López-Ruiz, E., Griñán-Lisón, C., García, MA., **Chocarro-Wrona, C**, Marchal, J.A., Kenyon, J. and Perán, M. *Pancreatic (pro)enzymes treatment suppresses BXPC-3 pancreatic Cancer Stem Cell subpopulation and impairs tumour engrafting*. **SCI REP 9, 11359 (2019). https://doi.org/10.1038/s41598-019-47837-7**
3. Martínez-Molina, E., **Chocarro-Wrona, C**., Martínez-Moreno, D., Marchal, J.A., and Boulaiz, H. *Large-Scale Production of Lentiviral Vectors: Current Perspectives and Challenges*. **PHARMACEUTICS 2020, 12, 1051. https://doi.org/10.3390/pharmaceutics12111051**
4. **Chocarro-Wrona, C**, de Vicente, J, Antich, C, et al. *Validation of the 1,4-butanediol thermoplastic polyurethane as a novel material for 3D bioprinting applications*. **BIOENG TRANSL MED. 2021; 6:e10192. https://doi.org/10.1002/btm2.10192**
5. D. Martínez-Moreno, G. Jiménez, **C. Chocarro-Wrona**, E. Carrillo, E. Montañez, C. Galocha-León, B. Clares-Naveros, P. Gálvez-Martín, G. Rus, J. de Vicente, J.A. Marchal. *Pore geometry influences growth and cell adhesion of infrapatellar mesenchymal stem cells in biofabricated 3D thermoplastic scaffolds useful for cartilage tissue engineering*. **MATERIALS SCIENCE AND ENGINEERING: C. Volume 122, 2021, https://doi.org/10.1016/j.msec.2021.111933**.
6. Antich, C., Jiménez, G., de Vicente, J., López-Ruiz, E., **Chocarro-Wrona, C**., Griñán-Lisón, C., Carrillo, E., Montañez, E., Marchal, J. A. *Development of a Biomimetic Hydrogel Based on Predifferentiated Mesenchymal Stem-Cell-Derived ECM for Cartilage Tissue Engineering*. **ADV. HEALTHCARE MATER. 2021, 10, 2001847. https://doi.org/10.1002/adhm.202001847**

7. Nardecchia, S., **Chocarro-Wrona, C**, Sánchez-Moreno, P., Zambrano-Marín, JR., Marchal, JA. and De Vicente, J. *Living magnetorheological composites: from the synthesis to the in vitro characterization*. 2021. **SMART MATER. STRUCT. 30 065015**
8. **Chocarro-Wrona, C**, López de Andrés, J, Rioboó-Legaspi, P, Antich, C, De Vicente, J, Gálvez-Martín, P, López-Ruiz, E, Marchal, JA. *Design and Evaluation of a Bilayered Dermal/Hypodermal 3D Model Using a Biomimetic Hydrogel Formulation.* **Manuscript under Submission.**
9. **Chocarro-Wrona, C**, Pleguezuelos-Beltrán, P, López de Andrés, J, Antich, C, De Vicente, J, Gálvez-Martín, P, López-Ruiz, E, Marchal, JA. *A bioactive three-layered skin substitute based on ECM components laden with human MSCs, fibroblasts, and keratinocytes effectively promotes skin wound healing and regeneration*. **Manuscript under Submission.**

Parte de los resultados también se han protegido bajo el tratado de cooperación en materia de patente (PCT):

1. Patente: Biomaterial para tratamiento de enfermedades que involucren la reparación o regeneración tisular.
    - País de inscripción: España
    - Inventores/autores/obtentores: Marchal Corrales, Juan Antonio Marchal; Chocarro Wrona, Carlos; López Ruiz, Elena; De Vicente Álvarez-Manzaneda, Juan; Antich Acedo, Cristina; Martínez Moreno, Daniel; Jiménez González, Gema; Perán Quesada, Macarena.
    - Fecha de registro: 16/09/2020
    - C. Autón/Reg. de inscripción: Andalucía
    - Entidad titular de derechos: University of Granada
    - Nº de solicitud: P202030939
2. Patente: Hidrogeles para su uso en ingeniería de tejidos de la piel.
    - País de inscripción: España
    - Inventores/autores/obtentores: Juan Antonio Marchal Corrales, Carlos Chocarro Wrona; Elena López Ruiz; Patricia Gálvez-Martin
    - Fecha de registro: Registrada.

- C. Autón./Reg. de inscripción: Madrid
- Entidad titular de derechos: Universidad de Granada, Bioiberica, Universidad de Jaén.
- Nº de solicitud: P202230432

Estancia Internacional en un centro de investigación

Estancia internacional de 4 meses en el grupo de investigación de 3d.FAB platform, Equipe Génie Enzymatique, Membranes Biomimétiques et Assemblages Supramoléculaires (GEMBAS), Institut de Chimie et Biochimie Moléculaires et Supramoléculaires, Centre national de la recherche scientifique (CNRS), Université Lyon 1, Villeurbanne, LYON. Trabajo dirigido por el Dr. Christophe Marquette (Director de investigación CNRS (Section 28); director adjunto de l'Institut de Chimie et Biochimie Moléculaires et Supramoléculaires (UMR 5246, Université Lyon1-CNRS)).

Financiación

Proyecto: Diseño de biotintas utilizando ácido hialurónico, colágeno y elastina para aplicaciones de Bioimpresión 3D. Análisis de caracterización celular para el desarrollo de cartílago artificial para tratar lesiones osteoarticulares.
Tipo de proyecto: Investigación, desarrollo y transferencia.
Entidad: Universidad de Granada.
Ciudad de la entidad: Granada, Andalucía, España.
Grado de contribución: Investigador.
Fecha de inicio: 01/05/2017.
Duración: 5 meses.

Proyecto: Diseño de biotintas utilizando ácido hialurónico, colágeno y elastina para aplicaciones de Bioimpresión 3D. Análisis de caracterización celular para el desarrollo de cartílago artificial para tratar lesiones osteoarticulares.
Tipo de proyecto: Investigación, desarrollo y transferencia.
Entidad: Universidad de Granada.
Ciudad de la entidad: Granada, Andalucía, España.
Grado de contribución: Investigador.
Fecha de inicio: 15/11/2017.
Duración: 5 meses.

Proyecto: Diseño y evaluación de biotintas utilizadas en Bioimpresión 3D para terapia celular.
Tipo de proyecto: Investigación, desarrollo y transferencia.
Entidad: Universidad de Granada.
Ciudad de la entidad: Granada, Andalucía, España.
Grado de contribución: Investigador.
Fecha de inicio: 15/06/2019.
Duración: 6 meses.

Proyecto: Contrato para apoyo técnico y gestión de I+D – Sistema de Garantía Juvenil.
Tipo de proyecto: Investigación, desarrollo y transferencia.
Entidad: Universidad de Granada.
Ciudad de la entidad: Granada, Andalucía, España.
Grado de contribución: Investigador.
Fecha de inicio: 01/01/2020.
Duración: 2 años.

Ayuda concedida por CONVOCATORIA DE PLAZAS DE **MOVILIDAD INTERNACIONAL DE ESTUDIANTES DE DOCTORADO DE LA UNIVERSIDAD DE GRANADA** en el marco de los programas **PLAN PROPIO DE INTERNACIONALIZACIÓN PROGRAMA 1.2,** Cursos Académicos 2020/2021 y 2021/2022, financiado por el Banco Santander, para la estancia internacional de doctorado.

En la teoría del caos, una rama científica que estudia sistemas complejos y dinámicos no lineales muy sensibles a variaciones en las condiciones iniciales, existe lo que el matemático y meteorólogo estadounidense Edward Norton Lorenz acuñó en 1972 como "*efecto mariposa*". Según este concepto, en determinadas circunstancias de tiempo y condiciones iniciales de un sistema dinámico caótico, cualquier pequeña discrepancia entre dos escenarios con una variación mínima en las condiciones iniciales dará lugar a dos sistemas que en ciertos aspectos evolucionarán de forma completamente distinta. Esto implica que si se produce una pequeña perturbación inicial en un sistema, tras un proceso de amplificación se podrá generar un efecto considerablemente grande a corto o medio plazo. Cris, gracias por haber sido esa mariposa el 10 de Enero de 2016.

Does the flap of a butterfly's wings in Brazil set off a tornado in Texas?

Edward Norton Lorenz (American Association for the Advancement of Science (MIT))

No solo me enseñaste todo lo que aprendí en el máster, también a darlo todo por la ciencia y a hacerlo con pasión. Incluso montamos juntos nuestra primera impresora 3D. Me siento muy afortunado de haber podido hacer la tesis al mismo tiempo que tú, gracias por ser como eres. Siempre has sido mi referencia durante todo este tiempo.

Quiero agradecer de forma especial al Profesor Juan Antonio Marchal por acogerme en su grupo de investigación para realizar el trabajo de fin de máster, y más tarde la tesis doctoral bajo su codirección y tutorización. Gracias por ofrecerme la oportunidad de hacer la tesis con vosotros, haberme entrenado en el mundo de la investigación, y por ser tan cercano como IP y como persona. De igual manera, agradecer a Elena López Ruiz y Patricia Gálvez Martín por ser mis codirectoras de tesis doctoral. Por haberse involucrado en la evolución de mi trabajo, y haber promovido mi participación en congresos y proyectos de investigación. En conjunto, quiero agradecer a mis 3 codirectores/as por haber guiado el desarrollo de mi tesis, así como mi formación como investigador.

Gracias a todas las personas del grupo de investigación CTS963. A Macarena, Mariang, Houria, Esmeralda, estuvisteis presentes en algunas etapas de mi doctorado. Ya fuera por impartirme clase cuando fui alumno de máster, tutorizarme en el TFM, trabajar en proyectos de investigación, o mentorizar TFMs, gracias por contar conmigo. A Gema, Saúl, Carmen, por enseñarnos y aconsejarnos siempre a los predoctorales en diversas técnicas y protocolos de laboratorio. A Julia, por ser siempre tan alegre. Las horas

interminables de procesar muestras de piel no se olvidan, aprendimos a trabajar coordinando 4 manos dejándonos "la piel" y los dedos. A Aitor por su arte para preparar NaOH 10M, y sus frases ("¡Que fantasía!", "Esa gitana está looocaaaa…♫"). A Belén Toledo, aunque solo haya coincidido contigo el último año, el *hype* de *Shingeki no Kyojin* (y *Solo Leveling*, ojo) fue intenso. Belén García, gracias por ser tan *apañá* y cariñosa como eres. Por haberte doctorado con el esfuerzo que le pusiste a la tesis. Aunque no trabajáramos en la misma línea, siempre me has parecido de las personas más trabajadoras y con más coraje del grupo. Gracias también a los demás integrantes del grupo con los que he podido compartir el laboratorio: Mª Eugenia, Yaiza, Jesús Peña, Pablo Graván, Jesús Ruiz (el calvo), Pablo Hernández, Gloria.

A Juan de Vicente, gracias por ser siempre tan profesional y amable. Ha sido un placer trabajar contigo. Siempre te tomaste la molestia de explicarnos las bases físicas de los ensayos que íbamos a hacer. Además, aunque solía pasar tiempo entre las veces que trabajábamos juntos siempre me preguntabas por cómo estaba yo y como estaba mi familia. Stefania, gracias por haber querido contar conmigo para los primeros ensayos celulares de tus estudios del campo electromagnético triaxial en 2019. Me gustó mucho trabajar contigo, y siempre tengo presente las conclusiones de tu tesis sobre cómo el tiempo de esterilización óptimo de polvos de alginato por ultravioleta es de 17 minutos.

Haber podido participar y ayudar en la formación de alumnos de trabajo de fin de máster (TFM) del máster de Investigación Traslacional y Medicina Personalizada, ha sido una experiencia que me ha gustado mucho. No solo porque yo también hice ese máster, también por haber podido participar en su aprendizaje, compartir el laboratorio, y trabajar juntos: Araceli y Alba (2017), Pablo Rioboó y Julia (2018), Marta, Mª José, Javi Rubio y Rafa (2019), Paula y Edu (2020), Elena Contreras y Alazne (2021). Ha sido una experiencia de la que he podido aprender mucho, y que también me ha llenado como predoctoral en los buenos y malos momentos. Gracias.

A las chicas de inmuno, Tatiana, Cristina, Patricia, Mabel, Mª José, gracias por ser unos soles. Aunque no hayamos sido del mismo grupo de investigación siempre habéis intentado ayudar en lo que pudierais, prestándonos lo que nos hiciera falta sonriendo y charlando de cosas de las tesis.

También pude conocer a mucha gente en el CIBM con la que compartí muchos momentos, y de la que podré guardar buenos recuerdos. Marisol, Antonio, Clara, Sergio,

y todos con los que comí durante mucho tiempo en la salita 39.

3d.fab m'as accueilli comme si j'étais du groupe dès le début, et à la fin j'ai fini par l'être hahaha ! La première fois que j'ai rencontré le groupe c'était en septembre 2017, lorsque Léa a publié son papier et je l'ai lu au début de ma thèse. A ce moment j'ai découvert le site web de 3d.fab avec les photos des membres, et maintenant j'en fais partie. Vous ne savais pas à quel point ça me fais illusion. Christophe, j'ai toujours aimé ta façon d'être, tu apportes de la joie et de la sécurité aux personnes avec qui tu travailles. Le tatouage a été trop cool, merci beaucoup ! Emma, je te remercie infiniment de m'avoir donné l'opportunité de débuter ma carrière postdoctorale avec toi. Le jour où tu me l'as offert dans la salle de réunion je ne m'y attendais pas (grâce à ça je pense que j'étais si calme !). Je ne me suis jamais senti aussi valorisé en tant que scientifique, merci beaucoup, vraiment. Hamza, I'll write in English specially for you: if you are reading this it means that I became PhD before you. I just wanted you to know. You were the first colleague at 3d.fab that I started to get to know, and you were so kind to me when I just arrived, thanks man, I really appreciate it. I hope that you'll manage to finish your PhD on time, I'm sure you'll be able to do it.

Alexandre, dès le premier jour où je t'ai rencontré tu râlais. Tu joues avec mes sentiments, ou tu râles ou tu dis des choses gênantes en japonais pendant qu'on travaille au PSM. Céline, c'était marrant parce qu'on est arrivée dans le groupe en même temps, et au début tu avais l'air d'une fille très calme, tu n'avais pas l'air d'être si folle. Je n'oublierai jamais le lait de baleine. Je continuerai d'être ton parasite du PSM. Meigg, on forme une bonne équipe de travail, autant pour faire des stickers que pour faire des manips. Lucie, je n'ai qu'une chose à te dire : Sasageyo. Voilà. Je déconne, merci d'avoir supporté toutes les bêtises que je fais avec les protocoles et les conta. Mehdi, tu me fais peur et rire en même temps, entre les massages, la danse de la banane, et me souhaiter la mort. Laura, j'ai toujours craint ta technique de Krav Maga, surtout pour comment tu fonce sur les gens dans les couloirs. Lucas, tu es un gars très poli et gentil, merci de m'avoir bien traité dès le premier jour. Arthur, je ne te vois pas beaucoup parce que tu te caches toujours avec ta poudre, mais tu es cool. Sarah, on va défendre la thèse presque en même temps, courage!

Et je ne pouvais pas oublier les biochimistes. Nicolas, bien qu'au début tu me donnés peur, finalement il s'avère que tu es un type bien, je suis grave surpris. Vraiment, les choses stupides que nous faisons dans nos bureaux sont les meilleures. Merci de m'avoir appris des mots français (margoulin) et de checker les kilomètres avec moi.

Quand tu as mis mon nom sur la porte à l'automne, ça m'a fait très plaisir, merci mec ! Numa, grâce à toi je n'oublierai jamais comment pipeter un Bradford ou préparer un tampon. Mon Dieu, 5 ans de thèse et quel mauvais moment j'ai eu en étant ton stagiaire ! Je plaisante, merci au deux de m'avoir aidé avec tout et d'être des si bonnes personnes. Et je ne pouvais pas oublier Bea, depuis que je suis arrivée, tu m'as toujours salué en espagnol, *gracias* d'être si gentille !

Quiero también dar las gracias a Ana Santos, Mohamed Tassi, Isabel Sánchez-Almazo, del Centro de Instrumentación Científica (Universidad de Granada), por su excelente trabajo, gran conocimiento e implicación que han demostrado todas las veces que he tenido oportunidad de trabajar con ellos. También, quiero agradecer a José Manuel Entrena del Instituto de Neurociencia y la Unidad de Investigación de Comportamiento Animal (Universidad de Granada) por su gran destreza trabajando con animales de experimentación, y por ser un grandísimo apoyo e implicación en los ensayos *in vivo* realizados en mi tesis doctoral.

Gracias Dani. Hicimos juntos el máster, un trabajo de revisión durante el máster (madre mía, que suplicio…), y empezamos la tesis también juntos en el mismo grupo. Desde entonces, nunca he olvidado que la primera vez que Cris y yo te dejamos solo tiraste a la lejía las muestras de grasa. Y nunca lo haré. Dejando de lado las bromas, siempre hemos podido desahogarnos juntos de las injusticias y de los problemas que compartíamos, siendo la persona más honesta y sincera del laboratorio (y no lo digo solo porque criticaras pelo). Eres de las pocas personas que se dio cuenta cuando estaba pasando por malos momentos, o de los pocos a los que les importó y que hicieron algo por animarme. No creas que no me di cuenta. A pesar de que tus chistes sean una mierda (aunque siempre me ha gustado la forma en que los cuentas).

Paula, si no fuera por ti habría estado solo los últimos meses de la tesis que pasé en Granada, no sé ni cómo habría sido capaz de sacar adelante el *in vivo* (vaya risas nos echamos durante esas más de 100 horas; sigo pensando que la sonda de pH solo me respondía a mi), y además, me apoyaste mucho durante la estancia. De los TFMs que he tenido a cargo durante los 5 años de mi tesis has sido la más capaz, la que más ha demostrado valerse por sí misma, y la que menos le ha tenido miedo sacrificarse por intentar hacer buenos experimentos. Me deja tranquilo saber que estás metiendo la cabeza en el mundo de la ciencia, se te da muy bien, y me alegra que sigas ese camino. Dale duro a la Ender, espero haberte dado un hilo del que tirar. Sabía que le ibas a dar utilidad, por

algo aprendiste tan rápido a imprimir. Me alegra que al final te hayas puesto a correr también, aunque me hayas puesto el nombre que me has puesto en tu teléfono (terrible…). Mucho ánimo con lo que te queda por delante, sé que podrás hacerlo por muy fea que se ponga la cosa.

Shih Wei, bien que tu sois entrée dans ma vie dans la dernière étape de ma thèse, tu es l'une des personnes les plus importantes pour moi. C'est la première fois de ma vie que j'ai une relation dans laquelle je ne ressens pas qu'il y a un déséquilibre, dans laquelle je sens une vraie réciprocité. Non seulement tu m'as donné de la force pour terminer la thèse, mais aussi pour commencer le postdoc avec plus d'enthousiasme. J'ai l'impression que si je suis venu à Lyon ce n'était pas seulement pour mon séjour et plus tard mon postdoc, c'était aussi pour te rencontrer. Merci beaucoup d'être venu avec moi pour m'accompagner et voir ma soutenance, tu ne te fais pas une idée de ce que cela signifie pour moi. Merci d'être entrée dans ma vie, tu me rends heureux à tous les niveaux. Je t'aime ❤

This part of my life... this little part... is called "Happiness"

The Pursuit Of Happyness

En último lugar, y más importante, a mi familia: Papá, Mamá, Mari Cruz, Izaro, Adri. Siempre habéis estado allí, tanto si os necesitaba como si no. Sois en quienes pienso cuando la gente me pregunta de dónde soy. Sois los que siempre me habéis ayudado cuando he estado en problemas. Sois los únicos que conocéis todo por lo que he pasado para llegar hasta aquí. En muchas ocasiones sentí ganas de dejarlo todo. En todas ellas lo último que me acababa deteniendo siempre era pensar en vosotros. Llevo años pensando en lo que iba a escribiros en los agradecimientos de mi tesis doctoral, pero lo primero que me ha venido a la cabeza al empezar ha sido las ganas de disculparme. Siento haber pasado tan poco tiempo con vosotros todos estos años; incluso en ocasiones haber pasado trabajando ese poco tiempo que podía dedicaros cada año; o no haber contestado siempre a las llamadas y los mensajes. Gracias por haber sido siempre tan comprensivos conmigo en este aspecto, y por entenderlo. Lo valoro más de lo que aparenta.

Me hacía especial ilusión defender la tesis en Mayo de 2022, siempre me han gustado cuidar los detalles, y creo que es una fecha perfecta en mi caso. Al final tuvo que ser un poco más tarde, pero no importa, no es tan lejos de esa fecha. Después de 15 años, bachillerato, selectividad, el grado, el máster, y ahora el doctorado (se dice pronto, jajaja),

sé que valió la pena seguir adelante. Ahora mismo estoy escribiendo esto desde la cama de mi estudio en Lyon, por la tarde, y soy feliz. Gracias por hacerme seguir adelante. Hoy no sería la persona que soy sin vosotros, y ahora mismo, por cómo soy, cómo estoy, dónde estoy, y con quien estoy, soy la persona más feliz del mundo.

PART ONE: THE CAVE AND THE FIRE

"SOCRATES: From the beginning, […] the prisoners have never been able to see anything except the shadows that are projected on the wall in front of them by the glow of the fire. […] In short, the chained prisoners would think that the only shadows cast by the things behind them are *real and true* – the shadows and nothing else."

PART TWO: THREE STAGES OF LIBERATION

FREEDOM (STAGE ONE): *A failed attempt within the cave*

"SOCRATES: […] Imagine someone pointing to one of the things being carried along […], asking the prisoner […] and forcing him to answer. The prisoner would probably be completely confused and would think the shadows he saw earlier were much clearer than what's being pointed out now."

FREEDOM (STAGE TWO): *The journey upward, and the sight of real things*

"SOCRATES: The prisoner who is being dragged up there will feel both pain and rage during the ascent. […] Later, he'll be able to look at the things themselves. […]."

FREEDOM (STAGE THREE): *Looking directly at the sun*

"SOCRATES: Do you think this prisoner, now that he is out of the cave, will envy the ones who are still down there? I can't imagine he'd want to compete with those who are held in high esteem in the cave or have the most power. I think the freed prisoner will instead prefer (as Homer says) "to live on the land [above ground] as the lowest paid servant of the poorest dirt farmer." I imagine the freed prisoner would put up with absolutely anything rather than be associated with the opinions that dominate in the cave. He'll do anything rather than be that kind of person, don't you think?"

PART THREE: THE PRISONER RETURNS TO THE CAVE

"SOCRATES: Imagine that the former prisoner has to go back to arguing with those who remained behind, that he has to get involved in the back-and-forth of making claims about the shadows and defending his opinions. […] And if they can get hold of that [bothersome] former prisoner as he is trying to free them from their chains and lead them out of the cave, and if they have the power, they certainly will kill him."

PLATO'S "ALLEGORY OF THE CAVE"

from The Republic, Book VII, 514a, 2 to 517a, 7

Translation by Thomas Sheehan, Stanford University

INDEX

ABSTRACT

Regenerative engineering (RE) is an interdisciplinary amalgam of technological fields that combine tissue engineering, material science, stem cell biology, developmental biology, and clinical translation to manufacture complex artificial tissues.

Tissue engineering (TE) has been described as the emerging fields of knowledge whose objective is to create artificial tissues and/or organs designed for mimicking their native form. Regenerative engineering combines cells, biomaterials, and biologically active molecules with proper manufacturing platforms to produce complex tissues. The main objective is to create functional constructs that can replace, preserve, or improve damaged tissues or organs. Artificial cartilage and skin substitutes are examples of devices that have been approved by the Food and Drug Administration (FDA), however, their use in humans is currently limited. Although TE manufacture strategies led to the first generations of engineered tissues, such processes usually consume time and are restricted to having mainly flat and pre-determined geometries. Furthermore, they also exhibit high manufacture costs, as well as human factors regarding surgeons and patients that may influence the success of the implantation.

In the last decades, advances in biofabrication have shown promising innovations in the manufacturing of complex scaffolds with biomechanical and structural characteristics like those found at the extracellular matrix (ECM). One of the most used biofabrication technology is 3D bioprinting. Its applications range from device prototyping, surgical planning, and personalized splints, towards 3D bioprinting of engineered tissues for drug testing/screening, regenerative medicine, and disease modelling, among others. 3D bioprinting is based on the combination of computer-aided design (CAD) and computer-aided manufacturing (CAM), which in the layer-by-layer fabrication nature of 3D printing, allows producing structures with different geometries, shapes and patterns while controlling the spatial distribution of the building blocks: cells, biomaterials, and growth factors. Also, 3D bioprinting brings advantages to the biomedical field such as shorter fabrication times, tailored production, and higher precision than conventional TE.

Several synthetic biomaterials have been developed to biofabricate bioinks to manufacture 3D bioprinted scaffolds as artificial tissues or organs. However, these biomaterials do not accurately reproduce the native tissue mechanical characteristics. Therefore, significant efforts are being made for manufacturing flexible constructs which

could bear with mechanical loads such as ligaments, tendons, cartilage, blood vessels, skin, or muscles. Similarly, despite quite a few progresses have been made in the development of bioinks and fabrication strategies for skin bioprinting, more biological mimicry regarding the design and molecular composition should be ameliorated in biomimetic skin bioprinting.

The first objective of this doctoral thesis was to validate the potential use of 1,4-Butanediol Thermoplastic Polyurethane (b-TPUe) elastomeric filament as a new 3D printing material for biomedical purposes. The analysis of its mechanical properties demonstrated that b-TPUe scaffolds had a much closer mechanical behaviour to native cartilage than other 3D bioprinting synthetic biomaterials. As well, b-TPUe printed scaffolds were also able to maintain proper human mesenchymal stem cells (hMSCs) proliferative potential, viability, and support chondrogenesis. Moreover, *in vivo* studies in immunocompetent mice demonstrated that b-TPUe printed scaffolds were firmly anchored and integrated within the subcutaneous tissue and no sign of oedema or macroscopic inflammation was detected. Also, in immunodeficient mice implanted 3D bioprinted cell-laden scaffolds showed good integration at the surrounding tissue 3 weeks post-implantation. Altogether, these results validated the biocompatibility of b-TPUe and suggest that this material could be exploited for 3D bioprinting of biomimetic tissues, such as cartilage, with tailorable mechanical properties.

The second objective was to develop skin layer-specific biomimetic bioinks for the design of a three-layered skin substitute. Different biomaterials and skin ECM-related biomolecules were screened and evaluated for the formulation of each bioink. The optimal composition for the biofabrication of an early dermo-hypodermal bi-layered hydrogel was achieved, combining them with hMSCs and human dermal fibroblasts (hDFs) in an attempt for reproducing the skin composition. At this stage, the developed bioinks already showed desirable physicochemical characteristics. As well, the hydrogels casted with these bioinks not only presented similar mechanical properties compared to human skin, but also showed good cytocompatibility. Furthermore, the bi-layered hydrogel was then upgraded by the addition of a third epidermal layer, with the subsequent seeding of human epidermal keratinocytes (hEKs), obtaining a bio-fabricated three-layered (BT) skin hydrogel. This construct did not only present good swelling and degradation behaviours, and mechanical properties comparable to those found in native skin, but also demonstrated to maintain good cell proliferation, viability, and showed

good results in the wound healing assay. Finally, the *in vivo* assay indicated that applying the BT Skin on wound healing mice models produced similar homeostatic and histological outcomes than the gold standard (autografting). Taken together, these results suggest that the BT Skin hydrogel could be suitable as a 3D bioprintable skin substitute for clinical application.

Summarizing, this doctoral thesis offers robust and extensive studies in which b-TPUe was validated for 3D bioprinting applications. Also, the design and biofabrication of a BT skin substitute are presented, demonstrating its biological and mechanical properties *in vitro* and *in vivo*, encouraging its future clinical application in RE of skin injuries.

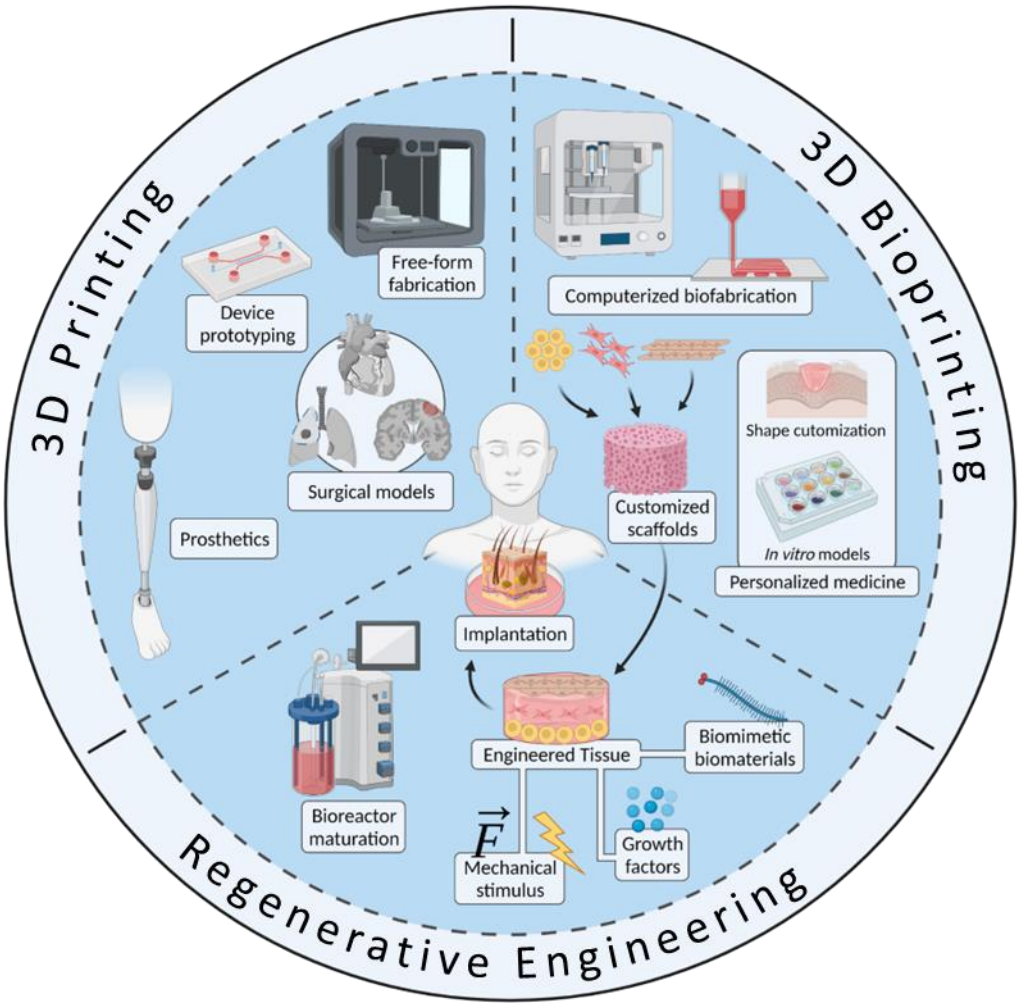

RESUMEN

La ingeniería regenerativa (IR) es una amalgama interdisciplinaria de campos tecnológicos que combinan ingeniería de tejidos, ciencia de materiales, investigación de células madre, biología del desarrollo y traslación clínica para fabricar tejidos artificiales complejos.

La ingeniería de tejidos (IT) ha sido descrita como los campos de conocimiento emergentes cuyo objetivo es crear tejidos y/u órganos artificiales diseñados para imitar su forma nativa. La ingeniería regenerativa combina células, materiales y moléculas biológicamente activas con plataformas de fabricación adecuadas para producir tejidos complejos. El objetivo principal es crear construcciones funcionales que puedan reemplazar, preservar o mejorar tejidos u órganos dañados. Los sustitutos de cartílago y piel son ejemplos de dispositivos que han sido aprobados por la *Food and Drug Administration* (FDA), sin embargo, su uso en humanos actualmente es limitado. Aunque las estrategias de fabricación de IT condujeron a las primeras generaciones de tejidos de ingeniería, dichos procesos suelen consumir tiempo y se limitan a tener geometrías principalmente planas y predeterminadas. Además, también presentan altos costes de fabricación, así como factores humanos de cirujanos y pacientes que pueden influir en el éxito de la implantación.

En las últimas décadas, los avances en biofabricación han mostrado innovaciones prometedoras en la fabricación de andamios complejos con características biomecánicas y estructurales como las que se encuentran en la matriz extracelular (ECM). Una de las tecnologías de biofabricación más utilizadas es la bioimpresión 3D. Sus aplicaciones van desde la creación de prototipos de dispositivos, la planificación quirúrgica y las férulas personalizadas, hasta la bioimpresión 3D de tejidos diseñados para pruebas/detección de fármacos, medicina regenerativa y modelado de enfermedades, entre otras. La bioimpresión 3D se basa en la combinación de diseño asistido por computadora (CAD) y fabricación asistida por computadora (CAM), que en la naturaleza de fabricación capa-por-capa de la impresión 3D, permite producir estructuras con diferentes geometrías, formas y patrones mientras controla la distribución espacial de los componentes básicos: células, biomateriales y factores de crecimiento. Además, la bioimpresión 3D aporta ventajas al campo biomédico, como tiempos de fabricación más cortos, producción a medida y mayor precisión que la IT convencional.

Se han desarrollado diversos materiales sintéticos para biofabricar biotintas para

generar andamios bioimpresos en 3D como tejidos u órganos artificiales. Sin embargo, estos materiales no reproducen con precisión las características mecánicas del tejido nativo. Por lo tanto, se están realizando esfuerzos significativos para fabricar construcciones flexibles que puedan soportar cargas mecánicas tales como ligamentos, tendones, cartílagos, vasos sanguíneos, piel o músculos. Del mismo modo, a pesar de que se han logrado bastantes avances en el desarrollo de biotintas y estrategias de fabricación para la bioimpresión de la piel, se debe mejorar más el mimetismo biológico con respecto al diseño y la composición molecular en la bioimpresión biomimética de la piel.

El primer objetivo de esta tesis doctoral fue validar el uso potencial del filamento elastomérico de poliuretano termoplástico de 1,4-butanodiol (b-TPUe) como un nuevo material de impresión 3D para fines biomédicos. El análisis de sus propiedades mecánicas demostró que los andamios de b-TPUe tenían un comportamiento mecánico mucho más cercano al cartílago nativo que otros materiales sintéticos de bioimpresión 3D. Además, los andamios impresos con b-TPUe también pudieron mantener el potencial proliferativo, la viabilidad y mantener la condrogénesis de las células madre mesenquimales humanas (hMSC). Además, los estudios *in vivo* en ratones inmunocompetentes demostraron que los andamios impresos de b-TPUe estaban firmemente anclados e integrados dentro del tejido subcutáneo y no se detectaron signos de edema o inflamación macroscópica. Además, en ratones inmunodeficientes implantados con andamios cargados de células bioimpresas en 3D mostraron una buena integración en el tejido circundante 3 semanas después de la implantación. En conjunto, estos resultados validaron la biocompatibilidad del b-TPUe y sugieren que este material podría explotarse para la bioimpresión 3D de tejidos biomiméticos, como el cartílago, con propiedades mecánicas adaptables.

El segundo objetivo era desarrollar biotintas biomiméticas específicas para cada capa de piel, con el fin de diseñar un sustituto de piel de tres capas. Se seleccionaron y evaluaron diferentes biomateriales y biomoléculas relacionadas con ECM de la piel para la formulación de cada biotinta. Se logró la composición óptima para la biofabricación de un hidrogel bicapa dermo-hipodérmico temprano, combinándolos con hMSC y fibroblastos dérmicos humanos (hDF) en un intento por reproducir la composición de la piel. En esta etapa, los biotintas desarrollados ya mostraban características fisicoquímicas deseables. Además, los hidrogeles moldeados con estos biotintas no solo presentaron propiedades mecánicas similares a las de la piel humana, sino que también mostraron una buena citocompatibilidad. Además, el hidrogel de dos capas se mejoró mediante la

adición de una tercera capa epidérmica, con la posterior siembra de queratinocitos epidérmicos humanos (hEK), obteniendo un hidrogel de piel de tres capas biofabricado (BT). Esta construcción no solo presentó buenos comportamientos de hinchazón y degradación, y propiedades mecánicas comparables a las encontradas en la piel nativa, sino que también demostró mantener una buena proliferación celular, viabilidad, y buenos resultados en el ensayo de cicatrización de heridas. Finalmente, el ensayo *in vivo* indicó que la aplicación de BT Skin en modelos de ratones con cicatrización de heridas produjo resultados homeostáticos e histológicos similares a los del *gold standard* (autoinjerto) utilizado en clínica. En conjunto, estos resultados sugieren que el hidrogel BT podría ser adecuado como sustituto de la piel bioimprimible en 3D para aplicaciones clínicas.

En resumen, esta tesis doctoral ofrece estudios sólidos y extensos en los que se validó b-TPUe para aplicaciones de bioimpresión 3D. Asimismo, se presenta el diseño y biofabricación de un sustituto de piel trilaminar, demostrando sus propiedades biológicas y mecánicas *in vitro* e *in vivo*, alentando su futura aplicación clínica en IR de lesiones cutáneas.

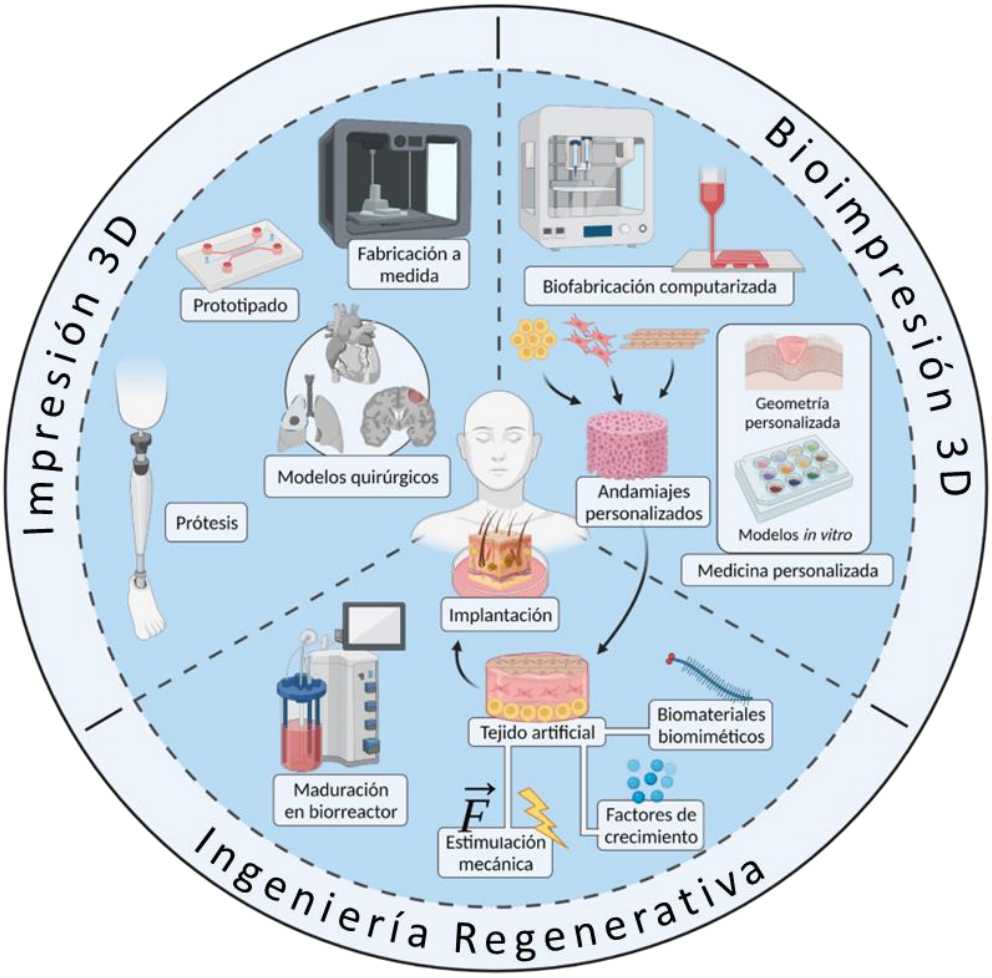

1. INTRODUCTION

1. INTRODUCTION

1.1. Regenerative engineering

Over the last half century, tissue and organ transplantation has made a paradigm change regarding our capacities to manage their medical care. The rapid progress of medicine, from post-mastectomy breast reconstruction to whole organ transplantation, and lately, allotransplantation of composite tissues, has allowed a broad spectrum of surgical procedures for tissue healing. However, these approaches still require autologous tissue transplantations, that frequently produce substantial donor site morbidity, or in the case of allogenic transplantation with a compatible donor it is required an immunosuppression treatment for the patient during the rest of his/her life (1). Altogether, the need to develop engineered tissues and organs is highlighted in all surgical specialities (2).

Tissue engineering (TE) has been described as the interdisciplinary field that gathers the researches aimed at creating of artificial tissues designed for mimicking native tissues (3–5). Regenerative engineering (RE) recently emerges as the amalgamation of TE combined with interdisciplinary fields such as material sciences, stem cell science, biophysics, developmental biology, and clinical translation (6) (**Figure 1**).

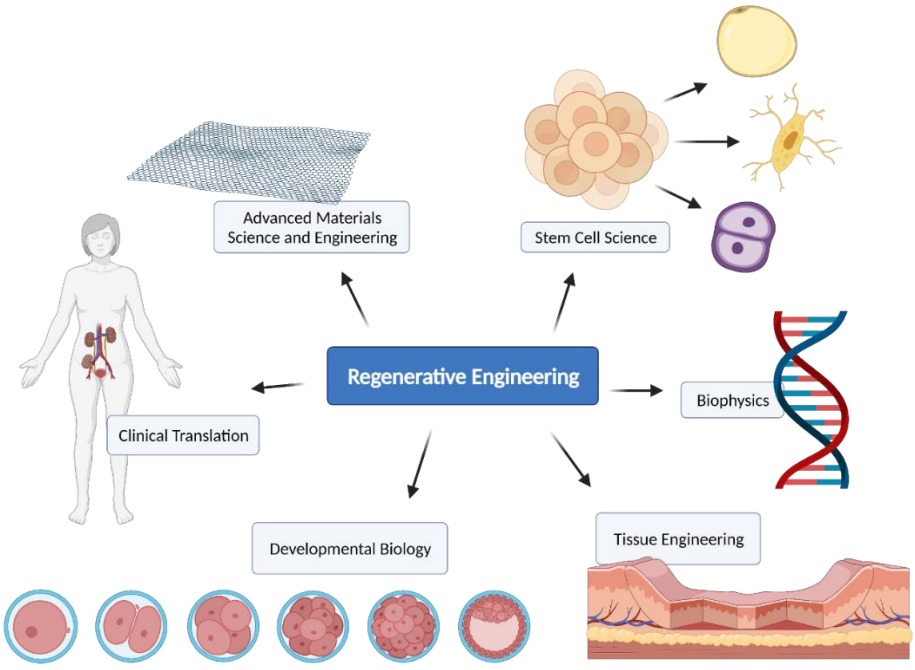

Figure 1. Regenerative engineering disciplines.

Combining cells, biomaterials, and bioactive molecules together with specific biofabrication techniques, RE is gradually evolving the development of optimized artificial tissues.

1.1.1. Biofabrication techniques

There are a broad range of biofabrication methods that are included in the RE field; some of the most remarkable techniques include decellularization, organoids, microfluidics, electrospinning, and 3D bioprinting. Each of those technologies presents advantages and disadvantages for their clinical application or their scaling-up possibilities.

1.1.1.1. Decellularization

The decellularization is a method that maintains a native microenvironment through depleting the cellular fraction of biological tissues, leaving behind only the ECM. Detergents are employed in this method for breaking down the cellular and nuclear elements, keeping the microarchitecture, proteins and growth factors, obtaining a scaffold with its inherent characteristic biomaterials (7). As a natural-based scaffold with tissue-specific cues, decellularized scaffolds even serve by itself as a biocompatible platform for living cells to proliferate and differentiate (8,9). This method can be applied to simple cell layers as well as whole organs, to obtain different levels of scaffold complexity (10). The decellularization process can be split in three stages: washing, rinsing, and sterilizing (11,12). First, a washing compound, either a denaturing agent, an enzyme, or a detergent is applied to the tissue sample to deplete the cellular fraction (13). Then, the sample is rinsed to remove the detergent residues due to its cytotoxicity, obtaining a clean decellularized extracellular matrix (dECM) (14).

Finally, the sample is sterilized at the sterilization stage to avoid cross-contamination from the host, or the fabrication protocol and to prevent an immune response from antigenic residues (15). Tissue-derived dECM can be re-cellularized *in vitro* or *in vivo*. Although the decellularization of tissues allows obtaining products with ideal ECM composition and low immunogenicity, the need of donors presents a main disadvantage on its application to the transplantation surgery field. Compared to tissue-derived dECM, cell-derived dECM not only offers functional matrices, which contain a highly complex blend of macromolecules, but hold the advantage of large-scale production, as well as outstanding biocompatibility and bioactive properties (16,17).

1.1.1.2. Organoids

Organoids can be defined as small aggregates of stem or differentiated cells that can self-organize into 3D spheroids, without the need of external biomaterials, and reproduce human tissue's structure and physiological function (18–20). Thus, this technology offers a great potential for personalized medicine strategies. As in all *in vitro* models, organoids provide a platform that mimics tissue regeneration in a controlled environment. Though, organoids outstand from other *in vitro* models in their ability to reproduce human organs physiologically and histologically (21–27). This special capacity arises from the stem cells ability to interact with cells in their native environment and produce their own ECM (20). Organoids represent small human tissue replicas whose value quickly increased given their applicability as disease progression and drug testing models (20). Nevertheless, they present the disadvantage of having a limited scaling-up. The development of systems with automated scalable organoid production and characterization may help to transform the organoid models into high-throughput platforms suitable for drug screening (20)

1.1.1.3. Microfluidics

Microfluidic devices have emerged as robust tools that offer the ability to produce monodisperse microgels at a high throughput rate (28,29). Microgels can be defined as 3D crosslinked particles which provide porous polymeric microenvironments for embedding cells, mimicking the native conditions of nutrient and metabolic waste diffusion (30–32). In microfluidics, microgels are generated in devices that create droplets of the desired polymers through water/oil emulsions, followed by chemical or physical crosslinking. The most commonly microfluidic devices use geometries like T-junctions, co-flowing, or flow-focusing laminar streams to produce the droplets (33–35). One of the bigger interests on microgels is their applicability as microcarriers, since their high surface/volume ratio promotes cell-matrix interactions and efficient mass transport (36). This technology allows a tight control on the components and flow rates in the microfluidic device channels, enabling to finely tune the particle's chemical composition and properties, proving to be a versatile biofabrication technique, in which different crosslinking approaches can be applied (33). In fact, microfluidics has recently been combined to bioprinting, complementing each other to generate functional engineered tissues and organs. Specifically, microfluidics can assist 3D bioprinting by regulating precise structures on micro- and nanoscale (37). Depending on how those two domains

interact, the generation of 3D tissues and organs by the synergistic combination of bioprinting and microfluidics can be divided into: printing nozzles modified by microfluidic devices; bioprinting into the microfluidic device; bioprinting of constructs with microchannels inside of them (37).

1.1.1.4. Electrospinning

Electrospinning is a 3D printing technology that creates micrometric to nanometric fibre scaffolds with different polymers that can be from synthetic or natural sources (38–41). The standard electrospinning set up presents a high voltage source, a pump to feed the material, a nozzle tip, and a grounded collector. Once the electric field between the nozzle and the collector generates electrostatic forces that are higher than the surface tension of the polymer at the nozzle tip, the material is jetted towards the collector plate, forming a mat with chaotically organised nanofibers (41,42). Specially, electrospinning has been highly studied in the biomedical field, since its scaffold small fibre scale, high porosity and surface area create intricate structures that can replicate the natural ECM microenvironment, promoting cell adherence, proliferation, and differentiation (43–46). However, this technology shows some shortcomings, such as the lack of control of the fibre organization, poor cell infiltration and distribution. An example of overcoming these limitations is the combination of two techniques: inkjet bioprinting together with melt electrowriting (MEW) (47). The MEW technique, which uses voltage-stabilized jets to accurately deposit micrometric fibres in pre-defined positions in a 3D space (48), is a promising stabilized form of the electrospinning technology.

1.1.1.5. 3D Bioprinting

3D Bioprinting can be defined as the production of biomedical elements that highly mimic natural tissue or organ characteristics using rapid prototyping mechanisms for bioprinting bioinks formulated from cells, biomaterials, and growth factors in a layer-by-layer approach (49,50). These technologies evolved as a derived application of additive manufacturing (AM) (51,52). AM generates complex 3D structures by the addition of biocompatible biomaterials with an automated, computer-aided design (CAD) and computer-aided manufacturing (CAM) technology. Regarding the different bioprinting strategies, 3D bioprinting technologies can be broadly classified into: Extrusion-Based Bioprinting (EBB), Droplet-Based Bioprinting (DBB), and

Stereolithography apparatus (SLA) (**Figure 2**) (53).

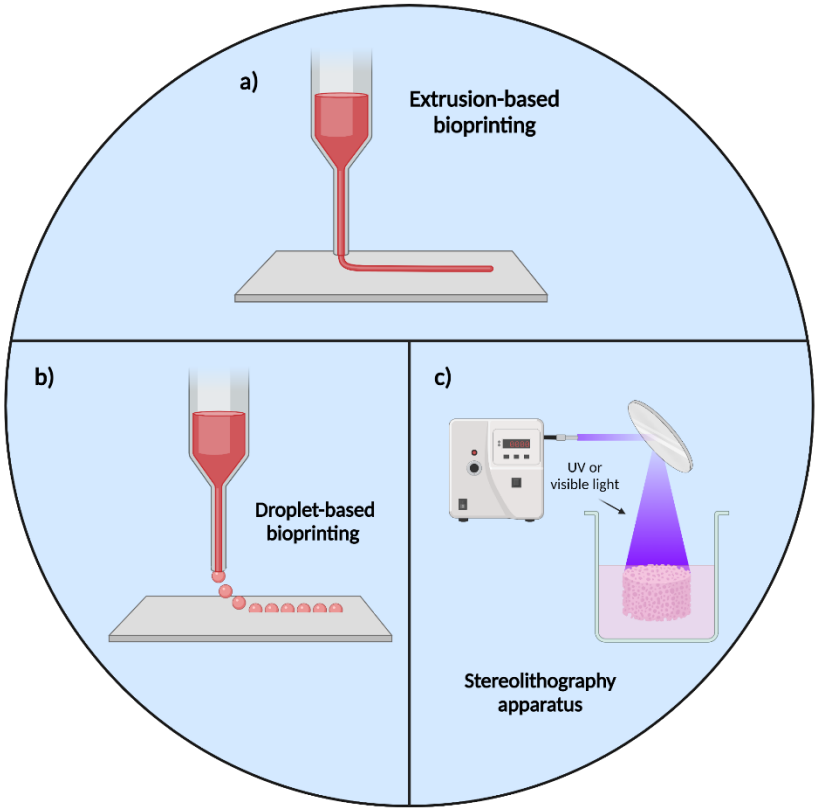

Figure 2. 3D bioprinting technologies: (a) Extrusion-based bioprinting, (b) Droplet-based bioprinting, and (c) Stereolithography apparatus.

1.1.1.5.1. Bioinks

Bioinks can be defined as biomaterials that can both be 3D printed and used as carriers for cells and bioactive compounds (54). The bioink microenvironment provides physical support and maintains the cell activity during the bioprinting process. Thus, an optimal bioink should have the following characteristics: a) the ability of supporting and promoting cell adhesion, proliferation, migration, and differentiation, b) biocompatibility, c) printability, d) mechanical stability, e) moderate degradability, and f) biologically mimic the extracellular microenvironment of the *in vivo* skin tissue (**Figure 3**) (55,56).

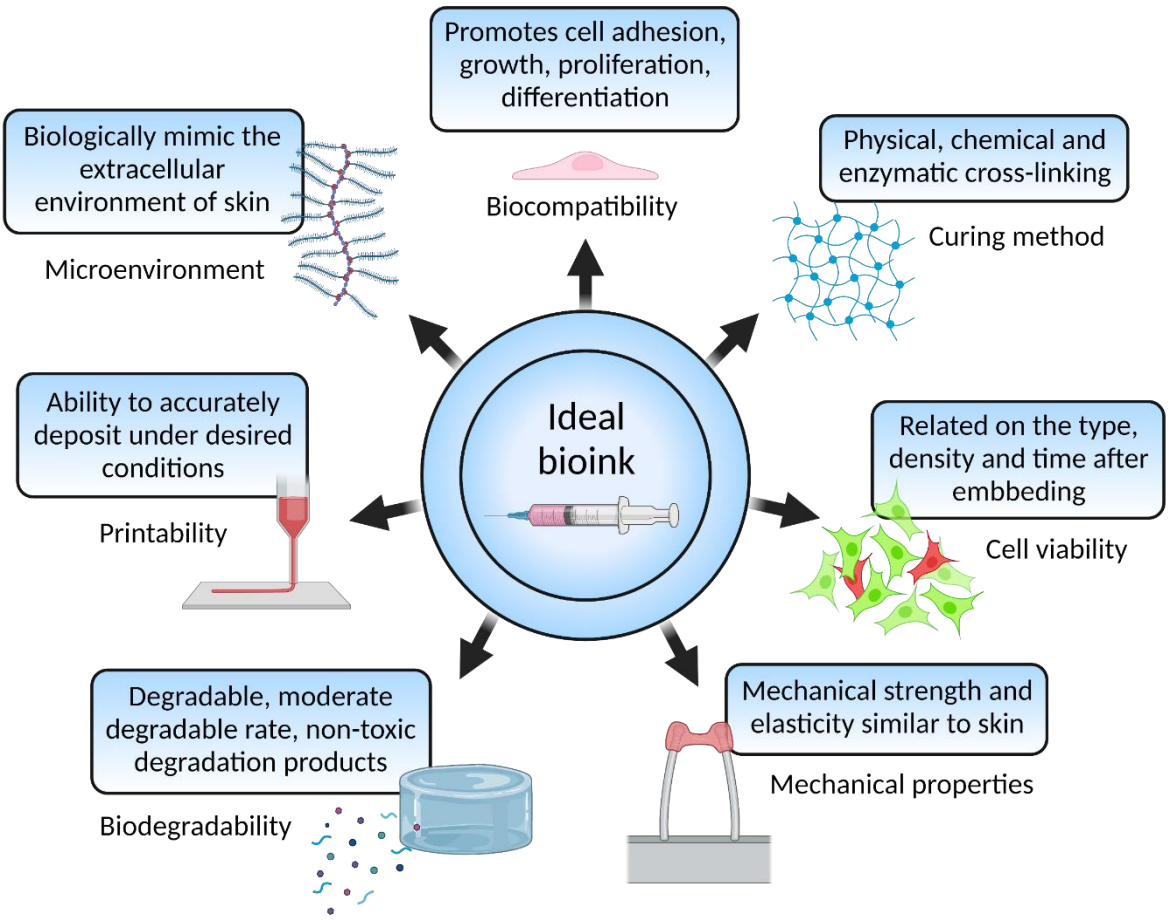

Figure 3. Ideal bioink properties.

1.1.1.5.2. Bioprinting technologies

Extrusion-based bioprinting (EBB)

The EBB method reaches highly controllable fluid distribution through an automated system (57). The cell-loaded bioink is extruded through a nozzle in a continuous filament using a piston, screw, or pneumatic-driven approaches. Once printed layer-by-layer, a full 3D object is obtained (58). The best performing bioinks for pneumatic-based bioprinting are hydrogels with shear thinning characteristics since they can maintain the filament shape once extruded. Structures created using screw-driven bioprinting can be printed using high-viscosity bioinks, thus obtaining more stable bioprinted constructs (59). Cutting-edge extrusion bioprinters are supplied with various print-heads, reducing cross-contaminations while allowing the simultaneous print of different bioinks (60). As well, EBB achieves a better control over parameters such as shape, cell-distribution, and porosity in the printed object. In comparison to the other

bioprinting approaches, EBB overcome DBB by having a faster bioprinting speed, being able to print a bigger range of bioinks, and obtaining printed constructs with better mechanical strength. Distinctively, EBB can create porous grid structures, thus promoting nutrient and metabolite diffusion. This kind of bioprinting technique is highly versatile, and an ideal approach to fabricate TE scaffolds or prosthetic devices (54). However, the major drawback of EBB is its low resolution, which lower limit usually exceeds 100 µm (60,61).

Droplet-based bioprinting (DBB)

DBB gathers Electrohydrodynamic Jetting Bioprinting (EHDJB), Inkjet Bioprinting (IJB), and Laser-Assisted Bioprinting (LAB). EHDJB employs an electric field to expel bioink droplets through an outlet, ejecting them onto the print surface (62). This characteristic enables EHDJB as a suitable technique for bioprinting bioinks with high volume weight (up to 20%) (63). IJB can be split into Continuous Inject bioprinting (CIJB) and Drop-On-Demand Bioprinting (DODB). Concisely, CIJB is based on the intrinsic predilection of a liquid to constantly disperse bioink droplets with connectivity. On the other hand, DODB creates droplets of ink over the bioprinting surface at demand. Although CIJB is able to expel droplets at a faster rate, DODB is more suited for material patterning since it shows a high deposition precision with minimal bioink waste production (64). As well, DODB is able to use thermal, electrostatic, or piezoelectric actuators to produce droplets, which offers the possibility to print different kind of biomaterials to manufacture heterogenous tissue-like structures (65). However, DODB presents some drawbacks, for instance, a particularly small ink-jet aperture (10 – 150 µm), which easily produces clogging, restricting this technique to only use low viscosity biomaterials (66); or the lack of porosity of the generated artificial tissues, limiting its clinical application due to its deficiency of tissue perfusion and substance exchange.

The LAB technology works as follows: a laser light is emitted from a pulsed laser source, focusing the laser light on a metal film on the backside of a silicate glass, rapidly evaporating the bioink that is deposited beneath the location of the heat, spraying liquid drops onto the substrate (67–69). LAB system prints using a nanosecond-driven laser with ultraviolet (UV)/near-UV wavelengths as an energy source, reaching a picogram level bioprinting resolution (70). It is also nozzle-free, and performs non-contact prints, being able to bioprint cells maintaining high resolution and viability. Nevertheless, it does not

have an adequate fast crosslinking mechanism, which restricts LAB to reaching high throughput (71–73).

Stereolithography apparatus (SLA)

The SLA method is a type of bioprinting that generates photopolymerization under a specific light to obtain solidified photopolymeric forms (74), holding the advantage of running with a fast bioprinting speed while maintaining a high resolution (≈ 1 μm). SLA is often used when high-precision shapes are needed to be printed, as well as high resolution tissues or scaffolds with intricated porous structures (75). It can achieve high cell viability rates (> 85%) without the need of using shear thinning biomaterials, however, it shows the drawback of having to use transparent liquids, otherwise, the light would not be able to uniformly pass through the material, obtaining a heterogenous crosslinking. Typically, some examples of biomaterials used in this kind of bioprinting technology are, for instance, poly(ethylene glycol) diacrylate (PEGDA), gelatine methacrylate (GelMA), or methacrylated hyaluronic acid (MeHA) (76). This drawback limits to maintain bioprinting cell densities under 10^8 cells/ml (77).

In summary, 3D bioprinting shows the advantages of allowing the controllable spatial deposition of multi-cell bioinks in a wide range of different cell densities, becoming the ideal method for generating *in vitro* 3D living biological structures. Then, the bioprinting results of the different 3D bioprinting systems rely on several parameters, such as gelation time of the bioprinting biomaterial, density, and viability of cells, bioprinting temperature, viscosity of the bioink, and bioprinting equipment. The comparison of the main parameters of the common bioprinting technologies are shown in **Tables 1 and 2**.

1.1.1.5.3. Bioinks for bioprinting

1.1.1.5.3.1 Bioink characteristics: biocompatibility, biodegradability, bioactivity, and printability

The biocompatibility of the material is an essential requirement to avoid adverse effects in the defect site and promote regeneration. Clearly, bioprinted constructs must not elicit any adverse, immunogenic, nor carcinogenic reaction, as any inflammatory or foreign body reaction to the implanted construct could eventually lead to the failure of the tissue restoration. On the other hand, to promote tissue repair, the biomaterials that

compose the bioink must also maintain cell viability throughout the 3D bioprinting process, as well as support further cell proliferation and adhesion.

Table 1. Main parameters of common bioprinting technologies

3D Bioprinting technologies	Print speed	Resolution (μm)	Viscosity of bioink (MPa s)	Cell concentration	Cell viability	References
Extrusion-based bioprinting	Slow	100-200	30^{-6}·10^{7}	High	80% - 90%	78
Droplet-based bioprinting						
Thermal inkjet bioprinting	Fast	30-60	-	-	70% - 90%	65
Electrostatic inkjet bioprinting	Fast	10-60	-	-	70%	65
Piezoelectric inkjet bioprinting	Fast	50-100	-	-	70% - 90%	65
Laser assisted bioprinting	Medium	pL level	1-300	$\leq 1 \cdot 10^{8}$/ml	> 95%	70,79
Stereolithography	Fast	High (≈ 1 μm)	No limitation	$\leq 1 \cdot 10^{8}$/ml	> 85%	71

-, no data obtained.

Table 2. Advantages and disadvantages of common bioprinting technologies

3D Bioprinting technologies	Advantages	Disadvantages	References
Extrusion-based bioprinting	Wide range of printable biomaterials High viscosity bioinks. Porous structures	Lower resolution	78
Droplet-based bioprinting			
Thermal inkjet bioprinting	Low cost and adaptable bioprinting process	Small range of biomaterials Cells can suffer damage in the bioprinting process	65
Electrostatic inkjet bioprinting	Low cost and adaptable bioprinting process		65
Piezoelectric inkjet bioprinting	Suitable for single channel bioprinting	Not suitable for specific biomaterials (like fibrinogen)	65
Laser assisted bioprinting	High-resolution, high cell viability (>95%)	Low bioprinting speed Relative high costs	70,79
Stereolithography	High cell viability, range of bioinks, and resolution	Transparent and photo-crosslinkable material required for bioinks	71

Biodegradability is also an important asset that must be considered when designing a bioink formulation, as well as its crosslinking method. Bioprinted constructs are meant to be grafted in the defect at tissue regeneration early stages, and slowly degrade as the host cells replace it with natural ECM. Nevertheless, the degradation rate

of the construct must also be carefully tailored to match the tissue restoration rate, since too fast degradation could lead to the mechanical failure of the graft (80). The bioink degradation can arise from biological, chemical, and/or physical processes, which can be driven by enzymatic, hydrolytic, or stimuli-ligated degradations (81). Also, the by-products of the construct degradation must be biocompatible and non-toxic, since they could provoke changes in the microenvironment, evoke immunologic reactions, or influence the nearby cellular activity (82).

How the construct interacts within the surrounding tissues/organs is what defines its bioactivity (83). One of the most interesting abilities of bioengineered constructs is how bioinks that compose them can interact and elicit a specific desired cellular activity while avoiding non-desired reactions. First, the bioink must offer anchorage for cells to attach to the biomaterial surface. Biomaterials obtained from natural sources present inherent cell adhesion sites; however, this is not often the case for synthetics. Synthetic biomaterials often require modifications on their surface to enable cell attachment, like coating with molecules, such as arginylglycylaspartic acid (RGD), silk fibroin, poly-L-lysine, Poly-D-lysine, or the addition of natural biomaterials into the bioink recipe to provide cell attachment sites (84,85).

One of the most important considerations when designing a bioink for extrusion-based bioprinting is to tailor its printability, in other words, its ability to be extruded through a nozzle in a controlled manner to print constructs with a high shape fidelity. A bioink printability is strongly relied on several of its properties, such as its rheology, viscosity, surface tension, homogeneity, as well as the bioprinting and crosslinking techniques used (86). When working with extrusion-based bioprinting, the bioprinting resolution is highly dependent on the nozzle diameter, when the nozzle diameter is decreased the resolution increases, but that also increases the extrusion force and shear stress, leading to a cell viability drop due to mechanical damage during the bioprinting process. Researchers have investigated the optimization possibilities of this process, finding, for instance, that by using conical needles, instead of cylindrical ones, higher viability rates could be maintained (97% of cell viability when bioprinting with a dispensing pressure of ≤ 1 kPa and a conical needle diameter of 200 μm; 87). Using higher needle diameters (0.25 mm), lower cell damage is produced when using conical needles (cell damage below 5%) instead of cylindrical ones (cell damage between 20-25%) employing the same pressure (flow rate of 0.015 mL/s) was also evidenced (88).

1.1.1.5.3.2 Cells

To produce biologically mimetic tissues and organs, the cells inside the bioink must proliferate and produce their natural tissue-specific ECM while degrading the material in which they are encapsulated. Cells used for bioprinting can be selected depending on two main factors: how printed cells maintain their viability, and how they can biologically mimic their physiological *in vivo* functions (50). Bioprinted tissues can be loaded either by using functional primary cells together with supporting cells (89–95), or seeded with stem cells that would undergo further differentiation (96–101). Bioprinting with several cell types increases the complexity of the protocol since it will entail bioprinting with multiple cell types simultaneously in parallel; however, that means preparing all the cell types, bioinks and reagents at the same time. Aligning the bioprinting steps and many bioinks involves a lot of multi-tasking effort, increasing the risk of introducing errors in the process. Using stem cells can reduce the number of total bioinks for a print, however, they may add their own set of complications such as bioink formulations with growth factor cocktails or supplementing small molecule signalling to guide site-specific differentiation. And even in post-printing culture there will be additional requirements since differentiation stimuli must be provided to ensure the differentiation control.

Although the supply of a reliable cell source has always been an issue for bioprinting research, for its clinical application the optimal option would be using the patient's isolated cells to avoid rejection (102). Nevertheless, not every cell type can regenerate after getting injured. Therefore, stem cells, which can grow and differentiate towards different cell types, are a promising cell source to apply in 3D bioprinting. hMSCs are an interesting cell type to be employed in bioprinting, since thanks to their wide range of differentiation possibilities they can be used to create different tissues. hMSCs can differentiate into the mesodermal lineages (adipocytes, osteocytes and chondrocytes) but they also have the capacity to differentiate towards ectodermal (neurocytes) or endodermal (hepatocytes) lineages (103). Obviously, besides stem cells, fully differentiated cells have also been used in 3D bioprinting. Chondrocytes have been typically used to generate artificial cartilage constructs (104); hepatocytes have been used to create a patient-specific bioprinted liver tissue for drug screening (105); or even vascularized constructs were bioprinted using MSCs, hDFs and human umbilical vein endothelial cells (HUVECS) (106). Examples of different cell types, with their target

tissues/organs, and the biomaterials used can be seen in **Table 3**.

Table 3. Examples of cell types used in bioprinting (107)

Target tissue	Cell types	Biomaterials	Bioprinting technology	References
Vessel	Smooth muscle cells	Carbon nanotube encapsulated alginate	Extrusion	95
	Smooth muscle cells and aortic valve leaflet interstitial cells	Gelatine and alginate	Extrusion	91
	Human umbilical vein endothelial cells (HUVEC) collagen	PEGDA, Matrigel, fibrin gel, alginate, agarose, and GelMA	Extrusion	108,109
Bone	Mouse osteoblastic cells	n-HA	Inkjet	89
	Human osteoprogenitor cells	n-HA	Laser-assisted	110
Cartilage	Patient's cartilage	poly(ethylene glycol) dimethacrylates (PEGDMA)	Inkjet	90
	Minced cartilage cells	Poly (ε-caprolactone) (PCL), and fibrin-collagen hydrogels	Inkjet	93
Skin	NIH3T3 fibroblast, HaCaT hEKs	Collagen	Laser-assisted	92
Neuronal tissue	Mouse bone marrow stem cells	Collagen, and agarose	Extrusion	100
Skeletal muscle	Mouse myoblasts	Polyurethane (PU), and PCL	Extrusion	111
Tumour	Hela cells	Gelatine-alginate- fibrinogen hydrogel	Extrusion	112
Adipose tissue	Adipose derived stem cells	Alginate	Laser-assisted	96

1.1.1.5.3.3. Biomaterials

Usually, biomaterials that conforms a bioink can be divided into two groups depending on its origin: naturals or synthetics. Biomaterials such as hyaluronic acid (HA), fibrin, collagen, and gelatine, as well as other such as dECM, chondroitin sulphate, dermatan sulphate (DS), agarose, silk fibroin, and alginate are considered natural biomaterials. Although natural biomaterials often offer good biocompatibility, they show the disadvantage of lacking long-lasting gelation times or enough mechanical properties. Otherwise, even though synthetic biomaterials lack of suitable biocompatibility and biodegradability, they have more customizable chemical and mechanical properties. Among the commonly used 3D bioprinting synthetic biomaterials we may find poly-L-lactic acid (PLA), poly-ε-caprolactone (PCL), polyethylene glycol (PEG), and GelMA, among others.

Natural biomaterials

Type I collagen (Col I), is a natural polymer that can be printed at low

temperatures after pH neutralization, obtaining a solidified gel at physiological temperature (113,114). Collagen shows interesting properties as a bioprinting biomaterial, since it promotes cell proliferation, adhesion, and migration, presents good biocompatibility, and is safe for the host as it does not trigger any serious immune rejection or inflammation responses (56). However, this biomaterial not only lacks mechanical strength, but also shows a slow speed of gelation, which significantly limits its application as a bioink ingredient by itself (115,116). Similarly, being a denatured form of collagen, gelatine is also biocompatible, it uses thermal gelation to crosslink, and its mechanical strength can be modified by adjusting its concentration (117,118). HA, an ECM anionic glycosaminoglycan (GAG) that can promote regeneration, cell differentiation and angiogenesis (119), is usually modified with acrylic acid to overcome its poor mechanical properties. Thanks to this modification, HA can be used to 3D print scaffolds by photocuring (120). Low melting temperature agarose, which melts at temperatures above 80ºC, stays melted at 37ºC while bioprinting, and forms a gel at room temperature (RT) (121). Agarose also shows the bioprinting advantages of having high mechanical strength while lacking immunogenicity, though its main drawback is that it does not offer cell adhesion (122). Alginate, which is a natural occurring linear polymer derived from brown algae cell wall (123), shows outstanding characteristics, such as high biocompatibility, lack of antigenicity, chelating ability, biodegradability, maintaining of cell viability, and short gelation times (124). However, the main drawback of alginate bioprinting is that it offers poor cell adhesion, weak mechanical properties, and the absence of enzymes able to degrade alginate in mammals (125,126). Chitin, the source from where the chitosan (Ch) is obtained, is a crustacean exoskeleton-derived polysaccharide (127) which can be crosslinked using NaOH, forming a gel matrix thanks to its linear structure (60). Ch shows a slow gelation speed, fast degradation speed, and poor mechanical properties; however, it offers good biodegradability and biocompatibility, and it also exerts a bacteriostatic effect (117,119).

dECM is an emerging TE biomaterial obtained through a combination of chemical and physical treatments that removes all cellular components to avoid rejection. dECM retains the complexity of native ECM elements, which makes this kind of biomaterial suitable to recreate the native microenvironment of the targeted tissue, enhancing the function and morphology of the printed cells (17,128). In addition, this lack of cellular components gives the dECM a low immunogenicity as well as a high biocompatibility.

dECM gelation can be triggered by pH neutralization at 37ºC. Probably, ECM inherent components, such as HA, Col I, and fibronectin, among others, might improve the cellular function of cells seeded within dECM (129). Though, this biomaterial shows some drawbacks, such as low printing resolution, poor mechanical properties, and the ease of collapsing or clogging if the printer lacks a heating module.

The blend of natural biomaterials to produce composite biomaterials is also commonly used for bioprinting applications. The combination of collagen and alginate is quite commonly used for bioprinting biological scaffolds. It has been seen that bioprinting this mixture with EBB allowed to obtain good cell viability and structural stability (130). Also, combining Ch with collagen showed to produce good pore sizes, low antigenicity, and good biocompatibility (131,132). However, even natural composite biomaterials retain poor mechanical properties, which make them prone to deform and shrink in the *in vivo* environment, hindering the maintenance of the original porous 3D structure. Those disadvantages limit the proliferation of cells, vascularization, and growth of tissues. Consequently, biomaterials with enhanced and controllable mechanical properties are needed for 3D bioprinting.

Synthetic biomaterials

The controllability and mechanical properties of synthetic biomaterials surpasses those of natural biomaterials (121). Polymeric biomaterials such as PLA, poly-glycolic acid (PGA), PCL, poly lactic-co-glycolic acid (PLGA), and GelMA are frequently used for skin bioprinting (133). PLA is widely used as a raw material in TE for scaffolds manufacture by 3D printing since it shows biocompatibility, good physical and mechanical properties, and can be fully biodegraded in the body, only producing residual CO_2 and water (134,135). PLGA, a polyester compound commonly used in TE for fabricating scaffolds and bioinks, shows good biocompatibility and mechanical properties. Its degradation rate can be modified by changing the ratio of glycolic acid to lactic acid (136,137). Likewise, PCL is another polyester which is biodegradable, presents a surface that is easily modifiable, is approved by the Food and Drug Administration (FDA), and a good candidate for tissue repair (138). The electrospinning technology allows creating PCL nanofibrous scaffolds that show enough mechanical strength to endure the *in vitro* and *in vivo* cell proliferation and differentiation. Remarkably, the PCL degradation rate is quite lower compared to other biomaterials such as poly-L-lactic acid (PLLA), PLGA or PGA, which enables PCL nanofibers to give long-

term mechanical support to damaged tissues (139). On the other hand, GelMA undertakes photo-polymerization under UV light exposure (with the presence of a photoinitiator), forming covalently cross-linked hydrogels (140). Photo-polymerization can be executed under neutral conditions (pH, RT, aqueous environment), and controlled in space and time (141), allowing the 3D bioprinters to generate unique hydrogels with the desired morphology, patterns, and structures. Besides, GelMA also shows good processability, biocompatibility, and biodegradability properties.

1.2. Cartilage regenerative engineering

Cartilage can be defined as a connective tissue that covers the surfaces of articulations, provides support to respiratory organs, and acts as a constituent of intra-articular menisci, auricles, and the intervertebral discs (142). It is aneural, flexible, and avascular, which means that it does not directly feed from blood supply but nourishes through nutrients that are contained in the synovial fluid. As a result of its aneurality and avascularity, this tissue is very restricted regarding self-regeneration, posing significant challenges to heal when is damaged. This suppose a relevant health issue, since those lesions can degenerate to osteoarthritis (OA), which is the most frequent joint disease in the world (143). Minor symptoms at the early stage of OA can be managed through medication; however, with the disease progression, the cartilage can be severely damaged, having a high impact on the patient's quality of life. Therefore, its major weakness is its poor regenerative capacity since it is not able to undergo self-repair after suffering degenerative or trauma injuries. Thus, novel regeneration strategies need to be developed (144).

1.2.1 Therapeutic strategies for cartilage regeneration

In the regenerative medicine field, many attempts have been done to restore cartilage defects, particularly articular cartilage. Current surgical strategies to deal with articular cartilage defects include subchondral drilling, microfracture, abrasion arthroplasty, mosaicplasty, perichondral and periosteal grafts, and advanced therapies medicinal products (ATMP) such as: i) ChondroCelect®, which is based on the autologous chondrocyte implantation (ACI), ii) MACI, which uses matrix-induced autologous chondrocyte implantation, or iii) Spherox, which employs autologous chondrocyte spheroids produced *ex vivo* to implant them in the patient's knee (145).

However, all these attempts to regenerate this tissue led, at best, to a reduction of painful symptoms. As a matter of fact, the obtained fibrous cartilage quite differs from native cartilage, failing to fully repair the injuries. Nevertheless, although widely applied in clinic, these techniques present the limitations of having high costs, donor site morbidity, graft hypertrophy, inconsistent tissue repair, short-term resolution, or the inability of reproducing the native cartilage architecture (146). Ultimately, a full joint replacement with prosthesis is required for last-stage defects. Therefore, the developments of new approaches to fully regenerate the injured cartilage tissue are necessary.

1.2.2 Clinical applications and future perspective

Currently, there are not so many clinical applications using hMSCs in human cartilage regeneration. However, the ability of hMSCs derived from adipose tissue to differentiate into chondrocytes makes them a promising candidate for cartilage regeneration, since unlike bone marrow-derived stem cells, they seem to grant a partial level of protection to other cell types, also presenting lower inflammatory responses (147,148).

Recent progress in addressing bioengineering approaches for articular cartilage has been made. An interesting approach for articular cartilage restoration is the *in situ* bioprinting strategy, which main strength lays in the ability to precisely print the construct directly on the wound site during the surgery (149). As a matter of fact, a hand-held bioprinting device called "*Biopen*", which consists of two bioink cartridges and a coaxial extrusion mechanism, has already been developed for direct manual bioprinting (150). The developers of the *Biopen* optimized the core/shell bioprinting technique with cells embedded in the bioink, testing the device *in vivo* in a sheep chondral defect model (151). Similarly, another work offered an *in situ* 3D bioprinting strategy, in which a six-degree-of-freedom robotic-arm was employed to repair osteochondral defects in an *in vivo* rabbit model. These researchers achieved to fill the defects with neo-formed hyaline cartilage after a 12 weeks healing period (152).

Regarding the integration of engineered constructs within the osteochondral interface, some researchers found a way of enhancing calcified cartilage differentiation optimizing biomaterials. This is the case of You *et al*., who perfected a combination of chitosan/alginate/hydroxyapatite hybrid to form a hydrogel that supported the production of a mineralized ECM (153). Other researchers mixed bone marrow (BM-MSCs) within

a β-tricalcium phosphate enriched bioink for cartilage bioprinting, characterizing its rheology and mechanical properties, as well as the expression of mineralization and chondrogenic-related markers (154).

Even though several relevant achievements have been made in the bioengineering of articular cartilage, many obstacles need to be overcome. Articular cartilage can be broadly zoned into four different sections regarding its matrix composition, heterogeneous cell density, and mechanical properties. The reproduction of this spatial zonation has not been achieved yet (155); besides, the cartilage graft have to be completely integrated within the underlying subchondral bone (156). Additional issues that need to be addressed relate to the specific cell density depending on the defect size, the long-lasting effectiveness of the engineered tissue, enhance the mechanical properties of the final tissue, or the xenobiological components of the artificial tissue and media employed for creating the tissue (157).

As previously stated, current cartilage regenerative strategies do not provide long-term solutions, frequently needing a joint prosthetic replacement. Cartilage RE strategies and cell therapy products offer alternative solutions that have been developing in the past few years. On one hand, TE-based approaches use combinations of cells, scaffolds, and growth factors to replace and stimulate cartilage defect regeneration (158). On the other hand, cell therapies, mainly based on the use of autologous chondrocytes and MSCs, apply those cells into the defect to promote the repair of the damaged tissues (159,160).

TE-based strategies for regenerating cartilage can be categorized in three groups: cell-scaffold, cell-free, and scaffold-free strategies. Therapies based on the cell-scaffold approach are currently the most used. Typically, cells are seeded inside a scaffold, and then the construct is implanted in the defect. Normally, the scaffolds are made of compatible biomaterials like Col I and III, alginate or agarose (161–163). Cell-free products that are used for articular cartilage repair are usually not completely cell-depleted, since in some cases they can be combined with autologous cells. Nevertheless, these products are initially based on synthetic biodegradable scaffolds which can further be combined with cells or their derivatives (secreted factors or cytokines) (164,165). Lastly, scaffold-free strategies use 3D culture techniques, like spheroid formation, where cells grow together generating their own matrix, to finally implant them in the defect (166–168). Following this last category we could locate cell therapy, since its basis

remains a scaffold-free strategy that focuses on injecting *ex vivo* cultured cell suspensions in the defect to help its regeneration. In **Table 4** are included some examples of products based on TE strategies that are available on the market or being tested in clinical trials. Hopefully, several TE and cell therapy products for treating cartilage defects have already completed clinical trials and are commercially available. Among them, the cell-scaffold products are present in ongoing clinical trials. Although those loaded with chondrocytes have already made quite some advances, medical products with stem cells still need to undergo clinical trials and further research to be approved and commercially available.

Table 4. Products based on TE strategies to cartilage regeneration

Category	Name	Composition	Status	References
Cell-scaffold	**BioSeed®-C**	Chondrocytes grown attached with fibrin glue on a polyglactin910/poly-p-dioxanone scaffold	Ongoing phase III clinical trial (2011-003594-28)	169
	Hyalograft® C	Chondrocytes seeded in a HA scaffold	Lack of phase III clinical trial; withdrawn from the market by the EMA	170,171
	CaReS®	Primary autologous chondrocytes seeded in Col I scaffolds	Prospective Multicentre Study (2003-2008): commercially available	172,173
	NeoCart®	Chondrocytes seeded in Col I scaffolds	Completed phase III clinical trial (2017)	174,175
	NOVOCART® 3D	Chondrocytes seeded in a biphasic Col I /III scaffold	Ongoing phase III clinical trial (NCT01656902)	-
Cell-free	**TruFit**	Scaffold made of PLGA copolymer, calcium sulphate, PGA fibres, and surfactant	Completed clinical pilot study (NCT01246635)	176–178
	MaioRegen	Three-layered Col I and hydroxyapatite scaffold	Completed phase IV clinical trial (NCT01282034)	179,180
Scaffold-free	**Spherox (Chondrosphere®)**	Chondrocyte spheroids suspension	Completed phase III clinical trial (NCT01222559; authorised by the EMA)	181
Cell therapy	**Carticel®**	Suspension of Autologous *ex vivo* cultured chondrocytes	Completed phase IV clinical trial (NCT00158613)	182
	ChondroCelect®	Characterised autologous *ex vivo* cultured chondrocytes expressing specific marker proteins	Completed phase III clinical trial (NCT00414700)	183
	Chondron™	Suspension of Autologous *ex vivo* cultured chondrocytes	Completed phase III clinical trial (NCT01050816)	184
	CARTISTEM®	Allogeneic HUVECs	Completer phase III clinical trial (NCT01626677)	185,186
	Invossa™	Injectable genetically engineered chondrocytes virally transduced with TGF-β1 (GEC-TGF-β1)	Ongoing phase III clinical trial (NCT03383471)	187
	JACC	Cultured autologous chondrocytes embedded in atelocollagen gel.	2-year follow-up prospective multicentre clinical trial in Japan	188

1.2.3. Cartilage 3D bioprinting

1.2.3.1. Essential elements for cartilage 3D bioprinting

1.2.3.1.1 Desirable properties of 3D bioprinted cartilage

The main objective of 3D bioprinted cartilage constructs is to simulate the cartilage microenvironment by combining biomaterials, growth factors, and cells, which can proliferate and generate this tissue. An optimal 3D cartilage construct should reproduce the biological and mechanical properties of native cartilage (articular, nasal, auricular, tracheal, or intervertebral) (189). However, tissues differ in its biological, physical, morphological, and chemical properties. In the 3D bioprinting domain, the bioprinter can define the structure and shape of the cartilage construct by bioink deposition. Essential properties that the 3D bioprinted constructs for cartilage regeneration should mimic include the architectural and mechanical properties of cartilage.

The global geometry together with the inner microarchitecture of a construct are the factors that define its specific properties. Regarding the inner microarchitecture, the pores density, size, and shape are critical parameters in the fabrication process. The pore density has a direct connection with the construct biological and mechanical properties, as it is defined by the void volume of the structure. An open and interconnected construct with high pore density holds a higher nutrient diffusion, stimulating cell growth, waste depletion, and can even promote vascularization, this latter characteristic not being of interest for cartilage regeneration (190). As a matter of fact, it has been seen that in cellular activity parameters, non-porous collagen constructs showed lower cell viability than porous collagen ones, reporting a high cell death rate in the core of the non-porous hydrogels after 7 days of *in vitro* culture (191). Similarly, the pore parameters are also an important consideration, since it has been seen that: i) bigger pore sizes reduce the surface area ratio, lowering cell attachment; ii) it can affect biomechanics; iii) pore size does not affect cell proliferation, but the angles produced by them can be critical on it (192). On the other hand, if the pore size is too small, nutrient diffusion and cell migration will be limited. Several researchers have studied this issue, and reported that optimal pore sized for collagen-based cartilage constructs may range between 150 – 250 μm (193) and 300 μm (194). Finally, the pore shape also plays an important role in the definition of constructs microarchitecture, since it has been demonstrated that, for instance, cubic pores

could influence MSCs chondrogenic differentiation (195). Latest studies in 3D bioprinting of cartilage constructs have aimed to recreate the zonal structure of native cartilage, developing mechanical and physicochemical properties, and biological composition gradients (196–199)

A bioprinted construct should match the mechanical properties of the native tissue that is trying to reproduce to achieve an optimal tissue regeneration (200). The articular cartilage Young's modulus ranges from 0.28 ± 0.16 MPa to 0.73 ± 0.26 MPa between its surface to its deeper zone, respectively (201). For achieving these properties, the mechanical strength of bioprinted constructs rely on the structure of the construct, the composition of the bioink, and the post-printing processes like the cross-linking methods (202). Usually, synthetic biomaterials like PCL are combined with hydrogels for reaching cartilage mechanical properties.

Also, several bioactive molecules have been investigated as supplements for bioprinting bioinks to enhance the differentiation into a specific tissue. This is the case of growth factors, like bone morphogenic proteins (BMPs) or transforming growth factors (TGFs) that have been proven to induce chondrogenic differentiation. For example, BMP-4/6, and TGFβ1/3/4 have already been successfully supplemented to bioinks as chondrogenic properties enhancers of 3D bioprinted constructs (203–205).

1.2.3.1.2 Cells

As the predominant cell in cartilage, chondrocytes are the most used cell type in the research and development of bioinks for cartilage bioprinting applications. This kind of cell can be isolated from articular cartilage and expanded *in vitro* to obtain enough biomass to be employed. Proof thereof is the fact that chondrocytes have been effectively used in the 3D bioprinting of chondrocyte-laden constructs in several studies (206–209). However, due to their limited availability given the donor site morbidity, as well as the high costs of *in vitro* cell production, several alternative cell sources have been extensively investigated. These alternative cell types mainly include the spectrum of stem cells, such as the MSCs isolated from infrapatellar fat pad (IFP-MSCs), adipose tissue (AD-MSCs) (210,211), BM-MSCs (47,212–214), synovium (sMSCs) (215), human embryonic stem cell-derived (hESC-MSCs) (216), and even human-derived induced pluripotent stem cells (iPSCs) (216,217). The main point of using stem cells, and specifically MSCs, is their ability to undergo chondrogenic differentiation through their

exposure to specific bioactive molecules. Though, a drawback of using this kind of cells is their propensity to undertake a cartilaginous hypertrophic differentiation. Nevertheless, it has been reported that IFP-MSC and sMSCs may display a low hypertrophic potential, being a more desirable option for cartilage TE (218,219). So far, there is no optimal stem cell source for 3D bioprinting, however, recent studies have investigated the co-culture of multiple cell types seeking to enhance of chondrogenesis in 3D bioprinted constructs. As a matter of fact, some researchers implemented the co-culture strategy to their studies, such as the combination of MSCs together with chondrocytes to create structurally organized spheroids (220); the creation of zonal-like articular cartilage models combining BM-MSCs, chondroprogenitor cells, and chondrocytes (221); or the bioprinting of constructs with IFP-MSCs and hESC-MSCs that showed the ability to promote the chondrogenic tissue neoformation after 2 weeks post-implantation in a subchondral defect rabbit *in vivo* model (216). The co-culture approach holds the potential of boosting the constructs chondrogenic properties, reducing the *in vitro* stage of cell expansion, unravelling this strategy to be clinically applicable and cost effective.

1.2.3.1.3 Biomaterials for Cartilage 3D bioprinting

Cartilage bioinks can be formulated using natural or synthetic biomaterials, depending on their source and their intended application (222). Due to their biological properties and similarities with native cartilage, hydrogels are often the better choice for cartilage extrusion-based bioprinting, since their hydrophilic crosslinked networks can hold up to 90% of water content, allowing good nutrient exchange while maintaining their structure (223,224). In fact, natural biomaterials are considered an ideal choice when designing a bioink for cartilage TE applications, since they are highly biocompatible, can mimic the natural ECM, are biodegradable, and provide cell attaching sites. However, their properties variability still poses some challenges. Synthetic biomaterials are more tricky to use in the biomedical field, as they tend to show less biocompatibility and cell interaction; however, they are capable of achieving optimal mechanical and rheological properties, that can be tailored by pH or temperature changes (225–227). In the cartilage research field there is a growing need for the formulation of bioinks with optimized bioprinting parameters, as well as the inherent biomaterial assets, which include physicochemical, biological and mechanical properties (228).

Natural-derived biomaterials employed for the formulation of bioinks for cartilage TE applications usually englobe the use of alginate, gelatine, agarose, HA, and Col I. The

bioprinted constructs fabricated using this kind of biomaterials often get crosslinked by physical, chemical and/or enzymatic agents such as temperature, pH, sodium chloride (NaCl), or thrombin (229–231). Several studies have created combinations of these biomaterials seeking the development of an optimized bioink (232–234).

Alginate, a biodegradable polymer derived from the brown algae (*Phaeophyceae*) cell walls is a polysaccharide that has been widely investigated to be applied in cartilage TE, due to its lack of immunogenicity and its biocompatibility (235). Regarding its printability, alginate has been extensively used as it presents a useful fast gelation process induced by exposure to calcium ions. It also exhibits shear-thinning properties, which protect the cell during the bioprinting process (236). Despite its advantages, alginate alone shows poor mechanical properties and it lacks of chondrogenic activity, thus, it has been frequently combined with other biomaterials, such as HA (237), cartilage ECM (238), or collagen (232). HA, as one of the main components of articular cartilage, is a polymeric GAG that provides lubrication and viscoelasticity to the joints (237). Its chondrogenic properties have made it ubiquitously used for cartilage regeneration applications (237,239); however, despite its advantages, it lacks of good mechanical properties, showing a poor printability (240–243). HA has already been used to fabricate a HA/alginate bioink to ameliorate its printability, showing good gelling, stiffness, degradability, printability properties, and even *in vitro* chondrogenesis (237).

The synthetic biomaterials most typically used for cartilage TE include poly-lactic acid (PLA), polycaprolactone (PCL), and poly-glycolic acid (PGA). Combinations of these polymers with other synthetic and natural biomaterials have also been studied to ameliorate the properties of their mixtures, like their printability, mechanical characteristics, or crosslinking method; seeking to optimize them for cartilage TE and even to help to stimulate their chondrogenic effect (244,245). Interestingly, synthetic polymeric biomaterials can also be used as sacrificial elements, to provide support to the construct structure during the bioprinting. This is the case of poloxamers, like Pluronic®, which hold thermos-reversible gelation properties making them suitable as sacrificial biomaterials (liquid at < 4ºC; gels at > 16ºC) (246). PCL is also a classically used polymer to bioprint cartilage TE constructs, often used for improving mechanical properties. It has been co-printed together with other polymers such as cartilage ECM, silk fibroin (247), MeHA, or PEG (248).

1.3. Skin regenerative engineering

Over the last decades, regenerative medicine has evolved tremendously in many areas, including wound healing and skin regeneration (249). However, treatment of acute and chronic skin wounds remains a clinical challenge and a lifesaving resource for many patients.

Skin-related diseases could be due to several reasons: acute or chronic wounds, skin-related pathologies (such as diabetic foot ulcers), perianal fistulae, epidermolysis bullosa, or the most common cause of major skin tissue loss: burn trauma (**Figure 4**). Deep dermal traumas and full-thickness skin wounds often prove to be difficult to treat due to the high risk of infection, the significance of the area involved, and the potential damage of deeper skin layers that include the dermis (250). Currently, in clinical practice, skin grafting with an autologous graft (autograft) is the "*gold standard*" treatment (251). However, the availability of healthy autologous tissue is often limited in patients suffering from major trauma. In response to these limitations, skin substitutes produced by RE offer alternative therapeutic approaches. Skin substitutes are defined as a heterogeneous group of substances that aim to restore the skin barrier function, facilitate wound healing, prevent infections, and manage pain. Most skin substitutes are acellular; however, in the past years an increasing attention has been paid to the development of cellular substitutes that are mainly manufactured using two skin cell types: hDFs and hEKs (252–254). Moreover, other researches also includes different skin-related cell types, such as melanocytes (255), MSCs (256), epidermal stem cells (ESCs) (257), hair follicle stem cells (258), or cell-based products such as platelet-rich-plasma (PRP) (259–261).

New approaches for skin RE are focused on combining natural or synthetic biomaterials with living cells for several biomedical and pharmaceutical applications. However, engineering a multiple layered skin architecture conforming the native skin structure is a tough goal that new RE advances aim to achieve. Currently, there is a broad spectrum of commercially acellular and cellular skin substitutes that are available for clinical use, as well as different therapeutic strategies that can be assessed for skin regenerative medicine, for instance, injectable cell solutions, cell sprays, cell sheets and 3D scaffolds. As well, clinical advances for the treatment of dermal injuries are being made, based on the clinical trials that are being carried out for the development of ATMPs, innovative strategies, and medical devices for a diverse range of skin disorders.

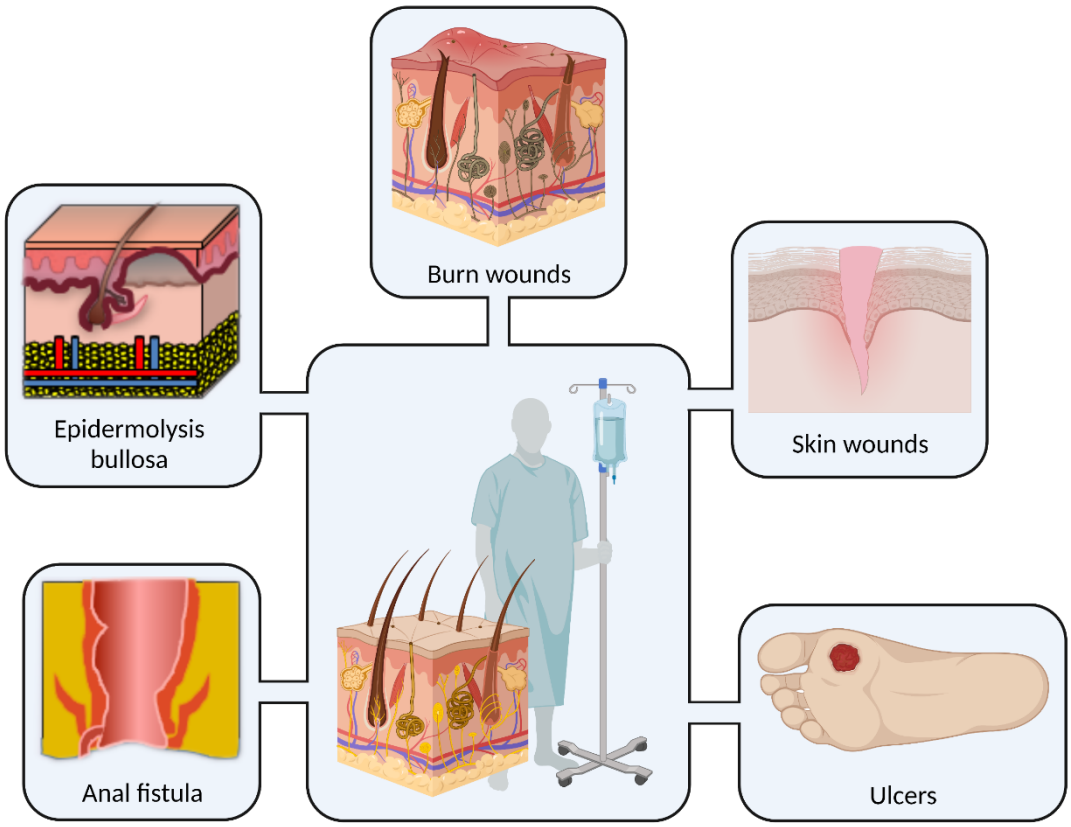

Figure 4. Most common skin-related diseases, namely: anal fistula, epidermolysis bullosa, burn wounds, different skin wounds and ulcers.

1.3.1. Acellular substitutes

Acellular skin substitutes are designed to act as a barrier to prevent water loss and infection of the wound bed. They are produced using different biomaterials such as collagen, silicone, or nylon meshes, but there are also some substitutes that are composed by cadaveric dermis. Different acellular skin substitutes are already employed in the clinical practice (**Table 5**). An example of a commercially available product is Integra®, which is composed of a silicone membrane, and a bovine collagen + shark chondroitin sulphate layer, which serve to prepare the wound bed for transplantation (262–264). It is widely used to treat different pathologies, such as full-thickness skin defects, deep partial and full-thickness burn wounds, soft tissue defects, chronic wounds.

Table 5. Acellular skin substitutes

Name	Composition	Clinical indications	References
Integra®	Epidermal equivalent – silicone membrane; Dermal equivalent – bovine collagen and shark chondroitin-6-sulphate	Large burns and limited autograft donor sites	262–264
Alloderm®	Acellular human dermis	Burns and other wounds; repair of soft tissue defects	265–267
Biobrane®	Epidermal equivalent – silicone membrane; Dermal equivalent – nylon mesh combined with porcine collagen	Superficial partial-thickness burns of limited extent, donor sites and temporary coverage of freshly excised deep partial- or full-thickness wounds.	268
AWBAT	3D nylon mesh with porcine type I collagen and a porous silicone membrane	Partial thickness burns	269
GammaGraft™	Decellularized human cadaveric dermis	Venous insufficiency ulcers, diabetic foot ulcers, full-thickness ulcers, skin graft donor sites, partial-thickness wounds, burns	270
Graftjacket®	Acellular human dermis	Periosteal patch or covering, protection and support of bone and tendons in foot & ankle and hand surgery	271–273
Matriderm®	Bovine matrix of Col I and elastin	Full-thickness wounds	274,275
DermaCELL®	Decellularized human dermal matrix	Implant-based breast reconstruction, diabetic foot ulcers, venous stasis ulcers, arterial ulcers, pressure ulcers	276
FlexHD®	Acellular human dermis	Replacement of damaged or inadequate integumental tissue or for the repair, reinforcement, or supplemental support of soft tissue defects.	277
Graftjacket Xpress®	Micronized (powdered) dermis	Deep dermal wounds or diabetic ulcers	278
MatriStem®	Porcine extracellular matrix	Deep partial-thickness burns	279
EZderm Mediskin®	Aldehyde cross-linked porcine dermis	Partial thickness skin loss injuries, donor sites, skin ulcerations and abrasions	280
OASIS®	Porcine acellular lyophilized small intestine submucosa	Wound closure stimulation in acute and chronic full-thickness diabetic ulcers and burn wounds	281–283
MicroMatrix®	Porcine-derived extracellular matrix (urinary bladder matrix)	Partial and full-thickness wounds, pressure ulcers, venous ulcers, diabetic ulcers, chronic vascular ulcers, surgical wounds, trauma wounds, and draining wounds	284

Acellular substitutes can also be obtained from cadaveric dermis. This kind of substitutes are decellularized human dermal matrix that keeps the ECM while reducing rejection and inflammation, allowing revascularization and cellular repopulation. Examples of allografts from cadaveric dermis include Alloderm™, GammaGraft™ and Graftjacket®. Alloderm™, is employed as a dermal substitute to treat deep and full-thickness burns to facilitate the following autologous split-thickness skin graft (265). Beyond its use as a dermal substitute, Alloderm™ has also been used for laryngoplasty, vaginal prolapse repair, implantable prosthesis coverage, pelvic and abdominal wall defect restoration, and other forms of soft tissue substitutions. Compared to Alloderm™,

Integra® shows a higher induced foreign body reaction; however, this response is expected given the fact that it is produced by chemical cross-linking. Assuming those drawbacks, and with the lack of clinical studies that compare these two skin substitutes, Integra® is not yet considered as a favoured option over human-derived skin substitutes such as AlloDerm™.

GammaGraft™ is a gamma-irradiated human skin allograft that provides epidermis and dermis structures. It presents the advantage of being able to be stored for 2 years at RT, unlike bioengineered tissues, which need cold storage and must be used when received. Graftjacket™ is a decellularized human dermal matrix where cellular components are removed. (278).

The biomaterials used to produce acellular skin substitutes can also be animal-derived, obtaining acellular xenografts such as Matriderm®, which is based on a bovine matrix of Col I and elastin (EL), and employed for dermal regeneration (274,275) This skin substitute shows an improved vascularization and elasticity of the regenerated tissue.

Unfortunately, acellular skin substitutes show some limitations, such as poor barrier function and short shelf-life. In addition, there is a risk of disease transmission when using cadaveric skin allografts since residual deoxyribonucleic acid remains in the tissue. To ameliorate these limitations, different types of cells are included in skin substitutes, improving the production of ECM, and extending the time of wound coverage.

1.3.2. Cellular substitutes

The inclusion of living cells within the skin substitutes promotes the regeneration of natural-like skin tissue due to the secretion of growth factors and ECM components. Among commercially available cellular substitutes, some are based on sheets of allogenic cells obtained from human neonatal foreskin (**Table 6**). TransCyte™, for example, consists in a nylon mesh, which is populated with neonatal hDFs (285). However, to reduce rejection, cells are eliminated before grafting by freezing to conserve the matrix and the growth factors. On the other hand, Dermagraft® is an allogenic skin substitute which uses the same cells as TransCyte™, but in this case hDFs are embedded in a biodegradable mesh of PLGA and cryopreserved to attain a better cell viability. (286).

Cellular substitutes often require cultured autologous hEKs for a permanent coverage. One of the few commercially cultured epithelial autografts (CEAs) is Epicel®,

which is produced under Good Manufacturing Practice (GMP) conditions and consists of sheets of the patient's hEKs seeded over a petrolatum gauze. This CEA is of great importance in patients who suffer large burns (over 60% of the total body surface area), as they lack available donor sites (287,288). Also, although it has a long generation time, taking almost 3 weeks to culture the tissue, it presents a very low risk of rejection (289).

Autologous hDFs are also used for dermal skin substitutes. One example is the TISSUEtech Autograft System™, which combines two TE biomaterials such as Hyalograft 3D™, as a dermal equivalent, and Laser skin®, an autologous epidermal substitute, as an epidermal equivalent (290,291). In addition, Hyalograft 3D™ is composed by seeding autologous hDFs over a 3D HA-derived scaffold named Hyalomatrix®.

Table 6. Cellular skin substitutes

Name	Composition	Clincial indications	References
TransCyte™	Nylon mesh substitute populated with hDFs	Excised burns awaiting placement of autograft	285,292
Dermagraft™	Combination of a biodegradable mesh of polyglycolic acid and neonatal foreskin hDFs	Full-thickness foot ulcers	286
Epicel™	Cultured autologous hEKs	Permanent closure in greater burn wounds	287,288
TissueTech Autograft System™	Combination of Hyalograft 3D™ as a dermal equivalent and Laser Skin as an epidermal equivalent	Diabetic foot ulcers, full-thickness ulcers	290,291
Hyalomatrix®	Bilayer composed of an external silicone membrane and an internal hyaluronan scaffold	Pressure ulcers, diabetic foot ulcers and deep second-degree burns	293–295
Hyalograft 3D™	Autologous hDFs seeded over Hyalomatrix®	Extensive dermal wounds, including burns and difficult-to-heal chronic wounds	-
Laser Skin	Cultured autologous hEKs in laser-perforated HA	Diabetic foot ulcers and venous leg ulcers, partial thickness burns, vitiligo	290,291
Apligraf™	Bilayered bovine collagen matrix seeded with neonatal hEKs and foreskin hDFs	Venous leg ulcers and diabetic foot ulcers	296,297
OrCel™	Type I collagen matrix seeded with neonatal foreskin hDFs and hEKs	Split-thickness donor sites in patients with burn wounds	298
Stratagraft®	Bilayered dermal hDFs and hEK-derived fully stratified epidermis	First-line treatment of burn wounds, until autografts are prepared	299,300
Permaderm™	Collagen-glycosaminoglycan substrates seeded with autologous hDFs and hEKs	Full-thickness burns	-
Tiscover™	Autologous full thickness cultured skin	Chronic therapy-resistant leg/foot ulcers	-
DenovoDerm™	Autologous dermal substitute	Large Deep Partial and Full Thickness Skin Defects	-
DenovoSkin™	Autologous full thickness substitute consisting of dermal and epidermal layers		-

-, no data obtained.

Hyalomatrix® consists of a bilayer composed by an outer silicone membrane, that acts as a temporary epidermal barrier, and an internal hyaluronan scaffold (293–295). The TISSUEtech Autograft System™ represents a good attempt to biomimic the histology of the human skin (291).

Other skin substitutes made of synthetic polymers, such as PLGA, PCL, or polypyrrole are investigated to generate membranes as platforms to seed hDFs (301–306). Regarding composite allografts, Apligraf® is a bovine collagen-based substitute which is more complex than previous substitutes since it includes both hDFs and hEKs cell types (296,297). OrCel® is another similar, although slightly thicker composite allograft compared to Apligraf® as it also contains the same cell types and provides a bovine Col I sponge to treat partial-thickness wounds (298).

In traumatic skin wounds, such as in burn patients, the wound bed often needs to be prepared before autografting. In this situation, the use of cellular substitutes is replacing the use of cadaveric allografts to cover full-thickness skin wounds. Within the skin substitutes that are used to cover full-thickness skin wounds, Stratagraft® is an allogenic epidermal substitute composed of dermal hDFs and neonatal hEKs. This skin substitute is used as an intermediate step before autografting burn wounds, showing good tolerability and non-acute immune reactions (299,300,307).

1.3.3. Therapeutic strategies for skin regeneration

Many products have been developed and applied for therapeutic applications to mimic the native skin architecture and its microenvironment properties (308–313). There are different strategies of procedures for the treatment of skin injuries, such as injectable cell solutions, cell sprays, sheets, and 3D scaffolds.

1.3.3.1 Injectable cell solutions

Many types of cells are being administered via subcutaneous injection within different kinds of solutions composed of HA, PRP, Col I, Ch, poly(ethylene glycol)-poly(L-alanine), ECM, or methylcellulose, among others (309,314–318). Moreover, cells can be delivered embedded in injectable hydrogels that provide a scaffold for *in situ* tissue regrowth and regeneration, allowing surgeons to fill complex shapes with a minimal invasive procedure (319,320). Several biomaterials have been employed for developing injectable hydrogels to mimic the biological cues of native ECM; however, they cannot reproduce the complex functions of natural ECM. In the last decade, increasing attention

has been paid to the development of tissue-derived ECM as a biomaterial to generate injectable hydrogels (321–325), some of them based on dermal ECM or hybrid injectable hydrogels of thermosensitive soluble ECM and methylcellulose as stem cell delivery systems in skin wound treatments (317,326).

1.3.3.2 Cell spray

To avoid mesh grafting, non-cultured autologous cell-spray grafting has been presented as a treatment for deep and partial-thickness wounds. Cells are isolated from a donor skin tissue and applied to the wound bed by spraying. This non-invasive treatment strategy aims to facilitate the re-epithelialization process, reducing the healing time in the hospital and minimizing complications (327). However, for the treatment of full-thickness wounds a dermal element to achieve functional permanent skin is still required.

1.3.3.3 Sheets

As explained above, engineered sheets could be used with or without cells. When cells are seeded on the sheets, they produce their own ECM upon confluence. The inclusion of multiple to single cell layers forms a thicker matrix easier to handle for implantation at the wound site; however, the risk of starving the basal cells complicates a successful survival on the wound bed (328,329).

1.3.3.4 3D scaffolds

Skin scaffolds are being studied to enhance the control of the wound healing process (330–332). To fabricate 3D scaffolds that recreate the physiological conditions of the skin, several 3D cell culture systems have been developed employing protein-based biomaterials, such as collagen, gelatine, or silk, among others (333,334). These biomaterials have proven to be advantageous since they are composed of biomolecules similarly found in natural tissues and can be degraded and cleared by the host native physiological processes. Moreover, complete decellularization of skin tissue to create ECM based matrix scaffolds for skin regeneration has been developed (335). A growing body of studies highlights the relevance of the combination of different biomaterials to create products with enhanced properties. For example, to generate a full-thickness skin substitute, fibrin and agarose can be mixed with hDFs and subsequently seeded with hEKs. This model of fibrin-agarose skin equivalent, achieved to reproduce the histological architecture and structure of the human skin, suggests the possibility of being applied as a skin substitute to treat skin wounds such as burns (336). Another example

can be found in the combination of biodegradable polyurethane and porcine dermal ECM to generate an elastomeric electrospun patch that provides better bioactivity and mechanical properties compared with digested dermal ECM alone (337). Another interesting strategy is to blend native ECM elements like keratin (Kt) fibres (the structural protein present in the epidermis ECM) or HA, with cross-linkable biomaterials such as alginate or agarose (a naturally occurring anionic polysaccharide) in order to prepare a biocompatible film (334,338–341).

In brief, these strategies are intended to improve the wound healing and the treatment of skin-related diseases. However, skin wound healing therapies are evolving towards the personalization of the treatment for each patient, to facilitating their clinical use, and shortening waiting times to generate skin substitutes.

1.3.4. Current and future clinical applications

In the las decade, various cell therapies and TE skin products have moved from *in vitro* and animal studies into human clinical trials as therapeutic clinical applications for a diverse range of skin disorders (**Table 7**). Among the different cell types applied by injectable cell solutions, several have been used, such as MSCs (NCT02669199, NCT01750749), human autologous adipose-derived stromal vascular fraction (NCT01813279), bone marrow-derived cells (NCT01750749), human placenta-derived cells (NCT01859117), melanocytes and hEKs (NCT0251065), and even human umbilical cord blood derived-universal stem cells (hUCB-MSCs) (NCT01927705). With the use of intramuscular human placenta-derived mesenchymal stromal-like cells in patients with peripheral arterial disease (PAD) and a diabetic foot ulcer (DFU), preliminary evidence of ulcer healing was shown in 7 out of 15 patients, and circulating endothelial cell levels (as a vascular trauma in peripheral artery disease biomarker) were decreased within 1 month (NCT01859117; 342).

Regarding hUCB-MSCs, clinical application in the treatment of atopic dermatitis (AD) demonstrated for the first time, a remarkably improvement of AD features with cell therapeutics without noteworthy adverse events (343). Nevertheless, other cell-based products such as the use PRP (NCT02832583), platelet-rich-fibrin (NCT01957124) and amnion-derived cellular cytokine (NCT02389777, NCT01715012) are also addressed.

Table 7. Completed Clinical Trials

Pharmaceutical form	NTC number	Title	Phase	Indication	Cell type	References
Injectable Cell Solution	NCT02669199	MSCs Source of Sweat Gland Cells of Large Area Skin Injury Patients Transplant of the Wound	1	Skin Burns	MSCs	-
	NCT01813279	Assessment of the Subcutaneous Reinjection of Human Autologous Adipose-derived Stromal Vascular Fraction (Celution® System) in the Hands of Patients Suffering from Systemic Sclerosis	1	Scleroderma	Human Autologous Adipose-derived Stromal Vascular Fraction	344,345
	NCT01750749	Cell Therapy for Venous Leg Ulcers Pilot Study	1	Venous Ulcer	Bone marrow-derived cells	-
	NCT01669746	A Study to Evaluate and Compare Injections of Autologous Mixed Population of Dermal Cells into the Balding Scalp of Subjects with Hair Loss (CA-0006931)	2	Androgenetic Alopecia, Male Pattern Baldness, Female Pattern Baldness	Autologous cultured mixed population of dermal cells	-
	NCT02458417	Autologous Cell Suspension Grafting Using ReCell in Vitiligo and Piebaldism Patients	4	Vitiligo and Piebaldism	Autologous cells	-
	NCT01859117	Study of Human Placenta-derived Cells (PDA002) to Evaluate the Safety and Effectiveness in Subjects with PAD and DFU	1	PAD, DFU	Human placenta-derived cells	346
	NCT01743053	A Pilot Trial of the Use of ReCell® Autologous Cell Harvesting Device for Venous Leg Ulcers	4	Venous Leg Ulcers	Autologous cells	-
	NCT01927705	Safety and Efficacy of FURESTEM-AD Inj. in Patients with Moderately Subacute and Chronic AD	1/2	AD	hUCB-USCs	347
	NCT02510651	Effect of Procedural Variables on Outcome of Surgical Treatment of Vitiligo	1	Vitiligo	Melanocyte-KC	-
	NCT02832583	Autologous PRP Combined to HA Obtained with Regen-Kit BCT-HA in Aesthetic Medicine		Skin Wrinkling	PRP-HA	-
	NCT02134132	Utilization of Platelet Gel for Treatment of DFU	1/2	DFU	Platelet Gel	-
	NCT02389777	ACCS Solution in UV-induced Inflammation	2	Skin Burns	ACCS	-
Spray	NCT01656889	Study Investigating the Safety and Efficacy of HP802-247 in the Treatment of Venous Leg Ulcers	3	Venous Leg Ulcers	hEKs and hDFs	348
Skin substitute	NCT02668055	Slow-release Tb4 Collagen and chondroitin sulphate Porous Sponge Scaffolds Skin Substitute Treatment is Difficult to Heal Wounds (TB4)	1	Skin wounds		-
	NCT01908088	Autologous Transplantation of Cultured hDFs on Amniotic Membrane in Patients with Epidermolysis Bullosa	1	Epidermolysis Bullosa with Mitten Hands	Autologous hDFs	-
	NCT02394886	Safety of ALLO-ASC-DFU in the Patients With DFU	1	DFU	Allogenic adipose-derived MSCs	-

BCT, blood cell therapy; ACCS, amnion-derived cellular cytokines; TB4, thymosin beta 4

Moreover, new devices are being evaluated, such as the ReCell kit (Avita Medical Europe Ltd, Cambridge, UK; NCT02458417, NCT01743053), which uses autologous epidermal cells (349). As well, innovative strategies are being assessed to ameliorate the cell dispensing systems, such as the topical wound spray HP802-247, a fibrinogen and thrombin solution spray containing living, irradiated and growth-arrested hEKs and hDFs (NCT01656889; 348).

Furthermore, there are also clinical trials that address the treatment of DFU, epidermolysis bullosa and other skin traumas with different skin substitutes. These include MatriStem, MicroMatrix and MatriStem Wound Matrix (NCT01858545) (ACell, Columbia, MD, USA), the umbilical cord allograft NEOX CORD 1K (NCT02166294) (AMNIOX, Miami, FL, USA), a skin substitute based on autologous hDFs seeded on an amniotic membrane (NCT01908088), and collagen-CS porous sponge scaffolds (NCT02668055).

It should be noted that the clinical use of living cells in advanced therapies and regenerative medicine has to be carried out under the GMP standards, which imply that for any development of a skin substitute with living cells, a manufacturing protocol and a quality control program have to be previously defined and validated (350). The quality controls include the following: (i) the biological characterization of the cellular component (identity, viability, dose, purity, potency, karyotype, and tumorigenicity); (ii) the microbiological quality of the product (sterility, mycoplasma detection, pyrogen and endotoxins testing, and adventitious viruses); and (iii) the environment quality control where the skin substitute is manufactured (surfaces, air, personnel, and facilities; 351).

Despite the substantial progress made in clinical assays, it remains a great challenge to produce a precise and complex new tissue that mimics the native skin by including several cell types arranged in a specific 3D pattern. To overcome the limitations of current skin TE technologies, new techniques such as the 3D bioprinting approach (**Figure 5**) allow a highly automated fabrication of complex bioengineered constructs using different cell types and biomaterials simultaneously to increase the homology to the native skin.

The biomaterial selection is one of the key steps in 3D bioprinting. Although collagen hydrogels prevail in research relating to skin 3D bioprinting, other biomaterials have been studied as bioink ingredients. For example, given its biocompatibility and ease

of obtaining, plasma-derived fibrin has been recently used to print human artificial skin (352). Also, mixtures of different biomaterials such as combining gelatine, low viscosity alginate and fibrinogen have been used as a bioink that allows bioprinting of a complete skin model using a scaffold-free approach. This bioink is combined with hDFs to generate the dermis layer, with the subsequent seeding of hEKs on the top of the cultured construct, providing an optimal rheology, as well as similar characteristics to those found in human skin (353).

The optimizations of skin 3D scaffold fabrication strategies include the use of novel composite biomaterials such as a gelatine-sulfonated silk composite scaffold, which is used to stimulate neovascularization within the construct (354), and the applications of innovative technologies in scaffold fabrication such as stereolithographic 3D bioprinting, a layer-by-layer photopolymerization system which provides good resolution, material availability, speed, and low surface roughness (355,356).

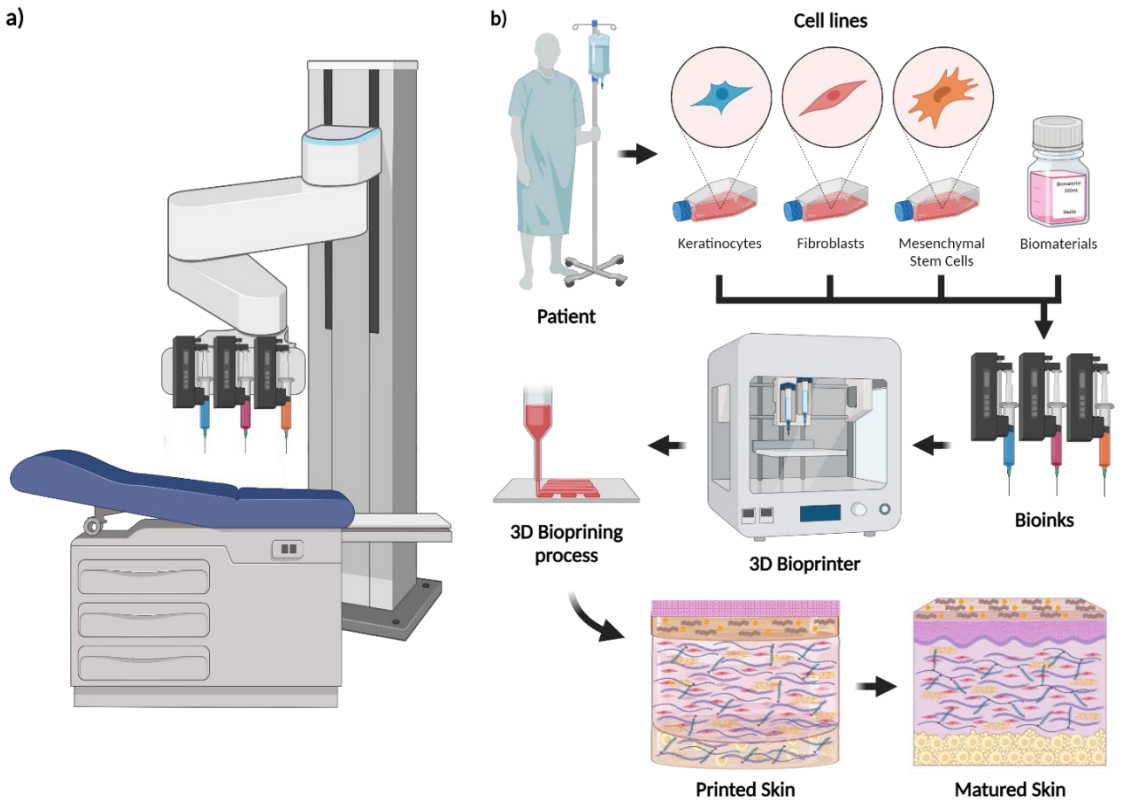

Figure 5. Skin 3D bioprinting technology: (a) Schematic representation of an *in-situ* 3D bioprinting approach for skin surgery. (b) Skin 3D bioprinting flowchart: cells are isolated from patient and cultured *in vitro*. Bioinks are used to 3D bioprint skin tissues. The tissues can be matured in bioreactors.

Another example is the use of mechanical micromilling technology, a precise fabrication of undulated micro-topographies of poly(methyl methacrylate) to mimic dermal papillae of skin (357). These innovative technologies allow overcoming one of the main problems in skin TE which is the deficiency of dermal vascularization, as well as improving the resolution and biomimicry of the scaffolds. Overall, the new strategies based on bioengineering and 3D bioprinting offer the possibility of personalizing and tailoring the properties of artificial skin substitutes and hold the promise of producing a paradigm shift in the biomedical field.

1.3.5 Skin 3D bioprinting

1.3.5.1 Essential elements for Skin 3D bioprinting

For carrying out a skin 3D bioprinting process firstly the bioink must be prepared. Then, the next step is to print the skin substitute accordingly to the specific clinical requirements. The resulting skin substitutes can be implanted to the skin wound bed after *in vitro* culture or bioreactor maturation. The scaffolding biomaterial will be degraded and/or absorbed by the host body, and eventually replaced by ECM secreted by the surrounding host cells and/or the grafted cells, achieving the regeneration of the lost skin tissue, finally repairing the skin wound.

Bioactive factors have a relevant role in the skin 3D bioprinting process. They can stimulate cell migration, growth, proliferation, and induce stem cell differentiation towards the desired direction. Commonly growth factors used in skin bioprinting are the epidermal growth factor (EGF), fibroblast growth factor (FGF), vascular endothelial growth factor (VEGF), and platelet-derived growth factor (PDGF), since they can improve wound healing thanks to upregulating the proliferation of hDFs, hEKs and endothelial cells, and even increasing collagen production (358,359). The use of different bioactive factors can also be combined, to simultaneously boost regenerative effects, like incorporating BMP-2 and VEGF for promoting angiogenesis and cell proliferation at the same time (360).

1.3.5.1.1 Cells

Native skin bears at least a dozen of differentiated cell lineages and stem cell types, with some of them with a specific related position among them. Currently, the main cell types that are used for skin bioprinting are hEKs, hDFs, and stem cells, such as MSCs, adipose-derived stem cells (ADSCs), ESCs, amniotic fluid-derived stem cells (AFSCs),

iPSCs, and BM-MSCs.

hDFs are the principal cell type of the dermis; they can promote wound healing by generating collagen and EL, and regulate the function of epidermal cells by producing FGF (361). hEKs are the main cells of the epidermis; they migrate from the basal membrane towards the stratum corneum during the keratinization process. hEKs are the cells that synthetize Kt in the epidermis (362) and increase their replication rate during stages of injury, inflammation, or disease (363). Therefore, hDFs and hEKs are generally used together for skin 3D bioprinting.

In ideal conditions, a 3D bioprinted skin should show functional characteristics such as natural pigmentation levels, skin appendages (sweat glands, sebaceous glands, hair follicles), and functional blood vessel networks. Endothelial cells have been used in skin bioprinting strategies in an attempt to promote angiogenesis (115,364,365). Also, melanocytes (MCs) have also been used to try to reproduce the native skin pigmentation, since it occurs by the transfer of melanin from MCs to hEKs (366). Then, hEKs and MCs are expected to be co-bioprinted for 3D skin bioprinting for solving the pigmentation issue. It has been seen that hair papilla cells (HPCs) and hair follicle stem cells (HFSCs), which include hair follicle dermal stem cells (HFDSCs; which play an important role in the maintenance of the amount of HPCs), and hair follicle epidermal stem cells (HFESCs; which show the ability of regenerating skin tissue and produce epidermal structures, such as sweat glands, hair follicles, and sebaceous glands), play an important role in the regeneration of hair follicles (367).

Skin TE strategies are being focused on the use of autologous cells for avoiding graft rejection and personalizing treatments. In patients that need a skin graft the cell obtaining is difficult since the injury is usually extensive, so alternative cell sources must be used. With the emergence of stem cell technology, several stem cell types have been studied to be applied in skin TE. Due to the easy availability of adipose tissue, and the popularity of plastic surgery liposuctions, high quantities of ADSCs can be obtained from tissue isolation to be applied in bioprinting. ADSCs can exert several positive functions in skin regeneration, such as liberating cytokines that promote hDFs migration in the wound healing process, and promote neovascularization by secreting VEGF (368). MSCs hold great therapeutic potential for tissue regeneration and repair, since they have been seen to increase the epithelialization, accelerate wound closure, generate granulation tissue, and promote angiogenesis in acute and chronic wounds (369). It has also been

demonstrated that BMSCs represent an ideal source of stem cells for skin appendages regeneration, since they play an essential role in tissue regeneration and wound repair (370). AFSCs are also an interesting source of stem cells for regenerative medicine due to their multipotency, immunomodulatory activity, lack of immunogenicity, high proliferation rate, and, unlike ESCs, AFSCs do not produce teratomas in immunodeficient mice (370,371). As well, these cells are an easy to isolate, achieving high outcomes of cells from only 2 ml of amniotic fluid (371,372). On the other hand, iPSCs shows the great potential of being able to differentiate *in vivo* into any cell type of the three germ layers. It has been seen that iPSCs can differentiate into skin cell types with the ability to generate a differentiated epidermis with glands and hair follicles (373), as well as into iPSCs-derived hEKs, hDFs, and MCs (364). Stem cells hold great potential in the Skin TE field, although several mechanisms by which these cells help the wound healing process remains unclear, and it is not easy to avoid potential risks such as tumorigenicity.

1.3.5.1.2 Biomaterials for skin 3D bioprinting

The mechanical performance of biomaterials used in bioinks formulation need to be improved while maintaining a good biocompatibility. Previous studies have reported that mixing PCL with gelatine could overcome the drawbacks of both natural and synthetic biomaterials, improving the physical, chemical, and mechanical properties while maintaining good biocompatibility (374–377). It has also been seen that blending PCL with chondroitin sulphate allowed to fabricate, *via* electrospinning, a 3D bilayered structure that could mimic the ECM hierarchy of found in the skin. This nanofibrous 3D structure allows the inflow of host cells, grafting successfully in the wound bed, preventing water loss, and offering a base for the KC migration (378). As well, several studies have shown that combining GelMA with natural polymers could significantly enhance its mechanical properties (379). The addition of HA (380) or collagen (381) to GelMA was evidenced to improve the rheological an biological features over GelMA alone.

1.3.5.2 Dermis bioprinting

The structural reliability of the dermal layer is strongly related to the flexibility and elasticity of the skin. The ability to reconstruct the continuity and integrity of a dermal skin tissue structure using 3D bioprinting has provided a significant progress towards the effective skin wound repair. Researchers have already achieved to create dermal

substitutes using laser-assisted bioprinting by laying hDFs on a commercial collagen matrix (MatriDerm®) (79). This dermal substitute was grafted over a full-thickness skin wound in nude mice. After 11 days blood vessel formation was observed at the wound bed and edges, and normal skin was found growing into the printed dermis. 3D bioprinting of dermis has also been achieved using composite biomaterials, such as polyelectrolyte gelatine-CS hydrogels (117), which inherent antimicrobial activity and haemostatic properties made it an adequate blend for skin wound healing applications. This hydrogel was showed good high shape-fidelity printability at RT, as well as good biocompatibility towards hDFs.

1.3.5.3. Full-thickness skin 3D bioprinting

Skin 3D bioprinting enables the production of customized autologous skin for a specific patient wound, or even to perform *in situ* bioprinting of the patient. Studies have shown that 3D bioprinted skin could closer recreate the native skin properties after maturation. Lee *et al*. (382) used Col I as a dermal skin matrix, and hEKs and hDFs were printed to reproduce a bilayered skin construct. The optimization of the bioink bioprinting parameters is essential to maximize the cell viability, as well as the cell seeding densities in the dermis and epidermis for physiologically mimic the human native skin. The 3D bioprinted skin tissue showed outstanding results compared to native human skin regarding the histological and immunostaining assays. Likewise, Cubo *et al*. (352) used a free-form fabrication bioprinting technique to fabricate also a bilayered skin with bioinks based on human plasma and human hEKs and hDFs. Similarly, Pourchet *et al*. (353) used a scaffold-free approach to also bioprint a bilayered skin, where hDFs were embedded in the dermal equivalent matrix, and hEKs seeded on the top. They used a mixture of gelatine, alginate, and fibrinogen, obtaining a nicely developed skin bioink that not only assured to not damage the cells due to shear forces thanks to its shear-thinning properties, but also demonstrated to be highly 3D-printable. In addition, their printed skin also showed similar histological and immunostaining characteristics that resembled the human native skin structure. To extend the cross-linking duration and overcome the poor printability of collagen-based biomaterials, researchers have designed, and printed scaffolds structured as a bilayered membrane (BLM) composed by an external layer of a PLGA membrane, and an internal layer of alginate, trying to reproduce the epidermal and dermal structure, respectively (383). The alginate layer promoted *in vitro* cell proliferation and adhesion, while the PLGA membrane maintained the hydrogel

moisture and prevented bacterial infection.

In situ bioprinting can be described as the deposition of cells over the patient's injury for wound healing, enabling the skin maturation directly on the wound bed. The accurate bioprinting of cells over the wound bed, reducing the number of multiple surgeries, or avoiding time-consuming and expensive *in vitro* differentiation are some of the advantages that the *in situ* bioprinting technology shows towards the burn wound treatment (384). Inkjet bioprinting was used to carry out *in situ* bioprinting on nude mice full-thickness injured backs with wounds of 7.5 cm^2 using a hDFs -laden bioink based on a fibrinogen-collagen blend, furtherly seeding 10^7 hEKs/cm^2 on top of the hDFs layer (385). The developed device was as a portable, relatively affordable, user-friendly *in situ* bioprinting system that was able to scan the wound bed continuously with a 3D laser scanner, while converting the topographical scanned area into a 3D model. The results showed an accelerated wound closure of < 15% of the starting wound size after 14 days, reaching the full wound closure 21 days after surgery. The regenerated skin showed a similar dermal structure and composition compared to native skin.

The aforementioned studies have enlightened the feasibility of the 3D bioprinting of artificial skin substitutes, acting as precursors for clinical applications. Besides wound healing, skin 3D bioprinting can also be used for creating *in vitro* models for personalized drug screening or cosmetic tests, as well as skin pathological models for pathophysiological research (386).

2. HYPOTHESIS

3D printing is an emerging technology that evolved fast since it was firstly developed, showing amazing applications in several fields for the past few decades. Regarding the biomedical field, it has been used for prototyping biomedical devices, translating clinical imaging to 3D physical objects to help the planning of surgical approaches, creating customized prosthesis, and even for bioprinting artificial tissues. However, these applications have required the selection of suitable biomaterials that should be biocompatible and able to provide support to be used with cells, as well as the development of protocols and bioinks to produce artificial tissues.

This PhD thesis is based on the following hypothesis:

1) RE seeks to fabricate biomimetic implants that reproduce the mechanical and biological features of the native target tissue. For this purpose, biomaterials with tailorable properties are the most attractive. We hypothesize that the validation of 1,4-Butanediol thermoplastic polyurethane (b-TPUe) as a novel material for 3D bioprinting applications would not only enable the production of scaffolds capable of sustaining high load-bearing environments, but also, the development of elastic biomedical devices as well.

2) The use of natural biomaterials has been one of the most attractive strategies for the design of bioinks for skin TE, since they show high biocompatibility. However, the obtained extracellular environment usually lacks complexity and similarity towards the target tissue. One of the growing trends in TE is the development of biomimetic bioinks for obtaining biological constructs that resembles more closely the native tissue. Here, we hypothesize that the use of skin-related elements, such as Col I, DS, HA, EL, Kt, and sphingolipids (Sph), used in a layer-specific structure and in combination with hMSCs, hDFs and hEKs, would allow to obtain bioinks for producing full-thickness skin models and substitutes with enhanced biomimicry.

3. OBJECTIVES

Main objectives

1) To validate the 1,4-Butanediol thermoplastic polyurethane elastomer (b-TPUe) derivative filament as a novel elastic and high load-bearing environment 3D bioprinting material for cartilage regeneration.

2) To develop a three-layered skin model/substitute using layer-specific biomimetic bioinks for its future application in skin 3D bioprinting.

Specific objectives (per chapters):

Specific objectives of *Chapter I:*

1) To characterize the frictional and elastic behaviour of b-TPUe scaffolds compared to PCL and PLA.

2) To determine the *in vitro* biocompatibility of b-TPUe with toxicity, proliferation and viability assays using hMSCs.

3) To analyse the ability of b-TPUe scaffolds to support hMSCs chondrogenic differentiation.

4) To determine the *in vivo* biocompatibility and integration of b-TPUe scaffolds in mice.

Specific objectives of *Chapter II:*

1) To design a biomimetic hydrogel formulation mixed with skin extracellular matrix-related components.

2) To physically characterize the biomimetic Agarose/Col I/DS/HA/EL (ACDHE) hydrogel formulation.

3) To analyse the wound healing ability of the biomimetic ADCHE hydrogel

formulation.

4) To develop a bi-layered ADCHE hydrogel using hDFs and hMSCs.

Specific objectives of *Chapter III:*

1) To biofabricate a three-layered skin model/substitute using layer-specific biomimetic bioinks, adding an epidermal layer to the dermo-hypodermal bilayered hydrogel designed in Chapter II.

2) To physically characterize the three-layered hydrogels.

3) To evaluate, *in vitro* and *in vivo*, the biocompatibility and functionality properties of the three-layered hydrogel as a skin substitute.

CHAPTER I:
Validation of an elastic 3D printing material for cartilage TE application

1. Background

The biofabrication research field is currently emerging as a powerful approach for the design and production of artificial living tissues that are urgently required for regenerative medicine and disease models (387). Several lesions that provoke tissue loss require replacements, for instance, cartilage, as an avascular and stratified tissue, presents a limited capacity of repair. However, the clinical surgical treatments, such as the autologous chondrocyte implantation (ACI) or the matrix-induced ACI (MACI), which uses a bilayer type I/III collagen membrane, lack of long-term effectiveness (388–390). Mosaicplasty, a treatment for focal chondral lesions, shows results that are relatively acceptable for the first 2 years but develops a sudden failure rate (approximatively 55%) over the successive 2 years (391). Currently, the strategies for cartilage repair are concentrated on Tissue Engineering (TE) (392), consisting in the creation of a complex material that biologically mimics the native tissue. Hence, many biomaterials are being used to create scaffolds for cartilage TE, such as fibrin, silk, HA, CS, PLA or PCL (393), but, on one hand, natural-based biomaterials do not show enough mechanical integrity, and on the other hand, synthetic-based biomaterials lack sufficient elasticity. Nevertheless, new biomaterials that aim to get close to the biomechanical properties of native cartilage are being developed. In the last few years the 3D bioprinting technology has shown promising results in the biofabrication of artificial tissues for TE applications (394). This emerging technology uses CAD and CAM techniques, which in combination with the layer-by-layer fabrication nature of 3D printing, allows to create structures with different geometries while controlling the spatial distribution of cells, biomaterials, and growth factors (395,396). Furthermore, 3D bioprinting brings advantages to the clinical field such as shorter fabrication time, higher precision than conventional TE techniques, and tailored production (397).

The main 3D bioprinting techniques are extrusion-based, laser-assisted, inkjet and stereolithography (SLA) (398). Each of these approaches shows both advantages and disadvantages regarding material availability, printing resolution, speed, and precision. Among these techniques, extrusion-based bioprinting is the most extended as it offers the possibility to print a wide variety of biomaterial viscosities and is the most adaptable technology to be transferred to the clinical field (399). Additionally, there are several commercially available extrusion-based bioprinters, and they can also be adapted for testing novel biomaterials. Although this approach holds great promises for TE and regenerative medicine, as an emerging technology it also entails some bottlenecks. One

of the main challenges is the restricted accessibility of biomaterials necessary to produce constructs that can properly mimic the native tissue properties. The most common type of material used for this purpose are hydrogels, since they can offer a suitable 3D microenvironment that mimics the extracellular matrix (ECM) of natural tissues, promoting cell attachment and proliferation (400). However, hydrogel scaffolds usually lack mechanical strength and structural integrity, therefore, their mechanical properties need to be tuned or combined with synthetic stiffer biomaterials to enhance its mechanical properties (401).

Several synthetic biomaterials such as PLA (402–404), PCL (405–408) or polylactic-co-glycolic acid (PLGA) (409–412) have been used to generate bioprinted scaffolds for TE applications. However, these biomaterials do not easily achieve to mimic the native tissue mechanical characteristics. The stiffness of porous scaffolds produced using rigid biomaterials, such as PLA (413), are in the MPa magnitude order comparable to those found in hard tissues such as porous bone (414). Therefore, significant efforts are being made for engineering flexible tissues that suffer mechanical loading such as ligaments, tendons, cartilage, blood vessels, skin, or muscles (415).

On other hand, polyurethane elastomers are a type of adaptable synthetic biomaterials broadly applied to biomedical purposes because of their biocompatibility and good mechanical properties (416–418). Recently, a novel elastic 3D printing filament consistent of a 1,4-Butanediol Thermoplastic Polyurethane (b-TPUe) derivative shows a combination of mechanical properties that makes it a promising candidate for TE (419).

In this study we evaluate, for the first time, the potential use of b-TPUe filament as a new 3D bioprinting material for biomedical applications. We carried out a rheological characterization to analyse their mechanical properties (in shear and compression) and a tribological study to evaluate the frictional behaviour in synovial fluid-lubricated b-TPUe-cartilage tribopairs. Moreover, we compared *in vitro* and *in vivo* the biocompatibility of b-TPUe 3D printed scaffolds versus PCL and showed the potential application of this material for cartilage tissue engineering. Finally, we described the induced chondrogenic differentiation of MSCs isolated from infrapatellar fat pad when cultured in 3D bioprinted b-TPUe scaffolds. In conclusion we present a novel use of b-TPUe filament with potential to support the development of cartilage-like phenotype as a promising TE biomaterial.

2. Materials and Methods

2.1. Patients

Human infrapatellar fat pad, cartilage tissue and synovial fluid were obtained from patients with knee OA during joint replacement surgery. Ethical approval for the study was obtained from the Ethics Committee of the Clinical University Hospital of Málaga, Spain. Informed patient consent was obtained for all samples used in this study. None of the patients had a history of inflammatory arthritis or crystal-induced arthritis. Hoffa's fat pad was harvested from the inside of the capsule excluding vascular areas and synovial regions. Human articular cartilage was obtained from the femoral side, selecting the non-overload compartment. Only cartilage that looked normal macroscopically was used for this study. Samples collected at joint arthroplasty were transported to the laboratory in Dulbecco's modified Eagle's medium (DMEM; Sigma, St. Louis, MO, USA) with 1% penicillin/streptomycin (P/S). Synovial fluid (SF) was pooled from knee joints and mixed on an orbital shaker. Only samples that were free of blood contamination were used, as assessed visually. SF was stored at -20°C between testing sessions (420).

2.2. Isolation and culture of human MSCs from infrapatellar fat pad

Infrapatellar fat pad tissue was minced and digested with an enzymatic solution of 1 mg/mL collagenase type IA (Sigma) and incubated in shaking at 37ºC for 1 h. Once digested, collagenase was removed with a single wash of sterilized phosphate-buffered saline (PBS), followed by two washes of DMEM supplemented with 10% foetal bovine serum (FBS) (Sigma). The cell pellet was resuspended in DMEM supplemented with 10% FBS and 1% Penicilin/Sreptomycin, placed into tissue culture flasks, and cultured at 37 ºC in a 5% CO_2 atmosphere. After 48 h the medium was removed to discard non-adherent and dead cells (421). When 80% of confluence was reached, cells were released with Tryple Express (Gibco) and sub-cultured.

2.3. Bioprinting process

A Regemat 3D V1 bioprinter (REGEMAT 3D S.L., Spain) was used for 3D printing with a direct extruder to fabricate the scaffolds (422). Commercial PCL (3D4Makers, 1.75 mm filament, printing temperature: 70 - 90 ºC; semi-crystalline aliphatic polyester) was melted at 75 ºC and printed at rate of 1.1 mm/s. Commercial PLA (Smart materials 3D, Spain, 1.75 mm filament, printing temperature: 190 - 210 ºC; polymerized polylactic acid) was melted at 200 ºC and printed at rate of 1.2 mm/s. Commercial b-TPUe (Recreus industries S.L., 1.75 mm filament, printing temperature: 200 - 230 ºC; based on methylene diphenyl diisocyanate (MDI) and 1,4-Butanediol) was

melted at 200 ºC and printed at rate of 1.4 mm/s. Printing parameters were optimized for each material in order to obtain the best printability and scaffold quality layout. PCL, PLA and b-TPUe scaffolds were designed to be extruded with triangular patterns for the infill with a pore size of 0.6 mm, solid walls consisting of a perimeter of 0.4 mm width, and 3 solid layers for the bottom, with a 0.2 mm layer height (**Figure 6A**). The scaffolds were printed as 3D cylindrical frameworks in a triangular inner lattice from alternately stacking filament fibres (**Figure 6B**). For 3D bioprinting with cells, the Regemat 3D V1 bioprinter was placed in a laminar flow hood. In the same process, the thermal extruder unit of the bioprinter was used to print the scaffolds, and then the syringe unit of the bioprinter was used to seed the cell suspension into the porous structure with a 200 µm diameter needle (1 x 10^5 cells/scaffold). PCL was used as a control material instead of PLA as it is more used for biomedical purposes than its counterpart. For all *in vitro* assays the scaffold dimensions were designed to fit in a 24-well plate (10 mm in diameter and 3 mm in height; 15 layers), with smaller dimensions for the *in vivo* assays (5 mm in diameter and 3 mm in height; 15 layers). Once bioprinted, the scaffolds were introduced in a 24-well plate and incubated for at least 1 h to allow the cells to adhere to the fibres. Finally, the scaffolds were submerged in culture medium containing DMEM supplemented with 10% FBS and 1% P/S and then, stored at 37 ºC in a 5% CO_2 atmosphere. Scaffolds used to support MSCs chondrogenic differentiation were cultured in DMEM supplemented with 10% FBS, 1% P/S, 50 µg/µL l-ascorbic acid 2-phosphate (Sigma), 40 µg/mL proline (Sigma), 1% insulin-transferrin-selenium (ITS) (Gibco), 40 µg/µL L-proline (Sigma), and 10 ng/mL TGF-β3 (423).

2.4. Tribological tests

A ball-on-three plates tribometer was adapted to a rheometer (Anton Paar, Austria) to interrogate the lubricating behaviour of the different materials. The contact consisted in a plastic ball (made of PLA, PCL or b-TPUe) that slides along three cartilage surfaces (cartilage disks with a diameter of 5 mm) lubricated by synovial fluid. The MCR501 rheometer head (Anton Paar) was used to calculate the friction coefficient. A schematic diagram of the test set-up is shown in **Figure 7A**. In this set-up, a ball is pressed at a given normal force F_N against three plates that are mounted on a movable stage. The experimental protocol was as follows. First, the test rig was assembled, and 400 µL of SF was added. This amount was enough to fully immerse the three-point contacts to a depth of 1 mm. Next, temperature was stabilized at 25 ºC and the plastic ball was loaded against the cartilage plates. Then, the ball was made to slide over the plates at a controlled

(decreasing) speed V, from 2500 to 0.1 rpm under a normal force of F_N = 1 N (5 s per data point), while the resulting torque T sensed by the ball was monitored. The friction coefficient μ was computed with $\mu = T/(F_N R)$ being R the radius of the ball.

2.5. Mechanical assays

Specimens for mechanical assays were printed with 20 mm in diameter and 5 mm in height, solids and porous to analyse the effect of the infill over the mechanical characteristics of the scaffold (n = 3). Porous samples were printed with the same pattern of the ones used for cell culture tests. A MCR302 (Anton Paar) head was used to carry out rheological measurements at 25 ºC. A three-step test was designed to obtain information on the compression and shearing characteristics of specimen. First, the scaffold was placed onto the base of the rheometer. Then, the rheometer head was approached at a constant speed (10 µm/s) up to a normal force of 40 N. Next, the specimen was oscillatory sheared according to a strain amplitude of 0.00001% at a frequency of 1 Hz and normal force of 40 N to determine the shear viscoelastic moduli and, finally, the upper plate was separated at a constant speed (10 µm/s).

2.6. Cell viability assay

Cell viability in the 3D printed scaffolds was determined on days 7 and 21 after bioprinting using Live/Dead™ Viability/Cytotoxicity Kit (Invitrogen). The printed constructs were incubated in PBS containing calcein AM (2µM) and ethidium homodimer (4 µM) at 37 ºC for 30 min to stain live and dead cells (424). Scaffolds were imaged by confocal microscopy (Nikon Eclipse Ti-E A1, Amsterdam, Netherlands) and analysed using NIS-Elements software (Amsterdam, Netherlands).

2.7. Scanning electron microscopy (SEM)

The morphology and structure of b-TPUe scaffolds were analysed using a variable-pressure and environmental scanning electron microscope (ESEM) FEI, mod. Quanta 400 (Oregon, USA). The analysis was performed in high vacuum mode to characterize the surface structure of scaffolds and cell growth. Samples were fixed with 2% glutaraldehyde and then, were rinsed in 0.1 M cacodylate buffer and incubated overnight at 4 °C. For critical point, the samples were then maintained with Osmium tetroxide 1% RT during 1h and dehydrated in a series of ethanol solutions (50%, 70%, 90%, 100%, 100%, 100%), by soaking the samples in each solution for 15 min. Subsequently, samples were critical point dried (Anderson, 1951) in a desiccator (Leica EMCPD300), and covered by evaporating them in a carbon evaporator (Emitech K975X).

2.8. *In vitro* cytotoxicity test

MSCs culture medium aliquots were conditioned with b-TPUe samples as previously described (425). Briefly, b-TPUe sterilized scaffolds for a total mass of 3 g were placed in T-75 tissue culture flasks and soaked in 100 mL of complete cell culture medium for 10 days at 37 °C in a cell culture incubator on a rocking platform. Control medium was incubated in parallel, but without the b-TPUe scaffolds. MSCs were plated in a 6-well plate at 1 x 10^5 cells/well. After 24 h the medium was replaced with a mix of a 1:1 fresh medium: b-TPUe-conditioned medium or with fresh control medium. Cell growth was analysed at different time points: 1, 3, 5 and 7 days using AlamarBlue® assay (Bio-Rad Laboratories, Inc., manufactured by Trek Diagnostic System. U.S.). Cells were incubated with AlamarBlue® solution at 37 ºC for 3 h. Fluorescence of reduced AlamarBlue® was determined at 530/590 nm excitation/emission wavelengths (Synergy HT, BIO-TEK).

2.9. Cell proliferation assay

Cell proliferation was analysed using AlamarBlue® assay after 1, 3, 5, 7, 14 and 21 days. The scaffolds were incubated with AlamarBlue® solution at 37 ºC for 3 h. Fluorescence of reduced AlamarBlue® was determined at 530/590 nm excitation/emission wavelengths.

2.10. RNA isolation and real time-PCR analysis

Total cellular RNA was isolated using TriReagent (Sigma) and reverse transcribed using the Reverse Transcription System kit (Promega). Real-time PCR was performed using the SYBR-Green PCR Master mix (Promega) according to the manufacturer's recommendations. PCR reactions were performed as follows: an initial denaturation at 95 °C for 2 min, 40 cycles of 95 °C for 5 s followed by 60 °C for 30 s, and final cycle of dissociation of 60 – 95 °C. The gene expression levels were normalized to corresponding GAPDH values and are shown as relative fold expression to the control sample. All samples were analysed in triplicate for each gene. Primer sequences used are shown in **Table 8**.

Table 8. Primer sequences

Gene	Forward	Reverse
Col 1	ATGGATGAGGAAACTGGCAACT	GCCATCGACAAGAACAGTGTAAGT
Col 2	GAGACAGCATGACGCCGAG	GCGGATGCTCTCAATCTGGT
Acan	AGGATGGCTTCCACCAGTGC	TGCGTAAAAGACCTCACCCTCC
Sox 9	GAGCAGACGCACATCTC	CCTGGGATTGCCCCGA
Gapdh	TGCACCACCAACTGCTTAGC	GGCATGGACTGTGGTCATGAG

2.11. Glycosaminoglycan quantification

The dimethylmethylene blue (DMMB) assay was used to study the glycosaminoglycans (GAGs) content as previously described (426). Briefly, 50 µL of papain-digested sample harvested at day 21 were added in triplicate to a 96-well plate and combined with 200 µL of DMMB dye, and the absorbance at 540 nm was immediately read. To determine the GAGs content of the samples chondroitin sulphate from shark cartilage (Sigma) was used as standard.

2.12. Type II Collagen quantification

Type II collagen content produced in the scaffolds was quantified by ELISA (Type II Collagen Detection kit #6018; Chondrex, Redmond, WA) according to manufacturer's instruction. Briefly, samples were digested using pepsin in 0.5 M acetic acid: collagen ratio of 1:10 (w/w) for 2 days. Once digested, samples were incubated at 4 ºC overnight in elastase: collagen ratio of 1:10 (w/w). Then, standard and samples were placed in a pre-coated 96-well plate with capture antibodies and incubated for 30 min. The detection antibody was added and incubated for 1.5 h and then washed. The plate was incubated with streptavidin peroxidase for 1 h, washed, and incubated with ortho-phenyldiamine (OPD) solution for 30 min. A solution of 2N sulphuric acid was added to stop the reaction, and the content of type II collagen was quantified by absorbance at 490 nm.

2.13. *In vivo* assays

In vivo assays were carried out in accordance with the approved guidelines of University of Granada following institutional and international standards for animal welfare and experimental procedure. The Research Ethics Committee of the University of Granada approved all experimental protocols. Experiments were performed in immunocompetent CD-1 mice and immunodeficient NOD SCID (NOD.CB17-Prkdcscid/NcrCrl) (NSG) mice purchased from Charles River (Barcelona, Spain). To evaluate the biocompatibility, PCL and b-TPUe cell-free scaffolds were transplanted into

two independent small subcutaneous pockets made on the back of CD-1 mice anesthetized by isoflurane inhalation (n = 5 per group). In addition, MSCs cell-laden scaffolds cultured for 21 days were implanted into two independent small subcutaneous pockets created on the back of NSG mice anesthetized by isoflurane inhalation to evaluate engraftment. Cell-laden or cell-free scaffolds were implanted in each pocket with a single biomaterial per mouse (b-TPUe or PCL) (n = 5 per group). Animals were maintained in a micro-ventilated cage system with a 12-h light/dark cycle with food and water *ad libitum*. Mice were manipulated within a laminar airflow hood to maintain pathogen-free conditions. Three weeks later, mice were sacrificed *via* an overdose injection of an aesthetic, and the scaffolds were photographed to evaluate the implantation within the surrounding mouse tissue and recovered for histological analyses. For the histological analysis, samples were dehydrated, embedded in Technovit 7200 and polymerized. The blocks were sectioned with a diamond-coated band saw (Exakt 310 CP) and then, grounded, and polished with a high precision grinder (Exakt 400). The total histological processing, including Toluidine Blue and Masson staining, were performed by Histology Unit of BIONAND (Málaga, Spain) following the Donath and Bruener cutting/grinding technique (427).

2.14. Statistical analysis

Statistical calculations were performed using SPSS 13.0 software for Windows (SPSS, Chicago, IL, USA). All graphed data represent the mean ± standard deviation (SD) from at least three experiments. Differences between treatments were tested using the two-tailed Student´s T test. Assumptions of Student´s T test (homoscedasticity and normality) were tested and assured by using transformed data sets [log(dependent variable value + 1)] when necessary. P-values < 0.05 (*) and P-values < 0.01 (**) were considered statistically significant in all cases.

3. Results

3.1. Scaffold fabrication

3D b-TPUe scaffolds were designed with a regular geometry and structure to enable an adequate cell bioprinting (**Figure 6A**) and successfully fabricated with the desired shape and dimensions, like the CAD model (**Figure 6B**). Scanning electron microscope (SEM) images (**Figure 6C and D**) show the obtained scaffold pores and filament surfaces and demonstrate that the thickness of the fibres of the b-TPUe printed scaffolds (200 - 400 µm) is maintained during the fabrication process (**Figure 6E-J**). As

can be clearly seen, the pores are large, ranging from 500 to 700 µm (**Figure 6C and D**) and have a regular structure, uniformly distributed, and interconnected.

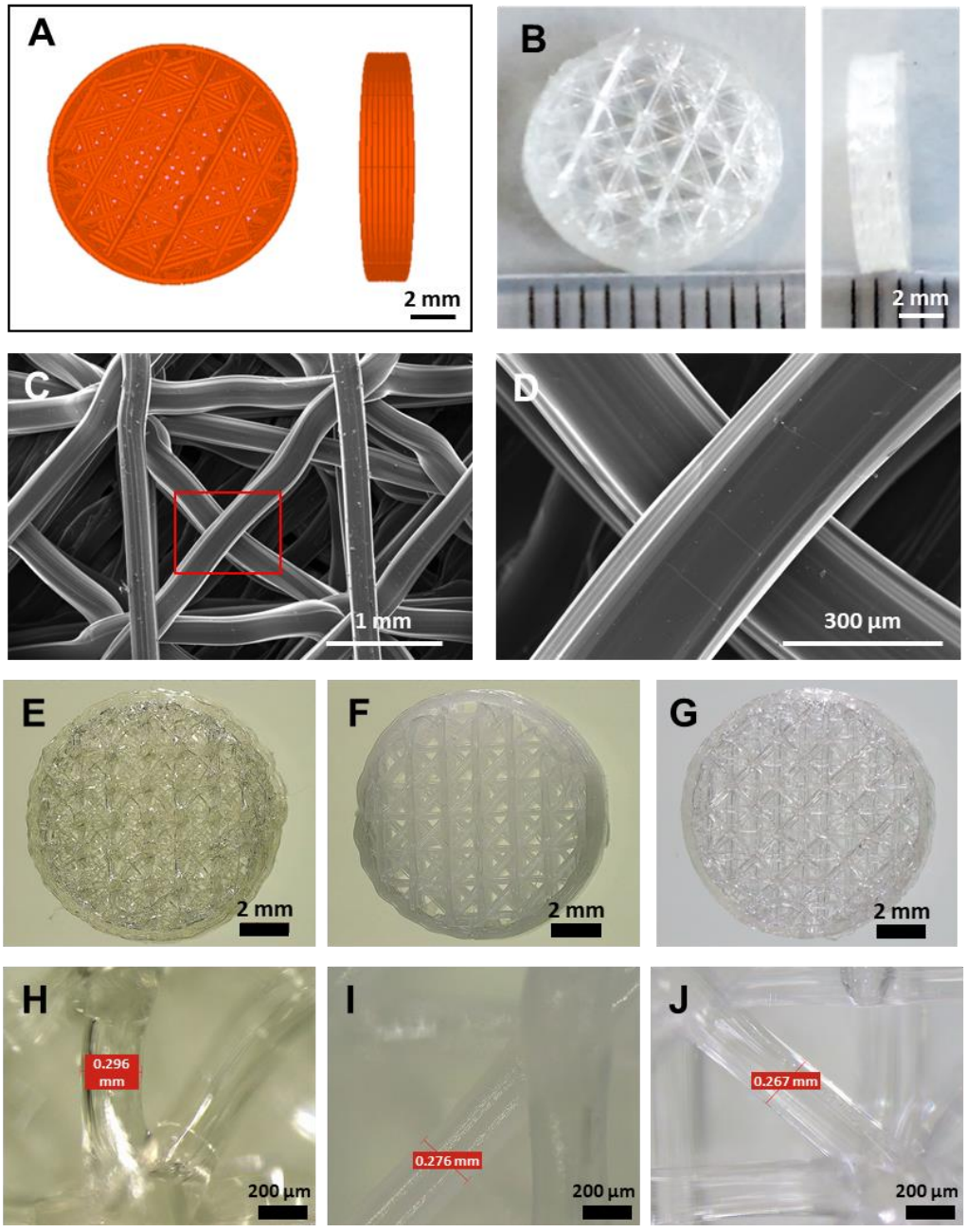

Figure 6. b-TPUe scaffolds design: (A) CAD model of the scaffold design. (B) 3D printed b-TPUe scaffold (10 mm in diameter and 3 mm in height). (C, D) SEM images of the top surface of b-TPUe 3D printed scaffolds (scale bars: 1 mm and 300 µm respectively). (E-G) Macroscopic view of b-TPUe, PCL and PLA scaffolds, respectively. (H-J) Scaffold fiber width of b-TPUe, PCL and PLA scaffolds, respectively.

3.2. Frictional test

The frictional behaviour of the different plastics used in this work is exemplified in **Figure 7A and B**. For this, plastic-cartilage point contacts were lubricated by synovial fluid and data are plotted in terms of a Stribeck curve, where friction coefficient is represented as a function of the sliding speed for a constant normal load of 1 N. Only for b-TPUe, the contact operates in the full film lubricated regime as demonstrated by the increase in friction for large sliding speeds. As observed, a lower friction was measured for b-TPUe, with average friction coefficients (μ) under 0.1, closer to the cartilage-to-cartilage interaction (0.03 μ) (428), followed by PCL and PLA, with average μ above 0.1, as seen in **Figure 7B**.

3.3. Compression test

The compression curves of PLA, PCL, b-TPUe and cartilage are shown in **Figure 7C**. These strongly non-linear curves clearly demonstrate that b-TPUe is more compliant than the other biomaterials investigated (PLA and PCL). Also, unlike PLA and PCL, results for solid (s) and porous (p) b-TPUe scaffolds showed different behaviours in compression. Interestingly, porous b-TPUe scaffolds were significantly softer than their solid counterparts, suggesting that b-TPUe scaffold elasticity can be tailored by changing the porosity. So, b-TPUe scaffolds with greater porosity present a mechanical behaviour closer to the one of native cartilage. In addition, for low strains ε, the mechanical behaviour of b-TPUe was closer to that observed in natural cartilage when compared with PCL or PLA. Moreover, the shear moduli obtained in the second interval of the test showed a clear correlation with the compression data, again demonstrating that b-TPUe exhibited a much lower storage modulus in contrast to the conventional plastics, PCL, and PLA (**Figure 7D**).

3.4. Effects of b-TPUe-conditioned medium on MSCs proliferation

We conducted a proliferation assay to evaluate if the exposure to b-TPUe could have a negative effect in the proliferative potential of MSCs. Results showed no adverse effects in the proliferative potential of MSCs cultured in b-TPUe-conditioned medium for 7 days when compared with MSCs cultured with control medium (**Figure 8A**).

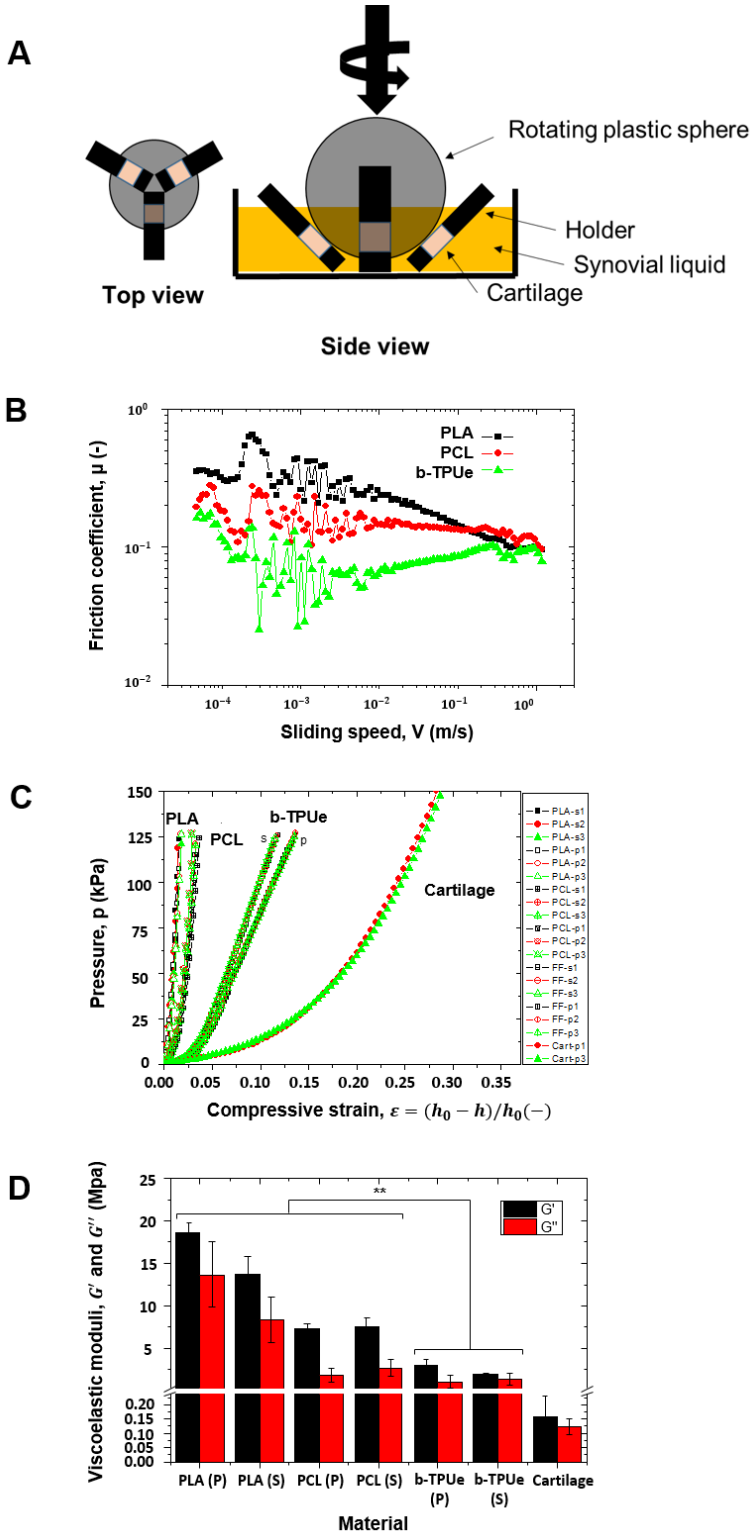

Figure 7. Tribological and mechanical characterization. (A) Schematic diagram of the tribological set-up. (B) Frictional behaviour of PLA (black), PCL (red) and b-TPUe (green). (C) Compression curves corresponding to the studied samples (s: solid; p: porous). (D) Linear viscoelastic moduli (G' and G'') for the biomaterials studied (** = $p < 0.01$). Graphs created using the Origin 9.0 software.

3.5. Proliferation and viability of MSCs cultured in b-TPUe scaffolds

Cell proliferation of MSCs cultured in b-TPUe bioprinted scaffolds was evaluated with an AlamarBlue® assay. PCL filament was used as a control material since it is a reference biomaterial used in cartilage bioprinting (429–432). As can be observed in **Figure 8B**, cell proliferation increased from day 1 to day 21 with a significant increase at day 7 of culture in both bioprinting biomaterials, while at day 21 no significant differences were observed in the proliferation rate between cells printed in b-TPUe and those in PCL control scaffolds (**Figure 8B**).

The viability of MSCs was also evaluated to validate the biocompatibility of b-TPUe printed scaffolds using a live/dead assay. Confocal images (**Figure 8C**) show a majority of green viable MSCs covering both b-TPUe and PCL scaffold fibre surfaces at day 7 and 21 after bioprinting.

3.6. Chondrogenic differentiation of MSCs cultured in b-TPUe bioprinted scaffolds

To investigate the capacity of b-TPUe scaffolds to support the induction of cartilage-like phenotype, chondrogenic key markers were evaluated by RT-PCR after 21 days of culture of bioprinted cell-seeded b-TPUe scaffolds under chondrogenic conditions. Cells extracted from b-TPUe bioprinted scaffolds cultured under chondrogenic media showed a significant increment in type II collagen, aggrecan and Sox9 gene expression when compared with cells grown in monolayer and onto b-TPUe scaffolds without chondrogenic media (**Figure 9A**).

The ECM produced under induction of chondrogenic differentiation was evaluated assessing glycosaminoglycans (GAGs) and type II collagen concentration in cell culture supernatants of MSCs monolayers and printed MSCs b-TPUe scaffolds cultured with (Diff) or without (CTL) chondrogenic medium for 21 days. The GAGs analysis showed that b-TPUe printed scaffolds in chondrogenic conditions produced a high significant number of GAGs compared to control b-TPUe scaffolds or monolayer conditions (**Figure 9B**). Similarly, collagen type II production was also markedly greater in b-TPUe printed scaffolds cultured under chondrogenic conditions at 21 days compared to control b-TPUe scaffolds and monolayer conditions (**Figure 9C**).

Moreover, SEM images showed cell growth and wide cell spread throughout the scaffold over the b-TPUe filament after 21 days of cell growth with and without differentiation conditions. It is relevant to note that cells attached to the filament surface and junctions *via* formation of filopodia and started to form a network of cell and matrix (**Figure 9D-F**). Also, an enhanced cell growth that covered the pore spaces (**Figure 9G**

and H) and over the filament surfaces was observed (**Figure 9I**).

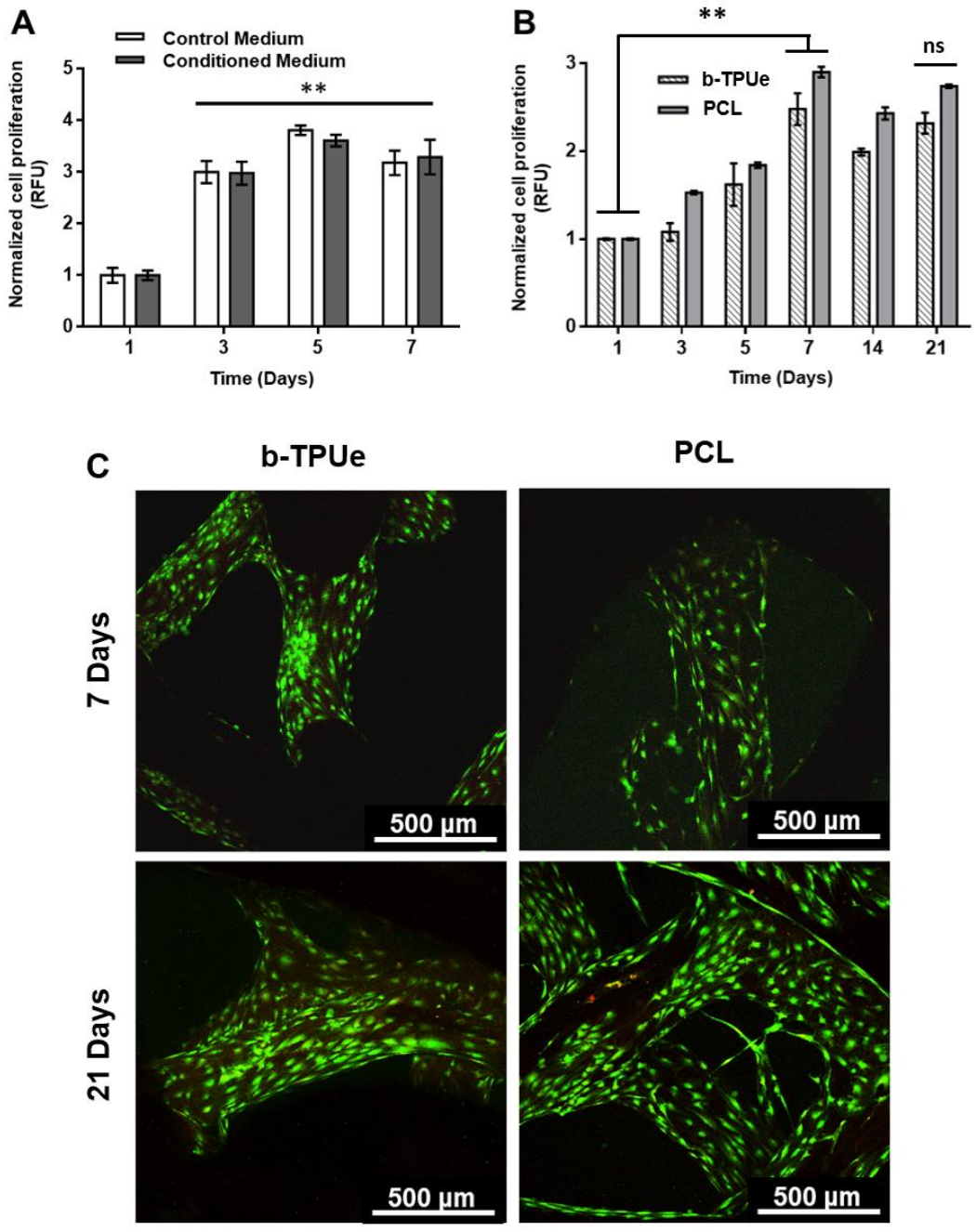

Figure 8. *In vitro* biocompatibility of b-TPUe bioprinted scaffolds with MSCs. (A) Proliferative potential of MSCs cultured with control (DMEM 10% FBS, 1% P/S) or b-TPUe-conditioned medium up to 7 days (** = $p < 0.01$). (B) MSCs proliferation cultured in both b-TPUe and PCL bioprinted scaffolds up to 21 days with no significant differences between PCL and b-TPUe (no significance: ns). Significant cell growth was observed at day 7 of culture in both biomaterials (** = $p < 0.01$) (RFU: Relative fluorescence units).

(C) Representative confocal images of MSCs grown in both b-TPUe and PCL bioprinted scaffolds at day 7 and 21. Live/dead assay was employed, using calcein (green) and ethidium homodimer (red), live cells were stained green while dead cells were stained red. Scale bars: 500 µm. Graphs created using the GraphPad Prism 6.01 software.

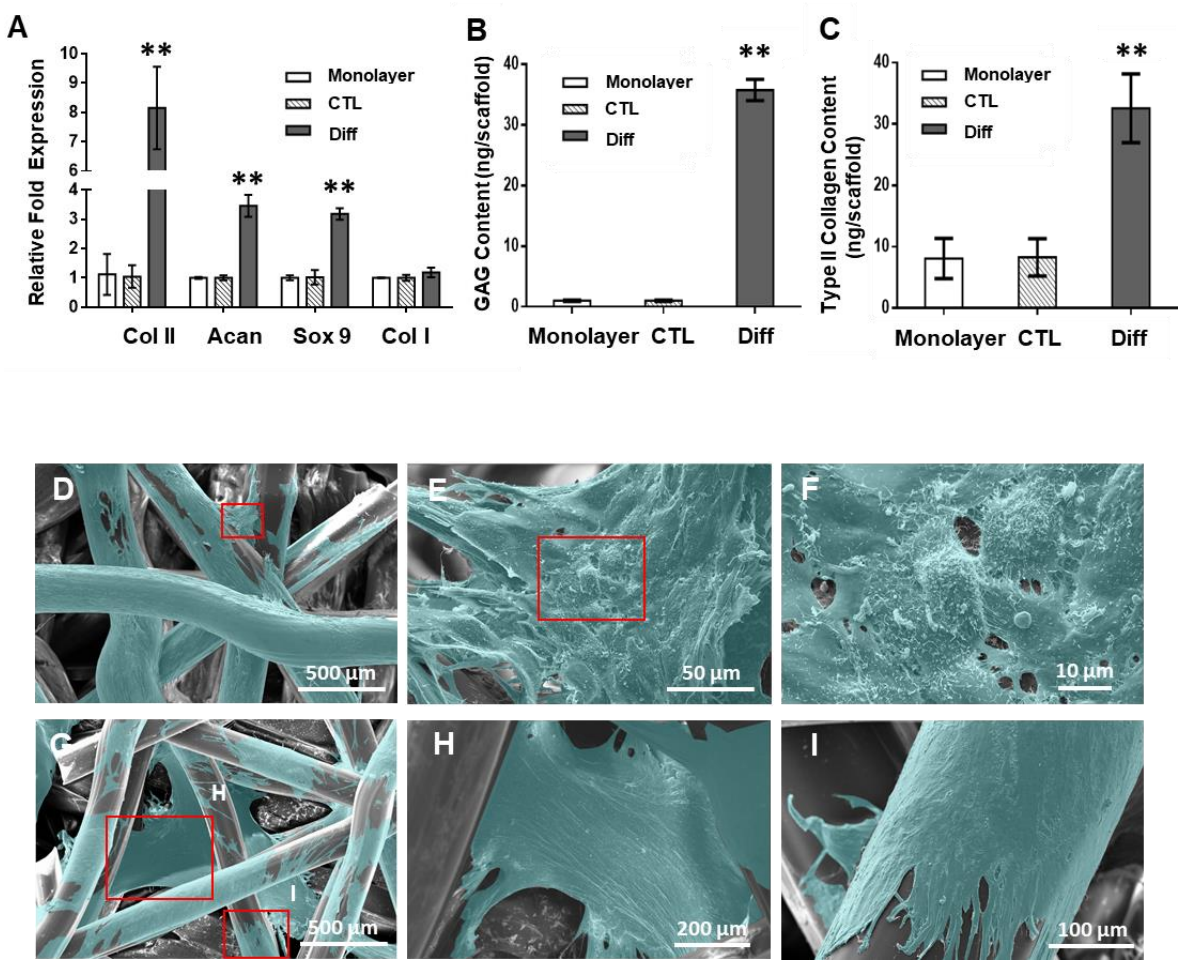

Figure 9. MSCs chondrogenic differentiation in b-TPUe bioprinted scaffolds. Chondrogenic differentiation was evaluated in MSCs cultured in monolayer, b-TPUe scaffolds (CTL), and b-TPUe scaffolds under differentiation conditions (Diff) after 21 days in culture. (A) RT-PCR analysis of chondrogenic key markers. (B) GAGs quantification. (C) Type II collagen quantification. (D-F) SEM representative images of MSCs growing in b-TPUe bioprinted scaffolds at day 21 (** = $p < 0.01$). (G-I) SEM representative images of MSCs growing in b-TPUe bioprinted scaffolds under chondrogenic differentiation conditions. Scale bars: 500 µm (D), 50 µm (E), 10 µm (F), 500 µm (G), 200 µm (H), 100 µm (I). Graphs created using the GraphPad Prism 6.01 software. SEM images false-coloured using the cross-platform image editor GIMP

(version 2.10.14).

3.7. *In vivo* assay

Biocompatibility of cell-free b-TPUe scaffolds was assessed *in vivo* by subcutaneous *in situ* implantation in the back of immunocompetent CD-1 mice using PCL as control material (**Figure 10A-D**). During the study, no cases of mice showing pain behaviour that could be induced by the scaffold implantation or infection were observed. The scaffolds were excised 21 days after implantation, and both scaffolds and mice were photographed to evaluate their appearance and integration within the subcutaneous surrounding tissue. Both b-TPUe and PCL scaffolds were firmly anchored and integrated within the subcutaneous tissue maintaining their shape and integrity. Moreover, no sign of oedema or macroscopic inflammation was detected (**Figures 10B and D**).

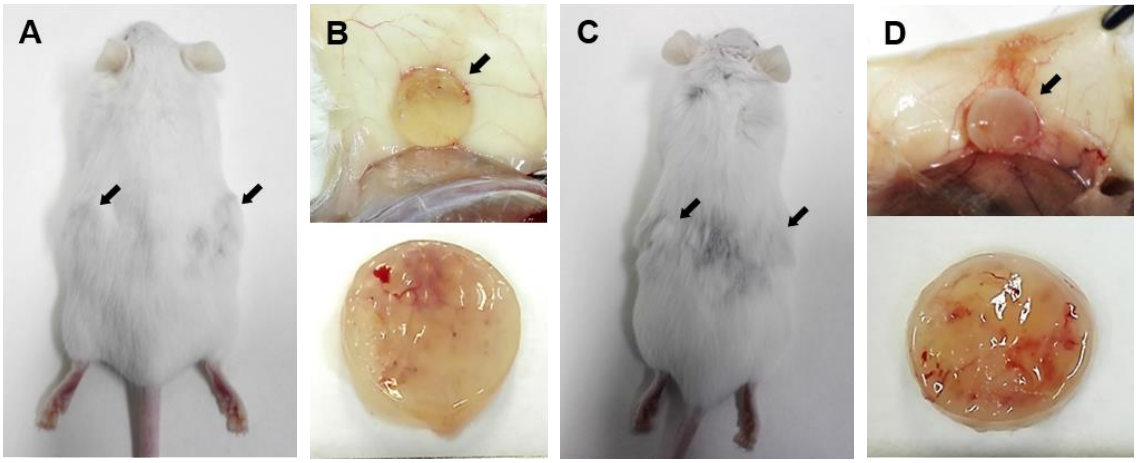

Figure 10. *In vivo* biocompatibility of b-TPUe. (A) Macroscopic image of the locations of implanted b-TPUe scaffolds in CD1 mice. Scaffolds were implanted in the dorsal region of 8 weeks old CD1 mice and resected 21 days after surgery procedure. (B) Images of b-TPUe scaffolds recovered from CD1 mice. (C) Macroscopic image of the locations of implanted PCL scaffolds in CD1 mice. (D) Images of PCL scaffolds implanted in the dorsal region of CD1 mice.

To assess the integration of the scaffolds within the surrounding tissue, both b-TPUe-MSCs and PCL- MSCs bioprinted scaffolds cultured for 21 days were transplanted into subcutaneous tissue on the flanks of immunodeficient NSG mice, as well as b-TPUe and PCL cell-free scaffolds and harvested 3 weeks later for subsequent analysis. The

implanted bioprinted cell-laden scaffolds were well tolerated by the mice showing the integration of both polymer scaffolds (**Figure 11A**). Toluidine blue staining showed the presence of GAGs in both b-TPUe and PCL scaffolds. Masson´s Trichrome staining showed that the deposition of collagenous fibres occurred in both biomaterials and in both cell-free and cell-laden conditions (**Figure 11B**).

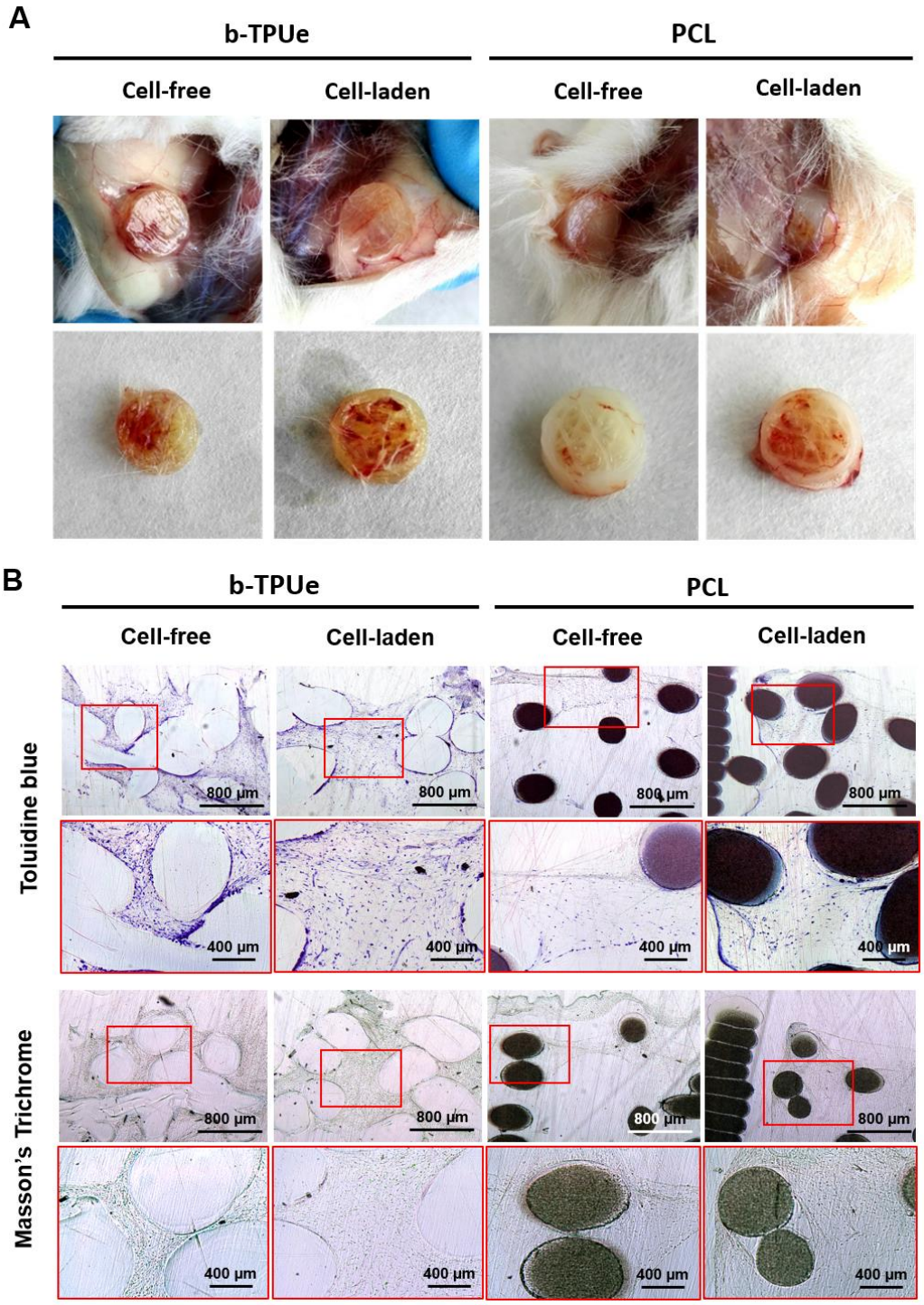

Figure 11. *In vivo* biocompatibility of b-TPUe bioprinted scaffolds with MSCs. (A)

Macroscopic images for cell-free and cell-laden b-TPUe and PCL scaffolds fabricated by 3D bioprinting. Scaffolds were implanted in the dorsal region of 8 weeks old female NSG mice and resected 21 days after surgery procedure. (B) Histologic analysis of Toluidine blue and Masson´s Trichrome staining of cell-free and cell-laden b-TPUe and PCL scaffolds 3 weeks post-implantation. Scale bars: 800 µm for black-labelled images, and 400 µm for red-labelled images.

4. Discussion

The 3D bioprinting technology allows high precision, fabrication, and customized production, which are important features for biomedical applications. Traditional methods for scaffold manufacturing comprise phase separation (433), electrospinning (434), freeze-drying (337), and gas forming (435). Comparing this methods to 3D bioprinting, they lack a high precision control of the pore size and shape (436).

In this study, a polyurethane-based 3D printing material, b-TPUe, was successfully used to fabricate scaffolds by 3D bioprinting that were able to maintain cellular viability and growth. We selected the b-TPUe since it belongs to the polyurethane thermoplastics, an adaptable category of biomaterials broadly used for biomedical purposes thanks to their biocompatibility, elasticity and strength (79,437–440). Similarly to the PEG-based adhesive-hydrogels composites, which are designed to fill and integrate irregular cartilage wounds, and are also already being tested in clinical trials (441), the b-TPUe can be designed to be printed with the customized shape of the patient wound. As well, the 3D bioprinting technology allows to fabricate the b-TPUe scaffolds with the desired thickness of fibre and pore size, biomimicking the tissue microstructure, and thus ameliorating the integration of the scaffold within the specific location. The porosity and interconnectivity of the scaffold plays a significant role in nutrient supply, gas diffusion and metabolic waste removal (442,443). Therefore, cells can penetrate the pores following their growth on the scaffold (444).

A selected biomaterial for treating joint replacements is expected to preserve the remaining native cartilage from degradation while maintaining the frictional properties of the joint (445). Analysing the friction profile of the studied biomaterials, b-TPUe showed to exert less friction towards the native cartilage surface than PLA and PCL, showing µ values closer to the cartilage-to-cartilage interaction (428). Also, the mechanical properties of a scaffold are important for engineering tissues, especially for cartilage, which is subjected to cyclic mechanical forces (446). Although scaffolds based

on hydrogels mimic more adequately the mechanical properties found in native tissues (447), their compressive modulus are typically an order of magnitude less than native cartilage tissue (448,449). Otherwise, scaffolds produced with thermoplastics possess higher Young's modulus than those based on hydrogels (450,451). The obtained results suggests that b-TPUe scaffold elasticity can be tailored, by changing the porosity, to achieve a closer values to the natural cartilage Young's modulus than hydrogel scaffolds and synthetic polymers such as PCL or PLA (447), thus exhibiting promising customizable elastic properties.

Polyurethanes are considered to have good biocompatibility properties and are widely used for long-term medical implants, such as cardiac pacemakers and vascular grafts (452). Since b-TPUe is a recently developed polyurethane-based 3D printing filament, no previous data concerning the possible cytotoxicity of this material on cell growth has been previously published. Biocompatibility must be a priority when selecting biomaterials for TE (453), therefore, and regarding the results of the cytotoxicity, proliferation and viability assays, b-TPUe showed no cytotoxic effects, that it can provide an environment that supports MSCs proliferation in a same manner as PCL (454). In fact, large spaces between the fibres allowed the adhered cells to start accommodating between the stacking fibres.

Regarding cartilage ECM production, type II collagen and aggrecan genes, which appear to be the main proteins of the hyaline cartilage ECM (455), showed to be upregulated in cells cultured in b-TPUe scaffold under chondrogenic media compared with control conditions. Similarly, Sox9, which is a known transcription factor of chondrogenesis that acts in the early stages of chondrogenic differentiation inducing type II collagen production (456) also shown to be upregulated. In addition, non-increased expression of Col I in b-TPUe scaffolds under chondrogenic media compared with their counterparts cultured in non-differentiated media or cells cultured in monolayer without chondrogenic media was observed. Type I collagen has been described in fibroblastic differentiation and could indicate the formation of fibrous cartilage (457). The upregulation of chondrogenic genes, together with the low expression of Col I of hMSCs bioprinted in b-TPUe scaffolds, indicate the ability of this material to support the differentiation of MSCs into chondrocyte-like cells. In accordance with these results, an increased GAGs and collagen type II deposition in the ECM of b-TPUe MSCs printed scaffolds cultured under chondrogenic conditions indicated the development of a cartilaginous-like matrix (458).

In the present study, we tried to evaluate qualitatively the macroscopic response to b-TPUe scaffolds in an *in vivo* environment. The lack of pain behaviour, infection, oedema or macroscopic tissue inflammation during the *in vivo* assay with immunocompetent CD-1 mice, as well as the maintenance of shape and integrity of the scaffold, and its integration within the implantation surrounding tissue indicate the *in vivo* biocompatibility of b-TPUe as previously described for other 3D polyurethanes (459). Similarly, when implanted in immunodeficient NSG mice, cell-free scaffolds showed that b-TPUe can promote the formation of new tissue since host cells infiltrated, adhered, and grew into the scaffold, confirming the integration of b-TPUe within the host's tissue. These results suggest that b-TPUe can allow *in vivo* GAGs and collagenous fibre production as well as PCL. Thus, it can be stated that b-TPUe polymer scaffolds showed good *in vivo* ECM deposition and host integration (460).

CHAPTER II:
Design and evaluation of a bilayered dermal/hypodermal 3D model

1. Background

The skin, also known as the integumentary system, is one of the largest organs of the body. Comprising 15% of the total adult body weight, skin plays a vital role in maintaining the homeostasis of the body, as it protects the inner organs from potential chemical, biological and physical threats. It also exerts many other functions, such as preventing and excessive water loss, thermoregulation, excretion, and perception through specialized receptors (461–463).

Skin pathologies can occur from diverse origins, either by genetic diseases, such as dermatitis or psoriasis (464,465); infections, like those caused by *Staphylococcus aureus* (466); or caused by injuries, such as burns, wounds derived from acute trauma, surgery; or other diseases like diabetic ulcers (467–469). A standard approach for the treatment of severe and chronic skin wounds is to replace the injured skin with a graft from the patient (autograft), a donor's skin (allograft), or from animal species (xenograft). Despite, these techniques cannot be applied in two main scenarios: low donor's healthy skin availability, and large wounds (470,471). To overcome these restrictions, the skin TE field research is trying to develop skin substitutes loaded with cells that can biologically mimic the native human skin to meet the growing demand of skin substitutes.

Due to their unique properties, such as biocompatibility, elasticity, and high water content, hydrogels are considered the best option for manufacturing skin substitutes (472,473). For instance, hydrogels hold great potential due to their intrinsic cellular interaction capacity (474), providing a 3D network similar to the native ECM that supplies mechanical support, as well as an adequate porosity, facilitating the encapsulation of living cells (475).

Different biomolecules and cell types can be incorporated into hydrogels, offering the possibility of customizing their composition to mimic native skin. Collagen is the main component of the skin ECM and represents approximatively the 25% of the total dry weight of mammal tissues (476). It is the principal skin ECM protein (477) and has been widely used in skin TE, as it provides an optimal environment by enhancing the structure of the hydrogel, promoting cell adhesion and proliferation (468,478,479). Col I is the current gold standard in the field of TE, not only providing tensile strength, but also will provide a substrate on which cells can migrate, sensing the ECM constituents (480). Collagen is produced by fibroblasts and after an injury it is able to accelerate and support the wound healing process, remodelling the ECM of the wound for regenerating the loss tissue (481). GAGs are complex polysaccharides that are present in diverse tissues,

including skin, and play a key role in cell proliferation, differentiation and migration (482). For instance, HA, the main skin GAG, has been widely used in skin care products and TE since it promotes lubrication, wound healing, and angiogenesis (341). The GAGs water-binding properties help to maintain skin's hydration, lowering the transepidermal water loss (483). HA interacts with different cell surface receptors, such as the receptor for hyaluronan-mediated motility (RHAMM) (484), which is up regulated in keratinocytes and migrating fibroblasts in the wound healing process to enhance the wound contraction and re-epithelization (485,486). On the other hand, DS is a sulphated GAGs that contributes to the ECM reconstruction during the wound healing process (487,488). In addition, EL is one of the main proteins of the native skin ECM, specifically in the dermal ECM, where it confers elasticity to the tissue matrix. As it is a highly crosslinked protein, soluble forms, such as tropoelastin or α-elastin are frequently used for developing elastin-based biomaterials (489).

Among polysaccharide-based biomaterials, agarose (Ag) it is not only a promising choice for skin substitutes fabrication, but has also been investigated for biofabrication of artificial human organs and tissues such as corneas (490), or skin (336), obtaining optimal physical properties that allowed surgical implantation.

Regarding the cellular fraction, typically the dermal compartment of artificial skin is populated by hDFs to mimic the biological feature of the dermis (478). hDFs do not only generate and remodel the skin ECM, but they also play an essential role in intercellular communication, regulating the skin physiology, which also involves wound healing processes (491). On the other hand, the use of hMSCs could provide healing capacities, since they have been seen to migrate to the injury, differentiate, and replace the damage tissue by promoting regeneration (492,493).

In this study we designed and characterized an Ag-based hydrogel enriched with skin native components, such as Col I, DS, HA, and EL, loaded with hDFs and hMSCs to obtain an optimized bilayered hydrogel for its application in skin TE. The present manuscript describes the biomaterials screening for the hydrogel formulation with adequate physicochemical properties, as well as their *in vitro* ability effect of these biomaterials on wound healing. Once optimized, the hydrogel formulation was used to biofabricate a bilayered hydrogel using hDFs and hMSCs, and its physicochemical, mechanical and biocompatibility properties were analysed.

2. Materials and Methods

2.1. Cell culture

hDFs were obtained from American Type Culture Collection (ATCC® PCS-201-012) and cultured in DMEM (Sigma) containing 10% FBS (Sigma), 100 U/mL penicillin, and 100 mg/mL streptomycin (Invitrogen) at 37ºC in a humidified atmosphere at 5% CO_2. Medium was changed every 3 days. When 80% of confluence was reached, cells were released with Tryple Express (Gibco) and sub-cultured. hDFs were used between passages 4 and 6 for all the experiments.

hMSCs were obtained from human adipose tissue and characterized as reported previously (494,495). All human samples used in this study were obtained after informed consent (Hospital Vithas, Granada, Spain) and authorization was provided from the Granada Provincial Ethics Committee (Ministry of Health and Families, Andalusia, Spain, reference: 0467-N-20). hMSCs were cultured in high-glucose DMEM (Sigma) supplemented with 10% FBS, 100 U/mL penicillin, and 100 mg/mL streptomycin (Invitrogen) at 37°C in a humidified atmosphere containing 5% CO_2. Medium was changed every 3 days. At 80% of confluence, cells were sub-cultured. hMSCs were used between passages 4 and 6 for all the experiments.

2.2. Hydrogel formulation

To prepare the hydrogel two different concentrations of Ag were prepared, an Ag-Col I (AC) hydrogel formulation previously reported (Ag 1.5% w/v) (479), and an AC hydrogel with a decreased agarose concentration (1.2% w/v) (AC_{low}). Ag solutions were prepared by dissolving Agarose UltraPure Low Melting Point (Thermo Scientific) powder in PBS. This solution was autoclaved at 120ºC for 2 h and stored at 4ºC. Before its use, Ag was preheated up to 70ºC and kept in a water bath at 37ºC to temper and avoid gelation. Col I solution (4.42 mg/mL rat tail collagen I, Corning) was kept on ice prior to its use, and neutralized with 0.8 M $NaHCO_3$, as Col I gels at neutral pH. The pH of the Col I solution after neutralization was 7.4. Then, three stock solutions were prepared using DS, HA, and EL (Bioiberica S.A.U) diluted in PBS (DS; DS + HA; DS + HA + EL) and added to Col I at final concentrations shown in **Table 9**. Col I solutions were filter-sterilized through a 0.22 μm membrane (Merck Millipore) before their use. Similarly, DS, HA, and EL freeze-dried powder were sterilized using UV irradiation for at least 30 min. Finally, cell-laden hydrogels were prepared by mixing the solutions with hDFs or hMSCs and pre-heated Ag was added to the blend, obtaining 1.1 mL of hydrogel with 1×10^6 cells/mL.

Table 9. Hydrogel formulations (mg/ml)

(mg/ml)	**Agarose**	**Collagen**	**Dermatan sulphate**	**Hyaluronic acid**	**Elastin**
AC	15.0	2.2	-	-	-
ACD	15.0	2.2	8.4	-	-
ACDH	15.0	2.2	8.4	1.0	-
ACDHE	15.0	2.2	8.4	1.0	1.0

2.2.1. Preparation of hDFs-loaded ACDHE hydrogels

ACDHE hydrogels loaded with hDFs were prepared as described above (see section 2.2) and manually casted to create a dermal equivalent using a sterile pipette, obtaining a hydrogel with 30 x 15 x 1.4 mm (x, y, z) dimensions.

2.3. Physical characterization of the ACDHE hydrogel

2.3.1. Tube inversion test

To analyse the hydrogel gelation the tube inversion test was carried out, and AC and ACDHE formulations were assayed. The hydrogel mixture was poured into a glass vial for the preparation of the hydrogels. To check the formation of a stable gel the vial was inverted upside down every 1 minute and time for gelation was noted.

2.3.2. pH determination

pH values of hydrogels at room temperature were determined using a calibrated digital pHmeter Hach Sension$^+$ (Hach Lange S.L.) at 25.0 ± 0.5 °C. Measurements were conducted by direct contact of the pHmeter electrode on hydrogels.

2.3.3. Environmental Scanning Electron Microscopy (ESEM)

ESEM was used to observe the surface morphology of the hydrogel blends and the inner cell distribution. Hydrogel samples were fixed with glutaraldehyde 2.5% w/v (Merck) during 1 h at 4ºC, then washed and kept in 0.1 M sodium cacodylate buffer (EMS, Electron Microscopy Science). Before its analysis, samples were processed using the critical point drying technique. Four samples were fixed with osmium tetroxide 1% w/v, dehydrated in a series of ethanol solutions of increasing concentration (50, 70, 90 and 100%) for 15 min each, and critical point dried in a Leica EM CPD300 dryer. Finally, the samples were covered in carbon using the EMITECH K975X carbon evaporator.

Images were acquired using the ESEM QEMSCAN 650F and hydrogel pore sizes were analysed using the software ImageJ (Fiji) (496).

2.3.4. Swelling assay

The swelling rate was calculated as previously described (497). Briefly, pre-weighed freeze-dried hydrogels were submerged in PBS. The weight of the prepared hydrogels was calculated at different time points. Swelling ratio was calculated [1].

$$Swelling\ ratio\ (\%) = \left(\frac{(W_t - W_0)}{W_0}\right) x\ 100 \quad [1]$$

Where W_0 represents the sample dry weight at day zero, and W_t represents the wet weight of the samples at a specific time point.

2.3.5. Degradation test

The degradation behaviour of hydrogels was analysed by weighing known amounts of hydrogel samples. Hydrogel samples were then incubated under gentle agitation in a hybridization oven at 37°C. Samples were retrieved at different time points from the hybridization oven and centrifuged at 5000 rpm for 2 min. After removing the supernatant, hydrogel samples were finally weighed (498). The degradation rate (%) as a measure of weight loss was calculated [2].

$$Degradation\ ratio\ (\%) = \left(\frac{(W_t - W_0)}{W_0}\right) x\ 100 \quad [2]$$

Where W_0 represents the initial weight of the sample, and W_t represents the wet weight of the samples at a specific time point.

2.3.6. Mechanical studies

Mechanical analyses were carried out in a torsional rheometer MCR302 (Anton Paar) at 25ºC. Cell-free and hDFs-laden hydrogels were casted with a cylindrical shape in moulds (20 x 5 mm). A three-step test was designed to obtain information on the compression and shearing characteristics of the samples. Firstly, the samples were placed on the base of the rheometer. Then, the rheometer head was approached at a constant speed (10 µm/s) up to a normal force of 0.5 N. Next, the specimen was oscillatory sheared according to a strain amplitude of 0.00001% at a frequency of 1 Hz and normal force of

0.5 N to determine the shear viscoelastic moduli and, finally, the upper plate was separated at a constant speed (10 µm/s).

2.4. Wound healing assay

hDFs and hMSCs were seeded in 12-well multiwell plates and cultured at 37ºC for 72 h (499). Culture media was removed, cells were rinsed with PBS, and incubated with culture medium supplemented with 8.4 mg/mL DS, 1.0 mg/mL HA, and 1.0 mg/mL elastin for 24 h. Culture medium without supplements was used as a non-treated control condition. After 24 h, medium was removed, and cells were washed with PBS and wounded by manual scratching with a 200 µL pipette tip. Supplemented and control media were replaced, and images of the wounds were taken at 0, 6, 12, 24, 48 and 72 h. Samples were maintained at 37ºC in a 5% CO_2 atmosphere. Images were taken using a Leica DMi8 microscope (Leica Microsystems) with the Leica Application Suite (LAS) X software and analysed using the software ImageJ (Fiji) (496).

2.5. Cell viability assay

Cell viability was determined using the LIVE/DEAD™ Viability/Cytotoxicity Kit (Invitrogen). Samples were incubated in PBS containing calcein AM (2 µM) and ethidium homodimer (4 µM) at 37ºC for 30 min to stain live (green) and dead (red) cells. Hydrogels were imaged by confocal microscopy at different time points and analysed using NIS-Elements software (Nikon Eclipse Ti-E A1). Live and dead cells were counted using the ImageJ (Fiji) software (496), and cell viability was determined as follows:

$$Cell\ viability\ (\%) = \frac{Live\ cells}{(Live\ cells + Dead\ cells)}\ x\ 100 \quad [3]$$

2.6. Cell proliferation assay

Cell proliferation was analysed using the AlamarBlue® assay (Invitrogen) at 1, 3, 5, 7, 14 and 21 days. This reagent is a resazurin solution, a blue non-fluorescent cell-permeable compound that is modified by the reducing environment of the viable cells into resorufin, a red fluorescent compound. Fluorescence after incubation can be measured, and therefore, the generated signal related to the metabolic activity of the samples. Hydrogels were incubated with AlamarBlue® solution at 37ºC for 3 h. Fluorescence of reduced AlamarBlue® was determined at 530/590 nm excitation/emission wavelengths.

2.7. Bilayered hydrogel design

Separate ACDHE hydrogels laden with hMSCs or hDFs were prepared in conical tubes and loaded in 3 mL sterile syringes. Then, hydrogel layers were stacked sequentially locating the hMSCs layer at the bottom and the hDFs layer at the top **(Figure 12)**. The bilayered hydrogels were allowed to gel and then placed in a rectangular 4-well multiwell plate with DMEM containing 10% FBS and 1% penicillin/streptomycin and cultured at 37°C in a 5% CO_2 atmosphere.

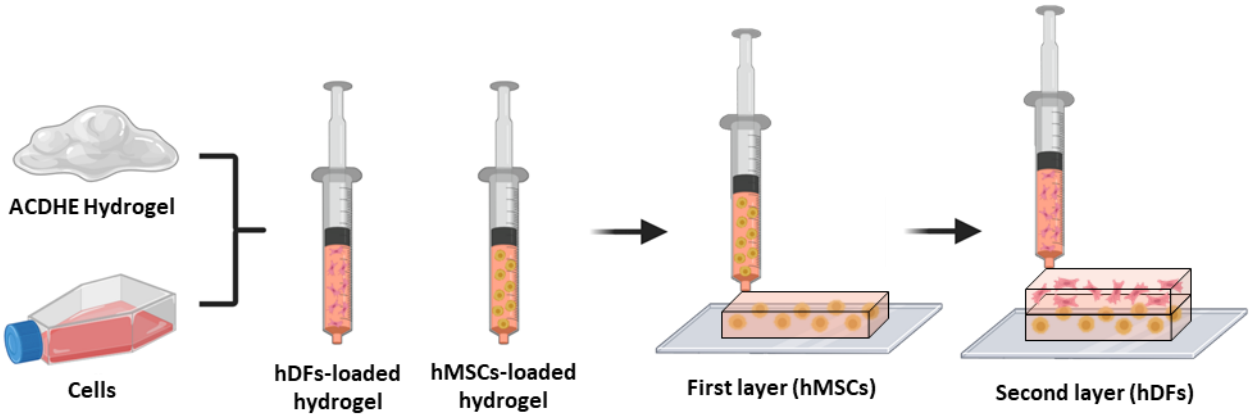

Figure 12. Bi-layered hydrogel design fabrication process. hMSCs or hDFs were cultured and mixed with an ACDHE hydrogel solution in separate conical tubes, loaded in 3 mL sterile syringes, and stacked sequentially, locating the hMSCs and hDFs at the bottom and at the top, respectively. Figure created with BioRender.com.

2.8. Morphological characterization of the bilayered hydrogels

The monitorization of the hydrogel shape maintenance was carried out over a culture period of 21 days. To observe the size of the hydrogels overtime, three hydrogel samples were prepared and seeded with hDFs and hMSCs, submerged in culture medium and maintained in an incubator. At preestablished time intervals (0, 7, 14 and 21 days) hydrogels were retrieved from the solution, the excess of medium was removed using a filter paper, and the length and width of the samples was measured (500).

2.9. Statistical analysis

Results in this work are represented as mean ± SD. Differences between two groups of data were tested using the two-tailed Student's T test for non-paired samples. Differences were considered statistically significant at $p < 0.05$ (*), $p < 0.01$ (**), and $p < 0.005$ (***).

3. Results

3.1. Hydrogel formulation

To determine the fittest Ag concentration, cell viability of AC_{low} and AC hydrogels was investigated with the Live/Dead assay. Confocal images were used to calculate the cell viability percentage. Although both concentrations showed good viability rates, cell viability at AC_{low} hydrogels was significantly lower compared with AC hydrogels at days 7 and 14 **(Figure S1)**. Moreover, a loss of structural integrity was observed at AC_{low} hydrogels after 7 days in culture. Hence, the referenced Ag concentration was maintained in further experiments (479).

To create a hydrogel that mimics the skin ECM composition, AC-based hydrogels were supplemented with skin native components. Therefore, DS and HA, GAGs found in native human skin; and EL, a protein responsible for the skin ECM elasticity, were added to the AC blend generating three formulations: Ag-Col I-DS (ACD), Ag-Col I-DS-HA (ACDH) and Ag-Col I-DS-HA-EL (ACDHE). Hydrogel solutions loaded with hDFs were pipetted on a petri dish surface, allowed to gel, gently transferred to a multiwell culture plate, and cultured for 21 days. All conditions were mostly populated by live cells, showing a uniformed distribution within the hydrogels **(Figure 13A)**. Results for all the formulations displayed no negative effects on hDFs viability up to 21 days. Control (AC samples) and hydrogel formulations enriched with skin-related materials were able to maintain hDFs viability levels above 78 and 86%, respectively **(Figure 13B)**, for at least 21 days. These results match with the viability specifications of pharmaceutical products before administration to patients, based on the primary criteria for quality stablished by the FDA and the European Medicines Agency (EMA) (≥70% and ≥80%, respectively) (501). The ACDHE hydrogels showed higher viability levels after 21 days compared to AC, ACD and ACDH hydrogels. Cell viability rates of the ACDHE condition remained higher than 93% during the entire experiment. Therefore, the ACDHE hydrogel formulation with all ECM components was used for the subsequent experiments.

3.2. Physicochemical properties of ACDHE hydrogel

3.2.1. Tube inversion test and pH

The elapsed time for the solution to turn into a gel was recorded using the tube inversion test. The average gelling times of AC and ACDHE hydrogels were 3.4 ± 0.2 and 4.1 ± 0.2 min, respectively. **Figure 14A** shows evidence of AC (white cap vial) and ACDHE (black cap vial) hydrogels in their liquid and gelled form. The pH value of ACDHE hydrogels was 7.36 ± 0.05.

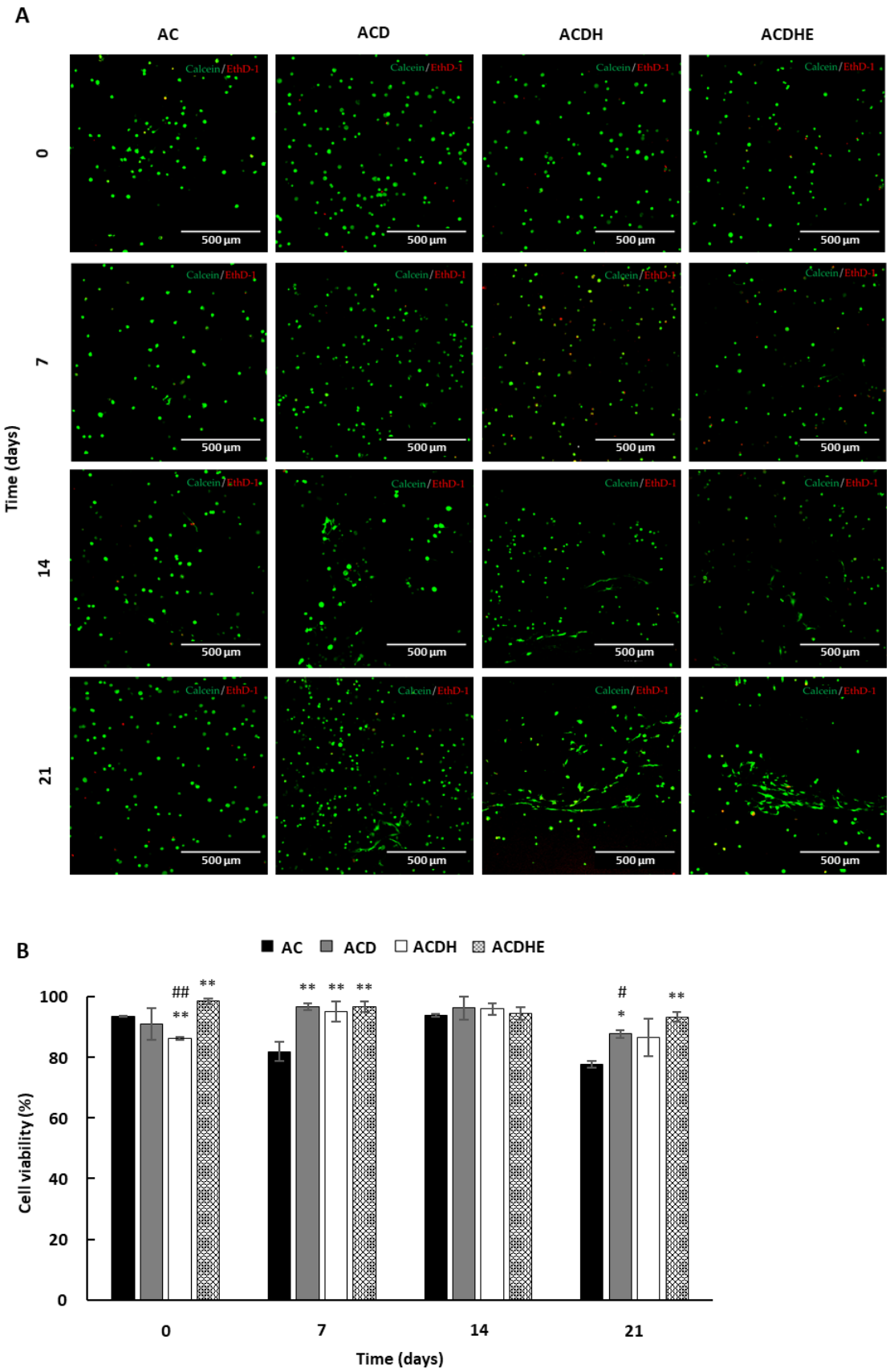

Figure 13. Cell viability assay of AC, ACD, ACDH and ACDHE hydrogel samples. (A)

Confocal images of hDFs-loaded hydrogels at 0, 7, 14 and 21 days. Calcein (green fluorescence) stains live cells, while EthD-1 (red fluorescence) stains dead cells. Scale bar = 500 µm. (B) Cell viability (%) in the hydrogel scaffolds after 0, 7, 14 and 21 days. Two-tailed Student T test analysis were performed for ACD, ACDH, ACDHE samples compared to AC samples at each time point at significance levels of: * $p < 0.05$, and ** $p < 0.01$; and for ACDHE samples compared to ACD, ACDH samples at each time point at significance levels of: # $p < 0.05$, and ## $p < 0.01$.

3.2.2. Hydrogel's ultrastructure

To physically characterize the hydrogels, ESEM analysis was carried out for ACD, ACDH and ACDHE formulations. The three hydrogel formulations showed a uniform and homogeneous lattice organization, with an interconnected porous network **(Figure 14B)**. Mean pore size increased proportionally with the complexity of the hydrogel formulation, (0.17 ± 0.03 µm, 0.38 ± 0.04 µm, and 0.73 ± 0.04 µm for the ACD, ACDH, and ACDHE hydrogels respectively) **(Figure 14C)**.

3.2.3. Swelling and degradation behaviour of ACDHE hydrogels

Freeze-dried ACDHE hydrogels were immersed in PBS (pH 7.4) to study the swelling behaviour of this formulation. Hydrogel swelling kinetics results are shown in **Figure 15A**. The average swelling rate of the ACDHE hydrogel was found to be 42 ± 8%. The swelling kinetics of the ACDHE hydrogel reached an intake plateau phase around 3 days after starting the assay, with a maximum peak at day 14. To study the stability of the ACDHE formulation, hydrogel degradation was determined by measuring weight variation overtime up to 21 days **(Figure 15B)**. Maximum degradation rate was found after 14 days with 7.14 ± 0.22 %.

3.2.4. Mechanical properties of the hydrogels

The mechanical properties of AC and ACDHE hydrogels were determined by compression assays. As stated in the materials and methods section, cell-free and hDFs-loaded hydrogels were casted in cylindrical-shaped moulds (20 mm in diameter and 5 mm in height) and maintained at 37ºC in a 5% CO_2 atmosphere. In **Figure 15C** the Young moduli obtained from the compression assays for AC and ACDHE hydrogels up to 21 days in culture are shown and compared with human skin.

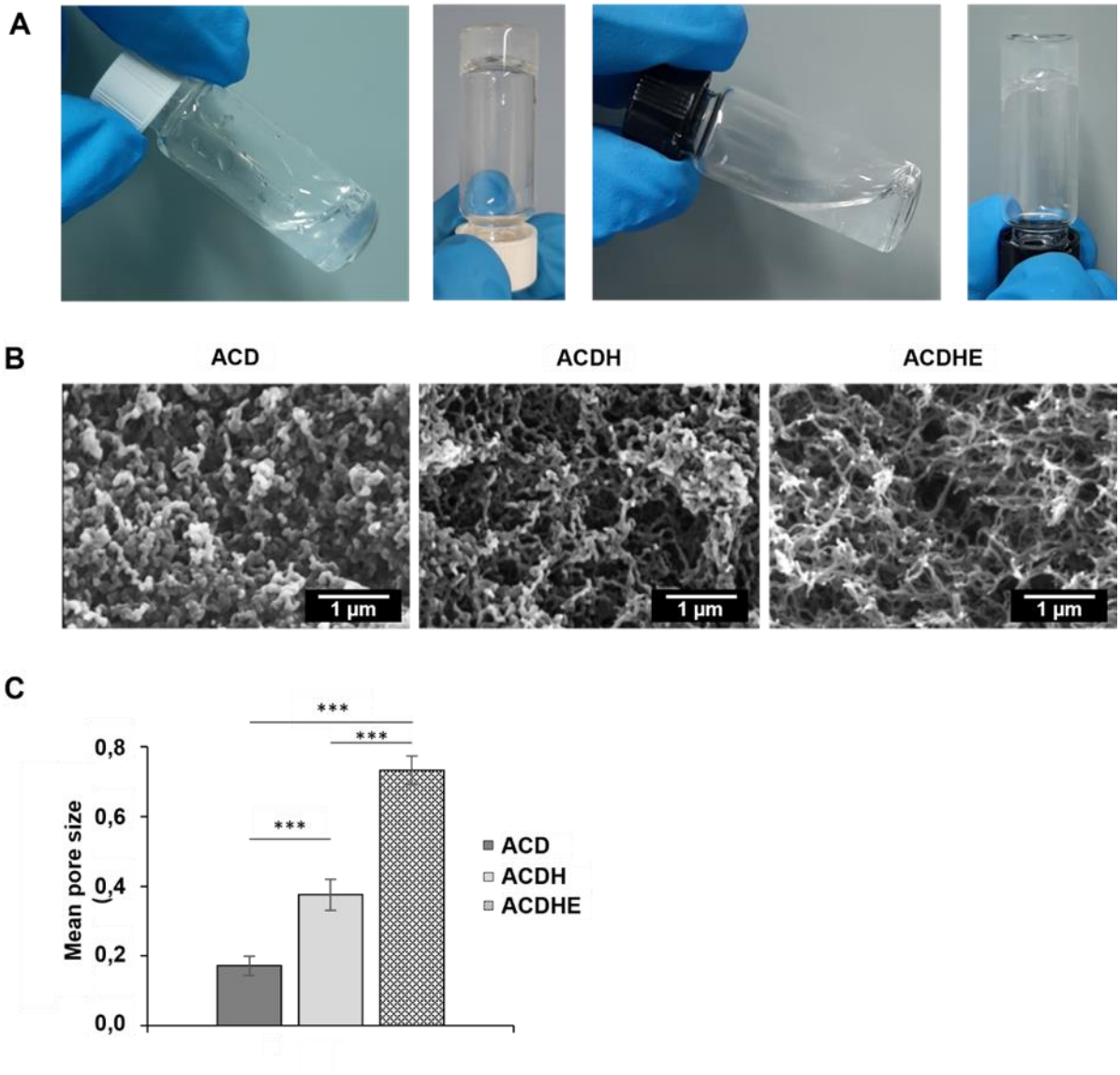

Figure 14. Tube inversion test and ultrastructure of the hydrogels. (A) Representation of AC (white cap) and ACDHE (black cap) hydrogels withstanding the tube inversion test. (B) ESEM images (scale bar = 1 µm) and (C) pore size characterization of the ACD, ACDH and ACDHE hydrogels. Two-tailed Student T test analysis were performed for ACDH and ACDHE samples compared to ACD samples at significance level of: *** $p < 0.05$.

Despite slight variations were found between Young moduli of cell-free AC and ACDHE hydrogels over time, cell-free AC hydrogel after 21 days in culture (10.14 ± 0.72 kPa) showed significant differences compared with the elasticity range observed in human native skin samples (5.22 ± 0.39 kPa), while no significant differences were found at day 21 of culture in ACDHE cell-free hydrogels (7.50 ± 0.94 kPa) compared with human native skin. On the other hand, besides Young moduli of cell-loaded hydrogels

also showed variations over time, after 21 days of culture neither AC (5.68 ± 0.00 kPa) nor ACDHE hydrogels (5.86 ± 0.38 kPa) showed significant differences compared with human native skin (5.22 ± 0.39 kPa). The range of strain analysed for the Young moduli obtained in hydrogels and skin samples is depicted in **Figure S2**.

The viscoelastic moduli of AC and ACDHE hydrogels, with and without cells, are shown in **Figure 15D and E**. The storage moduli of AC and ACDHE hydrogels, either cell-free (3.19 ± 0.61 and 2.56 ± 0.29 kPa, respectively) or cell-laden (2.49 ± 0.03 kPa and 1.89 ± 0.12 kPa, respectively) showed an oscillation in a range around the values obtained from human native skin samples (2.94 ± 0.27 kPa) (**Figure 15D**).

On the other hand, as it can be observed in **Figure 15E** when analysing the loss moduli, significant differences were found at day 21 for AC and ACDHE hydrogels, either for cell-free (0.19 ± 0.04 kPa and 0.17 ± 0.00 kPa, respectively) or cell-laden hydrogels (0.14 ± 0.00 kPa and 0.12 ± 0.00 kPa, respectively) when compared with human native skin samples (0.63 ± 0.13 kPa).

3.3. Scratch wound assay

To study the wound healing effect of the soluble biological compounds supplemented in the hydrogel formulation, a scratch wound assay was carried out on hDFs and hMSCs adding DS-HA-EL (DHE) solution to culture media **(Figure 16A)**. Interestingly, hDFs cultured with DHE-supplemented media displayed an important wound healing effect, showing a higher wound closure rate after 6 and 12 h, even achieving a 100% of wound closure 24 h earlier than the control group **(Figure 16B)**. As well, the wound closure effect of the DHE formulation on hMSCs showed a significant higher wound healing rate at 48 h compared with the control group; however, full wound closure was achieved at 72 h in treated and control conditions **(Figure 16C)**. These results indicate that the DHE supplementation can significantly promote the wound healing rate, especially for hDFs.

3.4. ACDHE bilayered hydrogel

For the biofabrication of a bilayered hydrogel two types of cells were used. On one hand, hDFs, an essential component of skin dermis, and on the other hand, hMSCs, which can provide growth factors, cytokines, and chemokines that promote cell survival and regulate the tissue regeneration. The ACDHE hydrogel formulation was prepared in a bilayered way with hDFs located at the top layer and hMSCs at the bottom layer.

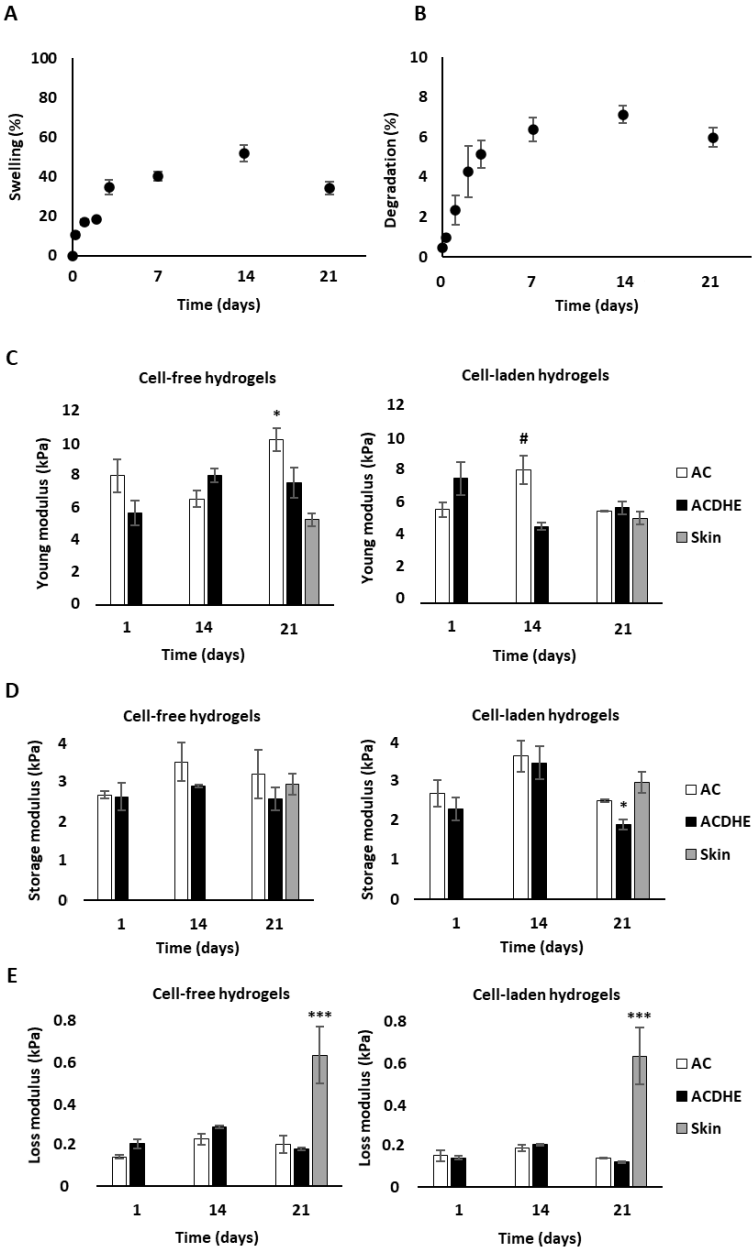

Figure 15. Swelling, degradation, and mechanical assays. (A) Swelling behaviour and (B) degradation rates of ACDHE hydrogel in a time lapse of 21 days. (C-E) Mechanical measurements: (C) Young moduli, (D), storage and (E) loss moduli of AC and ACDHE hydrogels without cells and cell-laden at 1, 14 and 21 days under culture conditions, compared with human native skin. Two-tailed Student T test analysis were performed for human skin samples compared to AC and ACDHE samples at day 21 at significance levels of: * $p < 0.05$, and *** $p < 0.005$; and for AC samples compared to ACDHE samples at each time point at a significance level of: # $p < 0.05$.

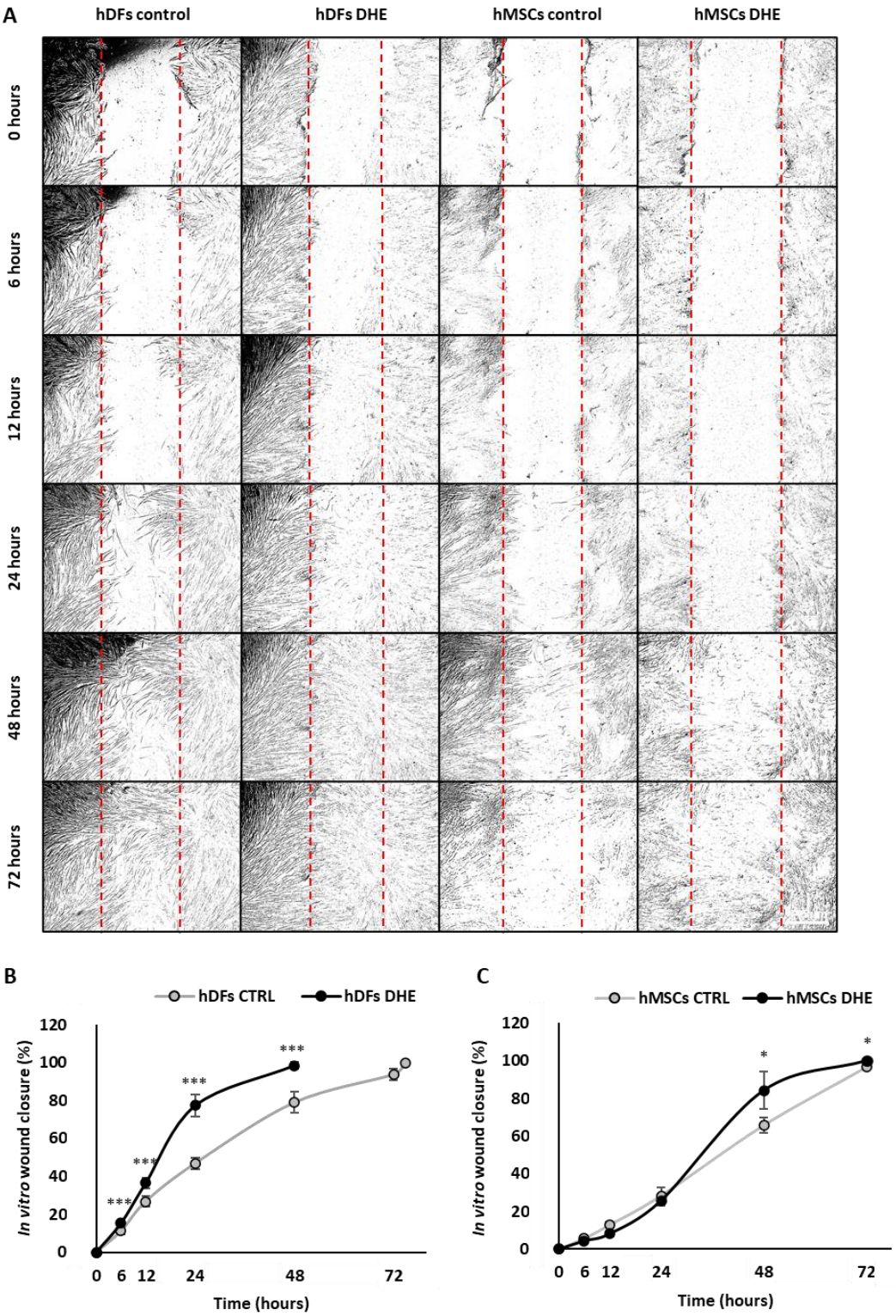

Figure 16. *In vitro* scratch wound healing assay of hDFs and hMSCs treated with DHE supplemented media. Culture medium without supplements was used as a control for non-treated cells. The images (A) and the analysed results (B, C) showed the wound closure after 0, 6, 12, 24, 48 and 72 hours. Statistical significance: * $p < 0.05$; *** $p < 0.005$.

An hMSCs-loaded ACDHE layer was placed on a petri dish surface and allowed to gel while preparing the hDFs-loaded ACDHE solution. Then, the hDFs-loaded ACDHE layer was added on the top of the hMSCs-loaded ACDHE layer. Due to the viscosity of the ACDHE formulation, the two layers did not mix during the process, but remained adhered together while gelling. Once fully gelled, the samples were transferred to multiwell culture plates and submerged in cell culture medium. **Figure 17A** shows the macroscopic appearance of the ACDHE bilayered hydrogel at days 0 and 21, demonstrating that it could hold its shape overtime.

To assess the distribution of the cells within the hydrogels, hDFs and hMSCs were previously stained with CellTracker^{TM} Green CMFDA and CellTracker^{TM} Red CMTPX, respectively. Two well differentiated layers with the two different cell types could be observed **(Figure 17B)**. The bottom view of the cross section allowed seeing the cells evenly distributed along the bilayered structure. Furthermore, this structure kept its distribution, and both layers could be observed during the entire culture time. Cell viability images acquired at days 0, 7, 14 and 21 showed that most of the cells were viable, with few dead cells. Bilayered ACDHE hydrogel samples showed to support cell viability up to 21 days **(Figure 17C)**, maintaining the bilayered distribution clearly differentiated, with hDFs showing a fibroblastic cell morphology (top), and the hMSCs showing a spherical shape (bottom) **(Figure 17D)**. Proliferation rate of the bilayered hydrogels displayed an initial decrease in proliferation rate (at days 1 - 5) and a later significant increase (from day 10 – 21).

Also, cell laden ACDHE bilayered hydrogels were also analysed by ESEM. Cells were observed encapsulated inside the hydrogel matrix **(Figure 18A** and **B)**, and it even seemed that they were able to produce ECM-like structure **(Figure 18C** and **D)**. **Figure 18E** and **F** show false-coloured cells in blue and deposited ECM in red.

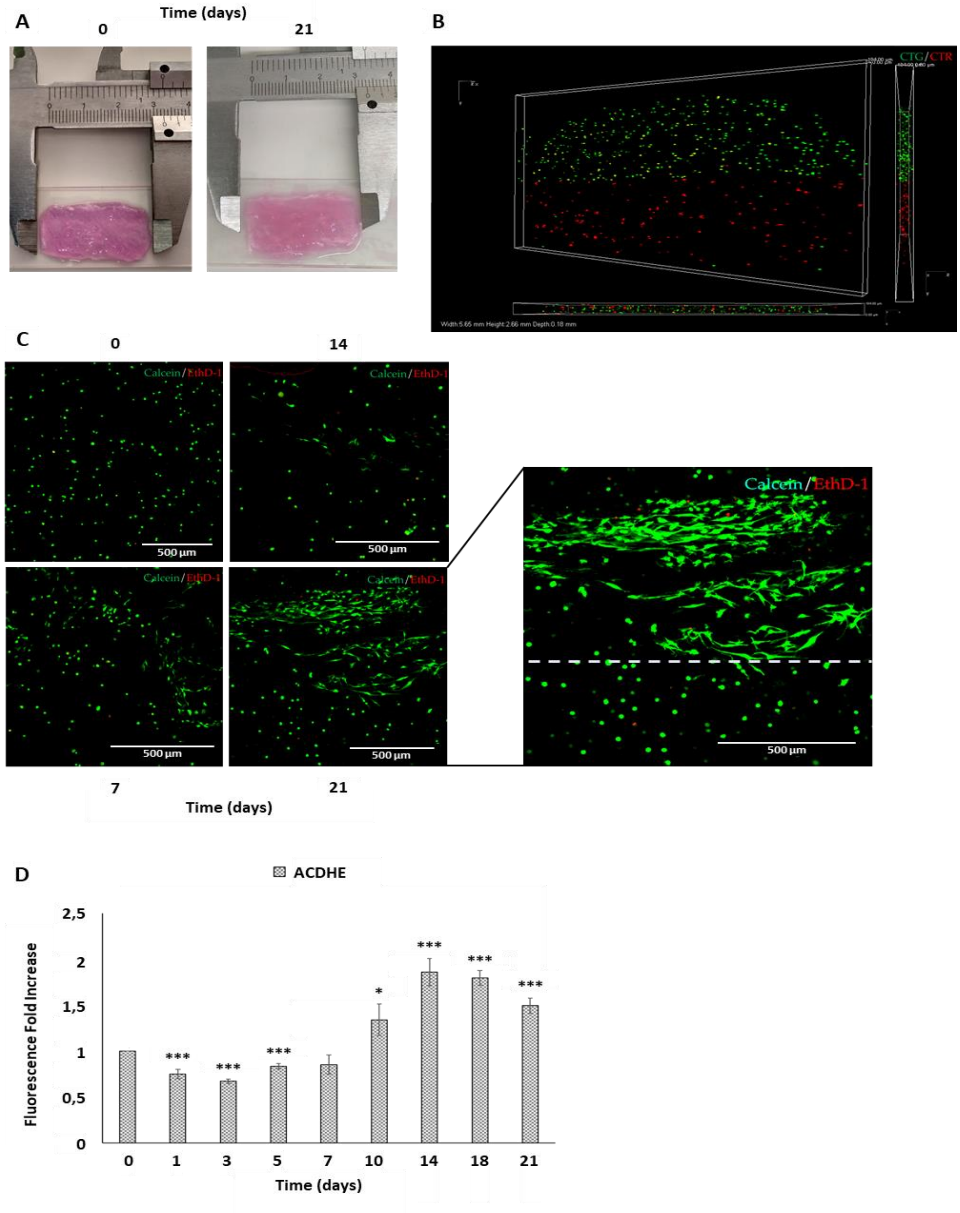

Figure 17. Bi-layered ACDHE hydrogel. (A) Macroscopic appearance of the bi-layered ACDHE hydrogels. (B) Vertical cross section image of the bi-layered hydrogel acquired by confocal microscopy. Side and bottom views are also included on the right-hand and bottom sides of the figure. hDFs and hMSCs are stained with CellTracker^{TM} Green CMFDA (CTG, green) and CellTracker^{TM} Red CMTPX (CTR, red), respectively. Dimensions = width: 5.65 mm; Height: 2.66 mm; Depth: 0.18 mm. (C) Confocal microscopy images of the cell viability of the ACDHE hydrogel at days 0, 7, 14 and 21. (D) Augmented image of the bi-layered ACDHE hydrogel at day 21, the white dotted line separates the fibroblast layer (top) from the hMSCs layer (bottom). Scale bar = 500 µm. (E) Proliferation results of the ACDHE hydrogels up to 21 days.

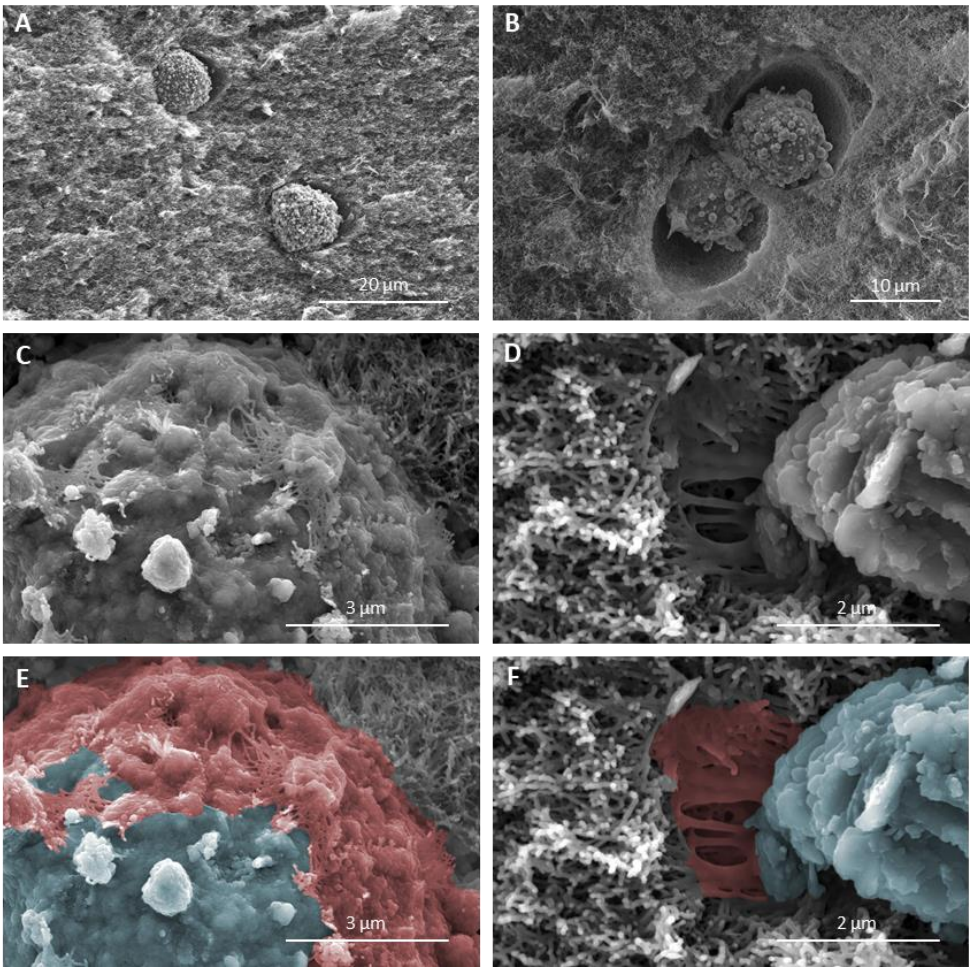

Figure 18. ACDHE bi-layered hydrogel ESEM. (A-F) ESEM images (Scale bar = 1 µm) of ACDHE hydrogels. Scale bars: (A) 20 µm; (B) 10 µm; (C and E) 3 µm; (D and F) 2 µm. (E and F). False-coloured ESEM images showing cells (light blue) and cell-produced ECM-like structures (light red).

4. Discussion

A future perspective of TE strategies is the treatment of patient's injuries by isolating specific autologous or allogenic cells taken from a biopsy, and implant them in the patient within a supporting matrix (57). For this purpose, the use of biomimetic hydrogels for the development of TE and regenerative medicine therapies could provide enhanced biological and physicochemical properties to reproduce those found at the human native tissue ECM (502–504). Hydrogel cultures have been shown to improve cell proliferation, differentiation, spreading and migration compared to traditional 2D culture conditions (505). Indeed, in skin TE most of the current approaches for the manufacture

of full-thickness skin substitutes involve embedding hDFs in hydrogels. Nevertheless, it has also been demonstrated that hMSCs can be an optimal option for healing skin wounds, as they can reduce the inflammatory response, promote angiogenesis, and even help to improve the aesthetic appearance (506). Collagen-based hydrogels have been widely used for 3D cell cultures, showing optimal results; however, they lack mechanical stability and biological complexity (507). In this study, the AC hydrogel was chosen as a core formulation since it has shown to have a good gelation kinetic, allowing its injectability through a small lumen. Also, to mimic the skin native ECM and recreate a microenvironment that closely simulates the physicochemical and biological cues of the native tissue, DS, HA, and EL were incorporated into the AC hydrogel. Then, the ACDHE hydrogel formulation was loaded with cells to study its applicability for skin TE.

As a first stage, different combinations of DS, HA and EL were combined with AC hydrogel, where Ag acts as a fast gelling thermosensitive agent, and Col I as a slower gelling pH-dependent biomaterial that provides biomimicry since it is the most ECM ubiquitous protein of the dermis (508,509). All studied formulations showed good cytocompatibility, maintaining viability levels over 86% up to 21 days. In fact, the ACDHE hydrogel formulation endowed with all the supplements showed the highest viability rates compared with the control and the other formulations. This is because DS, HA and EL are biological components of the dermal ECM, that act enriching the biomimetic properties of the formulation (510–512). Those components also exert biological properties related to wound healing in the skin. DS, besides being a ubiquitous dermal glycan, it is released at high concentrations during wound repair to act as a cofactor for important growth factors in the proliferative phase of wound healing (513). HA displays anti-inflammatory activity, helps the skin to maintain moisture, it is also involved in the regulation of collagen synthesis, and promotes wound healing during the non-scar healing of foetal skin (514), as well as during wound healing after injury. EL, which promotes biological responses in cells through its role as a biologically active ligand (515), inducing a range of cell activities, such as cell migration, proliferation, ECM synthesis, and protease production (516). In a wound healing context, EL properties can establish a parallelism with the characteristics found in foetal skin, which can heal skin wounds with no scar formation (517).

The gelling time and pH value of the ACDHE hydrogel were suitable for skin TE applications (518). An appropriate gelation time plays a vital role in wound healing since too short gelation times are unfavourable for surgery, which needs enough time for

applying treatments, while a long gelation time cannot timely seal the wounded site (519). The temperature-sensitive properties of the hydrogel allow its injectability as well as an *in situ* gelation to ensure matrix cohesion and its cytocompatibility. ACDHE hydrogel displayed a neutral pH of 7.36, optimal for skin applications as it has been seen that collagen-based hydrogels should be neutral for maintaining a good skin barrier function (520).

We observed that ACD, ACDH and ACDHE formulations showed porous structures similar to previously reported AC hydrogels (479). Interestingly, the pore size of the enriched hydrogels with the supplements proportionally increased together with the complexity of the formulation. In effect, it has been reported that the addition of different components, such as Col I or chitosan to Ag hydrogels could increase the hydrogel porosity, offering an attractive topology for cell adhesion and migration, promoting cell growth and proliferation (521). This highly porous micro/nanostructure enables the flow of nutrients and metabolic waste, and could positively affect migration and cellular activity (522).

The ability to absorb liquid or swelling is an important feature in the development of hydrogel scaffolds, since it affects the nutrient transport with the surrounding environment and can provide high mechanical resiliency (523). The water content that the hydrogel is able to hold will favour the cell viability of the encapsulated cells by lowering the interfacial tension, and will also increase the nutrients, ions and metabolites exchange with the surrounding environment (524). ACDHE hydrogel formulation also showed long-term degradation rates, revealing an 8% maximum mass loss over an incubation period of 21 days. Still, the ACDHE samples kept their original shape, which indeed qualifies this combination for long-term incubation after the cell encapsulation (525). These results about the time-related swelling and mass loss of the ACDHE hydrogel agree with those found in AC hydrogel formulation which are suitable for applications that require shape fidelity and volumetric accuracy (526).

Matching the mechanical properties of target tissues is crucial in terms of promoting an adequate tissue regeneration (527). Since Young's modulus of Col I-based hydrogels range around units of kPa (528), blending Ag with Col I and adding the DHE supplements could combine the mechanical and biological advantages of those elements. Compression and viscoelastic moduli of ACDHE hydrogels were analysed, using AC hydrogels as a control condition, and human skin as a target tissue mechanical behaviour reference. It was observed that after 21 days of culture the Young modulus of both cell-

free and cell-laden ACDHE hydrogels were in the human skin sample range of kPa (529). In addition, regarding viscoelastic modulus, although significant differences were found for loss modulus between the studied hydrogels and human skin, ACDHE hydrogel samples shared a similar storage modulus (G', elastic modulus) range of kPa found in human skin tissue. In addition, our results also match with those found in the literature related to hydrogels studied for skin applications. For instance, other researchers also obtained similar values (G' = 2 – 4 kPa; G" = 0,1 – 0,4 kPa) when developing polysaccharide-based hydrogels for skin (530). These results point out that the ACDHE hydrogels demonstrate an elastic behaviour as same as skin does, since G' > G" corresponds to an elastic behaviour (531,532).

The wound healing is an intricate process of multiple biological events and coordinated collaboration of several different cell types. Among them, fibroblast proliferation and ECM production, epithelial-mesenchymal interaction, and neovascularization of the wound bed are relevant (533,534). Our results showed that the DHE supplementation induced a shorter wound healing on hDFs than the control non-treated hDFs. Otherwise, DHE supplementation did not induce a shorter wound healing on hMSCs, though it successfully prompted a faster wound healing. It has been demonstrated that hMSCs are prone to exert paracrine functions, reduce the inflammatory response and promote angiogenesis (535–537). hMSCs can modulate wound healing by secreting paracrine factors such as EGF, keratinocyte growth factor (KGF), VEGF, insulin growth factor (IGF), skin derived factor (SDF-1); and immunomodulatory cytokines such as interleukin 1 alpha (IL-1α), interleukin 1 beta (IL-1β), tumour necrosis factor alpha (TNF-α) and interferon-λ (538,539). The management and performance of these paracrine functions could explain the similar closure rate of the wounds of control non-treated hMSCs and hMSCs treated with DHE supplemented media. Together, the combined use of hDFs and hMSCs could synergistically improve the reconstruction of the dermal and hypodermal layers, respectively, of skin (540).

Then, the viability and proliferation studies of the bilayered ACDHE hydrogel with hDFs and hMSCs revealed the cytocompatible nature of the formulation for both cells. Additionally, encapsulated hDFs showed outstanding cell morphology after 21 days of culture. The influence of chondroitin sulphate-based hydrogels (structurally similar to DS (541), HA (99), and EL (542)) over cell motility and migration has already been described, showing an improvement of cell migration and morphology. Among important factors for TE applications, a scaffold microstructural architecture that can offer suitable

physical properties is essential. The ACDHE hydrogels showed a regular pore distribution with ECM-like structures that may have been produced by the encapsulated cells, since hDFs are known to synthesize collagen and other ECM components and other proteins which support the structural integrity of the skin (543). Similarly, in the past few years, commercially available bilayered *in vitro* skin models have already been developed; however, little attention has been paid to the hypodermal layer, as they mainly focus on reproducing the dermo-epidermal structure of the skin, like StrataTest® or EpiDerm™ (544,545). Moreover, those models are focused on producing tissue-like structures by 2D-culturing in collagen matrices, restricting their production in matters of size and time. In a biological approach, the ACDHE bilayer hydrogel not only reproduces the dermo-hypodermal structure of the skin, but also includes skin-related molecules, enhancing its biological mimicry. This model enables the incorporation of other cells, such as endothelial cells, sweat gland cells, dermal papilla cells for hair follicles, melanocytes, or keratinocytes to address the engineering of more complex skin substitutes. Additionally, conversely to the 2D produced skin models, using a bioink widens the fabrication possibilities, allowing adapting their use to an automatized manufacturing. Taken altogether, these preliminary studies suggest that the ACDHE formulation could be a promising bioink candidate to develop skin biofabrication research. Among all the potential applications of this formulation, this hydrogel could be used to produce models of disease, cosmetic product testing, identification of potentially harmful substances, and 3D bioprinting bioinks.

CHAPTER III:
Biofabrication and *in vivo* assessment of a three-layered skin substitute

1. Background

The skin, one of the largest organs of the body, comprising approximately 15% of the total body weight, plays paramount roles in preserving the body homeostasis, and protects inner organs from physical, chemical, and biological hazards. It is also involved in many essential functions, such as preventing an excessive transepidermal water loss (TEWL), thermoregulation, sensorial perception through specialized receptors, or excretion (463,546,547). In addition, the skin may also operate as a biofactory that synthesizes, processes and/or metabolizes a wide range of proteins, glycosaminoglycans (GAGs), lipids and signalling molecules (548).

Skin substitutes, typically manufactured by TE, are an important field of research with great impact on dermatological pathology treatments. Skin substitutes should show biocompatible properties, help to restore the epidermal barrier function and cutaneous homeostasis (temperature, pH, TEWL, elasticity and moisture), and ensure a correct clinical outcome (549).

Although conventional TE manufacture strategies led to the first generations of engineered tissue, such processes usually consume time and are restricted to having mainly flat and predetermined geometries. To overcome these limitations, first skin 3D bioprinting approaches were achieved (550), and the potential of skin bioprinting has already been demonstrated using different techniques to create complex engineered tissues with a predefined structural architecture (353,551–554).

However, despite these progresses, more mimicry regarding design and biomolecule composition should be ameliorated in skin models. To conduct such research, our laboratory has developed three biomimetic bioinks, each one designed to resemble the ECM found in each skin layer (**Figure 19A**). The epidermal bioink was based on Col I as a scaffolding biomaterial, supplemented with Kt, a natural structural protein mainly found in epithelial tissues (e.g., epidermis, hair, wool), which is used in biomedical research (555,556), and Sph, which contribute to the maintenance of the epidermal barrier against desiccation and penetration of xenobiotics (557). The dermal and hypodermal bioinks were based on Ag, which provides mechanical support and fast gelation, and Col I, which provides slow gelation and represents the most ubiquitous protein in dermal ECM (477). Both bioinks were supplemented with a blend of DS, a highly relevant glycan in skin ECM that participates in the ECM reconstruction at the wound healing process (487,488), and HA, which it is the main GAG found at the dermal ECM. HA is commonly used in skin care products and TE, promoting wound healing,

skin moisture maintenance and cell proliferation (485,558–561). As well, EL was added to the dermal bioink supplementation, a highly crosslinked protein which is frequently used to develop EL-based biomaterials in TE (562,563), as it is the main protein in the native skin that confers elasticity to the dermal ECM (564).

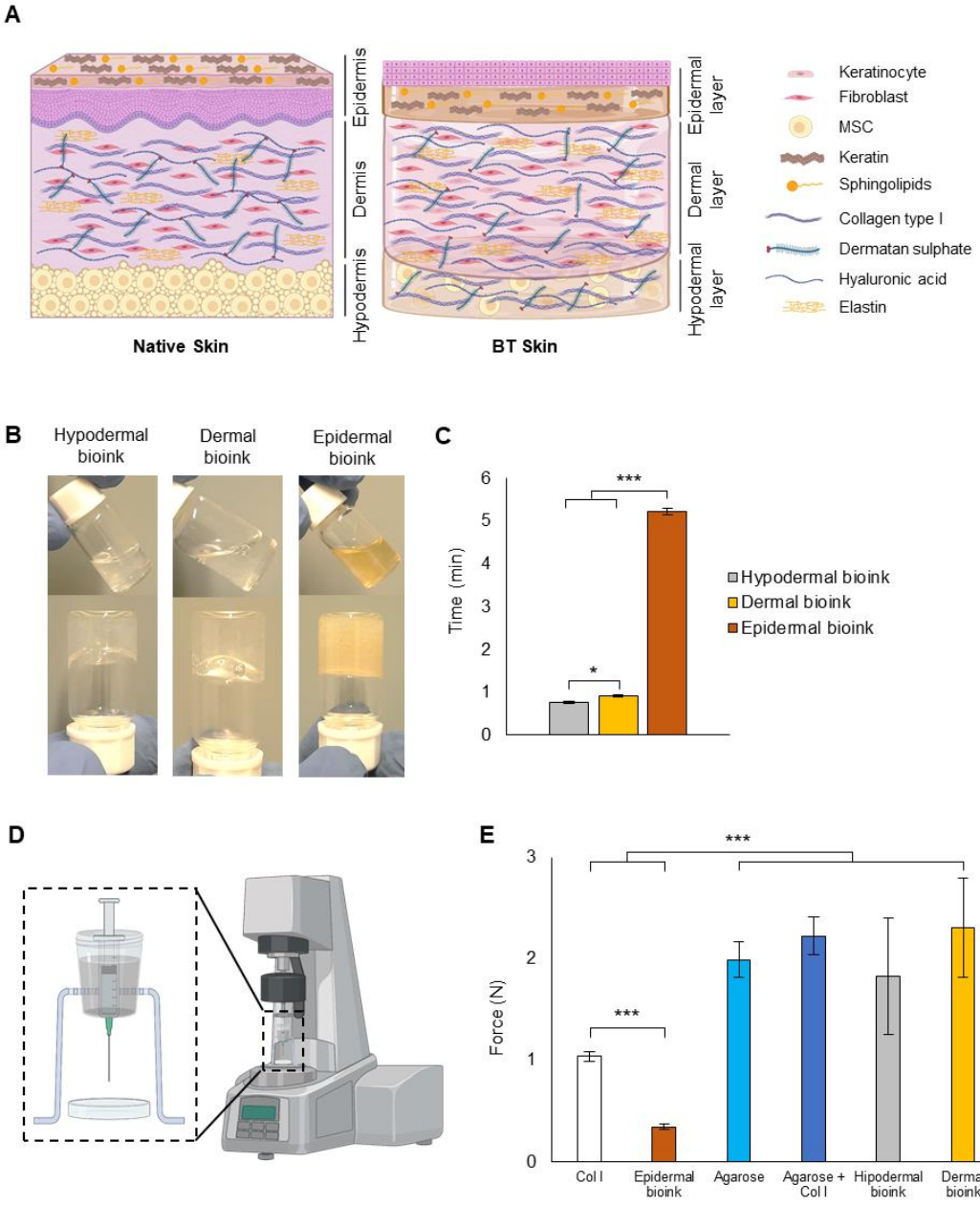

Figure 19. (A) Design of the BT Skin hydrogel compared with Native Skin. Cells such as hEKs, hDFs and hMSCs, and biological components such as Kt, Sph, Col I, DS, HA, and EL are depicted. Tube inversion test images (B) and results (C) of Hypodermal, Dermal and Epidermal bioinks. (D) Experimental design of the injectability assay. (E) Minimum force needed to extrude bioinks through a 3 mL bioprinter syringe. Statistical significance: *P < 0.05; ***P < 0.005

Regarding the cellular fraction, the epidermis is typically populated by human epidermal hEKs and the dermis by human dermal hDFs. Therefore, to mimic the biological features of the epidermis and the dermis, epidermal and dermal bioinks were populated with hEKs and hDFs, respectively (341,353). On the other hand, human hMSCs were used at the hypodermal layer, as they can promote wound healing and have been described to migrate to the wound site, differentiate and repopulate the injured tissue by promoting regeneration (565).

Consequently, the main objective of this study was to develop and characterize bioactive and biomimetic hydrogels for fabricating a skin substitute with epidermal, dermal, and hypodermal layers for skin TE. After evaluation of the diverse physicochemical, mechanical, and biological properties of the bionks formulated specifically to simulate each layer of the skin, we BT skin substitute that was characterized *in vitro*, and its full-thickness skin wound healing properties were assessed *in vivo*.

2. Materials and Methods

2.1. Cell cultures

hMSCs were isolated from human adipose tissue and characterized as previously reported (494,495). These samples were transported to the laboratory in DMEM (Sigma) with 1% P/S (Invitrogen). hMSCs were cultured in high-glucose DMEM supplemented with 10% FBS and 1% P/S, at 37 ºC in a humidified atmosphere containing 5% CO_2. Medium was refreshed every 3 days. At 80% of confluence, cells were passaged, and used between passages 4 and 6 for all the experiments. hDFs and hEKs were isolated from human skin samples obtained from donors as previously reported (30). Once skin samples were excised, they were transported to the laboratory in sterile recipients containing high-glucose DMEM without phenol red (Sigma) supplemented with antibiotics (341). Once isolated, hDFs and hEKs were cultured as previously described (336). All human samples used in this study were obtained after informed consent and authorization was provided from the Granada Provincial Ethics Committee (Ministry of Health and Families, Andalusia, Spain, reference: 0467-N-20).

2.2. Bioinks and BT skin substitute preparation

Firstly, an Ag (UltraPure™ Low Melting Point Agarose Thermo Scientific™) solution was prepared in PBS, autoclaved at 120ºC for 2 h and stored at 4ºC until use. Ag was preheated and maintained at 37 ºC in a water bath to avoid gelation and stabilize its

temperature at 37ºC. Col I solution (3.3 mg/mL rat tail collagen I, Corning®) was neutralized with 0.8 M $NaHCO_3$. Then, three solutions using Kt (Kerapro S, Proalan S.A., Barcelona, Spain), Sph, DS, HA, and EL (Bioiberica S.A.U, Barcelona, Spain) diluted in PBS were prepared: i) Kt + Sph (KS); ii) DS + HA (DH); iii) DHE. Each solution was blended with Col I at final concentration as shown in **Table 10**. All component solutions were filtered through a 0.22 μm membrane (Merck Millipore) before their use. To biofabricate the BT skin substitute, cell-loaded dermal and hypodermal bioinks were prepared by mixing Col I + DHE with hDFs and Col I + DH with hMSCs, respectively, and pre-heated Ag was added to each blend, obtaining a final concentration of 1 x 10^6 cells/mL. Once both hypodermal and dermal layers were obtained, the epidermal bioink (Col I + KS) was laid on top and let to gel inside an incubator at 37ºC during 15 min. Once the epidermal layer gelled, $2 \cdot 10^6$ hEKs were seeded on top of the BT skin hydrogel and cultured for 1 week. After this time, samples were partially dehydrated by the application of 100 g of pressure for 2 min, giving the hydrogels a higher resistance and enhancing their stiffness and mechanical properties (341,566,567).

Table 10. Final concentrations of the bioinks

(mg/ml)	**Agarose**	**Collagen I**	**DS**	**HA**	**EL**	**Kt**	**Sph**
Epidermal bioink	-	4.4	-	-	-	15.2	5.0
Dermal bioink	15	2.2	8.4	1.0	1.0	-	-
Hypodermal bioink	15	2.2	8.4	1.0	-	-	-

2.3. Physical characterization of hydrogel bioinks

2.3.1. Macroscopic characteristics

The physical appearance of the hydrogel bioinks was inspected visually before and after sterilisation. Macroscopic aspect, turbidity and colour were also evaluated.

2.3.2. Tube inversion test

The tube inversion test was used to define the gelation time of the hydrogel bioinks. The bioinks were poured in glass vials, inverting the vials upside down every 1 min to check the formation of stable gels. The gelation time was estimated as the time point when the samples formed a stable gel that remained at the bottom of the vials when inverted.

2.3.3. pH determination

The pH of the hydrogels obtained from the bioinks was determined using a calibrated digital pH meter Hach Sension$^+$ (Hach Lange S.L., Spain) at room temperature (RT).

2.3.4. Injectability test

The force required to extrude the different biomaterial blends was measured using a torsional rheometer MCR302 (Anton Paar, Austria). The equipment used for the assay was disposed as seen in **Figure 19D**, where a 3 mL syringe was maintained surrounded by heated water at a temperature of 37 ºC to avoid fast gelation and reproduce the environment of a 3D bioprinter heated syringe. Samples were placed in the syringe, and the force required to extrude the bioinks was monitored.

2.4. Physical characterization of BT skin substitute

2.4.1. Swelling test

Swelling rates of freeze-dried samples were determined as previously described (497). Briefly, samples were pre-weighed and submerged in PBS. The swelling rate of the BT skin substitute was calculated at different time points as follows [1]:

$$Swelling\ ratio\ (\%) = \left(\frac{(W_t - W_0)}{W_0}\right) x\ 100 \text{ [1]}$$

W_0 represents the initial weight of samples at day zero and W_t represents the wet weight of samples at the corresponding time point.

2.4.2. Degradation test

The degradation rate was analysed quantifying the weight loss of samples over time. The BT skin substitute was incubated under gentle agitation at 37ºC, retrieved at different time points, and centrifuged at 5000 rpm for 2 min. Supernatant was removed, and samples were weighed (498). Degradation rate (%) was calculated as a measure of weight loss as follows [2]:

$$Degradation\ ratio\ (\%) = \left(\frac{(W_t - W_i)}{W_i}\right) x\ 100 \text{ [2]}$$

W_i represents the initial weight of samples and W_t represents the wet weight of hydrogels at the corresponding time point.

2.4.3. Mechanical analysis

Mechanical properties were evaluated using a torsional rheometer MCR302 (Anton Paar, Austria). BT skin samples were casted using a 20 mm in diameter and 5 mm in height mould. A three-step assay was designed to obtain data on the compression and shearing characteristics of hydrogels. At the first step, specimens were placed on the base of the rheometer, approaching the rheometer head at 10 µm/s up to a normal force of 0.5 N. Secondly, the samples were oscillatory sheared with a strain amplitude of 0.00001% at a frequency of 1 Hz and normal force of 0.5 N to analyse the shear viscoelastic moduli, and lastly, the upper plate was removed at a constant speed of 10 µm/s. Cell-free and cell-loaded BT skin substitute before (pre cell-free BT skin and pre BT skin) and after (cell-free BT skin and BT skin) partial dehydration were generated and maintained at 37 ºC in a 5% CO_2 atmosphere until measurement.

2.5. Cell viability assay

The LIVE/DEAD™ Viability/Cytotoxicity Kit (Invitrogen, Massachusetts, EEUU) was used to analyse cell viability. Separated hydrogels for hypodermal and dermal layers and BT skin substitute were stained using a calcein AM (2 µM; green) and ethidium homodimer (4 µM; red) solution diluted in PBS at 37 ºC for 30 min. Samples were observed using confocal microscopy (Nikon Eclipse Ti-E A1) at different times and analysed using NIS-Elements software. Live and dead cells were quantified using the ImageJ (Fiji) software (496), determining the cell viability percentage as follows [3]:

$$Cell\ viability\ (\%) = \frac{Live\ cells}{(Live\ cells + Dead\ cells)}\ x\ 100 \quad [3]$$

2.6. Cell proliferation assay

The AlamarBlue HS® assay (Invitrogen) was used to analyse the cell proliferation of the samples after 1, 3, 5, 7, 14 and 21 days of culture. The fluorescence after incubation was measured, separated hydrogels for hypodermal and dermal layers and BT skin substitute were incubated with the AlamarBlue HS® solution at 37 ºC for 1h. The fluorescence of the reduced solution was determined at 530/590 nm excitation/emission wavelengths.

2.7. *In vivo* assay

2.7.1. Wound healing animal model, surgical procedures, and experimental groups

A total of 32 ATHYM-Foxn1nu/nu male and female, immunodeficient, athymic,

nude and albino mice of 4 weeks of life, were employed for the *in vivo* assay (Janvier Labs, Le Genest-Saint-Isle, France). All animal handling procedures followed the national and European Union legislation (Spanish RD 53/2013 and EU Directive 2010/63) for the protection of animals used for scientific purposes and in accordance with the Ethical Principles and Guidelines for the Use of Animals approved by Provincial Ethics Committees of Granada.

A surgery to remove a skin area of 2 cm^2 from the upper dorsal, in a longitudinal position to the mouse spine, was performed using surgical scissors. A sterile, 3D printed 1,4-butanediol thermoplastic polyurethane elastomer (b-TPUe) (568), donut-shaped, porous splint designed with a hinged lid (**Figure S3**) was centred over the wound and secured with seven interrupted sutures (569). Then, mice were transplanted with a BT skin, a cell-free BT skin, a skin autograft from the lower back (autograft) or were left untreated as control conditions (Control) (n = 8 per group). Finally, the splint lid was closed with eight interrupted sutures.

For all groups, samples and splints were grafted and an antibiotic ointment (Mupirocina 20 mg/g; ISDIN) was applied. Also, an analgesic (Bupredine 0.3 mg/mL 10 mL; Fatro Ibérica, Desvern, Barcelona, Spain) and an antibiotic (Ganadexil Enrofloxacino 5% 100 mL; Industrial Veterinaria, S.A. Invesa) were subcutaneously injected as postoperative treatment.

2.7.2. Skin repair monitoring

Throughout 8 weeks, a follow-up was carried out, collecting clinical information, such as scar/wound area, and several homeostasis parameters. As well, after 8 weeks, scars were evaluated using an adaptation of the Patient and Observer Scar Assessment Scale (POSAS) (570,571). Each 2 weeks, mice were anesthetized using isoflurane inhalation to avoid unnecessary stress and homeostasis skin parameters were measured using the Microcaya probe system (Microcaya S.L., Bilbao, Spain), allowing to monitor: the Thermometer® probe allowed to measure skin temperature in ºC; the Skin pH-meter® probe measured the skin pH; the Tewameter® probe determined the TEWL, as the evaporation of water in g/h/m^2; the Cutometer® probe analysed the skin elasticity (µm) with suction (450 mbar of negative pressure – 2 s); the Corneometer® probe determined the skin moisturization through the capacitance of a dielectric medium; and the Mexameter® probe, based on the light absorption/reflection of three wavelengths, was able to measure the erythema and pigmentation of the skin, obtaining indirect information about the vascularization (haemoglobin levels) and pigmentation (melanin), respectively.

Values of healthy skin were obtained by measuring a healthy area of skin (native skin) from each mouse from the study.

2.7.3. Histological and Immunohistochemical analysis

Four and eight weeks later, mice were sacrificed by cervical dislocation once anesthetized by isoflurane inhalation. Graft biopsies and native skin samples were collected, fixed in 4% paraformaldehyde, dehydrated, embedded in paraffin or in Optimal Cutting Temperature (OCT) compound (Tissue-Tek®, Sakura Finetek), and cut into 5 µm or 8 µm sections using a microtome and a cryostat, respectively.

Paraffin sections were deparaffinized, rehydrated, and stained with haematoxylin & eosin (H&E) and Masson's Trichrome to reveal the histological structure. For immunofluorescence analysis, cryosections were incubated with primary antibodies against fibronectin (Santa Cruz Biotechnology, 1:100) and cytokeratin (Invitrogen, 1:100). Sections were then incubated with a secondary Alexa-488-conjugated anti-rabbit antibody (ThermoFisher, 1:500) and counterstained with Hoechst. Images were obtained using a Leica DM 5500B microscope and analysed with Image J software.

2.8. Statistical analysis

Results in this work are represented as mean ± standard deviation (SD). Differences between two groups of data were tested using the two-tailed Student's T test for unpaired samples. Differences were considered statistically significant at $P < 0.05$ (*/#), $P < 0.01$ (**/##) and $P < 0.005$ (***/###).

3. Results

3.1. Physicochemical properties of bioinks

3.1.1. Macroscopic characteristics

In **Figure 19B** the three bioinks in their liquid state can be observed. Both hypodermal and dermal bioinks presented a whitish nearly transparent aspect, while the epidermal bioinks showed a brownish colour, quite turbid. The brownish colour of the epidermal bioink is given by its Kt component, which holds this shade.

3.1.2. Tube inversion test and pH

The gelling time was monitored by applying the tube inversion test for hypodermal, dermal, and epidermal bioinks. **Figure 19B** shows representative images of the bioinks in their liquid and gelled form. The average gelling times of the hypodermal, dermal, and

epidermal bioinks were 0.76 ± 0.03, 0.91 ± 0.03 and 5.22 ± 0.09 min (**Figure 19C**), respectively.

3.1.3. Injectability of bioinks

To characterize the injectability of the bioinks, the force required to extrude the solutions from a 3 mL syringe was measured. Results ranged between 0.34 to 2.3 N (**Figure 19E and S4**). The epidermal bioink (0.34 ± 0.03 N) showed the lowest value, even lower than the force needed to extrude Col I (1.04 ± 0.04 N). Regarding the hypodermal (1.82 ± 0.57 N) and dermal bioinks (2.30 ± 0.49 N), although they showed no differences between them, they showed a higher range of N (1.25 – 2.79 N) than both Col I and epidermal bioink conditions (0.34 – 1.08 N).

3.2. Physicochemical properties of the BT skin substitute

3.2.1. Macroscopic characteristics

Figure 20A shows the macroscopic aspect of the BT Skin (black arrow signalling the epidermal layer), as it can be observed, two main sections can be visually differentiated: a) the upper opaque epidermal layer, made of Col I with Kt and Sph supplementation, seeded with hEKs on its top; and b) the lower double dermal and hypodermal layers made of the blend of Col I and Ag, supplemented with DS-HA-EL and DS-HA, respectively. Both hypodermal and dermal layer showed a translucid whitish shade, remaining undifferentiated from each other. **Figures 20B and C** show the height difference of the hydrogel before and after the partial dehydration process, where 2 mm of the hydrogel height is reduced.

3.2.2. pH, swelling and degradation performance of BT skin hydrogels

The pH value of the full BT skin hydrogel was 7.5 ± 0.1**.** Moreover, freeze-dried BT skin hydrogels were immersed in PBS (pH 7.4) to observe their swelling behaviour. Swelling kinetics of the BT skin for an elapsed time of 21 days is shown in **Figure 20D**. The average swelling was 70 ± 7 %. The BT skin (freeze-dried) hydrogel showed to reach a plateau stage after 7 days. To analyse the endurance over time, a degradation assay was carried out by measuring the weight change up to 21 days (**Figure 20E**) showing that the maximum degradation rate was reached after 14 days with an 8.8 ± 1.5 % of mass loss.

3.2.3. Mechanical behaviour of the BT Skin hydrogels

The Young moduli of the hydrogels maintained up to 21 days compared to human native skin biopsies are depicted in **Figure 20F**. Even though variations were found in pre BT Skin (7.49 ± 0.62 kPa) and cell-free BT Skin (13.24 ± 0.30 kPa) compared to

native skin (9.46 ± 0.79); however, BT skin (9.06 ± 0.21 kPa) showed no significant differences in comparison with the target tissue.

The viscoelastic moduli of cell-free and cell-loaded BT skin hydrogels before and after dehydration were also measured and are shown in **Figure 20G**. Although the four tested conditions were found to share the same loss modulus range of the native skin (2.92 ± 0.91 kPa), only the BT skin hydrogels loss modulus (0.28 ± 0.10 kPa) showed no significant differences when compared to the native skin loss modulus (0.83 ± 0.33 kPa).

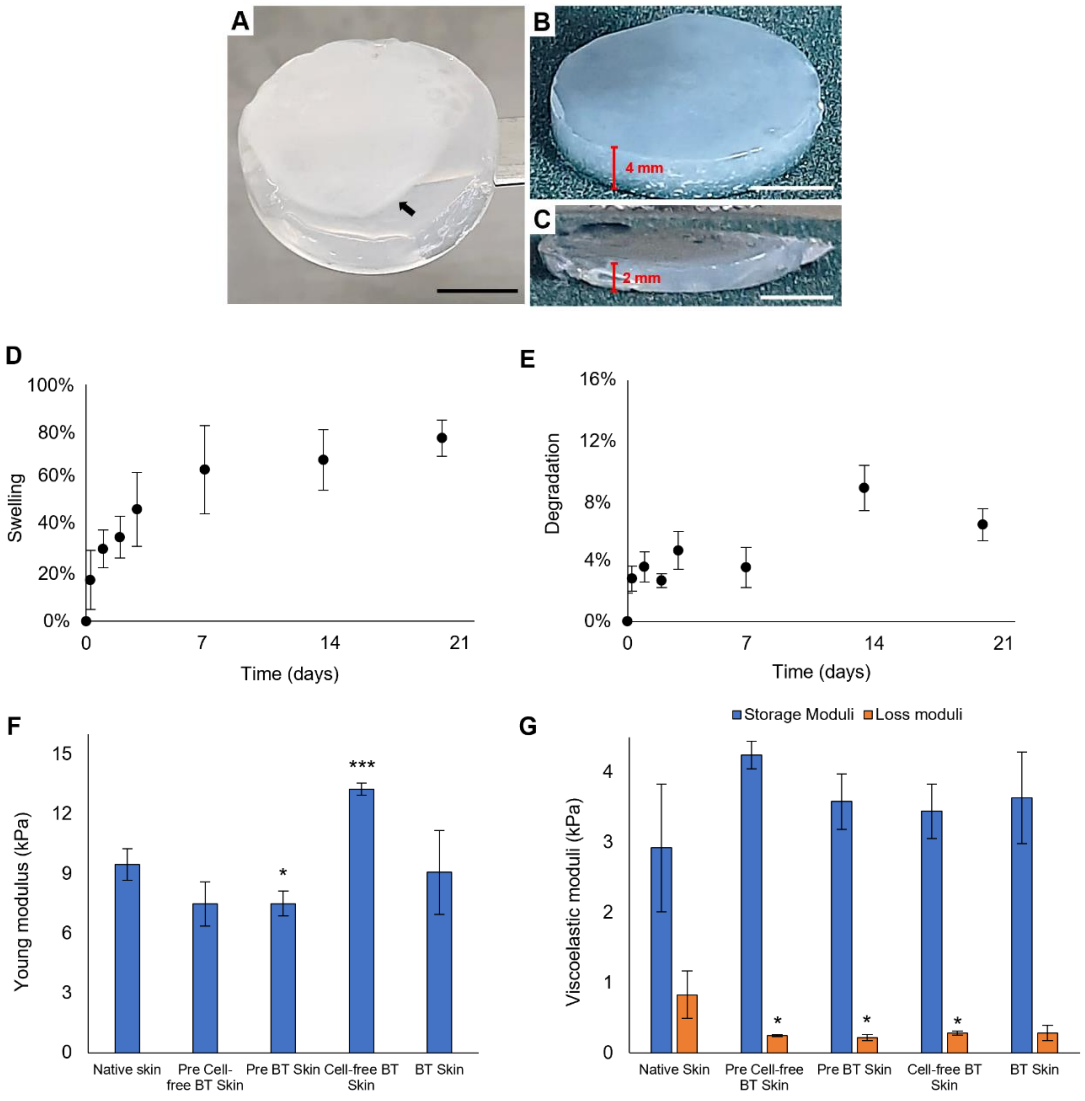

Figure 20. Macroscopic images of the BT Skin hydrogel (A; black arrow: epidermal layer), before (B) and after (C) partial dehydration (Scale bars = 5 mm). Swelling (D), degradation (E) and rheological assays (F and G). (D) Swelling behaviour and (E) degradation percentage of BT Skin hydrogel over 21 days. Young moduli (F) and viscoelastic moduli (G) of BT Skin hydrogels, with or without cells, before and after

partial dehydration process, after 21 days in culture, compared with native skin. Statistical significance: *P < 0.05, ***P < 0.005.

The viscoelastic moduli of cell-free and cell-loaded BT skin hydrogels before and after dehydration were also measured and are shown in **Figure 20G**. Although the four tested conditions were found to share the same loss modulus range of the native skin (2.92 ± 0.91 kPa), only the BT skin hydrogels loss modulus (0.28 ± 0.10 kPa) showed no significant differences when compared to the native skin loss modulus (0.83 ± 0.33 kPa).

3.3. Biological characterization of bioinks and the BT Skin model

A biological characterization of the hypodermal and dermal bioinks was carried out with cell proliferation and viability assays. Since epidermal bioink manipulation was complicated, as it showed to be brittle once gelled, this bioink was incorporated to the BT skin substitute once the biological characterization of the full skin substitute was carried out. Cell proliferation rates of both hypodermal and dermal bioink hydrogels at days 0, 1, 3, 5, 7, 10, 14, 18 and 21 are shown in **Figures 21A and C**, respectively. Hypodermal hydrogels showed an increase of cell proliferation at day 5, maintaining a plateau stage until the end of the experiment. Likewise, the dermal bioinks increased their cell proliferation from day 14, maintaining its level until the end of the experiment. Both bioinks were able to maintain cell viability level above 97% during the duration of the assay (**Figures 21B, D and E**), as evidenced by the images acquired at 0, 7, 14 and 21 days.

The BT skin substitute was prepared in a three-layered way with the hypodermal layer at the bottom, a middle dermal layer, and the epidermal layer over the top (**Figure 21A**), and partially dehydrated.

Similarly, to the hypodermal and dermal bioinks, the BT Skin substitute showed a rise in cell proliferation rate from day 5, remaining in a plateau stage until the end of the experiment (**Figure 22A**). As well, BT skin substitute showed cell viability rates between 90.9 – 98%. Moreover, to observe the distribution of the three cell types within each layer, hMSCs, hDFs and hEKs were stained with CellTracker™ Green CMFDA, CellTracker™ Red CMTPX, and CellTracker™ Green CMFDA, respectively (**Figure 22B**). In some areas of the hydrogels, cells were able to adhere and grow in contact with the surrounding cells (**Figure 22C**). As it can be observed in **Figure 22D** the three layers of the bioactive BT skin hydrogel were well differentiated and maintained the structure throughout all the study time.

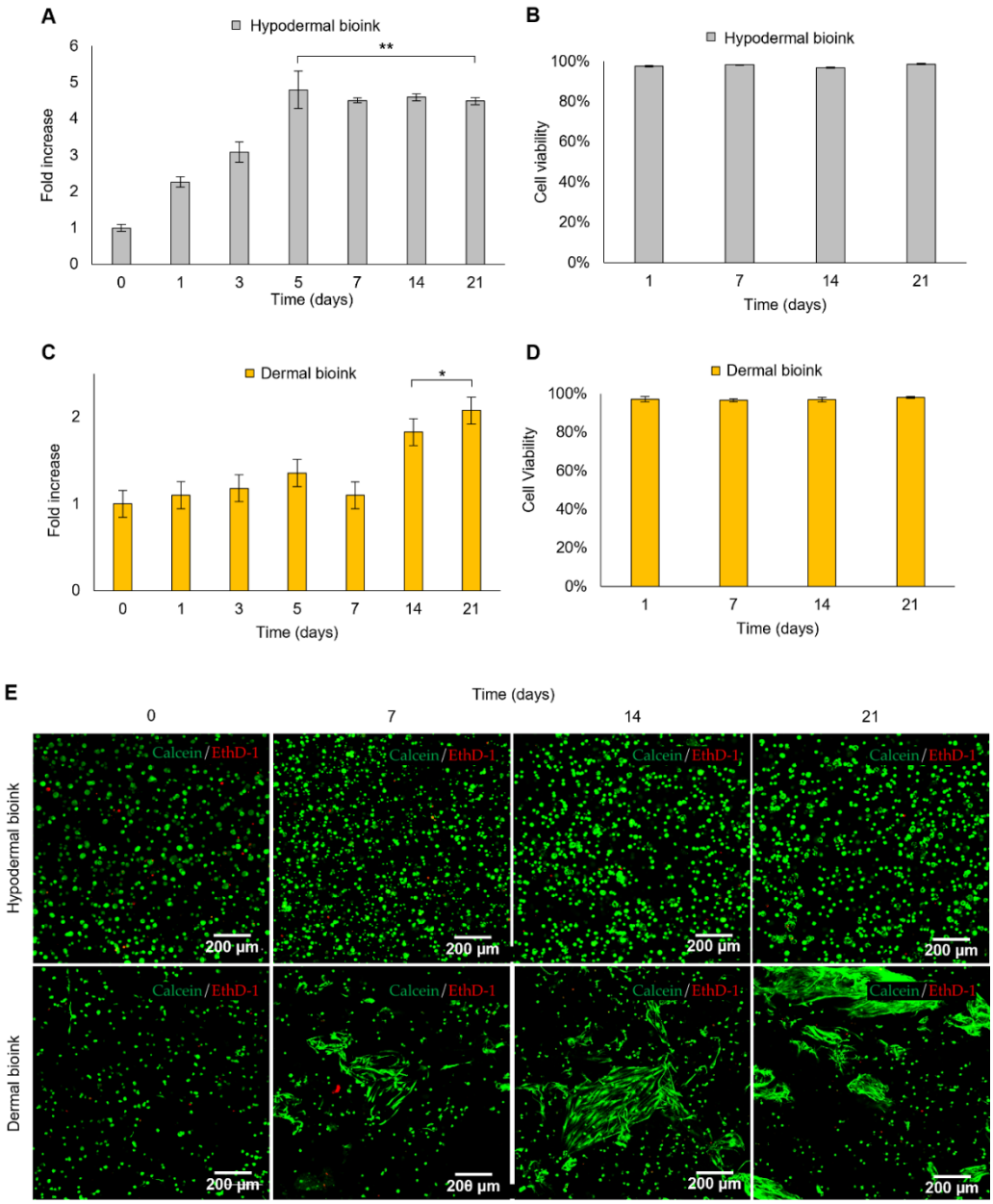

Figure 21. Hypodermal bioink cell proliferation (A) and viability (B). Dermal bioink cell proliferation (C) and viability (D). Representative confocal images of Hypodermal and Dermal bioinks at days 0, 7, 14 and 21. Live/dead assay was employed, using calcein (green) and ethidium homodimer (red), live cells were stained green while dead cells were stained red. Scale bars: 200 µm.

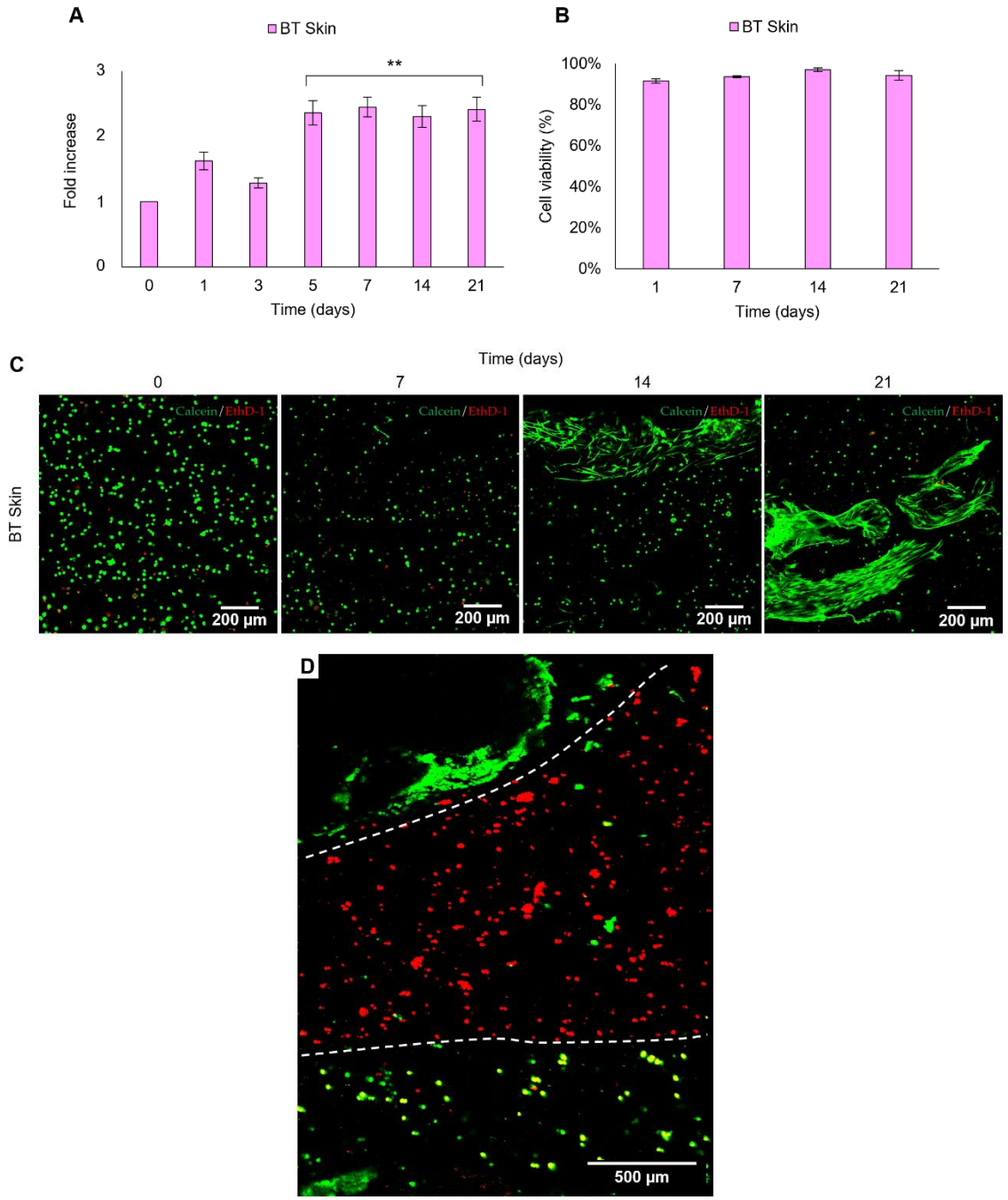

Figure 22. BT Skin hydrogel cell proliferation (A) and viability (B and C). Confocal fluorescence image of BT Skin hydrogel after 21 days of culture (D; hEKs labelled in green at the top, hDFs labelled in red in the middle, and hMSCs labelled in green at the bottom).

3.4. *In vivo* assay

3.4.1. Clinical assessment

An adequate stabilization of the wound was observed for all groups of mice after 4 weeks, with no complications (**Figure 23A**). Wound resolution was faster in the case of the groups treated with autograft, cell-free BT skin, and the BT skin substitute than in the control group. Similarly, wound repair was faster and more effective in the case of the BT skin group, while control, autograft, and cell-free BT skin groups experienced slower improvement. In the case of BT skin, total skin repair was observed after 8 weeks.

Results evaluation by visual clinical observation (**Figure 23A**) correlated with quantitative analysis of wound/scar area (**Figure 23B and C**), where significant differences were found between cell-free BT skin and the BT skin substitute groups when compared with control group at week 2, indicating a positive effect of these conditions on the wound healing process, but at the end of the experiment, only the BT skin group showed significant differences with the control group.

3.4.2. Homeostasis study

Temperature, pH, TEWL, elasticity and moisture were monitored (**Figures 24 and S5**), comparing all groups towards native skin of mice. Temperature (**Figures 24A, H, O and V**) and pH results (**Figures 24B, I, P and W**) showed a homogeneous evolution in all groups overall the study, with no differences compared to native skin. Temperature values of all groups during the study ranged 31.8 ºC– 36.6 ºC, overlapping the range of the native skin temperature (34.0ºC – 36.0 ºC). Similarly, pH ranges of all groups (5.2 – 7.8) and native skin (6.4 – 7.3) also overlapped overall the duration of the experiment. TEWL (**Figures 24C, J, Q and X**) showed a significant decrease after 2 weeks in all groups (**Figure S5**), reaching native skin levels. Regarding elasticity (**Figures 24D, K, R and Y**), although in control and BT skin groups showed an oscillatory behaviour throughout the experiment, there were no significant differences between all groups and the native skin overall the 8 weeks. Finally, similarly to TEWL results, moisture monitorization (**Figure 24E, L, S and Z**) showed a recovery after 2 weeks, restoring the native skin levels at 4 weeks in all groups.

3.4.3. Erythema and pigmentation evaluation

Erythema assessment (**Figure 24F, M, T and AA**) of control, autograft, and cell-free BT skin groups reported no significant differences towards native skin; however, BT skin showed significantly higher levels during the 8 weeks of the experiment. Regarding pigmentation (**Figure 24G, N, U and AB**), control and autograft groups were not able to

reach native skin melanin levels until 4 weeks; however, after 2 weeks cell-free BT skin and BT skin groups had already restored those levels.

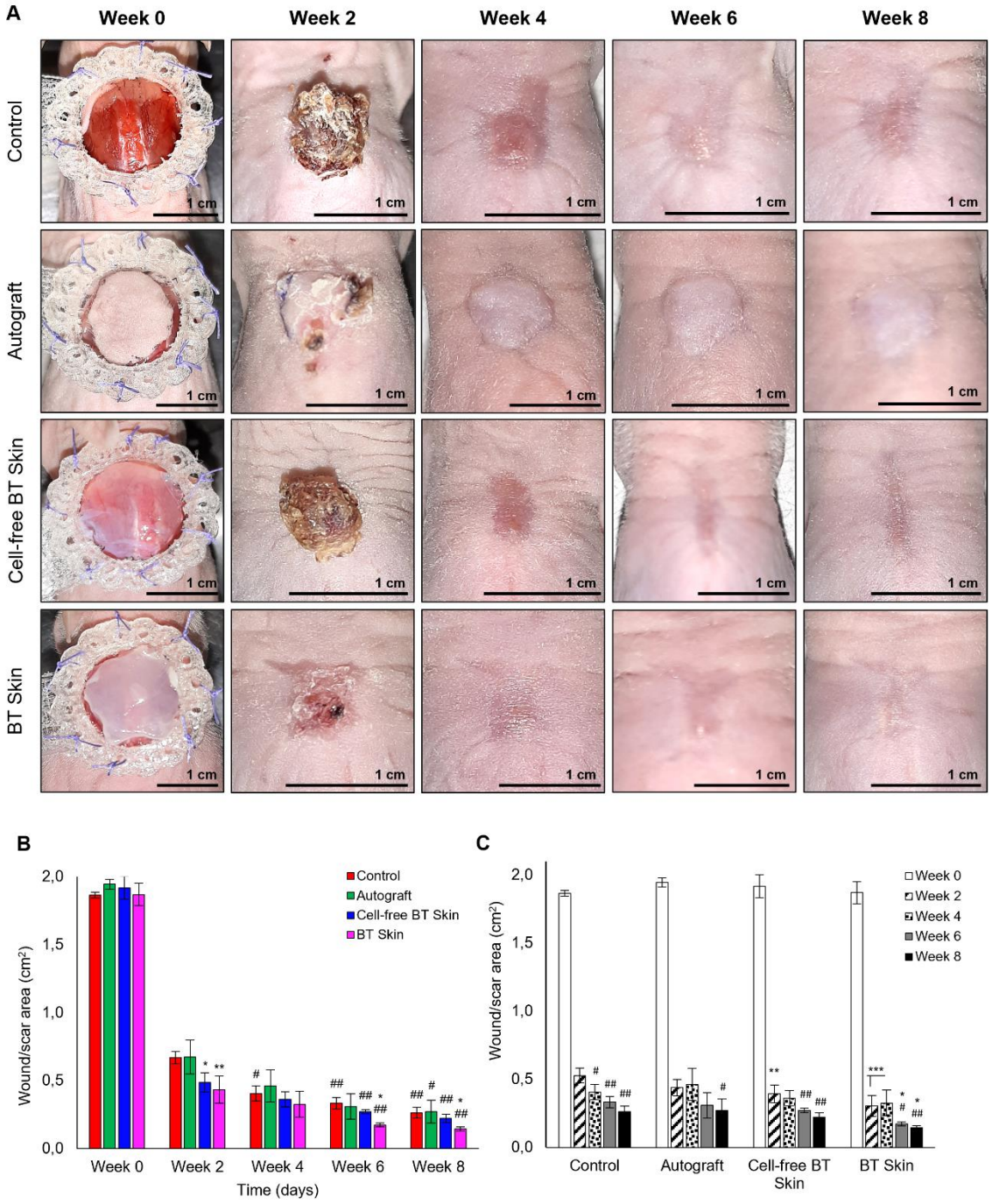

Figure 23. (A) Macroscopic images of wound healing process over time. Type of treatment is indicated in each row, while progression time (week 0, 2, 4, 6 or 8) is represented in each column. Scale bars are represented in each image: 1 cm. Quantitative evaluation of wound/scar area through time for all groups (B) and in separated groups

(C). Statistical significance compared to control: *P < 0.05; **P < 0.01; ***P < 0.005. Statistical significance compared to day 14: #P < 0.05; ##P <0.01.

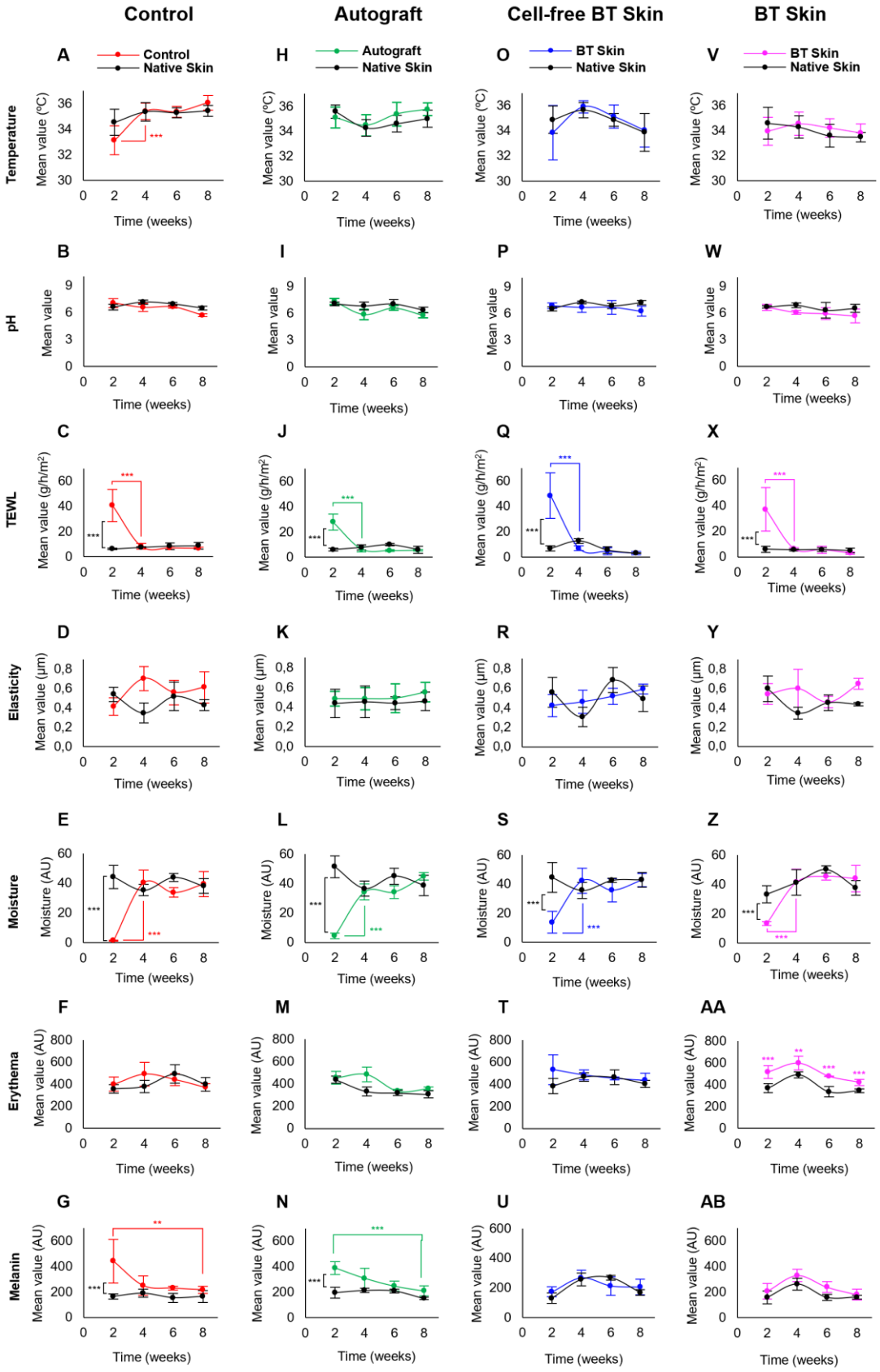

Figure 24. Analysis of homeostasis parameters per week and group. Graphics show results for each group of treatment against Native Skin group. (A, B, C, D, E, F and G) Control group; (H, I, J, K, L, M and N) Autograft group; (O, P, Q, R, S, T and U) Cell-free BT Skin; (V, W, X, Y, Z, AA and AB) BT Skin. Results per week were calculated as the mean value of all mice measures at each time of study; Control, Autograft, Cell-free BT Skin and BT Skin groups (n week 2, 4, 6, 8 = 8, 8, 4, 4); Native Skin group (n week 2, 4, 6, 8 = 32, 32, 16, 16). Statistical significance: *P < 0.05; **P < 0.01; ***P < 0.005.

3.4.4. Histological and Immunostaining analysis

H&E and Masson's Trichrome staining's of wound biopsies (**Figure 25 and S7**) showed a correct regeneration of the epidermis and dermis after 4 and 8 weeks in all groups; however, autograft, cell-free BT skin and BT skin groups presented a more complex dermal matrix structure closer to native skin than control group, which showed a less dense dermal matrix structure after 4 weeks of surgical procedure. As it can be observed in **Figure 26**, the immunohistological analysis showed an increased expression of fibronectin, a typical protein found in dermal ECM. As well, the expression of cytokeratin, a specific epidermal differentiation marker, was observed in all groups, showing that a good re-epithelialization and epidermal differentiation was achieved. Regarding the hypodermal layer, the absence of subcutaneous adipose tissue of the samples could have been caused by the histological processing of the samples.

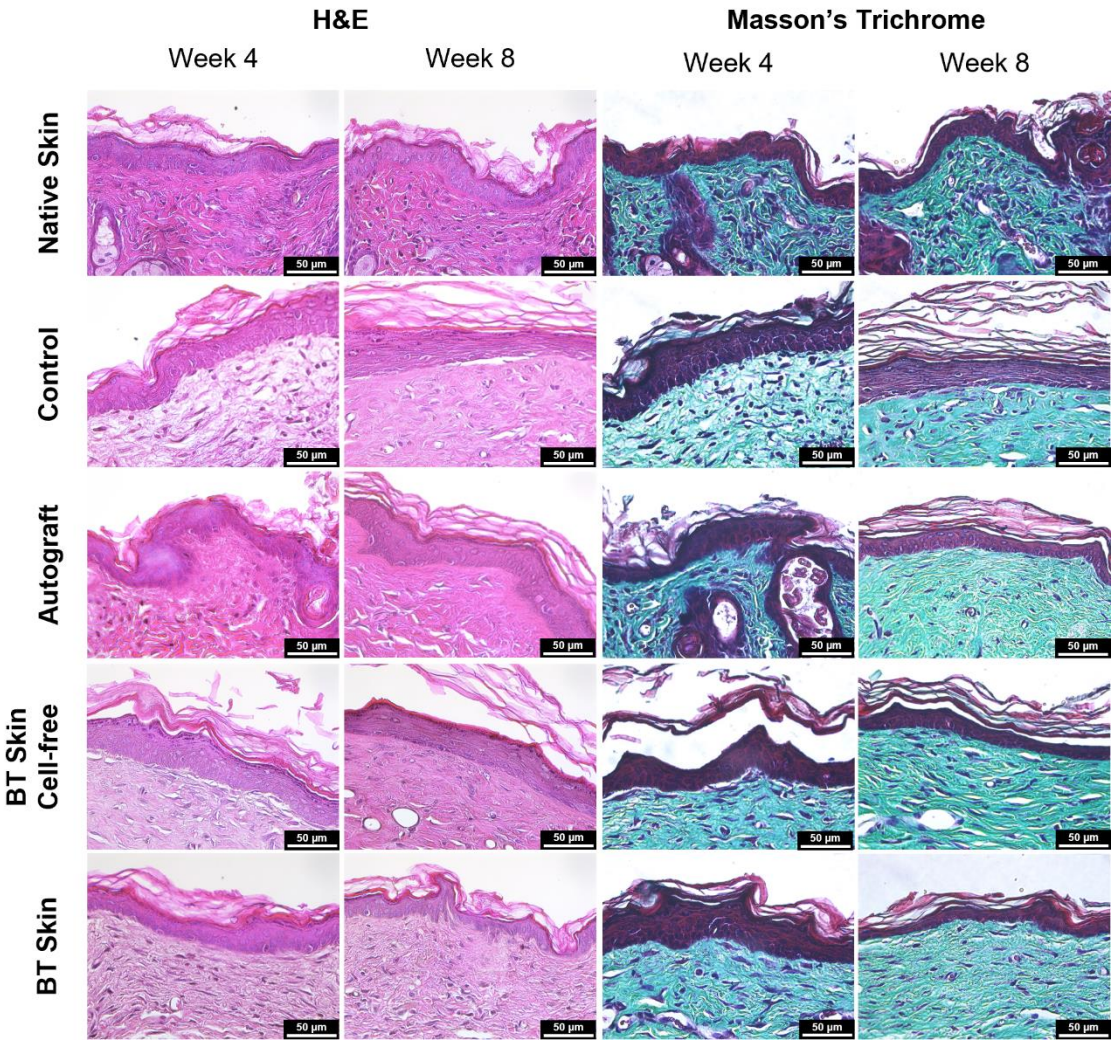

Figure 25. Haematoxylin and eosin (H&E) and Masson's Trichrome histological stainings from biopsies of mice wound/scar area and native skin after 4 and 8 weeks. Scale bar: 50 µm.

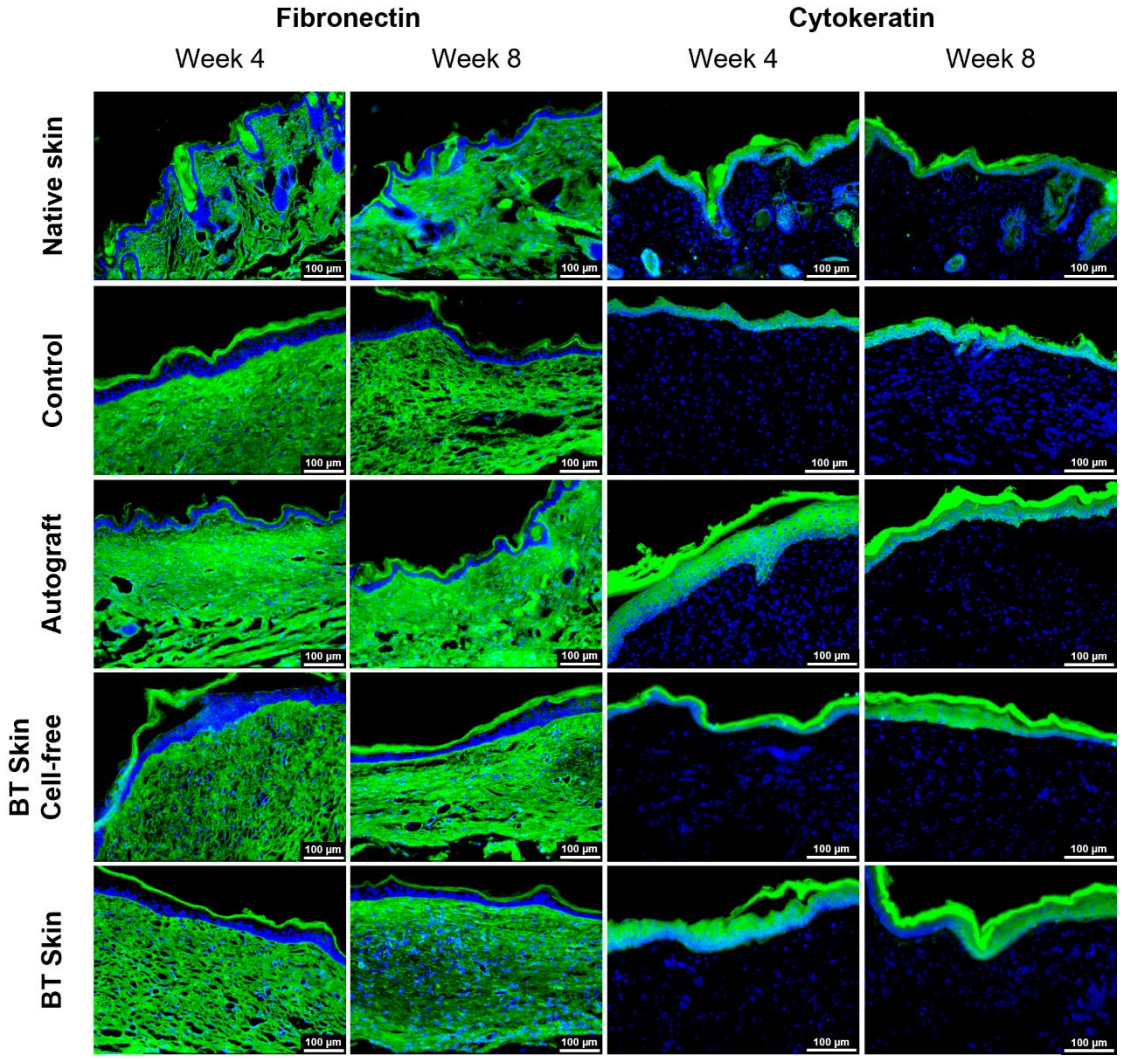

Figure 26. Fibronectin and cytokeratin profiles of mice wound/scar area and native skin biopsies after 4 and 8 weeks. Fluorescent microscopy observations. Scale bar: 100 µm.

4. Discussion

Recently, three-layered skin substitutes that intend to better mimic the anatomy of the skin (epidermis, dermis, and hypodermis) have attracted attention. The epidermal layer is populated by hEKs in a ECM enriched in Kt and Sph; the dermal layer mainly consists of hDFs embedded in a ECM formed by a variety of proteins (such as collagen and EL) and GAGs (such as HA and DS) which are produced by them; and the hypodermal layer mainly consists of adipocytes and MSCs conforming fat tissue, surrounded by connective tissue and basal membrane (572). However, most of these three-layered constructs only use a one-component hydrogel, such as col I (573,574) or a biomaterial that does not even relate to the native skin ECM, such as fibrin (575). Nevertheless, more biomimetic constructs are trying to be developed, such as using Kt to reproduce the epidermal ECM (576). Here, we present a study in which the ECM of each of the three layers of the skin have been customized to biofabricate a more bioactive and biomimetic skin substitute.

As a first step, a physicochemical characterization was carried out for each of the three bioinks and for the BT skin substitute. The gelling time of the bioinks was assessed since it is an important parameter during the biofabrication process. All three bioinks showed optimal gelling times, since good printability and 3D structures can be achieved with gelling times $t < 15$ min (577). The injectability of a bioink is essential to ensure their good printability and avoid syringe clogging due to an early gelation in 3D bioprinting applications. The three bioinks also showed that minimal forces are needed to be extruded without clogging, which would enable their application through bioprinter syringes (578).

Regarding the BT Skin, it showed a neutral pH (7.5 ± 0.1) suitable for skin TE as it has been observed that, to maintain an optimal skin barrier function, collagen-based hydrogels should be pH-neutral (520). Moreover, the hydrogel swelling is an essential characteristic as it is involved in nutrient and water transport within the surrounding media, also providing remarkable mechanical resiliency (523), lowering the interfacial tension, promoting metabolite exchange and improving cell viability (524). In our case, the BT skin substitute presented a high swelling capacity that stabilized after 3 weeks and showed slow degradation rates. Nevertheless, these swelling and degradation characteristics match for applications like 3D bioprinting, which require volumetric accuracy and shape fidelity (579).

Fitting the mechanical characteristics of the targeted tissue is a relevant issue to help in promoting a correct tissue regeneration (578). Since the core blend of the bioinks are Ag/Col I-based, the biological advantages of the DS-HA, DS-HA-EL and Kt supplementation could be combined with the Ag/Col I Young's modulus kPa range, which complies with native skin Young's modulus. Additionally, BT skin storage and loss moduli showed proper properties close to those found in native skin.

Once the physicochemical properties were characterized, the hypodermal and dermal bioinks, as well as the BT skin hydrogel's biological yield was assessed, revealing that both bioink hydrogels and the full BT skin substitute were able to maintain cell proliferation with high viability levels up to 21 days. Additionally, the BT skin substitute was also able to maintain its integrity after suffering a partial dehydration, decreasing its thickness, and displaying the three differentiated cellular layers along its height for 21 days. This partial dehydration was used as a plastic compression technique (566), which rapidly removes the excess fluid of the supersaturated hydrogels, to produce mechanically strengthened hydrogels with a dense matrix and cellular structure. One of the main advantages of this technique used in the clinical field (336,341,580), is the ability of introducing microlayering, mechanical properties, and micrometric topographies that increase the biomimetic potential in minutes instead of days or weeks (566).

Wound healing is a complex biological process that leads to resolution (regeneration) or repair (healing) (581). The tissue regenerates the ECM, cell population and function in wound resolution, while scarring or fibrosis due to the lack of ability to fully regenerate a tissue occurs in wound repair (582). In the current study we evaluated closure rates, homeostatic and histological characteristics of mice excision wound models treated with BT skin, cell-free BT skin, and autograft compared to an untreated control. Cell-free BT skin and BT skin showed higher reduction of the wound/scar area than control, as well as similar results than autograft in the POSAS scale. Regarding homeostasis and epidermal barrier function, autograft, cell-free BT skin and BT skin showed similar results than native skin. According to previous studies (341), it has been seen that similarly to humans, mice skin temperature varies in a range of 30 – 36 ºC in a stable environment (24 ºC). Therefore, the lack of significant differences between the groups indicates the correct restoration of this function.

When skin is harmed, its barrier function is compromised resulting in a high water loss (583,584) and, consequently, producing a reduction of skin moisture (585,586).

TEWL is considered as an *in vivo* indicator of the skin barrier integrity; in this study all groups were able to restore skin function, showing similar TEWL values than native skin.

The redness of the skin caused by hyperaemia in superficial blood vessels can be studied analysing the erythema. Control, autograft, and cell-free BT skin presented similar levels to native skin, except BT skin, which showed significantly higher values than native skin during all the duration of the experiment. This higher erythema levels could be a result of angiogenesis related to the hydrogel wound healing properties (559,560,564,587,588).

Melanin is a pigment produced by melanocytes whose main role is to minimize the deleterious effects of UVR (589). Within a wound, melanocytes would be expected to be the first cells to repopulate the damaged area, as part of the initial wound healing response. However, melanocytes seem to enter the wound later once it has re-epithelialized (590). In the present study, both cell-free BT skin and BT skin groups at week 2 had already recovered native skin melanin levels, while control and autograft groups were not able to reach those values until week 4. The outcome of this last condition was as expected, since skin autografts can experience an abrupt reduction of the melanocyte population of the graft when transplanted, which gradually increases between 1 and 3 weeks after transplantation (591).

In addition, histological and immunohistochemical staining revealed that healed skin showed a structure and morphology like native skin after 4 and 8 weeks, presenting a multi-layered epithelium, with an appropriate dermis and hDFs layout, although, absence of skin appendages and rete ridges was observed. Nevertheless, unlike the control group, which showed a less dense dermal matrix (592), autograft, cell-free BT skin and BT skin groups were able to develop a more reliable dermal matrix that resembled to native skin. As well, fibronectin and cytokeratin, which are involved in epidermal stability and re-epithelization, were abundantly expressed in mice healed skin, demonstrating the reconstruction and remodelling of wounds (593,594).

While the available variety of skin substitutes found on the market focus on restoring the dermal and epidermal structures, the subcutaneous layer is often neglected. To answer this pitfall several research groups have developed three-layered constructs in an attempt to reproduce the three-layered structure of the skin. Taking as a starting point single-material hydrogels, they used atelocollagen (595), type I collagen (573,596), or fibrin (597) and they successfully achieved to place hEKs at the epidermal layer, hDFs at the dermal layer, and AD-MSCs (595,597) or adipocytes (573,596) in the hypodermal

equivalent. Some results of these studies were improved with our BT skin substitute, like those obtained at the *in vivo* wound healing assay in a mouse model skin injury, where we reached an early wound closure after 14 days, instead of the 21 day-period with non-closure of the wound yet when using an atelocollagen three-layered construct (595). Additionally, the BT skin substitute showed an enhanced ECM complexity compared to its published counterparts, that only use a single-material component, adding a plus to our bioactive and biomimetic final product.

In summary, our results successfully demonstrate that the combination of human cells with the biomaterials conforming the BT skin were able to effectively promote skin wound healing and regeneration processes and could be the best alternative to autografts for skin wound treatment. Further studies will be taken into consideration to test the potential application of these hydrogel formulations as bioinks by using the 3D bioprinting technology and to implant this biofabricated BT skin substitute in the clinic.

7. CONCLUSIONS

1. The elastic characteristics of b-TPUe changes when modifying the porosity, improving the customization of the mechanical properties of the constructs, therefore offering the possibility to better adapt this parameter to the desired target tissue
2. b-TPUe demonstrated a much closer compression and shear behaviour to native cartilage than PCL and PLA, as well as closer tribological properties to native cartilage.
3. b-TPUe 3D printed scaffolds were able to maintain proper proliferative potential, cell viability, and supported hMSCs chondrogenesis.
4. *In vivo* studies revealed excellent biocompatibility after scaffolds implantation, and integration within the surrounding tissue.
5. The ACDHE biomimetic hydrogel shows the best cell viability outcome of the screened combinations.
6. The DHE supplement blend alone shows the ability to promote a faster *in vitro* wound healing.
7. The ACDHE hydrogel presents interesting physicochemical and mechanical properties for its application as a skin substitute or an injectable hydrogel.
8. The bilayered ACDHE hydrogel with hDFs and hMSCs allows the growth and proliferation of the hosted cells.
9. The BT Skin hydrogel simulates the three-layered distribution of skin-related biomolecules and cells.
10. The physicochemical characteristics of the BT Skin hydrogel support that this strategy has potential application for 3D bioprinting, allowing to achieve similar mechanical properties like those found in the native skin tissue.
11. The BT Skin substitute can help restore the *in vivo* physiological homeostatic

equilibrium and epidermal barrier function of skin wounds.

12. The BT Skin hydrogel promotes wound healing and the reconstruction of the histological architecture of native skin tissue in mice.

CONCLUSIONES

1. Las características elásticas de b-TPUe cambian al modificar la porosidad, mostrando una mayor capacidad de personalización de las propiedades mecánicas de los objetos impresos, ofreciendo así la posibilidad de adaptar mejor este parámetro al tejido objetivo deseado.
2. b-TPUe mostró comportamientos de compresión, cizallamiento, y fricción mucho más cercanos al cartílago nativo que el PCL y el PLA. Los andamiajes de b-TPUe impresos en 3D muestran una alta biocompatibilidad al cultivar hMSCs, manteniendo su proliferación.
3. Los andamiajes impresos en 3D con b-TPUe pudieron mantener un potencial proliferativo, viabilidad celular y condrogénesis de las hMSC adecuados.
4. Los estudios *in vivo* revelaron una biocompatibilidad excelente después de la implantación de andamiajes, así como la integración dentro del tejido circundante.
5. El hidrogel biomimético ACDHE muestra el mejor resultado de viabilidad celular de las combinaciones seleccionadas.
6. La mezcla de suplementos de DHE por sí sola muestra la capacidad de promover una cicatrización de heridas *in vitro* más rápida.
7. El hidrogel ACDHE presenta propiedades fisicoquímicas y mecánicas interesantes para su aplicación como sustituto de la piel o hidrogel inyectable.
8. El hidrogel de ACDHE bilaminar con hDF y hMSC permite el crecimiento y la proliferación de las células.
9. El hidrogel BT Skin simula la distribución en tres capas de biomoléculas y células relacionadas con la piel.
10. Las características fisicoquímicas del hidrogel BT Skin respaldan que esta estrategia tiene una aplicación potencial para la bioimpresión 3D, permitiendo alcanzar propiedades mecánicas similares a las del tejido de la piel nativa.

11. El sustituto de la piel trilaminar biofabricado puede ayudar a restaurar el equilibrio homeostático fisiológico *in vivo* y la función de barrera epidérmica de las heridas de la piel.

12. El hidrogel BT Skin favorece la cicatrización de heridas y la reconstrucción de la arquitectura histológica del tejido cutáneo nativo en ratones.

8. ABBREVIATIONS LIST

ABBREVIATIONS LIST

A

AC: Ag-Col I

ACCS: Amnion-derived cellular cytokines

ACDHE: AC hydrogels supplemented with DHE

ACI: Autologous chondrocyte implantation

AC_{low}: AC hydrogel with decreased agarose concentration

AD: Atopic dermatitis

AD-MSCs: Adipose derived mesenchymal stem cells

ADSCs: Adipose-derived stem cells

AFSCs: amniotic fluid-derived stem cells

Ag: Agarose

ALLO-ASC: Allogenic adipose-derived MSCs

AM: Additive manufacturing

ATMP: Advanced therapies medicinal products

B

BCT: Blood cell therapy

BM-MSCs: Bone marrow derived mesenchymal stem cells

BMPs: bone morphogenic proteins

BMSCs: Bone marrow mesenchymal stem cells

BMTs: Bone morphogenic proteins

BT: Bio-fabricated three-layered

b-TPUe: 1,4-Butanediol thermoplastic polyurethane elastomer

C

CAD: computer-aided design

CAM: computer-aided manufacturing

CCS: Collagen-Chitosan

CEAs: Cultured epithelial autografts

Ch: Chitosan

CIJB: Continuous inject bioprinting

Col I: Type I collagen

CTG: Cell tracker green

CTR: Cell tracker red

D

DBB: Droplet-based bioprinting

dECM: decellularized extracellular matrix

DFU: Diabetic foot ulcer

DH: DS-HA

DHE: DS, HA, and EL cocktail

DMEM: Dulbecco’s modified Eagle’s medium

DMMB: Dimethylmethylene blue

DODB: Drop-on-demand bioprinting

DS: Dermatan sulphate

E

EBB: Extrusion-based bioprinting

ECM: Extracellular matrix

EGF: epidermal growth factor

EHDJB: Electrohydrodynamic jetting bioprinting

EL: Elastin

ELISA: Enzyme-linked immunosorbent assay

EMA: European medicines agency

ESCs: Epidermal stem cells

ESEM: Environmental scanning electron microscope

F

FACS: Fluorescence-activated cell sorting

FBS: Foetal bovine serum

FDA: Food and Drug Administration

FGF: Fibroblast growth factor

G

GAG/s: Glygosaminoglycan/s

GAPDH: Glyceraldehyde-3-Phosphate Dehydrogenase

GelMA: Gelatine methacrylate

GelMA: gelatine methacrylate

GMP: Good Manufacturing Practice

H

H&E: Hematoxylin and eosin

HA: Hyaluronic acid

hDFs: human dermal fibroblasts

hEKs: Human epidermal keratinocytes

hESC-MSCs: Human embryonic stem cell-derived mesenchymal stem cells

HFDSCs: Hair follicle dermal stem cells

HFESCs: Hair follicle epidermal stem cells

HFSCs: Hair follicle stem cells

hMSCs: human mesenchymal stem cells

HPCs: Hair papilla cells

hUCB-USCs: Human umbilical cord blood derived-universal stem cells

HUVECs: human umbilical vein endothelial cells

I

IFP-MSCs: Infrapatellar fat pad mesenchymal stem cells

IJB: Inkjet bioprinting

iPSCs: Induced pluripotent stem cells

iPSCs: Induced pluripotent stem cells

ITS: Insulin-transferrin-selenium

K

KS: Kt-Sph

Kt: Keratin

L

LAB: Laser-assisted bioprinting

LAS: Leica application suite

M

MACI: Matrix-induced ACI

MCs: Melanocyte

MDI: Methylene diphenyl diisocyanate

MeHA: methacrylated hyaluronic acid

MEW: Melt electrowriting

MSCs: Mesenchymal stem cells

O

OA: Osteoarthritic

OCT: Optimal cutting temperature

OPD: Ortho-phenyldiamine

P

P/S: Penicillin and streptomycin

PAD: Peripheral arterial disease

PBB: Photocuring-based bioprinting

PBS: Phosphate-buffered saline

PCL: Poly-ε-caprolactone

PCR: Polymerase Chain Reaction

PDGF: platelet-derived growth factor

PEG: Polyethylene glycol

PEGDA: poly(ethylene glycol) diacrylate

PGA: Poly-glycolic acid

PLA: Poly-L-lactic acid

PLGA: Poly lactic-co-glycolic acid

PLGA: Polyglycolic acid

PLLA: Poly-L-lactic acid

POSAS: Patient and observer scar assessment scale

PRP: Platelet-rich-plasma

R

RFU: Relative fluorescence units

RGD: Arginylglycylaspartic acid

RHAMM: Receptor for hyaluronan-mediated motility

RNA: Ribonucleic acid

RT: Room temperature

S

SCID: Severe combined immunodeficiency

SD: Standard deviation

SEM: Scanning electron microscopy

SLA: Stereolithography

sMSCs: Synovium derived mesenchymal stem cells

Sph: Sphingolipids

T

TB4: Thymosin beta 4

TE: Tissue engineering

TEWL: Transepidermal water loss

TGFs: Transforming growth factors

TGF-β3: Transforming growth factor β3

U

UV: Ultraviolet

V

VEGF: Vascular endothelial growth factor

9. REFERENCES

1. Ikada Y. Challenges in tissue engineering. *J R Soc Interface*. 2006 Oct 22;3(10):589–601.

2. Ravnic DJ, Leberfinger AN, Koduru S V., et al. Transplantation of Bioprinted Tissues and Organs: Technical and Clinical Challenges and Future Perspectives. *Ann Surg*. 2017;266(1):48–58.

3. Cui H, Miao S, Esworthy T, et al. 3D bioprinting for cardiovascular regeneration and pharmacology. *Adv Drug Deliv Rev*. 2018 Jul 1;132:252.

4. Nichols JE, La Francesca S, Niles JA, et al. Production and transplantation of bioengineered lung into a large-animal model. *Sci Transl Med*. 2018 Aug 1;10(452):eaao3926.

5. Al-Himdani S, Jessop ZM, Al-Sabah A, et al. Tissue-Engineered Solutions in Plastic and Reconstructive Surgery: Principles and Practice. *Front Surg*. 2017 Feb 23;4:4.

6. Laurencin CT, Khan Y. Regenerative engineering. *Sci Transl Med*. 2012 Nov 14;4(160).

7. Xing H, Lee H, Luo L, et al. Extracellular matrix-derived biomaterials in engineering cell function. *Biotechnol Adv*. 2020 Sep 1;42:107421.

8. Badylak SF. Decellularized Allogeneic and Xenogeneic Tissue as a Bioscaffold for Regenerative Medicine: Factors that Influence the Host Response. *Ann Biomed Eng 2014 427*. 2014 Jan 9;42(7):1517–27.

9. Badylak SF. Regenerative medicine and developmental biology: The role of the extracellular matrix. *Anat Rec Part B New Anat*. 2005 Nov 1;287B(1):36–41.

10. Arenas-Herrera JE, Ko IK, Atala A, et al. Decellularization for whole organ bioengineering. *Biomed Mater*. 2013 Jan 25;8(1):014106.

11. Choudhury D, Yee M, Sheng ZLJ, et al. Decellularization systems and devices: State-of-the-art. *Acta Biomater*. 2020 Oct 1;115:51–9.

12. Schmitt A, Csiki R, Tron A, et al. Optimized protocol for whole organ decellularization. *Eur J Med Res*. 2017 Sep 8;22(1):1–9.

13. Crapo PM, Gilbert TW, Badylak SF. An overview of tissue and whole organ

decellularization processes. *Biomaterials*. 2011 Apr 1;32(12):3233–43.

14. White LJ, Taylor AJ, Faulk DM, et al. The impact of detergents on the tissue decellularization process: A ToF-SIMS study. *Acta Biomater*. 2017 Mar 1;50:207–19.

15. Kim BS, Kim H, Gao G, et al. Decellularized extracellular matrix: a step towards the next generation source for bioink manufacturing. *Biofabrication*. 2017 Aug 4;9(3):034104.

16. Lu H, Hoshiba T, Kawazoe N, et al. Autologous extracellular matrix scaffolds for tissue engineering. *Biomaterials*. 2011 Apr 1;32(10):2489–99.

17. Antich C, Jiménez G, de Vicente J, et al. Development of a Biomimetic Hydrogel Based on Predifferentiated Mesenchymal Stem-Cell-Derived ECM for Cartilage Tissue Engineering. *Adv Healthc Mater*. 2021 Apr 1;10(8).

18. Cobianchi L, Moeckli B, Croce S. Commentary: Insulin-Producing Organoids Engineered From Islet and Amniotic Epithelial Cells to Treat Diabetes. *Front Endocrinol (Lausanne)*. 2020 Oct 6;11:794.

19. Huch M, Koo BK. Modeling mouse and human development using organoid cultures. *Development*. 2015 Sep 15;142(18):3113–25.

20. Fennema E, Rivron N, Rouwkema J, et al. Spheroid culture as a tool for creating 3D complex tissues. *Trends Biotechnol*. 2013 Feb 1;31(2):108–15.

21. Kim J, Koo BK, Knoblich JA. Human organoids: model systems for human biology and medicine. *Nat Rev Mol Cell Biol 2020 2110*. 2020 Jul 7;21(10):571–84.

22. Sato T, Stange DE, Ferrante M, et al. Long-term expansion of epithelial organoids from human colon, adenoma, adenocarcinoma, and Barrett's epithelium. *Gastroenterology*. 2011 Nov 1;141(5):1762–72.

23. Fujii M, Matano M, Toshimitsu K, et al. Human Intestinal Organoids Maintain Self-Renewal Capacity and Cellular Diversity in Niche-Inspired Culture Condition. *Cell Stem Cell*. 2018 Dec 6;23(6):787-793.e6.

24. Lancaster MA, Renner M, Martin CA, et al. Cerebral organoids model human brain development and microcephaly. *Nat 2013 5017467*. 2013 Aug

28;501(7467):373–9.

25. Takasato M, Er PX, Chiu HS, et al. Kidney organoids from human iPS cells contain multiple lineages and model human nephrogenesis. *Nat 2015 5267574*. 2015 Oct 7;526(7574):564–8.

26. Hu H, Gehart H, Artegiani B, et al. Long-Term Expansion of Functional Mouse and Human Hepatocytes as 3D Organoids. *Cell*. 2018 Nov 29;175(6):1591-1606.e19.

27. Turco MY, Gardner L, Hughes J, et al. Long-term, hormone-responsive organoid cultures of human endometrium in a chemically defined medium. *Nat Cell Biol 2017 195*. 2017 Apr 10;19(5):568–77.

28. Chen Q, Chen D, Wu J, et al. Flexible control of cellular encapsulation, permeability, and release in a droplet-templated bifunctional copolymer scaffold. *Biomicrofluidics*. 2016 Nov 1;10(6).

29. Rossow T, Lienemann PS, Mooney DJ, et al. Cell Microencapsulation by Droplet Microfluidic Templating. *Macromol Chem Phys*. 2017 Jan 1;218(2):1600380.

30. Jiang W, Li M, Chen Z, et al. Cell-laden microfluidic microgels for tissue regeneration. *Lab Chip*. 2016;16(23):4482–506.

31. Agrawal G, Agrawal R. Functional Microgels: Recent Advances in Their Biomedical Applications. *Small*. 2018 Sep 1;14(39):1801724.

32. Newsom JP, Payne KA, Krebs MD. Microgels: Modular, tunable constructs for tissue regeneration. *Acta Biomater*. 2019 Apr 1;88:32–41.

33. Annabi N, Tamayol A, Uquillas JA, et al. 25th Anniversary Article: Rational Design and Applications of Hydrogels in Regenerative Medicine. *Adv Mater*. 2014 Jan 1;26(1):85–124.

34. Tumarkin E, Kumacheva E. Microfluidic generation of microgels from synthetic and natural polymers. *Chem Soc Rev*. 2009 Jul 21;38(8):2161–8.

35. Huang D, Gibeley SB, Xu C, et al. Engineering Liver Microtissues for Disease Modeling and Regenerative Medicine. *Adv Funct Mater*. 2020 Oct 1;30(44):1909553.

36. Mora-Boza A, Mancipe Castro LM, Schneider RS, et al. Microfluidics generation

of chitosan microgels containing glycerylphytate crosslinker for in situ human mesenchymal stem cells encapsulation. *Mater Sci Eng C*. 2021 Jan 1;120:111716.

37. Ma J, Wang Y, Liu J. Bioprinting of 3D tissues/organs combined with microfluidics. *RSC Adv*. 2018 Jun 13;8(39):21712–27.

38. Doshi J, Reneker DH. Electrospinning process and applications of electrospun fibers. *J Electrostat*. 1995 Aug 1;35(2–3):151–60.

39. Agarwal S, Wendorff JH, Greiner A. Use of electrospinning technique for biomedical applications. *Polymer (Guildf)*. 2008 Dec 8;49(26):5603–21.

40. Zanin MHA, Cerize NNP, de Oliveira AM. Production of Nanofibers by Electrospinning Technology: Overview and Application in Cosmetics. *Nanocosmetics and Nanomedicines*. 2011;311–32.

41. de Lima GG, Lyons S, Devine DM, et al. Electrospinning of Hydrogels for Biomedical Applications. 2018;219–58.

42. Vasita R, Katti DS. Nanofibers and their applications in tissue engineering. *Int J Nanomedicine*. 2006;1(1):15–30.

43. Chronakis IS. Novel nanocomposites and nanoceramics based on polymer nanofibers using electrospinning process—A review. *J Mater Process Technol*. 2005 Aug 30;167(2–3):283–93.

44. Wang X, Ding B, Li B. Biomimetic electrospun nanofibrous structures for tissue engineering. *Mater Today*. 2013 Jun 1;16(6):229–41.

45. Braghirolli DI, Steffens D, Pranke P. Electrospinning for regenerative medicine: a review of the main topics. *Drug Discov Today*. 2014;19(6):743–53.

46. Ghanavi J, Farnia P, Velayati AA. Nano design of extracellular matrix for tissue engineering. *Nanoarchitectonics Biomed*. 2019 Jan 1;547–83.

47. Dufour A, Gallostra XB, O'Keeffe C, et al. Integrating melt electrowriting and inkjet bioprinting for engineering structurally organized articular cartilage. *Biomaterials*. 2022 Apr 1;283:121405.

48. Brown TD, Dalton PD, Hutmacher DW. Direct Writing By Way of Melt Electrospinning. *Adv Mater*. 2011 Dec 15;23(47):5651–7.

49. Gu B, Choi D, Park S, et al. 3D Bioprinting Technologies for Tissue Engineering Applications. *Adv Exp Med Biol*. 2018;1078:15–28.

50. Murphy S V, Atala A. 3D bioprinting of tissues and organs. *Nat Biotechnol 2014 328*. 2014 Aug 5;32(8):773–85.

51. Arslan-Yildiz A, Assal R El, Chen P, et al. Towards artificial tissue models: past, present, and future of 3D bioprinting. *Biofabrication*. 2016;8(1).

52. Lee JM, Sing SL, Zhou M, et al. 3D bioprinting processes: A perspective on classification and terminology. *Int J Bioprinting*. 2018;4(2).

53. Papaioannou TG, Manolesou D, Dimakakos E, et al. 3D Bioprinting Methods and Techniques: Applications on ArtificialBlood Vessel Fabrication. *Acta Cardiol Sin*. 2019 May 1;35(3):284.

54. Matai I, Kaur G, Seyedsalehi A, et al. Progress in 3D bioprinting technology for tissue/organ regenerative engineering. *Biomaterials*. 2020 Jan 1;226.

55. Varkey M, Visscher DO, van Zuijlen PPM, et al. Skin bioprinting: the future of burn wound reconstruction? *Burn Trauma 2019 71*. 2019 Feb 12;7(1):1–12.

56. Li J, Chen M, Fan X, et al. Recent advances in bioprinting techniques: approaches, applications and future prospects. *J Transl Med 2016 141*. 2016 Sep 20;14(1):1–15.

57. Mironov V, Boland T, Trusk T, et al. Organ printing: Computer-aided jet-based 3D tissue engineering. *Trends Biotechnol*. 2003 Apr 1;21(4):157–61.

58. Shafiee A, Atala A. Printing Technologies for Medical Applications. *Trends Mol Med*. 2016 Feb 5;22(3):254–65.

59. Fielding G, Bandyopadhyay A, Bose S. Effects of silica and zinc oxide doping on mechanical and biological properties of 3D printed tricalcium phosphate tissue engineering scaffolds. *Dent Mater*. 2012 Feb;28(2):113–22.

60. Munaz A, Vadivelu RK, St. John J, et al. Three-dimensional printing of biological matters. *J Sci Adv Mater Devices*. 2016 Mar 1;1(1):1–17.

61. Liu W, Zhang Y, Heinrich M, et al. Rapid Continuous Multimaterial Extrusion Bioprinting. *Adv Mater*. 2017 Jan 1;29(3).

62. Onses M, Sutanto E, Ferreira P, et al. Mechanisms, Capabilities, and Applications of High-Resolution Electrohydrodynamic Jet Printing. *Small*. 2015 Sep 1;11(34):4237–66.

63. Jayasinghe S, Qureshi A, Eagles P. Electrohydrodynamic jet processing: an advanced electric-field-driven jetting phenomenon for processing living cells. *Small*. 2006 Feb;2(2):216–9.

64. Derby B. Inkjet Printing of Functional and Structural Materials: Fluid Property Requirements, Feature Stability, and Resolution. *http://dx.doi.org/101146/annurev-matsci-070909-104502*. 2010 Jul 2;40:395–414.

65. Saunders RE, Derby B. Inkjet printing biomaterials for tissue engineering: bioprinting. *http://dx.doi.org/101179/1743280414Y0000000040*. 2014 Nov 1;59(8):430–48.

66. Ozbolat IT, Hospodiuk M. Current advances and future perspectives in extrusion-based bioprinting. *Biomaterials*. 2016 Jan;76:321–43.

67. Keriquel V, Oliveira H, Rémy M, et al. In situ printing of mesenchymal stromal cells, by laser-assisted bioprinting, for in vivo bone regeneration applications. *Sci Reports 2017 71*. 2017 May 11;7(1):1–10.

68. Koch L, Gruene M, Unger C, et al. Laser Assisted Cell Printing. *Curr Pharm Biotechnol*. 2013 Jan 28;14(1):91–7.

69. Guillemot F, Souquet A, Catros S, et al. Laser-assisted cell printing: principle, physical parameters versus cell fate and perspectives in tissue engineering. *Nanomedicine (Lond)*. 2010 Apr;5(3):507–15.

70. Devillard R, Pagès E, Correa M, et al. Cell patterning by laser-assisted bioprinting. *Methods Cell Biol*. 2014;119:159–74.

71. Serra P, Duocastella M, Fernández-Pradas JM, et al. Liquids microprinting through laser-induced forward transfer. *Appl Surf Sci*. 2009 Mar 1;255(10):5342–5.

72. Patrascioiu A, Fernández-Pradas JM, Palla-Papavlu A, et al. Laser-generated liquid microjets: correlation between bubble dynamics and liquid ejection.

Microfluid Nanofluidics 2013 161. 2013 Jun 19;16(1):55–63.

73. Ali M, Pages E, Ducom A, et al. Controlling laser-induced jet formation for bioprinting mesenchymal stem cells with high viability and high resolution. *Biofabrication*. 2014 Dec 1;6(4).

74. Dhariwala B, Hunt E, Boland T. Rapid prototyping of tissue-engineering constructs, using photopolymerizable hydrogels and stereolithography. *Tissue Eng*. 2004 Sep;10(9–10):1316–22.

75. Melchels F, Feijen J, Grijpma D. A review on stereolithography and its applications in biomedical engineering. *Biomaterials*. 2010 Aug;31(24):6121–30.

76. Grigoryan B, Sazer DW, Avila A, et al. Development, characterization, and applications of multi-material stereolithography bioprinting. *Sci Reports 2021 111*. 2021 Feb 4;11(1):1–13.

77. Heinrich M, Liu W, Jimenez A, et al. 3D Bioprinting: from Benches to Translational Applications. *Small*. 2019 Jun 7;15(23).

78. Ramesh S, Harrysson OLA, Rao PK, et al. Extrusion bioprinting: Recent progress, challenges, and future opportunities. *Bioprinting*. 2021 Mar 1;21:e00116.

79. Michael S, Sorg H, Peck CT, et al. Tissue Engineered Skin Substitutes Created by Laser-Assisted Bioprinting Form Skin-Like Structures in the Dorsal Skin Fold Chamber in Mice. *PLoS One*. 2013;8(3).

80. Le X, Poinern GEJ, Ali N, et al. Engineering a biocompatible scaffold with either micrometre or nanometre scale surface topography for promoting protein adsorption and cellular response. *Int J Biomater*. 2013;2013.

81. Yang D, Xiao J, Wang B, et al. The immune reaction and degradation fate of scaffold in cartilage/bone tissue engineering. *Mater Sci Eng C Mater Biol Appl*. 2019 Nov 1;104.

82. O'Brien FJ. Biomaterials & scaffolds for tissue engineering. *Mater Today*. 2011 Mar 1;14(3):88–95.

83. Roseti L, Parisi V, Petretta M, et al. Scaffolds for Bone Tissue Engineering: State of the art and new perspectives. *Mater Sci Eng C Mater Biol Appl*. 2017 Sep

1;78:1246–62.

84. Theus AS, Ning L, Hwang B, et al. Bioprintability: Physiomechanical and Biological Requirements of Materials for 3D Bioprinting Processes. *Polym 2020, Vol 12, Page 2262*. 2020 Oct 1;12(10):2262.

85. Rodríguez-Lozano FJ, García-Bernal D, Aznar-Cervantes S, et al. Effects of composite films of silk fibroin and graphene oxide on the proliferation, cell viability and mesenchymal phenotype of periodontal ligament stem cells. *J Mater Sci Mater Med*. 2014 Nov 28;25(12):2731–41.

86. Schwab A, Levato R, D'Este M, et al. Printability and Shape Fidelity of Bioinks in 3D Bioprinting. *Chem Rev*. 2020 Oct 14;120(19):11028–55.

87. Billiet T, Gevaert E, De Schryver T, et al. The 3D printing of gelatin methacrylamide cell-laden tissue-engineered constructs with high cell viability. *Biomaterials*. 2014;35(1):49–62.

88. Wu D, Yu Y, Tan J, et al. 3D bioprinting of gellan gum and poly (ethylene glycol) diacrylate based hydrogels to produce human-scale constructs with high-fidelity. *Mater Des*. 2018 Dec 15;160:486–95.

89. Keriquel V, Guillemot F, Arnault I, et al. In vivo bioprinting for computer- and robotic-assisted medical intervention: preliminary study in mice. *Biofabrication*. 2010;2(1).

90. Cui X, Breitenkamp K, Finn MG, et al. Direct human cartilage repair using three-dimensional bioprinting technology. *Tissue Eng Part A*. 2012 Jun 1;18(11–12):1304–12.

91. Duan B, Hockaday LA, Kang KH, et al. 3D bioprinting of heterogeneous aortic valve conduits with alginate/gelatin hydrogels. *J Biomed Mater Res A*. 2013 May;101(5):1255–64.

92. Michael S, Sorg H, Peck CT, et al. Tissue engineered skin substitutes created by laser-assisted bioprinting form skin-like structures in the dorsal skin fold chamber in mice. *PLoS One*. 2013 Mar 4;8(3).

93. Xu T, Binder KW, Albanna MZ, et al. Hybrid printing of mechanically and biologically improved constructs for cartilage tissue engineering applications.

Biofabrication. 2013 Mar;5(1).

94. Zhang K, Chou C-K, Xia X, et al. Block-Cell-Printing for live single-cell printing. *Proc Natl Acad Sci*. 2014;201313661.

95. Dolati F, Yu Y, Zhang Y, et al. In vitro evaluation of carbon-nanotube-reinforced bioprintable vascular conduits. *Nanotechnology*. 2014 Apr 11;25(14).

96. Gruene M, Pflaum M, Deiwick A, et al. Adipogenic differentiation of laser-printed 3D tissue grafts consisting of human adipose-derived stem cells. *Biofabrication*. 2011 Mar;3(1).

97. Xu F, Sridharan BP, Wang SQ, et al. Embryonic stem cell bioprinting for uniform and controlled size embryoid body formation. *Biomicrofluidics*. 2011;5(2).

98. Duarte Campos DF, Blaeser A, Weber M, et al. Three-dimensional printing of stem cell-laden hydrogels submerged in a hydrophobic high-density fluid. *Biofabrication*. 2013 Mar;5(1).

99. Hong S, Song SJ, Lee JY, et al. Cellular behavior in micropatterned hydrogels by bioprinting system depended on the cell types and cellular interaction. *J Biosci Bioeng*. 2013 Aug;116(2):224–30.

100. Owens CM, Marga F, Forgacs G, et al. Biofabrication and testing of a fully cellular nerve graft. *Biofabrication*. 2013 Dec;5(4).

101. Visser J, Peters B, Burger TJ, et al. Biofabrication of multi-material anatomically shaped tissue constructs. *Biofabrication*. 2013 Sep;5(3).

102. Ozbolat IT, Yu Y. Bioprinting Toward Organ Fabrication : Challenges and Future Trends Bioprinting Toward Organ Fabrication : Challenges and Future Trends. 2015;60(November):691–9.

103. Ullah I, Subbarao RB, Rho GJ. Human mesenchymal stem cells - current trends and future prospective. *Biosci Rep*. 2015;35(2).

104. Ren X, Wang F, Chen C, et al. Engineering zonal cartilage through bioprinting collagen type II hydrogel constructs with biomimetic chondrocyte density gradient. *BMC Musculoskelet Disord*. 2016 Jul 20;17(1).

105. Nguyen DG, Funk J, Robbins JB, et al. Bioprinted 3D Primary Liver Tissues

Allow Assessment of Organ-Level Response to Clinical Drug Induced Toxicity In Vitro. *PLoS One*. 2016 Jul 1;11(7).

106. Kolesky DB, Homan KA, Skylar-Scott MA, et al. Three-dimensional bioprinting of thick vascularized tissues. *Proc Natl Acad Sci U S A*. 2016 Mar 22;113(12):3179–84.

107. Mandrycky C, Wang Z, Kim K, et al. 3D Bioprinting for Engineering Complex Tissues. *Biotechnol Adv*. 2016 Jul 1;34(4):422.

108. Miller JS, Stevens KR, Yang MT, et al. Rapid casting of patterned vascular networks for perfusable engineered three-dimensional tissues. *Nat Mater*. 2012;11(9):768–74.

109. Kolesky DB, Truby RL, Gladman AS, et al. 3D bioprinting of vascularized, heterogeneous cell-laden tissue constructs. *Adv Mater*. 2014 May 21;26(19):3124–30.

110. Catros S, Fricain JC, Guillotin B, et al. Laser-assisted bioprinting for creating on-demand patterns of human osteoprogenitor cells and nano-hydroxyapatite. *Biofabrication*. 2011 Jun;3(2).

111. Merceron TK, Burt M, Seol YJ, et al. A 3D bioprinted complex structure for engineering the muscle-tendon unit. *Biofabrication*. 2015 Jun 17;7(3).

112. Zhao Y, Yao R, Ouyang L, et al. Three-dimensional printing of Hela cells for cervical tumor model in vitro. *Biofabrication*. 2014;6(3).

113. Choi W, Ha D, Park S, et al. Synthetic multicellular cell-to-cell communication in inkjet printed bacterial cell systems. *Biomaterials*. 2011 Apr;32(10):2500–7.

114. Cui X, Boland T. Human microvasculature fabrication using thermal inkjet printing technology. *Biomaterials*. 2009 Oct;30(31):6221–7.

115. Yanez M, Rincon J, Dones A, et al. In vivo assessment of printed microvasculature in a bilayer skin graft to treat full-thickness wounds. *Tissue Eng Part A*. 2015 Jan 1;21(1–2):224–33.

116. Osidak EO, Kozhukhov VI, Osidak MS, et al. Collagen as Bioink for Bioprinting: A Comprehensive Review. *Int J Bioprinting*. 2020 Apr 1;6(3):1–10.

117. Ng WL, Yeong WY, Naing MW. Polyelectrolyte gelatin-chitosan hydrogel

optimized for 3D bioprinting in skin tissue engineering. *Int J Bioprinting*. 2016;2(1):53–62.

118. Huang S, Yao B, Xie J, et al. 3D bioprinted extracellular matrix mimics facilitate directed differentiation of epithelial progenitors for sweat gland regeneration. *Acta Biomater*. 2016 Mar 1;32:170–7.

119. Murphy S, Skardal A, Atala A. Evaluation of hydrogels for bio-printing applications. *J Biomed Mater Res A*. 2013 Jan;101(1):272–84.

120. Tirella A, Orsini A, Vozzi G, et al. A phase diagram for microfabrication of geometrically controlled hydrogel scaffolds. *Biofabrication*. 2009;1(4).

121. Huang Y, Zhang X, Gao G, et al. 3D bioprinting and the current applications in tissue engineering. *Biotechnol J*. 2017 Aug 1;12(8).

122. Köpf M, Campos D, Blaeser A, et al. A tailored three-dimensionally printable agarose-collagen blend allows encapsulation, spreading, and attachment of human umbilical artery smooth muscle cells. *Biofabrication*. 2016 May 20;8(2).

123. Sun J, Tan H. Alginate-Based Biomaterials for Regenerative Medicine Applications. *Mater (Basel, Switzerland)*. 2013;6(4):1285–309.

124. Glicklis R, Shapiro L, Agbaria R, et al. Hepatocyte behavior within three-dimensional porous alginate scaffolds. *Biotechnol Bioeng*. 2000;67(3):344–53.

125. Guillemot F, Souquet A, Catros S, et al. High-throughput laser printing of cells and biomaterials for tissue engineering. *Acta Biomater*. 2010;6(7):2494–500.

126. Axpe E, Oyen M. Applications of Alginate-Based Bioinks in 3D Bioprinting. *Int J Mol Sci*. 2016 Dec 1;17(12).

127. Chandy T, Sharma C. Chitosan--as a biomaterial. *Biomater Artif Cells Artif Organs*. 1990;18(1):1–24.

128. Ngo M, Aberman H, Hawes M, et al. Evaluation of human acellular dermis versus porcine acellular dermis in an in vivo model for incisional hernia repair. *Cell Tissue Bank*. 2011 May;12(2):135–45.

129. Seidlits S, Khaing Z, Petersen R, et al. The effects of hyaluronic acid hydrogels with tunable mechanical properties on neural progenitor cell differentiation. *Biomaterials*. 2010 May;31(14):3930–40.

130. Murakami K, Aoki H, Nakamura S, et al. Hydrogel blends of chitin/chitosan, fucoidan and alginate as healing-impaired wound dressings. *Biomaterials*. 2010 Jan;31(1):83–90.

131. Ma L, Gao C, Mao Z, et al. Collagen/chitosan porous scaffolds with improved biostability for skin tissue engineering. *Biomaterials*. 2003;24(26):4833–41.

132. Shi H, Han C, Mao Z, et al. Enhanced angiogenesis in porous collagen-chitosan scaffolds loaded with angiogenin. *Tissue Eng Part A*. 2008 Nov 1;14(11):1775–85.

133. Mota C, Puppi D, Chiellini F, et al. Additive manufacturing techniques for the production of tissue engineering constructs. *J Tissue Eng Regen Med*. 2015 Mar 1;9(3):174–90.

134. Aboudzadeh N, Imani M, Shokrgozar MA, et al. Fabrication and characterization of poly(D,L-lactide-co-glycolide)/hydroxyapatite nanocomposite scaffolds for bone tissue regeneration. *J Biomed Mater Res Part A*. 2010 Jul 1;94A(1):137–45.

135. Rogina A, Pribolšan L, Hanžek A, et al. Macroporous poly(lactic acid) construct supporting the osteoinductive porous chitosan-based hydrogel for bone tissue engineering. *Polymer (Guildf)*. 2016 Aug 19;98:172–81.

136. Wu L, Ding J. In vitro degradation of three-dimensional porous poly(D,L-lactide-co-glycolide) scaffolds for tissue engineering. *Biomaterials*. 2004 Dec;25(27):5821–30.

137. Agrawal C, Ray R. Biodegradable polymeric scaffolds for musculoskeletal tissue engineering [Internet]. Journal of Biomedical Materials Research - Wiley Online Library. 2001.

138. Gümüşderelioğlu M, Dalkıranoğlu S, Aydın RST, et al. A novel dermal substitute based on biofunctionalized electrospun PCL nanofibrous matrix. *J Biomed Mater Res Part A*. 2011 Sep 1;98A(3):461–72.

139. You Y, Min B-M, Lee SJ, et al. In vitro degradation behavior of electrospun polyglycolide, polylactide, and poly(lactide-co-glycolide). *J Appl Polym Sci*. 2005 Jan 15;95(2):193–200.

140. Yue K, Trujillo-de Santiago G, Alvarez M, et al. Synthesis, properties, and

biomedical applications of gelatin methacryloyl (GelMA) hydrogels. *Biomaterials*. 2015 Dec 1;73:254–71.

141. Nichol J, Koshy S, Bae H, et al. Cell-laden microengineered gelatin methacrylate hydrogels. *Biomaterials*. 2010 Jul;31(21):5536–44.

142. Chen S, Fu P, Wu H, et al. Meniscus, articular cartilage and nucleus pulposus: a comparative review of cartilage-like tissues in anatomy, development and function. *Cell Tissue Res*. 2017 Oct 1;370(1):53–70.

143. Bedi A, Feeley BT, Williams RJ. Management of articular cartilage defects of the knee. *J Bone Joint Surg Am*. 2010 Apr 1;92(4):994–1009.

144. Xiongfa J, Hao Z, Liming Z, et al. Recent advances in 3D bioprinting for the regeneration of functional cartilage. *Regen Med*. 2018 Jan 1;13(1):73–87.

145. Zylińska B, Silmanowicz P, Sobczyńska-Rak A, et al. Treatment of Articular Cartilage Defects: Focus on Tissue Engineering. *In Vivo (Brooklyn)*. 2018 Nov 1;32(6):1289.

146. Dhawan A, Kennedy PM, Rizk EB, et al. Three-dimensional Bioprinting for Bone and Cartilage Restoration in Orthopaedic Surgery. *J Am Acad Orthop Surg*. 2019 Mar 1;27(5):E215–26.

147. Fellows CR, Matta C, Zakany R, et al. Adipose, Bone Marrow and Synovial Joint-Derived Mesenchymal Stem Cells for Cartilage Repair. *Front Genet*. 2016;7(DEC):213.

148. Chen FH, Tuan RS. Mesenchymal stem cells in arthritic diseases. *Arthritis Res Ther*. 2008 Oct 10;10(5):223.

149. Singh S, Choudhury D, Yu F, et al. In situ bioprinting - Bioprinting from benchside to bedside? *Acta Biomater*. 2020 Jan 1;101:14–25.

150. O'Connell CD, Di Bella C, Thompson F, et al. Development of the Biopen: a handheld device for surgical printing of adipose stem cells at a chondral wound site. *Biofabrication*. 2016;8(1).

151. Di Bella C, Duchi S, O'Connell CD, et al. In situ handheld three-dimensional bioprinting for cartilage regeneration. *J Tissue Eng Regen Med*. 2018 Mar 1;12(3):611–21.

152. Ma K, Zhao T, Yang L, et al. Application of robotic-assisted in situ 3D printing in cartilage regeneration with HAMA hydrogel: An in vivo study. *J Adv Res*. 2020 May 1;23:123–32.

153. Sadeghianmaryan A, Naghieh S, Yazdanpanah Z, et al. Fabrication of chitosan/alginate/hydroxyapatite hybrid scaffolds using 3D printing and impregnating techniques for potential cartilage regeneration. *Int J Biol Macromol*. 2022 Apr 15;204:62–75.

154. Costantini M, Idaszek J, Szöke K, et al. 3D bioprinting of BM-MSCs-loaded ECM biomimetic hydrogels for in vitro neocartilage formation. *Biofabrication*. 2016 Jul 18;8(3):035002.

155. Ng WL, Chua CK, Shen YF. Print Me An Organ! Why We Are Not There Yet. *Prog Polym Sci*. 2019 Oct 1;97:101145.

156. Favreau H, Pijnenburg L, Seitlinger J, et al. Osteochondral repair combining therapeutics implant with mesenchymal stem cells spheroids. *Nanomedicine*. 2020 Oct 1;29.

157. Francis SL, Di Bella C, Wallace GG, et al. Cartilage Tissue Engineering Using Stem Cells and Bioprinting Technology—Barriers to Clinical Translation. *Front Surg*. 2018 Nov 27;5.

158. Huang BJ, Hu JC, Athanasiou KA. Cell-based tissue engineering strategies used in the clinical repair of articular cartilage. *Biomaterials*. 2016 Aug 1;98:1–22.

159. Harrell CR, Markovic BS, Fellabaum C, et al. Mesenchymal stem cell-based therapy of osteoarthritis: Current knowledge and future perspectives. *Biomed Pharmacother*. 2019 Jan 1;109:2318–26.

160. Caplan AI, Correa D. The MSC: An Injury Drugstore. *Cell Stem Cell*. 2011 Jul 8;9(1):11–5.

161. Kreulen C, Giza E, Walton J, et al. Seven-Year Follow-up of Matrix-Induced Autologous Implantation in Talus Articular Defects. *Foot Ankle Spec*. 2018 Apr 1;11(2):133–7.

162. Dekker TJ, Dekker PK, Tainter DM, et al. Treatment of Osteochondral lesions of the talus: A critical analysis review. *JBJS Rev*. 2017;5(3).

163. Giza E, Sullivan M, Ocel D, et al. Matrix-Induced Autologous Chondrocyte Implantation of Talus Articular Defects. 2010;

164. Joshi N, Reverte-Vinaixa M, Díaz-Ferreiro EW, et al. Synthetic resorbable scaffolds for the treatment of isolated patellofemoral cartilage defects in young patients: magnetic resonance imaging and clinical evaluation. *Am J Sports Med*. 2012 Jun;40(6):1289–95.

165. Condello V, Filardo G, Madonna V, et al. Use of a Biomimetic Scaffold for the Treatment of Osteochondral Lesions in Early Osteoarthritis. *Biomed Res Int*. 2018;2018.

166. Park IS, Jin RL, Oh HJ, et al. Sizable Scaffold-Free Tissue-Engineered Articular Cartilage Construct for Cartilage Defect Repair. *Artif Organs*. 2019 Mar 1;43(3):278–87.

167. Brenner JM, Ventura NM, Tse MY, et al. Implantation of scaffold-free engineered cartilage constructs in a rabbit model for chondral resurfacing. *Artif Organs*. 2014;38(2).

168. Yamashita A, Morioka M, Yahara Y, et al. Generation of Scaffoldless Hyaline Cartilaginous Tissue from Human iPSCs. *Stem Cell Reports*. 2015 Mar 10;4(3):404–18.

169. Kreuz PC, Müller S, Ossendorf C, et al. Treatment of focal degenerative cartilage defects with polymer-based autologous chondrocyte grafts: four-year clinical results. *Arthritis Res Ther*. 2009 Mar 5;11(2).

170. Nehrer S, Dorotka R, Domayer S, et al. Treatment of Full-Thickness Chondral Defects with Hyalograft C in the Knee: A Prospective Clinical Case Series with 2 to 7 Years' Follow-up. *Am J Sports Med*. 2009 Nov 1;37(1_suppl):81S-87S.

171. European Medicines Agency. Hyalograft C autograft - (Characterised viable autologous chondrocytes expanded in vitro, seeded and cultured on a hyaluronan-based scaffold). 2013;

172. Nehrer S, Halbwirth F, Luksch T. CaReS®, Cartilage Regeneration System: Autologous Chondrocyte Transplantation in a Collagen Gel. *Tech Cartil Repair Surg*. 2014 Jan 1;245–50.

173. Schneider U, Rackwitz L, Andereya S, et al. A prospective multicenter study on the outcome of type i collagen hydrogel-based autologous chondrocyte implantation (cares) for the repair of articular cartilage defects in the knee. *Am J Sports Med*. 2011 Dec 7;39(12):2558–65.

174. Crawford DC, DeBerardino TM, Williams RJ. NeoCart, an autologous cartilage tissue implant, compared with microfracture for treatment of distal femoral cartilage lesions: an FDA phase-II prospective, randomized clinical trial after two years. *J Bone Joint Surg Am*. 2012 Jun 6;94(11):979–89.

175. Anderson DE, Williams RJ, DeBerardino TM, et al. Magnetic Resonance Imaging Characterization and Clinical Outcomes after NeoCart Surgical Therapy as a Primary Reparative Treatment for Knee Cartilage Injuries. *Am J Sports Med*. 2017 Mar 1;45(4):875–83.

176. Dhollander AAM, Liekens K, Almqvist KF, et al. A Pilot Study of the Use of an Osteochondral Scaffold Plug for Cartilage Repair in the Knee and How to Deal With Early Clinical Failures. *Arthroscopy*. 2012 Feb 1;28(2):225–33.

177. Verhaegen J, Clockaerts S, Van Osch GJVM, et al. TruFit Plug for Repair of Osteochondral Defects—Where Is the Evidence? Systematic Review of Literature. *Cartilage*. 2015 Jan 19;6(1):12.

178. Dell'Osso G, Bottai V, Bugelli G, et al. The biphasic bioresorbable scaffold (Trufit®) in the osteochondral knee lesions: long-term clinical and MRI assessment in 30 patients. *Musculoskelet Surg 2015 1002*. 2015 Nov 3;100(2):93–6.

179. D'Ambrosi R, Valli F, De Luca P, et al. MaioRegen Osteochondral Substitute for the Treatment of Knee Defects: A Systematic Review of the Literature. *J Clin Med*. 2019 Jun 1;8(6).

180. Berruto M, Pasqualotto S, Uboldi F, et al. Traitement des lésions ostéocartilagineuses du genou avec implant biomimètique Maioregen® : résultats à moyen terme. *Rev Chir Orthopédique Traumatol*. 2014 Dec 1;100(8):e31–2.

181. Armoiry X, Cummins E, Connock M, et al. Autologous Chondrocyte Implantation with Chondrosphere for Treating Articular Cartilage Defects in the Knee: An Evidence Review Group Perspective of a NICE Single Technology

Appraisal. *Pharmacoeconomics*. 2019 Jul 1;37(7):879–86.

182. Kielpinski G, Prinzi S, Duguid J, et al. Roadmap to approval: use of an automated sterility test method as a lot release test for Carticel, autologous cultured chondrocytes. *Cytotherapy*. 2005 Dec;7(6):531–41.

183. Vanlauwe J, Huylebroek J, van Der Bauwhede J, et al. Clinical Outcomes of Characterized Chondrocyte Implantation. *Cartilage*. 2012 Apr;3(2):173–80.

184. Korpershoek J V., Vonk LA, Kester EC, et al. Efficacy of one-stage cartilage repair using allogeneic mesenchymal stromal cells and autologous chondron transplantation (IMPACT) compared to nonsurgical treatment for focal articular cartilage lesions of the knee: study protocol for a crossover randomized controlled trial. *Trials*. 2020 Oct 9;21(1).

185. Park Y-B, Ha C-W, Lee C-H, et al. Cartilage Regeneration in Osteoarthritic Patients by a Composite of Allogeneic Umbilical Cord Blood-Derived Mesenchymal Stem Cells and Hyaluronate Hydrogel: Results from a Clinical Trial for Safety and Proof-of-Concept with 7 Years of Extended Follow-Up. *Stem Cells Transl Med*. 2017 Feb 1;6(2):613–21.

186. Lim HC, Park YB, Ha CW, et al. Allogeneic Umbilical Cord Blood-Derived Mesenchymal Stem Cell Implantation Versus Microfracture for Large, Full-Thickness Cartilage Defects in Older Patients: A Multicenter Randomized Clinical Trial and Extended 5-Year Clinical Follow-up. *Orthop J Sport Med*. 2021;9(1).

187. Cherian JJ, Parvizi J, Bramlet D, et al. Preliminary results of a phase II randomized study to determine the efficacy and safety of genetically engineered allogeneic human chondrocytes expressing TGF-β1 in patients with grade 3 chronic degenerative joint disease of the knee. *Osteoarthr Cartil*. 2015 Dec 1;23(12):2109–18.

188. Tohyama H, Yasuda K, Minami A, et al. Atelocollagen-associated autologous chondrocyte implantation for the repair of chondral defects of the knee: a prospective multicenter clinical trial in Japan. *J Orthop Sci*. 2009;14(5):579–88.

189. Huang J, Xiong J, Wang D, et al. 3D Bioprinting of Hydrogels for Cartilage Tissue Engineering. *Gels*. 2021 Sep 1;7(3).

190. Zhang L, Yang G, Johnson BN, et al. Three-dimensional (3D) printed scaffold and material selection for bone repair. *Acta Biomater*. 2019 Jan 15;84:16–33.

191. Koo YW, Choi EJ, Lee JY, et al. 3D printed cell-laden collagen and hybrid scaffolds for in vivo articular cartilage tissue regeneration. *J Ind Eng Chem*. 2018 Oct 25;66:343–55.

192. Martínez-Moreno D, Jiménez G, Chocarro-Wrona C, et al. Pore geometry influences growth and cell adhesion of infrapatellar mesenchymal stem cells in biofabricated 3D thermoplastic scaffolds useful for cartilage tissue engineering. *Mater Sci Eng C*. 2021;122.

193. Zhang Q, Lu H, Kawazoe N, et al. Pore size effect of collagen scaffolds on cartilage regeneration. *Acta Biomater*. 2014;10(5):2005–13.

194. Matsiko A, Gleeson JP, O'Brien FJ. Scaffold mean pore size influences mesenchymal stem cell chondrogenic differentiation and matrix deposition. *Tissue Eng Part A*. 2015 Feb 1;21(3–4):486–97.

195. Ferlin KM, Prendergast ME, Miller ML, et al. Influence of 3D printed porous architecture on mesenchymal stem cell enrichment and differentiation. *Acta Biomater*. 2016 Mar 1;32:161–9.

196. Dimaraki A, Díaz-payno PJ, Minneboo M, et al. Bioprinting of a Zonal-Specific Cell Density Scaffold: A Biomimetic Approach for Cartilage Tissue Engineering. *Appl Sci 2021, Vol 11, Page 7821*. 2021 Aug 25;11(17):7821.

197. Gao F, Xu Z, Liang Q, et al. Direct 3D Printing of High Strength Biohybrid Gradient Hydrogel Scaffolds for Efficient Repair of Osteochondral Defect. *Adv Funct Mater*. 2018 Mar 1;28(13):1706644.

198. Chen L, Deng C, Li J, et al. 3D printing of a lithium-calcium-silicate crystal bioscaffold with dual bioactivities for osteochondral interface reconstruction. *Biomaterials*. 2019 Mar 1;196:138–50.

199. Nowicki MA, Castro NJ, Plesniak MW, et al. 3D printing of novel osteochondral scaffolds with graded microstructure. *Nanotechnology*. 2016 Sep 8;27(41).

200. Antons J, Marascio MGM, Nohava J, et al. Zone-dependent mechanical properties of human articular cartilage obtained by indentation measurements. *J*

Mater Sci Mater Med. 2018 May 1;29(5).

201. O'Connell G, Garcia J, Amir J. 3D Bioprinting: New Directions in Articular Cartilage Tissue Engineering. *ACS Biomater Sci Eng*. 2017 Nov 13;3(11):2657–68.

202. Roseti L, Cavallo C, Desando G, et al. Three-Dimensional Bioprinting of Cartilage by the Use of Stem Cells: A Strategy to Improve Regeneration. *Materials (Basel)*. 2018 Sep 17;11(9).

203. Zhu W, Cui H, Boualam B, et al. 3D bioprinting mesenchymal stem cell-laden construct with core-shell nanospheres for cartilage tissue engineering. *Nanotechnology*. 2018 Mar 8;29(18).

204. Wang B, Díaz-Payno PJ, Browe DC, et al. Affinity-bound growth factor within sulfated interpenetrating network bioinks for bioprinting cartilaginous tissues. *Acta Biomater*. 2021 Jul 1;128:130–42.

205. Sun Y, You Y, Jiang W, et al. 3D bioprinting dual-factor releasing and gradient-structured constructs ready to implant for anisotropic cartilage regeneration. *Sci Adv*. 2020 Sep 1;6(37).

206. Posniak S, Chung JHY, Liu X, et al. Bioprinting of Chondrocyte Stem Cell Co-Cultures for Auricular Cartilage Regeneration. *ACS omega*. 2022 Feb 22;7(7):5908–20.

207. Lan X, Liang Y, Erkut EJN, et al. Bioprinting of human nasoseptal chondrocytes-laden collagen hydrogel for cartilage tissue engineering. *FASEB J*. 2021 Mar 1;35(3).

208. Beketov EE, Isaeva E V., Yakovleva ND, et al. Bioprinting of Cartilage with Bioink Based on High-Concentration Collagen and Chondrocytes. *Int J Mol Sci*. 2021 Nov 1;22(21).

209. Chiesa-Estomba CM, Aiastui A, González-Fernández I, et al. Three-Dimensional Bioprinting Scaffolding for Nasal Cartilage Defects: A Systematic Review. *Tissue Eng Regen Med*. 2021 Jun 1;18(3):343–53.

210. Theodoridis K, Aggelidou E, Vavilis T, et al. Hyaline cartilage next generation implants from adipose-tissue-derived mesenchymal stem cells: Comparative

study on 3D-printed polycaprolactone scaffold patterns. *J Tissue Eng Regen Med*. 2019 Feb 1;13(2):342–55.

211. Zhou X, Tenaglio S, Esworthy T, et al. Three-Dimensional Printing Biologically Inspired DNA-Based Gradient Scaffolds for Cartilage Tissue Regeneration. *ACS Appl Mater Interfaces*. 2020 Jul 22;12(29):33219–28.

212. Daly AC, Critchley SE, Rencsok EM, et al. A comparison of different bioinks for 3D bioprinting of fibrocartilage and hyaline cartilage. *Biofabrication*. 2016 Oct 7;8(4).

213. De Moor L, Fernandez S, Vercruysse C, et al. Hybrid Bioprinting of Chondrogenically Induced Human Mesenchymal Stem Cell Spheroids. *Front Bioeng Biotechnol*. 2020 May 25;8:484.

214. Hauptstein J, Böck T, Bartolf-Kopp M, et al. Hyaluronic Acid-Based Bioink Composition Enabling 3D Bioprinting and Improving Quality of Deposited Cartilaginous Extracellular Matrix. *Adv Healthc Mater*. 2020 Aug 1;9(15).

215. Pan JF, Li S, Guo CA, et al. Evaluation of synovium-derived mesenchymal stem cells and 3D printed nanocomposite scaffolds for tissue engineering. *http://www.tandfonline.com/action/journalInformation?show=aimsScope&journalCode=tsta20#VmBmuzZFCUk*. 2015 Aug 1;16(4).

216. Grogan SP, Dorthé EW, Glembotski NE, et al. Cartilage tissue engineering combining microspheroid building blocks and microneedle arrays. *Connect Tissue Res*. 2020 Mar 3;61(2):229–43.

217. Nguyen D, Hgg DA, Forsman A, et al. Cartilage Tissue Engineering by the 3D Bioprinting of iPS Cells in a Nanocellulose/Alginate Bioink. *Sci Rep*. 2017 Dec 1;7(1).

218. Lopa S, Colombini A, Stanco D, et al. Donor-matched mesenchymal stem cells from knee infrapatellar and subcutaneous adipose tissue of osteoarthritic donors display differential chondrogenic and osteogenic commitment. *Eur Cell Mater*. 2014 Apr 23;27:298–311.

219. Kubosch EJ, Lang G, Furst D, et al. The Potential for Synovium-derived Stem Cells in Cartilage Repair. *Curr Stem Cell Res Ther*. 2018 Feb 23;13(3):174–84.

220. Daly AC, Kelly DJ. Biofabrication of spatially organised tissues by directing the growth of cellular spheroids within 3D printed polymeric microchambers. *Biomaterials*. 2019 Mar 1;197:194–206.

221. Levato R, Webb WR, Otto IA, et al. The bio in the ink: cartilage regeneration with bioprintable hydrogels and articular cartilage-derived progenitor cells. *Acta Biomater*. 2017 Oct 1;61:41–53.

222. Gungor-Ozkerim PS, Inci I, Zhang YS, et al. Bioinks for 3D bioprinting: an overview. *Biomater Sci*. 2018 May 1;6(5):915–46.

223. Henrionnet C, Messaoudi O, Pourchet L, et al. A Comparison of 3 Bioinks for 3D Bioprinting of Articular Cartilage. *Stem Cells Regen Med Proc 9th Int Eur Symp Strasbg 2-4 Oct 2019*. 2021 Jun 1;80:81–7.

224. Bahram M, Mohseni N, Moghtader M. An Introduction to Hydrogels and Some Recent Applications. *Emerg Concepts Anal Appl Hydrogels*. 2016 Aug 24;

225. Gopinathan J, Noh I. Recent trends in bioinks for 3D printing. *Biomater Res*. 2018 Apr 6;22(1).

226. O'Shea TM, Miao X. Bilayered scaffolds for osteochondral tissue engineering. *Tissue Eng Part B Rev*. 2008 Dec 1;14(4):447–64.

227. Occhetta P, Mainardi A, Votta E, et al. Hyperphysiological compression of articular cartilage induces an osteoarthritic phenotype in a cartilage-on-a-chip model. *Nat Biomed Eng*. 2019 Jul 1;3(7):545–57.

228. Groll J, Burdick JA, Cho DW, et al. A definition of bioinks and their distinction from biomaterial inks. *Biofabrication*. 2018 Jan 1;11(1).

229. Giuseppe M Di, Law N, Webb B, et al. Mechanical behaviour of alginate-gelatin hydrogels for 3D bioprinting. *J Mech Behav Biomed Mater*. 2018 Mar 1;79:150–7.

230. Gao Q, He Y, Fu J zhong, et al. Coaxial nozzle-assisted 3D bioprinting with built-in microchannels for nutrients delivery. *Biomaterials*. 2015 Aug 1;61:203–15.

231. Naghieh S, Karamooz-Ravari MR, Sarker MD, et al. Influence of crosslinking on the mechanical behavior of 3D printed alginate scaffolds: Experimental and

numerical approaches. *J Mech Behav Biomed Mater*. 2018 Apr 1;80:111–8.

232. Yang X, Lu Z, Wu H, et al. Collagen-alginate as bioink for three-dimensional (3D) cell printing based cartilage tissue engineering. *Mater Sci Eng C Mater Biol Appl*. 2018 Feb 1;83:195–201.

233. Gao T, Gillispie GJ, Copus JS, et al. Optimization of gelatin-alginate composite bioink printability using rheological parameters: a systematic approach. *Biofabrication*. 2018 Jun 29;10(3).

234. Hu X, Man Y, Li W, et al. 3D Bio-Printing of CS/Gel/HA/Gr Hybrid Osteochondral Scaffolds. *Polym 2019, Vol 11, Page 1601*. 2019 Sep 30;11(10):1601.

235. Hernández-González AC, Téllez-Jurado L, Rodríguez-Lorenzo LM. Alginate hydrogels for bone tissue engineering, from injectables to bioprinting: A review. *Carbohydr Polym*. 2020 Feb 1;229.

236. Axpe E, Oyen ML. Applications of Alginate-Based Bioinks in 3D Bioprinting. *Int J Mol Sci*. 2016 Dec 1;17(12).

237. Antich C, de Vicente J, Jiménez G, et al. Bio-inspired hydrogel composed of hyaluronic acid and alginate as a potential bioink for 3D bioprinting of articular cartilage engineering constructs. *Acta Biomater*. 2020 Apr 1;106:114–23.

238. Rathan S, Dejob L, Schipani R, et al. Fiber Reinforced Cartilage ECM Functionalized Bioinks for Functional Cartilage Tissue Engineering. *Adv Healthc Mater*. 2019 Apr 11;8(7).

239. Noh I, Kim N, Tran HN, et al. 3D printable hyaluronic acid-based hydrogel for its potential application as a bioink in tissue engineering. *Biomater Res*. 2019 Feb 6;23(1):1–9.

240. Poldervaart MT, Goversen B, De Ruijter M, et al. 3D bioprinting of methacrylated hyaluronic acid (MeHA) hydrogel with intrinsic osteogenicity. *PLoS One*. 2017 Jun 1;12(6).

241. Petta D, Armiento AR, Grijpma D, et al. 3D bioprinting of a hyaluronan bioink through enzymatic-and visible light-crosslinking. *Biofabrication*. 2018 Sep 25;10(4).

242. Kiyotake EA, Douglas AW, Thomas EE, et al. Development and quantitative characterization of the precursor rheology of hyaluronic acid hydrogels for bioprinting. *Acta Biomater*. 2019 Sep 1;95:176–87.

243. Lam T, Dehne T, Krüger JP, et al. Photopolymerizable gelatin and hyaluronic acid for stereolithographic 3D bioprinting of tissue-engineered cartilage. *J Biomed Mater Res B Appl Biomater*. 2019 Nov 1;107(8):2649.

244. Kundu J, Shim JH, Jang J, et al. An additive manufacturing-based PCL-alginate-chondrocyte bioprinted scaffold for cartilage tissue engineering. *J Tissue Eng Regen Med*. 2015 Nov 1;9(11):1286–97.

245. Narayanan LK, Huebner P, Fisher MB, et al. 3D-Bioprinting of Polylactic Acid (PLA) Nanofiber–Alginate Hydrogel Bioink Containing Human Adipose-Derived Stem Cells. *ACS Biomater Sci Eng*. 2016 Oct 10;2(10):1732–42.

246. Semba JA, Mieloch AA, Rybka JD. Introduction to the state-of-the-art 3D bioprinting methods, design, and applications in orthopedics. *Bioprinting*. 2020 Jun 1;18:e00070.

247. Jung CS, Kim BK, Lee J, et al. Development of Printable Natural Cartilage Matrix Bioink for 3D Printing of Irregular Tissue Shape. *Tissue Eng Regen Med*. 2017 Apr 1;15(2):155–62.

248. Mouser VHM, Abbadessa A, Levato R, et al. Development of a thermosensitive HAMA-containing bio-ink for the fabrication of composite cartilage repair constructs. *Biofabrication*. 2017 Mar 1;9(1).

249. Jaklenec A, Stamp A, Deweerd E, et al. Progress in the Tissue Engineering and Stem Cell Industry “Are we there yet?” *Tissue Eng Part B Rev*. 2012;18(3):155–66.

250. Zhang M, Sun L, Wang X, et al. Activin B Promotes BMSC-Mediated Cutaneous Wound Healing by Regulating Cell Migration via the JNK-ERK Signaling Pathway. *Cell Transplant*. 2014 Sep;23(9):1061–73.

251. Rowan MP, Cancio LC, Elster EA, et al. Burn wound healing and treatment: review and advancements. *Crit Care*. 2015 Jun 12;19(1).

252. Petrof G, Martinez-Queipo M, Mellerio J, et al. Fibroblast cell therapy enhances

initial healing in recessive dystrophic epidermolysis bullosa wounds: results of a randomized, vehicle-controlled trial. *Br J Dermatol*. 2013 Nov;169(5):1025–33.

253. McGrath H, Hormozi A, Hosseini S, et al. Comparison of the Application of Allogeneic Fibroblast and Autologous Mesh Grafting With the Conventional Method in the Treatment of Third-Degree Burns. *J Burn Care Res*. 2016;37(1):e90–5.

254. Kirsner R, Marston W, Snyder R, et al. Spray-applied cell therapy with human allogeneic fibroblasts and keratinocytes for the treatment of chronic venous leg ulcers: a phase 2, multicentre, double-blind, randomised, placebo-controlled trial. *Lancet (London, England)*. 2012;380(9846):977–85.

255. Ramos M, Ramos D, Gontijo G, et al. Non-cultured melanocyte/keratinocyte transplantation for the treatment of stable vitiligo on the face: report of two cases. *An Bras Dermatol*. 2013 Sep;88(5):811–3.

256. Xu Y, Huang S, Fu X. Autologous transplantation of bone marrow-derived mesenchymal stem cells: a promising therapeutic strategy for prevention of skin-graft contraction. *Clin Exp Dermatol*. 2012 Jul;37(5):497–500.

257. Orouji Z, Bajouri A, Ghasemi M, et al. A single-arm open-label clinical trial of autologous epidermal cell transplantation for stable vitiligo: A 30-month follow-up. *J Dermatol Sci*. 2018 Jan 1;89(1):52–9.

258. Kumar A, Mohanty S, Nandy S, et al. Hair & skin derived progenitor cells: In search of a candidate cell for regenerative medicine. *Indian J Med Res*. 2016 Feb 1;143(2):175–83.

259. Stessuk T, Puzzi M, Chaim E, et al. Platelet-rich plasma (PRP) and adipose-derived mesenchymal stem cells: stimulatory effects on proliferation and migration of fibroblasts and keratinocytes in vitro. *Arch Dermatol Res*. 2016 Sep 1;308(7):511–20.

260. Law J, Chowdhury S, Saim A, et al. Platelet-rich plasma with keratinocytes and fibroblasts enhance healing of full-thickness wounds. *J Tissue Viability*. 2017 Aug 1;26(3):208–15.

261. Takabayashi Y, Ishihara M, Kuwabara M, et al. Improved Survival of Full-Thickness Skin Graft With Low-Molecular Weight Heparin-Protamine

Micro/Nanoparticles Including Platelet-Rich Plasma. *Ann Plast Surg*. 2017;78(5):562–8.

262. Yannas I V, Burke JF. Design of an artificial skin. I. Basic design principles. *J Biomed Mater Res*. 1980 Jan;14(1):65–81.

263. Kopp J, Magnus Noah E, Rübben A, et al. Radical Resection of Giant Congenital Melanocytic Nevus and Reconstruction With Meek-Graft Covered Integra Dermal Template. *Dermatologic Surg*. 2003 Jun 1;29(6):653–7.

264. Heimbach D, Luterman A, Burke J, et al. Artificial dermis for major burns. A multi-center randomized clinical trial. *Ann Surg*. 1988 Sep;208(3):313–20.

265. Munster A, Smith-Meek M, Shalom A. Acellular allograft dermal matrix: immediate or delayed epidermal coverage? *Burns*. 2001;27(2):150–3.

266. Park S, Kim Y, Jang S. The application of an acellular dermal allograft (AlloDerm) for patients with insufficient conjunctiva during evisceration and implantation surgery. *Eye (Lond)*. 2018 Jan 1;32(1):136–41.

267. Jones G, Yoo A, King V, et al. Prepectoral Immediate Direct-to-Implant Breast Reconstruction with Anterior AlloDerm Coverage. *Plast Reconstr Surg*. 2017 Dec;140(6S Prepectoral Breast Reconstruction):31S-38S.

268. Tan H, Wasiak J, Paul E, et al. Effective use of Biobrane as a temporary wound dressing prior to definitive split-skin graft in the treatment of severe burn: A retrospective analysis. *Burns*. 2015 Aug;41(5):969–76.

269. Greenwood JE. A Randomized, Prospective Study of the Treatment of Superficial Partial-Thickness Burns: AWBAT-S Versus Biobrane. *Eplasty*. 2011 Feb 24;11:e10.

270. Sivak WN, Bourne DA, Miller MP, et al. Simplified Calvarial Reconstruction: Coverage of Bare Skull With Gammagraft Promotes Granulation and Facilitates Skin Grafting. *J Craniofac Surg*. 2016 Oct 1;27(7):1808–9.

271. Reyzelman A, Crews RT, Moore JC, et al. Clinical effectiveness of an acellular dermal regenerative tissue matrix compared to standard wound management in healing diabetic foot ulcers: a prospective, randomised, multicentre study. *Int Wound J*. 2009 Jun;6(3):196–208.

272. Winters CL, Brigido SA, Liden BA, et al. A Multicenter Study Involving the Use of a Human Acellular Dermal Regenerative Tissue Matrix for the Treatment of Diabetic Lower Extremity Wounds. *Adv Skin Wound Care*. 2008 Aug;21(8):375–81.

273. Brigido SA. The use of an acellular dermal regenerative tissue matrix in the treatment of lower extremity wounds: a prospective 16-week pilot study. *Int Wound J*. 2006 Sep;3(3):181–7.

274. Haslik W, Kamolz L-P, Manna F, et al. Management of full-thickness skin defects in the hand and wrist region: first long-term experiences with the dermal matrix Matriderm®. *J Plast Reconstr Aesthetic Surg*. 2010 Feb;63(2):360–4.

275. Ryssel H, Gazyakan E, Germann G, et al. The use of MatriDerm in early excision and simultaneous autologous skin grafting in burns--a pilot study. *Burns*. 2008 Feb;34(1):93–7.

276. Pittman TA, Fan KL, Knapp A, et al. Comparison of Different Acellular Dermal Matrices in Breast Reconstruction. *Plast Reconstr Surg*. 2017 Mar;139(3):521–8.

277. Eberli D, Rodriguez S, Atala A, et al. In vivo evaluation of acellular human dermis for abdominal wall repair. *J Biomed Mater Res Part A*. 2009 Jun 15;93(4):n/a-n/a.

278. Kirsner R, Bohn G, Driver V, et al. Human acellular dermal wound matrix: evidence and experience. *Int Wound J*. 2015 Dec 1;12(6):646–54.

279. Kim JS, Kaminsky AJ, Summitt JB, et al. New Innovations for Deep Partial-Thickness Burn Treatment with ACell MatriStem Matrix. *Adv Wound Care*. 2016 Dec 1;5(12):546–52.

280. El-Khatib HA, Hammouda A, Al-Ghol A, et al. Aldehyde-treated porcine skin versus biobrane as biosynthetic skin substitutes for excised burn wounds: case series and review of the literature. *Ann Burns Fire Disasters*. 2007 Jun 30;20(2):78–82.

281. Romanelli M, Dini V, Bertone M, et al. OASIS wound matrix versus Hyaloskin in the treatment of difficult-to-heal wounds of mixed arterial/venous aetiology. *Int Wound J*. 2007 Mar;4(1):3–7.

282. Niezgoda JA, Van Gils CC, Frykberg RG, et al. Randomized clinical trial comparing OASIS Wound Matrix to Regranex Gel for diabetic ulcers. *Adv Skin Wound Care*. 2005 Jun;18(5 Pt 1):258–66.

283. Hodde JP, Ernst DMJ, Hiles MC. An investigation of the long-term bioactivity of endogenous growth factor in OASIS Wound Matrix. *J Wound Care*. 2005 Jan;14(1):23–5.

284. Field JLC. Porcine urinary bladder matrix: a retrospective study and establishment of protocol. *http://dx.doi.org/1012968/jowc20122110476*. 2013 Aug 16;21(10):476–82.

285. Noordenbos J, Doré C, Hansbrough J. Safety and efficacy of TransCyte for the treatment of partial-thickness burns. *J Burn Care Rehabil*. 1999;20(4):275–81.

286. Marston W, Hanft J, Norwood P, et al. The efficacy and safety of Dermagraft in improving the healing of chronic diabetic foot ulcers: results of a prospective randomized trial. *Diabetes Care*. 2003 Jun 1;26(6):1701–5.

287. Williamson J, Snelling C, Clugston P, et al. Cultured epithelial autograft: five years of clinical experience with twenty-eight patients. *J Trauma*. 1995;39(2):309–19.

288. Carsin H, Ainaud P, Le Bever H, et al. Cultured epithelial autografts in extensive burn coverage of severely traumatized patients: a five year single-center experience with 30 patients. *Burns*. 2000 Jun;26(4):379–87.

289. Greenberg J, Falabella A, Bello Y, et al. Tissue-engineered skin in the healing of wound stumps from limb amputations secondary to purpura fulminans. *Pediatr Dermatol*. 2003 Mar;20(2):169–72.

290. Caravaggi C, De Giglio R, Pritelli C, et al. HYAFF 11-based autologous dermal and epidermal grafts in the treatment of noninfected diabetic plantar and dorsal foot ulcers: a prospective, multicenter, controlled, randomized clinical trial. *Diabetes Care*. 2003 Oct 1;26(10):2853–9.

291. Uccioli L. A clinical investigation on the characteristics and outcomes of treating chronic lower extremity wounds using the tissuetech autograft system. *Int J Low Extrem Wounds*. 2003 Sep;2(3):140–51.

292. Amani H, Dougherty W, Blome-Eberwein S. Use of Transcyte and dermabrasion to treat burns reduces length of stay in burns of all size and etiology. *Burns*. 2006 Nov;32(7):828–32.

293. Myers S, Partha V, Soranzo C, et al. Hyalomatrix: a temporary epidermal barrier, hyaluronan delivery, and neodermis induction system for keratinocyte stem cell therapy. *Tissue Eng*. 2007 Nov 1;13(11):2733–41.

294. Landi A, Garagnani L, Leti Acciaro A, et al. Hyaluronic acid scaffold for skin defects in congenital syndactyly release surgery: a novel technique based on the regenerative model. *J Hand Surg Eur Vol*. 2014 Nov 12;39(9):994–1000.

295. Simman R, Mari W, Younes S, et al. Use of Hyaluronic Acid–Based Biological Bilaminar Matrix in Wound Bed Preparation: A Case Series. *Eplasty*. 2018;18:e10.

296. Eaglstein W, Iriondo M, Laszlo K. A composite skin substitute (graftskin) for surgical wounds. A clinical experience. *Dermatol Surg*. 1995;21(10):839–43.

297. Stone R, Stojadinovic O, Rosa A, et al. A bioengineered living cell construct activates an acute wound healing response in venous leg ulcers. *Sci Transl Med*. 2017 Jan 4;9(371).

298. Still J, Glat P, Silverstein P, et al. The use of a collagen sponge/living cell composite material to treat donor sites in burn patients. *Burns*. 2003;29(8):837–41.

299. Schurr MJ, Foster KN, Centanni JM, et al. Phase I/II Clinical Evaluation of StrataGraft: A Consistent, Pathogen-Free Human Skin Substitute. *J Trauma*. 2009 Mar;66(3):866.

300. Centanni J, Straseski J, Wicks A, et al. StrataGraft skin substitute is well-tolerated and is not acutely immunogenic in patients with traumatic wounds: results from a prospective, randomized, controlled dose escalation trial. *Ann Surg*. 2011 Apr;253(4):672–83.

301. Akkouch A, Shi G, Zhang Z, et al. Bioactivating electrically conducting polypyrrole with fibronectin and bovine serum albumin. *J Biomed Mater Res A*. 2010;92(1):221–31.

302. Darabi M, Khosrozadeh A, Mbeleck R, et al. Skin-Inspired Multifunctional Autonomic-Intrinsic Conductive Self-Healing Hydrogels with Pressure Sensitivity, Stretchability, and 3D Printability. *Adv Mater*. 2017 Aug 18;29(31).

303. Sadeghi A, Nokhasteh S, Molavi A, et al. Surface modification of electrospun PLGA scaffold with collagen for bioengineered skin substitutes. *Mater Sci Eng C Mater Biol Appl*. 2016 Sep 1;66:130–7.

304. Sadeghi-Avalshahr A, Khorsand-Ghayeni M, Nokhasteh S, et al. Synthesis and characterization of PLGA/collagen composite scaffolds as skin substitute produced by electrospinning through two different approaches. *J Mater Sci Mater Med*. 2017 Jan 1;28(1).

305. Sharif S, Ai J, Azami M, et al. Collagen-coated nano-electrospun PCL seeded with human endometrial stem cells for skin tissue engineering applications. *J Biomed Mater Res B Appl Biomater*. 2018 May 1;106(4):1578–86.

306. Levengood S, Erickson A, Chang F, et al. Chitosan-Poly(caprolactone) Nanofibers for Skin Repair. *J Mater Chem B*. 2017;5(9):1822–33.

307. Límová M. Active wound coverings: bioengineered skin and dermal substitutes. *Surg Clin North Am*. 2010 Dec;90(6):1237–55.

308. Taghiabadi E, Beiki B, Aghdami N, et al. Amniotic Membrane Seeded Fetal Fibroblasts as Skin Substitute for Wound Regeneration. *Methods Mol Biol*. 2019;1879:211–9.

309. Qian X, Linru G, Sigen A, et al. Injectable hyperbranched poly(β-amino ester) hydrogels with on-demand degradation profiles to match wound healing processes. *Chem Sci*. 2018 Feb 21;9(8):2179–87.

310. Rameshbabu A, Bankoti K, Datta S, et al. Silk Sponges Ornamented with a Placenta-Derived Extracellular Matrix Augment Full-Thickness Cutaneous Wound Healing by Stimulating Neovascularization and Cellular Migration. *ACS Appl Mater Interfaces*. 2018 May 23;10(20):16977–91.

311. Gholipourmalekabadi M, Seifalian A, Urbanska A, et al. 3D Protein-Based Bilayer Artificial Skin for the Guided Scarless Healing of Third-Degree Burn Wounds in Vivo. *Biomacromolecules*. 2018 Jul 9;19(7):2409–22.

312. Ramió-Lluch L, Cerrato S, Brazis P, et al. Proof of concept of a new autologous skin substitute for the treatment of deep wounds in dogs. *Vet J*. 2017 Dec 1;230:36–40.

313. Held M, Medved F, Petersen W, et al. A Quantitative Analysis of Microcirculation in Skin Defects Covered with Topical Wound Dressings or a Newly Developed Collagen Matrix. *Adv Skin Wound Care*. 2017 Nov 1;30(11):517–21.

314. Hartwell R, Leung V, Chavez-Munoz C, et al. A novel hydrogel-collagen composite improves functionality of an injectable extracellular matrix. *Acta Biomater*. 2011 Aug;7(8):3060–9.

315. Nimal T, Baranwal G, Bavya M, et al. Anti-staphylococcal Activity of Injectable Nano Tigecycline/Chitosan-PRP Composite Hydrogel Using Drosophila melanogaster Model for Infectious Wounds. *ACS Appl Mater Interfaces*. 2016 Aug 31;8(34):22074–83.

316. Yun E, Yon B, Joo M, et al. Cell therapy for skin wound using fibroblast encapsulated poly(ethylene glycol)-poly(L-alanine) thermogel. *Biomacromolecules*. 2012 Apr 9;13(4):1106–11.

317. Eun Ji K, Ji Suk C, Jun Sung K, et al. Injectable and Thermosensitive Soluble Extracellular Matrix and Methylcellulose Hydrogels for Stem Cell Delivery in Skin Wounds. *Biomacromolecules*. 2016;17(1):4–11.

318. Kuo K, Lin R, Tien H, et al. Bioengineering vascularized tissue constructs using an injectable cell-laden enzymatically crosslinked collagen hydrogel derived from dermal extracellular matrix. *Acta Biomater*. 2015 Nov 1;27:151–66.

319. Song W, An D, Kao D-I, et al. Nanofibrous Microposts and Microwells of Controlled Shapes and Their Hybridization with Hydrogels for Cell Encapsulation. *ACS Appl Mater Interfaces*. 2014 May 28;6(10):7038–44.

320. Tran N, Joung Y, Lih E, et al. In situ forming and rutin-releasing chitosan hydrogels as injectable dressings for dermal wound healing. *Biomacromolecules*. 2011 Aug 8;12(8):2872–80.

321. Young Chan C, Ji Suk C, Beob Soo K, et al. Decellularized extracellular matrix derived from porcine adipose tissue as a xenogeneic biomaterial for tissue

engineering. *Tissue Eng Part C Methods*. 2012 Nov 1;18(11):866–76.

322. Wassenaar J, Braden R, Osborn K, et al. Modulating In Vivo Degradation Rate of Injectable Extracellular Matrix Hydrogels. *J Mater Chem B*. 2016 Apr 28;4(16):2794–802.

323. Tukmachev D, Forostyak S, Koci Z, et al. Injectable Extracellular Matrix Hydrogels as Scaffolds for Spinal Cord Injury Repair. *Tissue Eng Part A*. 2016 Feb 1;22(3–4):306–17.

324. Zhu Y, Hideyoshi S, Jiang H, et al. Injectable, porous, biohybrid hydrogels incorporating decellularized tissue components for soft tissue applications. *Acta Biomater*. 2018 Jun 1;73:112–26.

325. Li Y, Cao J, Han S, et al. ECM based injectable thermo-sensitive hydrogel on the recovery of injured cartilage induced by osteoarthritis. *https://doi.org/101080/2169140120181452752*. 2018 Nov 5;46(sup2):152–60.

326. Wolf M, Daly K, Brennan-Pierce E, et al. A hydrogel derived from decellularized dermal extracellular matrix. *Biomaterials*. 2012 Oct;33(29):7028–38.

327. Esteban-Vives R, Choi M, Young M, et al. Second-degree burns with six etiologies treated with autologous noncultured cell-spray grafting. *Burns*. 2016 Nov 1;42(7):e99–106.

328. Mizoguchi T, Ueno K, Takeuchi Y, et al. Treatment of Cutaneous Ulcers with Multilayered Mixed Sheets of Autologous Fibroblasts and Peripheral Blood Mononuclear Cells. *Cell Physiol Biochem*. 2018 Jun 1;47(1):201–11.

329. Chen L, Radke D, Qi S, et al. Protocols for Full Thickness Skin Wound Repair Using Prevascularized Human Mesenchymal Stem Cell Sheet. *Methods Mol Biol*. 2019;1879:187–200.

330. Ehterami A, Salehi M, Farzamfar S, et al. In vitro and in vivo study of PCL/COLL wound dressing loaded with insulin-chitosan nanoparticles on cutaneous wound healing in rats model. *Int J Biol Macromol*. 2018 Oct 1;117:601–9.

331. Im H, Kim S, Kim S, et al. Skin Regeneration with a Scaffold of Predefined Shape and Bioactive Peptide Hydrogels. *Tissue Eng Part A*. 2018 Oct 1;24(19–

20):1518–30.

332. Vulpe R, Popa M, Picton L, et al. Scaffolds Based on Collagen, Hyaluronan and Sericin with Potential Applications as Controlled Drug Delivery System. *J Nanosci Nanotechnol*. 2018 Oct 17;18(3):1528–33.

333. Hou X, Liu S, Wang M, et al. Layer-by-Layer 3D Constructs of Fibroblasts in Hydrogel for Examining Transdermal Penetration Capability of Nanoparticles. *SLAS Technol*. 2017 Aug 1;22(4):447–53.

334. Bhardwaj N, Sow W, Devi D, et al. Silk fibroin-keratin based 3D scaffolds as a dermal substitute for skin tissue engineering. *Integr Biol (Camb)*. 2015 Jan 1;7(1):53–63.

335. Morris A, Stamer D, Kunkemoeller B, et al. Decellularized materials derived from TSP2-KO mice promote enhanced neovascularization and integration in diabetic wounds. *Biomaterials*. 2018 Jul 1;169:61–71.

336. Carriel V, Garzón I, Jiménez J, et al. Epithelial and stromal developmental patterns in a novel substitute of the human skin generated with fibrin-agarose biomaterials. *Cells Tissues Organs*. 2012 Jun;196(1):1–12.

337. Zhang Y, Yang F, Liu K, et al. The impact of PLGA scaffold orientation on invitro cartilage regeneration. *Biomaterials*. 2012 Apr;33(10):2926–35.

338. Sow W, Lui Y, Ng K. Electrospun human keratin matrices as templates for tissue regeneration. *Nanomedicine (Lond)*. 2013;8(4):531–41.

339. Nayak K, Gupta P. Study of the keratin-based therapeutic dermal patches for the delivery of bioactive molecules for wound treatment. *Mater Sci Eng C Mater Biol Appl*. 2017 Aug 1;77:1088–97.

340. Gupta P, Nayak K. Compatibility Study of Alginate/Keratin Blend for Biopolymer Development: *https://doi.org/105301/jabfm5000242*. 2015 Dec 18;13(4):E332–9.

341. Sierra-Sánchez Á, Fernández-González A, Lizana-Moreno A, et al. Hyaluronic acid biomaterial for human tissue-engineered skin substitutes: Preclinical comparative in vivo study of wound healing. *J Eur Acad Dermatol Venereol*. 2020 Oct 1;34(10):2414–27.

342. Wu S, Pollak R, Frykberg R, et al. Safety and efficacy of intramuscular human placenta-derived mesenchymal stromal-like cells (cenplacel [PDA-002]) in patients who have a diabetic foot ulcer with peripheral arterial disease. *Int Wound J*. 2017 Oct 1;14(5):823–9.

343. Kim H, Lee J, Roh K, et al. Clinical Trial of Human Umbilical Cord Blood-Derived Stem Cells for the Treatment of Moderate-to-Severe Atopic Dermatitis: Phase I/IIa Studies. *Stem Cells*. 2017 Jan 1;35(1):248–55.

344. Greenwood JE. A Randomized, Prospective Study of the Treatment of Superficial Partial-Thickness Burns: AWBAT-S Versus Biobrane. *Eplasty*. 2011 Feb 24;11:e10.

345. Reyzelman A, Crews R, Moore J, et al. Clinical effectiveness of an acellular dermal regenerative tissue matrix compared to standard wound management in healing diabetic foot ulcers: a prospective, randomised, multicentre study. *Int Wound J*. 2009 Jun;6(3):196–208.

346. Palaia D, Arthur K, Cahan A, et al. Incidence of Seromas and Infections Using Fenestrated versus Nonfenestrated Acellular Dermal Matrix in Breast Reconstructions. *Plast Reconstr surgery Glob open*. 2015;3(11).

347. Eberli D, Rodriguez S, Atala A, et al. In vivo evaluation of acellular human dermis for abdominal wall repair. *J Biomed Mater Res A*. 2010 Jun 15;93(4):1527–38.

348. Kirsner R, Vanscheidt W, Keast D, et al. Phase 3 evaluation of HP802-247 in the treatment of chronic venous leg ulcers. *Wound Repair Regen*. 2016 Sep 1;24(5):894–903.

349. Lommerts J, Meesters A, Komen L, et al. Autologous cell suspension grafting in segmental vitiligo and piebaldism: a randomized controlled trial comparing full surface and fractional CO 2 laser recipient-site preparations. *Br J Dermatol*. 2017 Nov 1;177(5):1293–8.

350. Gálvez-Martín P, Clares B, Hmadcha A, et al. Development of a cell-based medicinal product: regulatory structures in the European Union. *Br Med Bull*. 2013 Mar;105(1):85–105.

351. Gálvez-Martín P, Clares B, Bermejo M, et al. Standard Requirement of a

Microbiological Quality Control Program for the Manufacture of Human Mesenchymal Stem Cells for Clinical Use. *Stem Cells Dev*. 2014 May 15;23(10):1074–83.

352. Cubo N, Garcia M, Del Cañizo J, et al. 3D bioprinting of functional human skin: production and in vivo analysis. *Biofabrication*. 2016 Mar 1;9(1).

353. Pourchet L, Thepot A, Albouy M, et al. Human Skin 3D Bioprinting Using Scaffold-Free Approach. *Adv Healthc Mater*. 2017 Feb 22;6(4).

354. Xiong S, Zhang X, Lu P, et al. A Gelatin-sulfonated Silk Composite Scaffold based on 3D Printing Technology Enhances Skin Regeneration by Stimulating Epidermal Growth and Dermal Neovascularization. *Sci Rep*. 2017 Dec 1;7(1).

355. Zou Y, Han Q, Weng X, et al. The precision and reliability evaluation of 3-dimensional printed damaged bone and prosthesis models by stereo lithography appearance. *Medicine (Baltimore)*. 2018 Feb 1;97(6).

356. Juskova P, Ollitrault A, Serra M, et al. Resolution improvement of 3D stereo-lithography through the direct laser trajectory programming: Application to microfluidic deterministic lateral displacement device. *Anal Chim Acta*. 2018 Feb 13;1000:239–47.

357. Yu J, E E, Berg M, et al. Biomimetic scaffolds with three-dimensional undulated microtopographies. *Biomaterials*. 2017 Jun 1;128:109–20.

358. Gainza G, Bonafonte DC eldra., Moreno B, et al. The topical administration of rhEGF-loaded nanostructured lipid carriers (rhEGF-NLC) improves healing in a porcine full-thickness excisional wound model. *J Control Release*. 2015 Jan 10;197:41–7.

359. Chen JD, Kim JP, Zhang K, et al. Epidermal Growth Factor (EGF) Promotes Human Keratinocyte Locomotion on Collagen by Increasing the α2 Integrin Subunit. *Exp Cell Res*. 1993 Dec 1;209(2):216–23.

360. Cui H, Zhu W, Nowicki M, et al. Hierarchical Fabrication of Engineered Vascularized Bone Biphasic Constructs via Dual 3D Bioprinting: Integrating Regional Bioactive Factors into Architectural Design. *Adv Healthc Mater*. 2016 Sep 7;5(17):2174.

361. El-Ghalbzouri A, Gibbs S, Lamme E, et al. Effect of fibroblasts on epidermal regeneration. *Br J Dermatol*. 2002;147(2):230–43.

362. Dinulos J. Clinical Dermatology by Habif 7th Ed. *J Chem Inf Model*. 2021;1:0–1051.

363. Bolognia J, Jorizzo J, and Schaffer J. Dermatology, 3rd edition — Northwestern Scholars. Elsevier Limited. London; 2012.

364. Abaci H, Guo Z, Coffman A, et al. Human Skin Constructs with Spatially Controlled Vasculature Using Primary and iPSC-Derived Endothelial Cells. *Adv Healthc Mater*. 2016 Jul 20;5(14):1800–7.

365. Kérourédan O, Bourget J, Rémy M, et al. Micropatterning of endothelial cells to create a capillary-like network with defined architecture by laser-assisted bioprinting. *J Mater Sci Mater Med*. 2019 Feb 1;30(2).

366. Liu Y, Suwa F, Wang X, et al. Reconstruction of a tissue-engineered skin containing melanocytes. *Cell Biol Int*. 2007 Sep;31(9):985–90.

367. Tumbar T, Guasch G, Greco V, et al. Defining the epithelial stem cell niche in skin. *Science*. 2004 Jan 16;303(5656):359–63.

368. Sheng-Ping H, Chun-Hsiang H, Jia-Fwu S, et al. Promotion of wound healing using adipose-derived stem cells in radiation ulcer of a rat model. *J Biomed Sci*. 2013;20(1):51.

369. Maxson S, Lopez E, Yoo D, et al. Concise review: role of mesenchymal stem cells in wound repair. *Stem Cells Transl Med*. 2012 Feb;1(2):142–9.

370. Moorefield EC, McKee EE, Solchaga L, et al. Cloned, CD117 Selected Human Amniotic Fluid Stem Cells Are Capable of Modulating the Immune Response. *PLoS One*. 2011;6(10):e26535.

371. De Coppi P, Bartsch G, Siddiqui M, et al. Isolation of amniotic stem cell lines with potential for therapy. *Nat Biotechnol*. 2007 Jan 5;25(1):100–6.

372. Skardal A, Mack D, Kapetanovic E, et al. Bioprinted amniotic fluid-derived stem cells accelerate healing of large skin wounds. *Stem Cells Transl Med*. 2012 Nov;1(11):792–802.

373. Aasen T, Raya A, Barrero M, et al. Efficient and rapid generation of induced

pluripotent stem cells from human keratinocytes. *Nat Biotechnol*. 2008 Nov;26(11):1276–84.

374. Zhang Y, Ouyang H, Lim C, et al. Electrospinning of gelatin fibers and gelatin/PCL composite fibrous scaffolds. *J Biomed Mater Res B Appl Biomater*. 2005 Jan 15;72(1):156–65.

375. Chong E, Phan T, Lim I, et al. Evaluation of electrospun PCL/gelatin nanofibrous scaffold for wound healing and layered dermal reconstitution. *Acta Biomater*. 2007;3(3):321–30.

376. Fee T, Surianarayanan S, Downs C, et al. Nanofiber Alignment Regulates NIH3T3 Cell Orientation and Cytoskeletal Gene Expression on Electrospun PCL+Gelatin Nanofibers. *PLoS One*. 2016 May 1;11(5).

377. Dias J, Baptista-Silva S, Sousa A, et al. Biomechanical performance of hybrid electrospun structures for skin regeneration. *Mater Sci Eng C Mater Biol Appl*. 2018 Dec 1;93:816–27.

378. Pal P, Dadhich P, Srivas PK, et al. Bilayered nanofibrous 3D hierarchy as skin rudiment by emulsion electrospinning for burn wound management. *Biomater Sci*. 2017 Aug 22;5(9):1786–99.

379. Xiao S, Zhao T, Wang J, et al. Gelatin Methacrylate (GelMA)-Based Hydrogels for Cell Transplantation: an Effective Strategy for Tissue Engineering. *Stem cell Rev reports*. 2019 Oct 1;15(5):664–79.

380. Schuurman W, Levett P, Pot M, et al. Gelatin-methacrylamide hydrogels as potential biomaterials for fabrication of tissue-engineered cartilage constructs. *Macromol Biosci*. 2013 May;13(5):551–61.

381. Stratesteffen H, Köpf M, Kreimendahl F, et al. GelMA-collagen blends enable drop-on-demand 3D printablility and promote angiogenesis. *Biofabrication*. 2017 Sep 1;9(4).

382. Lee W, Debasitis JC, Lee VK, et al. Multi-layered culture of human skin fibroblasts and keratinocytes through three-dimensional freeform fabrication. *Biomaterials*. 2009;30(8):1587–95.

383. Wang S, Xiong Y, Chen J, et al. Three Dimensional Printing Bilayer Membrane

Scaffold Promotes Wound Healing. *Front Bioeng Biotechnol*. 2019 Nov 19;0:348.

384. Ozbolat I. Bioprinting scale-up tissue and organ constructs for transplantation. *Trends Biotechnol*. 2015 Jul 1;33(7):395–400.

385. Albanna M, Binder K, Murphy S, et al. In Situ Bioprinting of Autologous Skin Cells Accelerates Wound Healing of Extensive Excisional Full-Thickness Wounds. *Sci Rep*. 2019 Dec 1;9(1).

386. Vijayavenkataraman S, Lu W, Fuh J. 3D bioprinting of skin: a state-of-the-art review on modelling, materials, and processes. *Biofabrication*. 2016 Sep 7;8(3).

387. Moroni L, Boland T, Burdick JA, et al. Biofabrication: A Guide to Technology and Terminology [Internet]. Vol. 36, Trends in Biotechnology. Elsevier Ltd; 2018. p. 384–402.

388. Zheng MH, Willers C, Kirilak L, et al. Matrix-Induced Autologous Chondrocyte Implantation (MACI®): Biological and histological assessment. *Tissue Eng*. 2007 Apr;13(4):737–46.

389. Legendre F, Ollitrault D, Hervieu M, et al. Enhanced hyaline cartilage matrix synthesis in collagen sponge scaffolds by using siRNA to stabilize chondrocytes phenotype cultured with bone morphogenetic protein-2 under hypoxia. *Tissue Eng - Part C Methods*. 2013 Jul 1;19(7):550–67.

390. Willers C, Chen J, Wood D, et al. Autologous chondrocyte implantation with collagen bioscaffold for the treatment of osteochondral defects in rabbits. In: Tissue Engineering. Tissue Eng; 2005. p. 1065–76.

391. Bentley G, Biant LC, Vijayan S, et al. Minimum ten-year results of a prospective randomised study of autologous chondrocyte implantation versus mosaicplasty for symptomatic articular cartilage lesions of the knee. *J Bone Jt Surg - Ser B*. 2012 Apr;94 B(4):504–9.

392. Raghunath J, Rollo J, Sales KM, et al. Biomaterials and scaffold design: key to tissue-engineering cartilage. *Biotechnol Appl Biochem*. 2007 Feb 1;46(2):73.

393. Vinatier C, Guicheux J. Cartilage tissue engineering: From biomaterials and stem cells to osteoarthritis treatments. Vol. 59, Annals of Physical and Rehabilitation

Medicine. Elsevier Masson SAS; 2016. p. 139–44.

394. Derakhshanfar S, Mbeleck R, Xu K, et al. 3D bioprinting for biomedical devices and tissue engineering: A review of recent trends and advances. *Bioact Mater*. 2018 Jun 1;3(2):144–56.

395. Hutmacher DW, Sittinger M, Risbud M V. Scaffold-based tissue engineering: rationale for computer-aided design and solid free-form fabrication systems. *Trends Biotechnol*. 2004 Jul 1;22(7):354–62.

396. Ozler SB, Bakirci E, Kucukgul C, et al. Three-dimensional direct cell bioprinting for tissue engineering. *J Biomed Mater Res Part B Appl Biomater*. 2017 Nov;105(8):2530–44.

397. Zhang YS, Yue K, Aleman J, et al. 3D Bioprinting for Tissue and Organ Fabrication. *Ann Biomed Eng*. 2017;45(1):148–63.

398. Bishop ES, Mostafa S, Pakvasa M, et al. 3-D bioprinting technologies in tissue engineering and regenerative medicine: Current and future trends. *Genes Dis*. 2017 Dec;4(4):185–95.

399. Hölzl K, Lin S, Tytgat L, et al. Bioink properties before, during and after 3D bioprinting. *Biofabrication*. 2016 Sep 23;8(3):032002.

400. Seliktar D. Designing Cell-Compatible Hydrogels for Biomedical Applications. *Science (80-)*. 2012 Jun 1;336(6085):1124–8.

401. Senatov FS, Niaza KV, Zadorozhnyy MY, et al. Mechanical properties and shape memory effect of 3D-printed PLA-based porous scaffolds. *J Mech Behav Biomed Mater*. 2016 Apr;57:139–48.

402. Diomede F, Gugliandolo A, Cardelli P, et al. Three-dimensional printed PLA scaffold and human gingival stem cell-derived extracellular vesicles: a new tool for bone defect repair. *Stem Cell Res Ther*. 2018 Dec 13;9(1):104.

403. Grémare A, Guduric V, Bareille R, et al. Characterization of printed PLA scaffolds for bone tissue engineering. *J Biomed Mater Res Part A*. 2018 Apr;106(4):887–94.

404. Gregor A, Filová E, Novák M, et al. Designing of PLA scaffolds for bone tissue replacement fabricated by ordinary commercial 3D printer. *J Biol Eng*. 2017 Dec

16;11(1):31.

405. Shkarina S, Shkarin R, Weinhardt V, et al. 3D biodegradable scaffolds of polycaprolactone with silicate-containing hydroxyapatite microparticles for bone tissue engineering: high-resolution tomography and in vitro study. *Sci Rep*. 2018 Dec 11;8(1):8907.

406. Su Y, Denbeigh JM, Camilleri ET, et al. Extracellular matrix protein production in human adipose-derived mesenchymal stem cells on three-dimensional polycaprolactone (PCL) scaffolds responds to GDF5 or FGF2. *Gene Reports*. 2018 Mar;10:149–56.

407. Kim J-Y, Ahn G, Kim C, et al. Synergistic Effects of Beta Tri-Calcium Phosphate and Porcine-Derived Decellularized Bone Extracellular Matrix in 3D-Printed Polycaprolactone Scaffold on Bone Regeneration. *Macromol Biosci*. 2018 Jun;18(6):1800025.

408. Dao TT-T, Vu NB, Pham LH, et al. In Vitro Production of Cartilage Tissue from Rabbit Bone Marrow-Derived Mesenchymal Stem Cells and Polycaprolactone Scaffold. In: Advances in experimental medicine and biology. 2017.

409. Park K-S, Kim B-J, Lih E, et al. Versatile effects of magnesium hydroxide nanoparticles in PLGA scaffold–mediated chondrogenesis. *Acta Biomater*. 2018 Jun;73:204–16.

410. Lin S, Cui L, Chen G, et al. PLGA/β-TCP composite scaffold incorporating salvianolic acid B promotes bone fusion by angiogenesis and osteogenesis in a rat spinal fusion model. *Biomaterials*. 2018 Apr 4;

411. Brown JH, Das P, DiVito MD, et al. Nanofibrous PLGA electrospun scaffolds modified with type I collagen influence hepatocyte function and support viability in vitro. *Acta Biomater*. 2018 Jun;73:217–27.

412. Dai Y, Shen T, Ma L, et al. Regeneration of osteochondral defects in vivo by a cell-free cylindrical poly(lactide-co-glycolide) scaffold with a radially oriented microstructure. *J Tissue Eng Regen Med*. 2018 Mar;12(3):e1647–61.

413. Serra T, Mateos-Timoneda MA, Planell JA, et al. 3D printed PLA-based scaffolds: a versatile tool in regenerative medicine. *Organogenesis*. 2013;9(4):239–44.

414. Maggi A, Li H, Greer JR. Three-dimensional nano-architected scaffolds with tunable stiffness for efficient bone tissue growth. *Acta Biomater*. 2017 Nov 1;63:294–305.

415. Serrano MC, Chung EJ, Ameer GA. Advances and Applications of Biodegradable Elastomers in Regenerative Medicine. *Adv Funct Mater*. 2010 Jan 22;20(2):192–208.

416. Jaganathan SK, Mani MP, Supriyanto E. Blood compatibility assessments of electrospun polyurethane nanocomposites blended with megni oil for tissue engineering applications. *An Acad Bras Cienc*. 2019 Jun 19;91(2):e20190018.

417. Ergene E, Yagci BS, Gokyer S, et al. A novel polyurethane-based biodegradable elastomer as a promising material for skeletal muscle tissue engineering. *Biomed Mater*. 2019 Feb 25;14(2):025014.

418. Ma Y, Hu N, Liu J, et al. Three-Dimensional Printing of Biodegradable Piperazine-Based Polyurethane-Urea Scaffolds with Enhanced Osteogenesis for Bone Regeneration. *ACS Appl Mater Interfaces*. 2019 Mar 6;11(9):9415–24.

419. Blaya F, Pedro PS, Pedro ABS, et al. Design of a Functional Splint for Rehabilitation of Achilles Tendon Injury Using Advanced Manufacturing (AM) Techniques. Implementation Study. *J Med Syst*. 2019 May 1;43(5).

420. Caligaris M, Canal CE, Ahmad CS, et al. Investigation of the frictional response of osteoarthritic human tibiofemoral joints and the potential beneficial tribological effect of healthy synovial fluid. *Osteoarthr Cartil*. 2009 Oct;17(10):1327–32.

421. López-Ruiz E, Perán M, Cobo-Molinos J, et al. Chondrocytes extract from patients with osteoarthritis induces chondrogenesis in infrapatellar fat pad-derived stem cells. *Osteoarthr Cartil*. 2013 Jan;21(1):246–58.

422. Baena J, Jiménez G, López-Ruiz E, et al. Volume-by-volume bioprinting of chondrocytes-alginate bioinks in high temperature thermoplastic scaffolds for cartilage regeneration. *Exp Biol Med*. 2019 Jan 10;244(1):13–21.

423. Kang H-W, Yoo JJ, Atala A. Bioprinted Scaffolds for Cartilage Tissue Engineering. In 2015. p. 161–9.

424. Akkineni AR, Ahlfeld T, Lode A, et al. A versatile method for combining different biopolymers in a core/shell fashion by 3D plotting to achieve mechanically robust constructs. *Biofabrication*. 2016 Oct 7;8(4):045001.

425. Penick KJ, Solchaga LA, Berilla JA, et al. Performance of polyoxymethylene plastic (POM) as a component of a tissue engineering bioreactor. *J Biomed Mater Res A*. 2005 Oct 1;75(1):168–74.

426. Burkhardt D, Hwa S-Y, Ghosh P. A novel microassay for the quantitation of the sulfated glycosaminoglycan content of histological sections: its application to determine the effects of Diacerhein on cartilage in an ovine model of osteoarthritis. *Osteoarthr Cartil*. 2001 Apr;9(3):238–47.

427. Donath K, Breuner G. A method for the study of undecalcified bones and teeth with attached soft tissues. The Säge-Schliff (sawing and grinding) technique. *J Oral Pathol*. 1982 Aug;11(4):318–26.

428. Kanca Y, Milner P, Dini D, et al. Tribological properties of PVA/PVP blend hydrogels against articular cartilage. *J Mech Behav Biomed Mater*. 2018 Feb 1;78:36–45.

429. Petrie Aronin CE, Cooper JA, Sefcik LS, et al. Osteogenic differentiation of dura mater stem cells cultured in vitro on three-dimensional porous scaffolds of poly(ε-caprolactone) fabricated via co-extrusion and gas foaming. *Acta Biomater*. 2008 Sep;4(5):1187–97.

430. Kim H-J, Lee J-H, Im G-I. Chondrogenesis using mesenchymal stem cells and PCL scaffolds. *J Biomed Mater Res Part A*. 2009;9999A:NA-NA.

431. Izquierdo R, Garcia-Giralt N, Rodriguez MT, et al. Biodegradable PCL scaffolds with an interconnected spherical pore network for tissue engineering. *J Biomed Mater Res Part A*. 2008 Apr;85A(1):25–35.

432. Li W-JW-J, Tuli R, Okafor C, et al. A three-dimensional nanofibrous scaffold for cartilage tissue engineering using human mesenchymal stem cells. *Biomaterials*. 2005 Feb;26(6):599–609.

433. Wei G, Ma PX. Partially nanofibrous architecture of 3D tissue engineering scaffolds. *Biomaterials*. 2009 Nov;30(32):6426–34.

434. Ghosh S, Laha M, Mondal S, et al. In vitro model of mesenchymal condensation during chondrogenic development. *Biomaterials*. 2009 Nov;30(33):6530–40.

435. Tai H, Mather ML, Howard D, et al. Control of pore size and structure of tissue engineering scaffolds produced by supercritical fluid processing. *Eur Cells Mater*. 2007;14:64–76.

436. Izadifar Z, Chen X, Kulyk W. Strategic Design and Fabrication of Engineered Scaffolds for Articular Cartilage Repair. *J Funct Biomater*. 2012 Nov 14;3(4):799–838.

437. Bacakova L, Filova E, Parizek M, et al. Modulation of cell adhesion, proliferation and differentiation on materials designed for body implants. *Biotechnol Adv*. 2011 Nov;29(6):739–67.

438. Monllau JC, Poggioli F, Erquicia J, et al. Magnetic Resonance Imaging and Functional Outcomes After a Polyurethane Meniscal Scaffold Implantation: Minimum 5-Year Follow-up. *Arthrosc J Arthrosc Relat Surg*. 2018 May;34(5):1621–7.

439. Shafaat S, Mangir N, Regureos SR, et al. Demonstration of improved tissue integration and angiogenesis with an elastic, estradiol releasing polyurethane material designed for use in pelvic floor repair. *Neurourol Urodyn*. 2018 Feb;37(2):716–25.

440. Mangera A, Bullock AJ, Roman S, et al. Comparison of candidate scaffolds for tissue engineering for stress urinary incontinence and pelvic organ prolapse repair. *BJU Int*. 2013 Sep;112(5):674–85.

441. Sharma B, Fermanian S, Gibson M, et al. Human cartilage repair with a photoreactive adhesive-hydrogel composite. *Sci Transl Med*. 2013 Jan 9;5(167):167ra6-167ra6.

442. Kumar A, Biswas K, Basu B. Hydroxyapatite-titanium bulk composites for bone tissue engineering applications. *J Biomed Mater Res Part A*. 2015 Feb;103(2):791–806.

443. Habib FN, Nikzad M, Masood SH, et al. Design and Development of Scaffolds for Tissue Engineering Using Three-Dimensional Printing for Bio-Based Applications. *3D Print Addit Manuf*. 2016 Jun 20;3(2):119–27.

444. Theodoridis K, Aggelidou E, Vavilis T, et al. Hyaline cartilage next generation implants from adipose-tissue-derived mesenchymal stem cells: Comparative study on 3D-printed polycaprolactone scaffold patterns. *J Tissue Eng Regen Med*. 2019 Feb 1;13(2):342–55.

445. Stojanović B, Bauer C, Stotter C, et al. Tribocorrosion of a CoCrMo alloy sliding against articular cartilage and the impact of metal ion release on chondrocytes. *Acta Biomater*. 2019 Jun 18;

446. Patel A, Gaharwar AK, Iviglia G, et al. Highly elastomeric poly(glycerol sebacate)-co-poly(ethylene glycol) amphiphilic block copolymers. *Biomaterials*. 2013 May;34(16):3970–83.

447. Liu J, Zheng H, Poh P, et al. Hydrogels for Engineering of Perfusable Vascular Networks. *Int J Mol Sci*. 2015 Jul 14;16(7):15997–6016.

448. Tatman PD, Gerull W, Sweeney-Easter S, et al. Multiscale Biofabrication of Articular Cartilage: Bioinspired and Biomimetic Approaches [Internet]. Vol. 21, Tissue Engineering - Part B: Reviews. Mary Ann Liebert Inc.; 2015. p. 543–59.

449. Little CJ, Bawolin NK, Chen X. Mechanical properties of natural cartilage and tissue-engineered constructs. *Tissue Eng - Part B Rev*. 2011 Aug 1;17(4):213–27.

450. Fedorovich NE, De Wijn JR, Verbout AJ, et al. Three-Dimensional Fiber Deposition of Cell-Laden, Viable, Patterned Constructs for Bone Tissue Printing. *Tissue Eng Part A*. 2008 Jan;14(1):127–33.

451. Cohen DL, Malone E, Lipson H, et al. Direct freeform fabrication of seeded hydrogels in arbitrary geometries. *Tissue Eng*. 2006;12.

452. Zdrahala RJ, Zdrahala IJ. Biomedical Applications of Polyurethanes: A Review of Past Promises, Present Realities, and a Vibrant Future. *J Biomater Appl*. 1999 Jul;14(1):67–90.

453. Kiradzhiyska DD, Mantcheva RD. Overview of Biocompatible Materials and Their Use in Medicine. *Folia Med (Plovdiv)*. 2019 Mar 1;61(1):34–40.

454. Rashad A, Mohamed-Ahmed S, Ojansivu M, et al. Coating 3D Printed Polycaprolactone Scaffolds with Nanocellulose Promotes Growth and Differentiation of Mesenchymal Stem Cells. *Biomacromolecules*. 2018 Nov

12;19(11):4307–19.

455. Fraser A, Fearon U, Billinghurst RC, et al. Turnover of type II collagen and aggrecan in cartilage matrix at the onset of inflammatory arthritis in humans: Relationship to mediators of systemic and local inflammation. *Arthritis Rheum*. 2003 Nov 1;48(11):3085–95.

456. Lefebvre V, Huang W, Harley VR, et al. SOX9 is a potent activator of the chondrocyte-specific enhancer of the pro alpha1(II) collagen gene. *Mol Cell Biol*. 1997 Apr;17(4):2336–46.

457. Goldwasser M, Astley T, van der Rest M, et al. Analysis of the type of collagen present in osteoarthritic human cartilage. *Clin Orthop Relat Res*. 1982 Jul;(167):296–302.

458. Singh P, Schwarzbauer JE. Fibronectin and stem cell differentiation - lessons from chondrogenesis. *J Cell Sci*. 2012 Aug 15;125(16):3703–12.

459. Jiménez G, Venkateswaran S, López-Ruiz E, et al. A soft 3D polyacrylate hydrogel recapitulates the cartilage niche and allows growth-factor free tissue engineering of human articular cartilage. *Acta Biomater*. 2019 May;90:146–56.

460. Feng B, Ji T, Wang X, et al. Engineering cartilage tissue based on cartilage-derived extracellular matrix cECM/PCL hybrid nanofibrous scaffold. *Mater Des*. 2020 Aug 1;193:108773.

461. Kanitakis J. Anatomy, histology and immunohistochemistry of normal human skin. *Eur J Dermatology*. 2002;12(4):390–401.

462. Kolarsick, P. A. J.; Kolarsick MA. Anatomy and Physiology of the Skin | Article | NursingCenter [Internet]. Journal of the Dermatology Nurses' Association. 2011. p. 203–13.

463. Sontheimer RD. Skin is not the largest organ. Vol. 134, Journal of Investigative Dermatology. Nature Publishing Group; 2014. p. 581–2.

464. Maver T, Maver U, Kleinschek KS, et al. Advanced therapies of skin injuries. Vol. 127, Wiener Klinische Wochenschrift. Springer-Verlag Wien; 2015. p. 187–98.

465. Danby SG. Biological Variation in Skin Barrier Function: From A (Atopic

Dermatitis) to X (Xerosis). In: Current Problems in Dermatology (Switzerland). S. Karger AG; 2016. p. 47–60.

466. Zanger P. Staphylococcus aureus positive skin infections and international travel. Vol. 122, Wiener Klinische Wochenschrift. 2010. p. 31–3.

467. Chua AWC, Khoo YC, Tan BK, et al. Skin tissue engineering advances in severe burns: review and therapeutic applications. *Burn Trauma*. 2016 Dec 1;4.

468. Vig K, Chaudhari A, Tripathi S, et al. Advances in skin regeneration using tissue engineering. *Int J Mol Sci*. 2017;

469. Peck MD. Epidemiology of burns throughout the world. Part I: Distribution and risk factors. *Burns*. 2011 Nov 29;37(7):1087–100.

470. Vrana NE, Lavalle P, Dokmeci MR, et al. Engineering functional epithelium for regenerative medicine and in vitro organ models: A review. Vol. 19, Tissue Engineering - Part B: Reviews. 2013. p. 529–43.

471. Santema TB, Poyck PPC, Ubbink DT. Skin grafting and tissue replacement for treating foot ulcers in people with diabetes. Vol. 2016, Cochrane Database of Systematic Reviews. John Wiley and Sons Ltd; 2016.

472. Kamoun EA, Kenawy ERS, Chen X. A review on polymeric hydrogel membranes for wound dressing applications: PVA-based hydrogel dressings [Internet]. Vol. 8, Journal of Advanced Research. Elsevier B.V.; 2017. p. 217–33.

473. Sood A, Granick MS, Tomaselli NL. Wound Dressings and Comparative Effectiveness Data. *Adv Wound Care*. 2014 Aug;3(8):511–29.

474. Cabodi M, Choi NW, Gleghorn JP, et al. A microfluidic biomaterial. *J Am Chem Soc*. 2005 Oct 12;127(40):13788–9.

475. He PL. Call for Special Issue Papers: Tissue Engineering: Part A—Special Issue on Hydrogels and Injectable Systems. *Tissue Eng Part C Methods*. 2020 May 1;26(5):241–241.

476. Alberts B., Johnson A., Lewis J., Raff M. RK. Molecular Biology of The Cell. Garland Science. New York, NY, USA; 2002.

477. Parenteau-Bareil R, Gauvin R, Berthod F. Collagen-based biomaterials for tissue engineering applications. *Materials (Basel)*. 2010;3(3):1863–87.

478. Lee V, Singh G, Trasatti JP, et al. Design and fabrication of human skin by three-dimensional bioprinting. *Tissue Eng Part C Methods*. 2014;20(6):473–84.

479. Köpf M, Campos DF, Blaeser A, Sen KS FH. A tailored three-dimensionally printable agarose-collagen blend allows encapsulation, spreading, and attachment of human umbilical artery smooth mu... - PubMed - NCBI [Internet]. Biofabrication. 2016. p. 025011.

480. Geiger B, Yamada KM. Molecular architecture and function of matrix adhesions. *Cold Spring Harb Perspect Biol*. 2011;3(5):1–21.

481. Norouzi M, Boroujeni SM, Omidvarkordshouli N, et al. Advances in Skin Regeneration: Application of Electrospun Scaffolds. Vol. 4, Advanced Healthcare Materials. Wiley-VCH Verlag; 2015. p. 1114–33.

482. Tu Y, Mithieux SM, Annabi N, et al. Synthetic elastin hydrogels that are coblended with heparin display substantial swelling, increased porosity, and improved cell penetration. *J Biomed Mater Res Part A*. 2010 Dec 15;95A(4):1215–22.

483. Wang ST, Neo BH, Betts RJ. Glycosaminoglycans: Sweet as Sugar Targets for Topical Skin Anti-Aging . *Clin Cosmet Investig Dermatol*. 2021 Sep 14;14:1227–46.

484. Lapčík L, Lapčík L, De Smedt S, et al. Hyaluronan: Preparation, structure, properties, and applications. *Chem Rev*. 1998;98(8).

485. Teh BM, Shen Y, Friedland PL, et al. A review on the use of hyaluronic acid in tympanic membrane wound healing. Vol. 12, Expert Opinion on Biological Therapy. Expert Opin Biol Ther; 2012. p. 23–36.

486. Turley E, Harrison R. RHAMM, a member of the hyaladherins [Internet]. Glycoforum. 1999. p. Vol.3, A3.

487. Penc SF, Pomahac B, Winkler T, et al. Dermatan sulfate released after injury is a potent promoter of fibroblast growth factor-2 function. *J Biol Chem*. 1998 Oct 23;273(43):28116–21.

488. Lee PHA, Trowbridge JM, Taylor KR, et al. Dermatan sulfate proteoglycan and glycosaminoglycan synthesis is induced in fibroblasts by transfer to a three-

dimensional extracellular environment. *J Biol Chem*. 2004 Nov 19;279(47):48640–6.

489. Silva R, Singh R, Sarker B, et al. Hydrogel matrices based on elastin and alginate for tissue engineering applications. *Int J Biol Macromol*. 2018 Jul 15;114:614–25.

490. González-Andrades M, Garzón I, Gascón MI, et al. Sequential development of intercellular junctions in bioengineered human corneas. *J Tissue Eng Regen Med*. 2009;3(6):442–9.

491. Dellambra E, Dimri GP. Cellular Senescence and Skin Aging. *Ski Aging Handb*. 2009 Jan 1;129–48.

492. Ullah M, Liu DD, Thakor AS. Mesenchymal Stromal Cell Homing: Mechanisms and Strategies for Improvement. Vol. 15, iScience. Elsevier Inc.; 2019. p. 421–38.

493. Jimenez-Puerta GJ, Marchal JA, López-Ruiz E, et al. Role of Mesenchymal Stromal Cells as Therapeutic Agents: Potential Mechanisms of Action and Implications in Their Clinical Use. *J Clin Med*. 2020 Feb 6;9(2):445.

494. López-Ruiz E, Jiménez G, Kwiatkowski W, et al. Impact of TGF-β family-related growth factors on chondrogenic differentiation of adipose-derived stem cells isolated from lipoaspirates and infrapatellar fat pads of osteoarthritic patients. *Eur Cells Mater*. 2018 Jan 1;35:209–24.

495. Gálvez-Martín P, Hmadcha A, Soria B, et al. Study of the stability of packaging and storage conditions of human mesenchymal stem cell for intra-arterial clinical application in patient with critical limb ischemia. *Eur J Pharm Biopharm*. 2014;86(3):459–68.

496. Schindelin J, Arganda-Carreras I, Frise E, et al. Fiji: An open-source platform for biological-image analysis. Vol. 9, Nature Methods. 2012. p. 676–82.

497. A-Rang Im, Jee Young Kim, Hyun-Seok Kim, Seonho Cho, Youmie Park YSK. Wound Healing and Antibacterial Activities of Chondroitin Sulfate- And Acharan Sulfate-Reduced Silver Nanoparticles - PubMed [Internet]. Nanotechnology. 2013.

498. Soriano-Ruiz JL, Gálvez-Martín P, López-Ruiz E, et al. Design and evaluation of mesenchymal stem cells seeded chitosan/glycosaminoglycans quaternary hydrogel scaffolds for wound healing applications. *Int J Pharm*. 2019 Oct 30;570.

499. Fronza M, Heinzmann B, Hamburger M, et al. Determination of the wound healing effect of Calendula extracts using the scratch assay with 3T3 fibroblasts. *J Ethnopharmacol*. 2009 Dec 10;126(3):463–7.

500. Rivera-Tarazona LK, Bhat VD, Kim H, et al. Shape-morphing living composites. *Sci Adv*. 2020 Jan 17;6(3):eaax8582.

501. Guadix JA, López-Beas J, Clares B, et al. Principal criteria for evaluating the quality, safety and efficacy of hMSC-based products in clinical practice: Current approaches and challenges. Vol. 11, Pharmaceutics. MDPI AG; 2019.

502. Wang Z, Han L, Sun T, et al. Extracellular matrix derived from allogenic decellularized bone marrow mesenchymal stem cell sheets for the reconstruction of osteochondral defects in rabbits. *Acta Biomater*. 2020 Oct;

503. Erben A, Hörning M, Hartmann B, et al. Precision 3D-Printed Cell Scaffolds Mimicking Native Tissue Composition and Mechanics. *Adv Healthc Mater*. 2020;

504. Ozpinar EW, Frey AL, Arthur GK, et al. Dermal Extracellular Matrix-Derived Hydrogels as an In Vitro Substrate to Study Mast Cell Maturation. *Tissue Eng Part A*. 2020 Oct 1;

505. Arnette C, Koetsier JL, Hoover P, et al. In Vitro Model of the Epidermis: Connecting Protein Function to 3D Structure. In: Methods in Enzymology. Academic Press Inc.; 2016. p. 287–308.

506. Oryan A, Alemzadeh E, Mohammadi AA, et al. Healing potential of injectable Aloe vera hydrogel loaded by adipose-derived stem cell in skin tissue-engineering in a rat burn wound model. *Cell Tissue Res*. 2019 Aug 14;377(2):215–27.

507. Lotz C, Schmid FF, Oechsle E, et al. Cross-linked Collagen Hydrogel Matrix Resisting Contraction to Facilitate Full-Thickness Skin Equivalents. *ACS Appl Mater Interfaces*. 2017 Jun 21;9(24):20417–25.

508. Malda J, Visser J, Melchels FP, et al. 25th anniversary article: Engineering hydrogels for biofabrication. Vol. 25, Advanced Materials. Adv Mater; 2013. p. 5011–28.

509. Boraschi-Diaz I, Wang J, Mort JS, et al. Collagen type i as a ligand for receptor-mediated signaling. Vol. 5, Frontiers in Physics. Frontiers Media S.A.; 2017. p. 12.

510. Smith MM, Melrose J. Proteoglycans in Normal and Healing Skin. *Adv Wound Care*. 2015 Mar;4(3):152–73.

511. Papakonstantinou E, Roth M, Karakiulakis G. Hyaluronic acid: A key molecule in skin aging [Internet]. Vol. 4, Dermato-Endocrinology. Landes Bioscience; 2012. p. 253.

512. Cole MA, Quan T, Voorhees JJ, et al. Extracellular matrix regulation of fibroblast function: redefining our perspective on skin aging [Internet]. Vol. 12, Journal of Cell Communication and Signaling. Springer Netherlands; 2018. p. 35–43.

513. Trowbridge JM, Rudisill JA, Ron D, et al. Dermatan sulfate binds and potentiates activity of keratinocyte growth factor (FGF-7). *J Biol Chem*. 2002 Nov 8;277(45):42815–20.

514. Zhao JY, Chai JK, Song HF, et al. Influence of hyaluronic acid on wound healing using composite porcine acellular dermal matrix grafts and autologous skin in rabbits. *Int Wound J*. 2013 Oct;10(5):562–72.

515. Duca L, Floquet N, Alix AJP, et al. Elastin as a matrikine. Vol. 49, Critical Reviews in Oncology/Hematology. Elsevier Ireland Ltd; 2004. p. 235–44.

516. Almine JF, Wise SG, Weiss AS. Elastin signaling in wound repair. *Birth Defects Res Part C Embryo Today Rev*. 2012 Sep 1;96(3):248–57.

517. Moore AL, Marshall CD, Barnes LA, et al. Scarless wound healing: Transitioning from fetal research to regenerative healing [Internet]. Vol. 7, Wiley Interdisciplinary Reviews: Developmental Biology. John Wiley and Sons Inc.; 2018.

518. Van Tomme SR, Storm G, Hennink WE. In situ gelling hydrogels for

pharmaceutical and biomedical applications. Vol. 355, International Journal of Pharmaceutics. Elsevier; 2008. p. 1–18.

519. Yang X, Liu G, Peng L, et al. Highly Efficient Self-Healable and Dual Responsive Cellulose-Based Hydrogels for Controlled Release and 3D Cell Culture. *Adv Funct Mater*. 2017 Oct 26;27(40).

520. Ciszek A. Variability of skin pH after the use of different collagen gels. *J Cosmet Dermatol*. 2017 Dec 1;16(4):531–6.

521. Campos DFD, Blaeser A, Korsten A, et al. The stiffness and structure of three-dimensional printed hydrogels direct the differentiation of mesenchymal stromal cells toward adipogenic and osteogenic lineages. *Tissue Eng - Part A*. 2015 Feb 1;21(3–4):740–56.

522. Loh QL, Choong C. Three-dimensional scaffolds for tissue engineering applications: Role of porosity and pore size [Internet]. Vol. 19, Tissue Engineering - Part B: Reviews. Mary Ann Liebert, Inc.; 2013. p. 485–502.

523. Gao Y, Kong W, Li B, et al. Fabrication and characterization of collagen-based injectable and self-crosslinkable hydrogels for cell encapsulation. *Colloids Surfaces B Biointerfaces*. 2018 Jul 1;167:448–56.

524. Bhattarai N, Gunn J, Zhang M. Chitosan-based hydrogels for controlled, localized drug delivery. Vol. 62, Advanced Drug Delivery Reviews. Adv Drug Deliv Rev; 2010. p. 83–99.

525. Tan YJ, Tan X, Yeong WY, et al. Hybrid microscaffold-based 3D bioprinting of multi-cellular constructs with high compressive strength: A new biofabrication strategy. *Sci Rep*. 2016 Dec 14;6.

526. Drury JL, Mooney DJ. Hydrogels for tissue engineering: Scaffold design variables and applications. Vol. 24, Biomaterials. Elsevier BV; 2003. p. 4337–51.

527. Ceccaldi C, Assaad E, Hui E, et al. Optimization of Injectable Thermosensitive Scaffolds with Enhanced Mechanical Properties for Cell Therapy. *Macromol Biosci*. 2017 Jun 1;17(6).

528. Buckley CT, Thorpe SD, O'Brien FJ, et al. The effect of concentration, thermal history and cell seeding density on the initial mechanical properties of agarose

hydrogels. *J Mech Behav Biomed Mater*. 2009 Oct 1;2(5):512–21.

529. Kalra A, Lowe A, Am A-J. Mechanical Behaviour of Skin: A Review. *J Mater Sci Eng*. 2016;5:4.

530. Almeida N, Mueller A, Hirschi S, et al. Rheological studies of polysaccharides for skin scaffolds. *J Biomed Mater Res Part A*. 2014 May 1;102(5):1510–7.

531. Martínez-Ruvalcaba A, Chornet E, Rodrigue D. Viscoelastic properties of dispersed chitosan/xanthan hydrogels. *Carbohydr Polym*. 2007 Feb 19;67(4):586–95.

532. Ross-Murphy SB, Shatwell KP. Polysaccharide strong and weak gels. *Biorheology*. 1993;30(3–4):217–27.

533. Stone RC, Pastar I, Ojeh N, et al. Epithelial-Mesenchymal Transition in Tissue Repair and Fibrosis. *Cell Tissue Res*. 2016 Sep 1;365(3):495.

534. Volk SW, Iqbal SA, Bayat A. Interactions of the Extracellular Matrix and Progenitor Cells in Cutaneous Wound Healing. *Adv Wound Care*. 2013 Jul;2(6):261.

535. Jiang LW, Chen H, Lu H. Using human epithelial amnion cells in human de-epidermized dermis for skin regeneration. *J Dermatol Sci*. 2016 Jan 1;81(1):26–34.

536. Mahmood R, Choudhery MS, Mehmood A, Khan SN RS. In Vitro Differentiation Potential of Human Placenta Derived Cells Into Skin Cells - PubMed [Internet]. Stem Cells International. 2015.

537. Mehanni SS, Ibrahim NF, Hassan AR, et al. New approach of bone marrow-derived mesenchymal stem cells and human amniotic epithelial cells applications in accelerating wound healing of irradiated albino rats. *Int J Stem Cells*. 2013;6(1):45–54.

538. Baraniak PR, McDevitt TC. Stem cell paracrine actions and tissue regeneration. Vol. 5, Regenerative Medicine. NIH Public Access; 2010. p. 121–43.

539. Liang X, Ding Y, Zhang Y, et al. Paracrine mechanisms of mesenchymal stem cell-based therapy: Current status and perspectives. Vol. 23, Cell Transplantation. Cognizant Communication Corporation; 2014. p. 1045–59.

540. Yates CC, Rodrigues M, Nuschke A, et al. Multipotent stromal cells/mesenchymal stem cells and fibroblasts combine to minimize skin hypertrophic scarring. *Stem Cell Res Ther*. 2017 Sep 5;8(1):193.

541. Kirker KR, Luo Y, Nielson JH, et al. Glycosaminoglycan hydrogel films as bio-interactive dressings for wound healing. *Biomaterials*. 2002;23(17):3661–71.

542. Ravi S, Caves JM, Martinez AW, et al. Incorporation of fibronectin to enhance cytocompatibility in multilayer elastin-like protein scaffolds for tissue engineering. *J Biomed Mater Res - Part A*. 2013 Jul;101 A(7):1915–25.

543. Tracy LE, Minasian RA, Caterson EJ. Extracellular Matrix and Dermal Fibroblast Function in the Healing Wound [Internet]. Vol. 5, Advances in Wound Care. Mary Ann Liebert Inc.; 2016. p. 119–36.

544. Rasmussen C, Gratz K, Liebel F, et al. The StrataTest® human skin model, a consistent in vitro alternative for toxicological testing. *Toxicol Vitr*. 2010 Oct 1;24(7):2021–9.

545. Kubilus J, Hayden PJ, Ayehunie S, et al. Full thickness epiderm^{TM}: A dermal-epidermal skin model to study epithelial-mesenchymal interactions. *ATLA Altern to Lab Anim*. 2004 Apr 9;32(SUPPL. 1A):75–82.

546. Baroni A, Buommino E, De Gregorio V, et al. Structure and function of the epidermis related to barrier properties. *Clin Dermatol*. 2012 May;30(3):257–62.

547. Boer M, Duchnik E, Maleszka R, et al. Structural and biophysical characteristics of human skin in maintaining proper epidermal barrier function. *Adv Dermatology Allergol Dermatologii i Alergol*. 2016 Feb 1;33(1):1.

548. Kligman AM. What is the 'true' function of skin? *Exp Dermatol*. 2002 Apr;11(2):159.

549. Dai C, Shih S, Khachemoune A. Skin substitutes for acute and chronic wound healing: an updated review. *J Dermatolog Treat*. 2020 Aug 17;31(6):639–48.

550. Lee V, Singh G, Trasatti JP, et al. Design and fabrication of human skin by three-dimensional bioprinting. *Tissue Eng - Part C Methods*. 2014 Jun 1;20(6):473–84.

551. Chen K, Ying Q, Hao X, et al. Elastic and Stretchable Double Network Hydrogel as Printable Ink for High-Resolution Fabrication of Ionic Skin. *Int J bioprinting*.

2021;7(3):377.

552. Jin R, Cui Y, Chen H, et al. Three-dimensional bioprinting of a full-thickness functional skin model using acellular dermal matrix and gelatin methacrylamide bioink. *Acta Biomater*. 2021 Jul 12;

553. Liu Y, Huang J, Xu Z, et al. Fabrication of gelatin-based printable inks with improved stiffness as well as antibacterial and UV-shielding properties. *Int J Biol Macromol*. 2021 Sep 1;186:396–404.

554. Patel J, Willis J, Aluri A, et al. Three-Dimensionally Printed Skin Substitute Using Human Dermal Fibroblasts and Human Epidermal Keratinocytes. *Ann Plast Surg*. 2021 Jun 1;86(6S Suppl 5):S628–31.

555. Ledford B, Barron C, Van Dyke M, et al. Keratose hydrogel for tissue regeneration and drug delivery. *Semin Cell Dev Biol*. 2021 Jul 2;

556. Hill P, Brantley H, Van Dyke M. Some properties of keratin biomaterials: Kerateines. *Biomaterials*. 2010 Feb 1;31(4):585–93.

557. Holleran WM, Takagi Y, Uchida Y. Epidermal sphingolipids: Metabolism, function, and roles in skin disorders. *FEBS Lett*. 2006 Oct 9;580(23):5456–66.

558. Greene J, Sidle D. The Hyaluronic Acid Fillers: Current Understanding of the Tissue Device Interface. *Facial Plast Surg Clin North Am*. 2015 Nov 1;23(4):423–32.

559. Leite M, Frade M. Efficacy of 0.2% hyaluronic acid in the healing of skin abrasions in rats. *Heliyon*. 2021 Jul 1;7(7).

560. AM J, DG M, A S, et al. Advantages of Hyaluronic Acid and Its Combination with Other Bioactive Ingredients in Cosmeceuticals. *Molecules*. 2021 Jul 22;26(15):4429.

561. Pardue EL, Ibrahim S, Ramamurthi A. Role of hyaluronan in angiogenesis and its utility to angiogenic tissue engineering. *Organogenesis*. 2008;4(4):203.

562. Rodriguez-Cabello J, Gonzalez De Torre I, Gonzalez De Torre M, et al. Fibrous Scaffolds From Elastin-Based Materials. *Front Bioeng Biotechnol*. 2021 Jul 16;9.

563. Stojic M, Ródenas-Rochina J, López-Donaire M, et al. Elastin-Plasma Hybrid Hydrogels for Skin Tissue Engineering. *Polymers (Basel)*. 2021 Jul 1;13(13).

564. Baumann L, Bernstein E, Weiss A, et al. Clinical Relevance of Elastin in the Structure and Function of Skin. *Aesthetic Surg journal Open forum*. 2021 Sep 1;3(3).

565. Riedl J, Popp C, Eide C, et al. Mesenchymal stromal cells in wound healing applications: role of the secretome, targeted delivery and impact on recessive dystrophic epidermolysis bullosa treatment. *Cytotherapy*. 2021 Aug;

566. Brown RA, Wiseman M, Chuo C-B, et al. Ultrarapid Engineering of Biomimetic Materials and Tissues: Fabrication of Nano- and Microstructures by Plastic Compression. *Adv Funct Mater*. 2005 Nov 1;15(11):1762–70.

567. Scionti G, Moral M, Toledano M, et al. Effect of the hydration on the biomechanical properties in a fibrin-agarose tissue-like model. *J Biomed Mater Res A*. 2014;102(8):2573–82.

568. Chocarro-Wrona C, Vicente J de, Antich C, et al. Validation of the 1,4-butanediol thermoplastic polyurethane as a novel material for 3D bioprinting applications. *Bioeng Transl Med*. 2021 Jan 1;6(1):e10192.

569. Kellar R, Diller R, Tabor A, et al. Improved Wound Closure Rates and Mechanical Properties Resembling Native Skin in Murine Diabetic Wounds Treated with a Tropoelastin and Collagen Wound Healing Device. *J Diabetes Clin Res*. 2020 Dec 31;2(3).

570. Draaijers L, Tempelman F, Botman Y, et al. The patient and observer scar assessment scale: a reliable and feasible tool for scar evaluation. *Plast Reconstr Surg*. 2004 Jun;113(7):1960–5.

571. van de Kar A, Corion L, Smeulders M, et al. Reliable and feasible evaluation of linear scars by the Patient and Observer Scar Assessment Scale. *Plast Reconstr Surg*. 2005 Aug;116(2):514–22.

572. Brohem C, da Silva Cardeal L, Tiago M, et al. Artificial skin in perspective: concepts and applications. *Pigment Cell Melanoma Res*. 2011 Feb 1;24(1):35–50.

573. Schmidt FF, Nowakowski S, Kluger PJ. Improvement of a Three-Layered in vitro Skin Model for Topical Application of Irritating Substances. *Front Bioeng Biotechnol*. 2020 May 8;0:388.

574. Zimoch J, Zielinska D, Michalak-Micka K, et al. Bio-engineering a prevascularized human tri-layered skin substitute containing a hypodermis. *Acta Biomater*. 2021 Oct 15;134:215–27.

575. Keck M, Gugerell A, Kober J. Engineering a Multilayered Skin Substitute with Keratinocytes, Fibroblasts, Adipose-Derived Stem Cells, and Adipocytes. *Methods Mol Biol*. 2019;1993:149–57.

576. Choi WS, Kim JH, Ahn CB, et al. Development of a Multi-Layer Skin Substitute Using Human Hair Keratinic Extract-Based Hybrid 3D Printing. *Polym 2021, Vol 13, Page 2584*. 2021 Aug 4;13(16):2584.

577. Rahimnejad M, Labonté-Dupuis T, Demarquette NR, et al. A rheological approach to assess the printability of thermosensitive chitosan-based biomaterial inks. *Biomed Mater*. 2020 Nov 26;16(1):015003.

578. Ceccaldi C, Assaad E, Hui E, et al. Optimization of Injectable Thermosensitive Scaffolds with Enhanced Mechanical Properties for Cell Therapy. *Macromol Biosci*. 2017 Jun 1;17(6).

579. Mancha Sánchez E, Gómez-Blanco JC, López Nieto E, et al. Hydrogels for Bioprinting: A Systematic Review of Hydrogels Synthesis, Bioprinting Parameters, and Bioprinted Structures Behavior. *Front Bioeng Biotechnol*. 2020 Aug 6;0:776.

580. Egea-Guerrero JJ, Carmona G, Correa E, et al. Transplant of Tissue-Engineered Artificial Autologous Human Skin in Andalusia: An Example of Coordination and Institutional Collaboration. *Transplant Proc*. 2019 Nov 1;51(9):3047–50.

581. Adzick NS. The Molecular and Cellular Biology of Wound Repair, 2nd Edition. *Ann Surg*. 1997;225(2):236.

582. Chandrasoma P, Taylor C. Chapter 6. Healing & Repair | Concise Pathology, 3e | AccessPhysiotherapy | McGraw Hill Medical [Internet].

583. Tsuruta D, Green KJ, Getsios S, et al. The barrier function of skin: how to keep a tight lid on water loss. *Trends Cell Biol*. 2002 Aug 1;12(8):355–7.

584. Akdeniz M, Gabriel S, Lichterfeld-Kottner A, et al. Transepidermal water loss in healthy adults: a systematic review and meta-analysis update. *Br J Dermatol*.

2018 Nov 1;179(5):1049–55.

585. Busch K, Aliu A, Walezko N, et al. Medical Needling: Effect on Moisture and Transepidermal Water Loss of Mature Hypertrophic Burn Scars. *Cureus*. 2018 Mar 26;10(3).

586. Maroto-Morales D, Montero-Vilchez T, Arias-Santiago S. Study of Skin Barrier Function in Psoriasis: The Impact of Emollients. *Life*. 2021 Jul 4;11(7):651.

587. Hauck S, Zager P, Halfter N, et al. Collagen/hyaluronan based hydrogels releasing sulfated hyaluronan improve dermal wound healing in diabetic mice via reducing inflammatory macrophage activity. *Bioact Mater*. 2021 Dec 1;6(12):4342–59.

588. Valachová K, Šoltés L. Hyaluronan as a Prominent Biomolecule with Numerous Applications in Medicine. *Int J Mol Sci*. 2021 Jul 1;22(13).

589. Brenner M, Hearing VJ. The Protective Role of Melanin Against UV Damage in Human Skin. *Photochem Photobiol*. 2008 May;84(3):539.

590. Chadwick S, Heath R, Shah M. Abnormal pigmentation within cutaneous scars: A complication of wound healing. *Indian J Plast Surg*. 2012 May;45(2):403.

591. Tsukada S. The melanocytes and melanin in human skin autografts. *Plast Reconstr Surg*. 1974;53(2):200–7.

592. Cerqueira MT, Pirraco RP, Martins AR, et al. Cell sheet technology-driven re-epithelialization and neovascularization of skin wounds. *Acta Biomater*. 2014 Jul 1;10(7):3145–55.

593. Kallioinen M, Koivukangas V, Järvinen M, et al. Expression of cytokeratins in regenerating human epidermis. *Br J Dermatol*. 1995 Dec 1;133(6):830–5.

594. Patten J, Wang K. Fibronectin in development and wound healing. *Adv Drug Deliv Rev*. 2021 Mar 1;170:353–68.

595. Zhang Y, Li D, Fang S, et al. Stimulatory effect of engineered three-layer adipose tissue-derived stem cells sheet in atelocollagen matrix on wound healing in a mouse model of radiation-induced skin injury. *J Biomater Appl*. 2019;34(4):498–508.

596. Huber B, Link A, Linke K, et al. Integration of Mature Adipocytes to Build-Up a

Functional Three-Layered Full-Skin Equivalent. *Tissue Eng Part C Methods*. 2016;22(8):756–64.

597. Kober J, Gugerell A, Schmid M, et al. Generation of a Fibrin Based Three-Layered Skin Substitute. *Biomed Res Int*. 2015;2015.

10. ANNEXES

10.1. Supplementary data

Figure S1. Cell viability of AC_{low} and AC hydrogel formulations. (A) Confocal images of hDFs-loaded hydrogels at 7 and 14 days. Calcein (green fluorescence) stains live cells, while EthD-1 (red fluorescence) stains dead cells. Scale bar = 500µm. (B) Cell viability (%) in the hydrogel scaffolds after 7 and 14 days. Two-tailed Student T test analysis were performed for AC_{low} and AC samples at a significance level of: *P < 0.05.

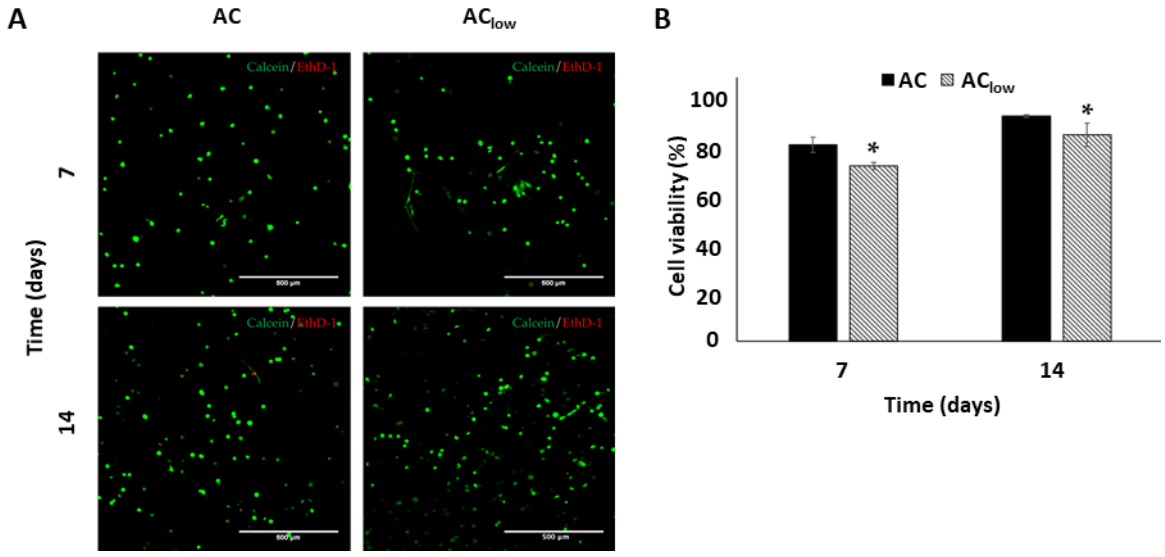

Figure S2. Range of strain analysed for the Young moduli obtained in cell-free and cell-laden AC and ACDHE hydrogels, and human skin samples.

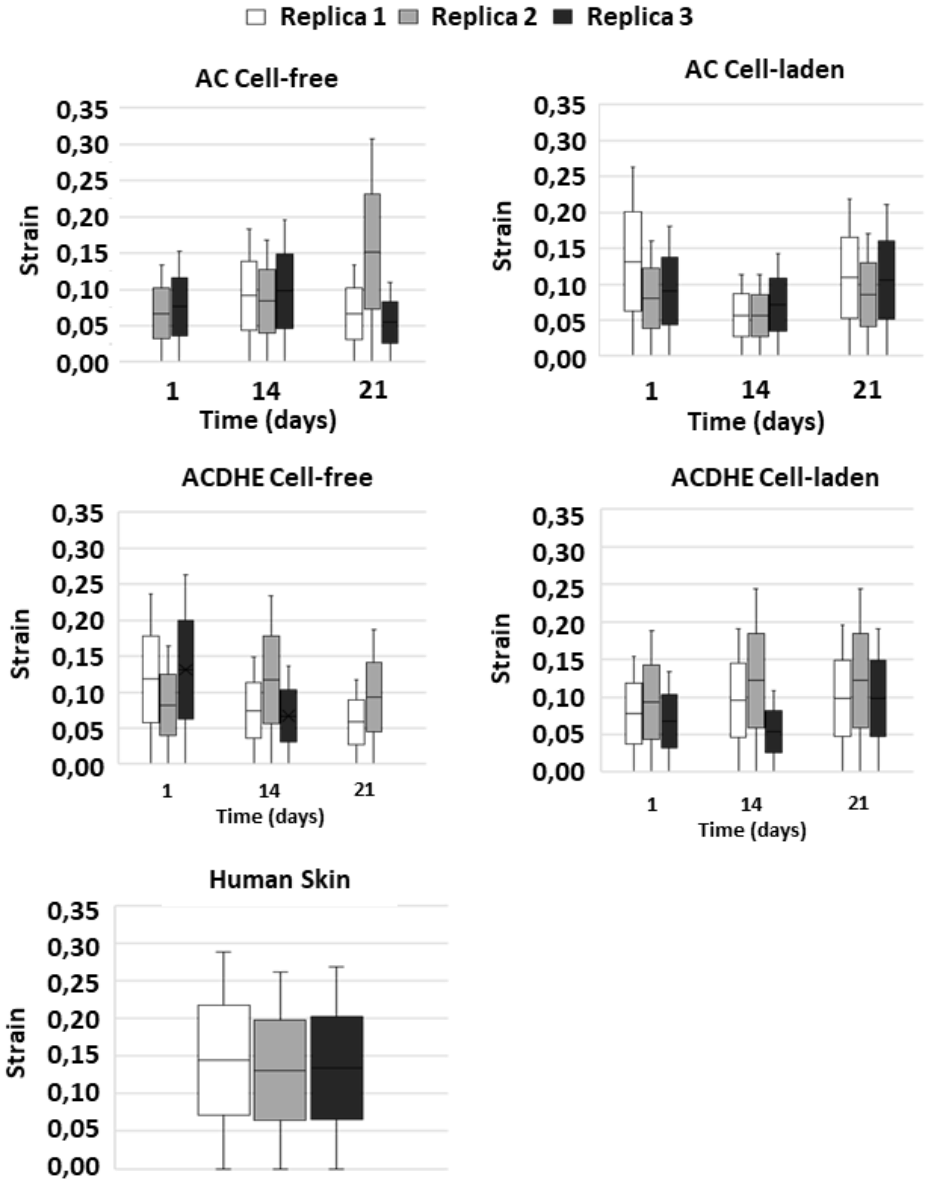

Figure S3. TPUe splint design and surgical protocol for the *in vivo* assay wound excision model.

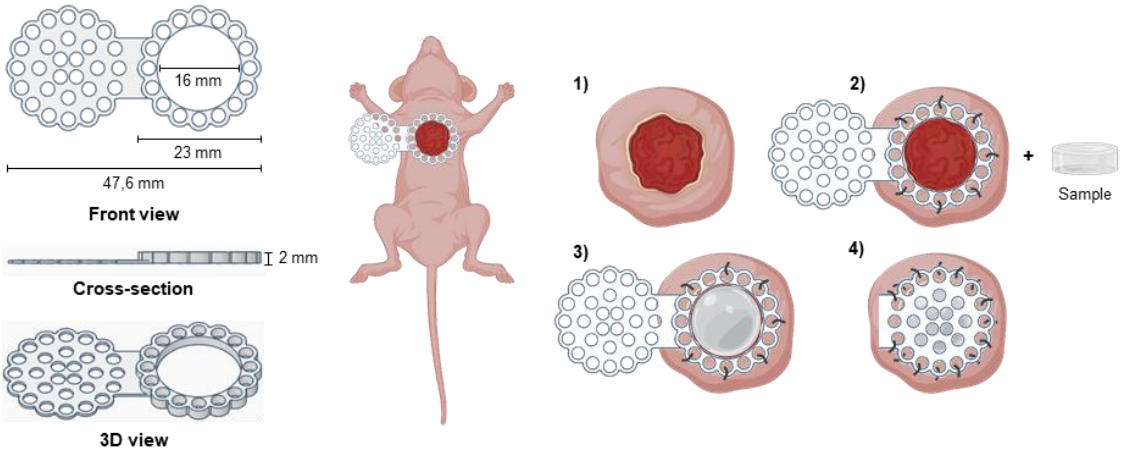

Figure S4. Injectability of bioink core biomaterials (Col I and Agarose) and bioinks (Epidermal, Hypodermal and Dermal bioinks).

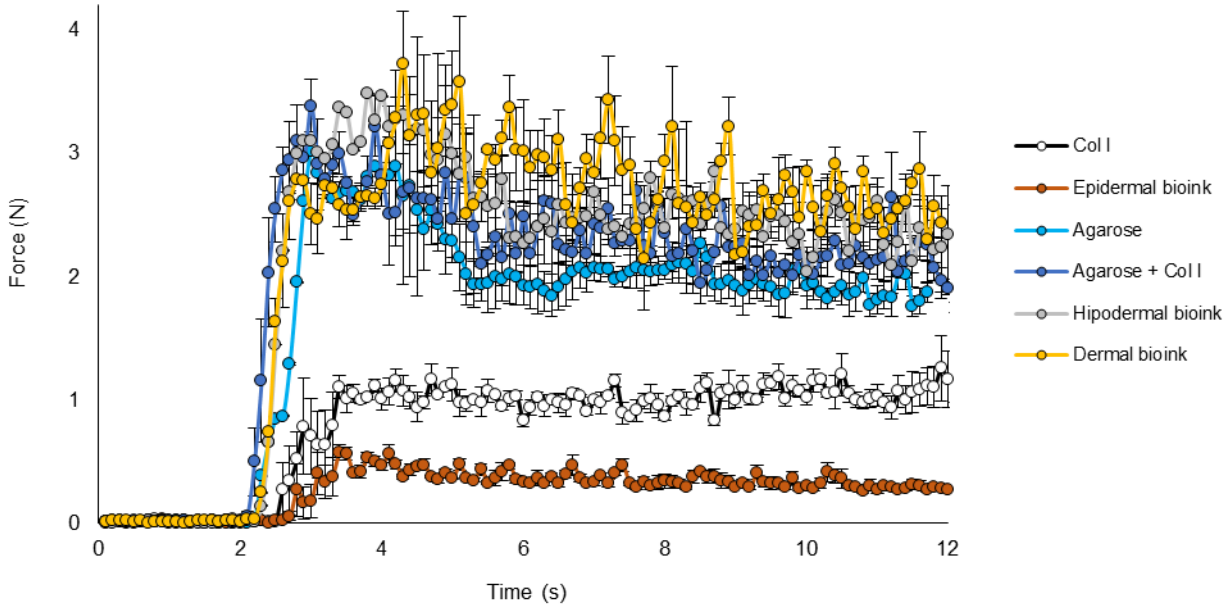

Figure S5. Analysis of individual homeostasis parameters. Graphics show results for each group of treatment against native skin group. Results per week were calculated as the mean value of all mice measures at each time of study: control, autograft, cell-free BT skin and BT skin substitute groups (n week 2, 4, 6, 8 = 8, 8, 4, 4); Native Skin group (n week 2, 4, 6, 8 = 32, 32, 16, 16). Statistical significance: ***P < 0.005.

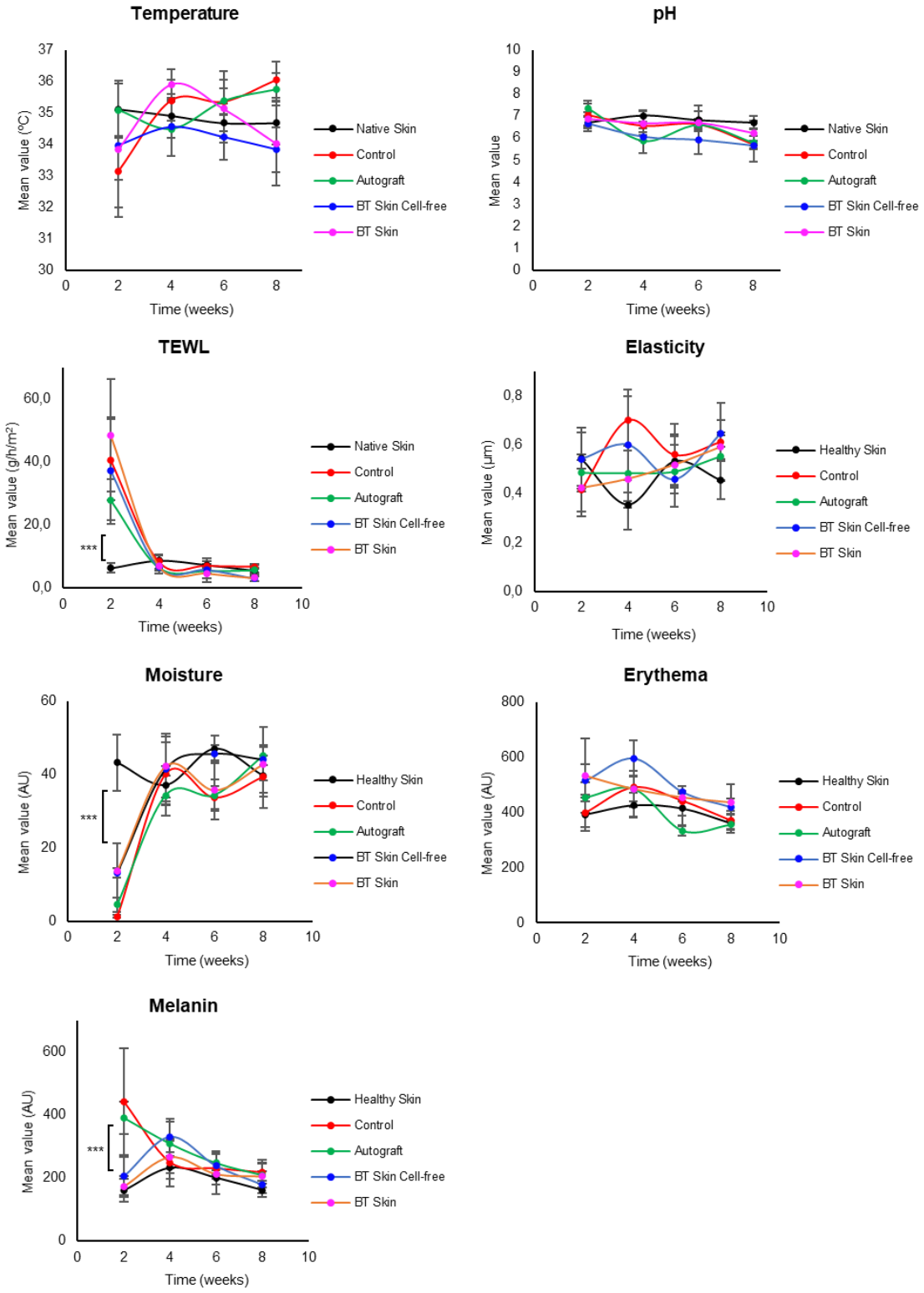

Figure S6. Haematoxylin and eosin (H&E) and Masson's Trichrome histological staining from biopsies of mice wound/scar area and native skin after 4 and 8 weeks. Scale bar: 500 µm.

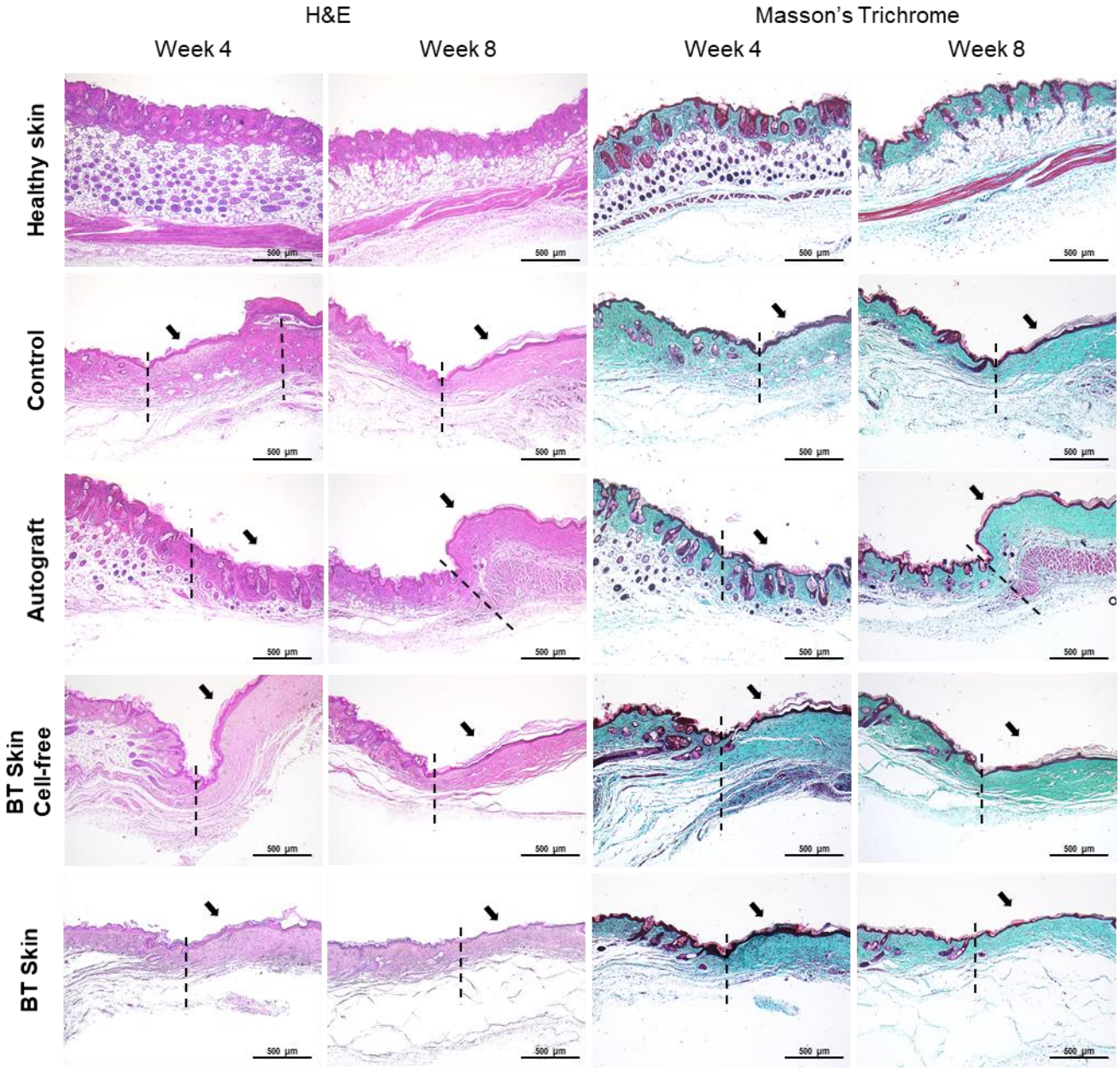

DO NOT GO GENTLE INTO THAT GOOD NIGHT

Dylan Thomas - 1914-1953

Do not go gentle into that good night,

Old age should burn and rave at close of day;

Rage, rage against the dying of the light.

Though wise men at their end know dark is right,

Because their words had forked no lightning they

Do not go gentle into that good night.

Good men, the last wave by, crying how bright

Their frail deeds might have danced in a green bay,

Rage, rage against the dying of the light.

Wild men who caught and sang the sun in flight,

And learn, too late, they grieved it on its way,

Do not go gentle into that good night.

Grave men, near death, who see with blinding sight

Blind eyes could blaze like meteors and be gay,

Rage, rage against the dying of the light.

And you, my father, there on the sad height,

Curse, bless, me now with your fierce tears, I pray.

Do not go gentle into that good night.

Rage, rage against the dying of the light.